INVESTIGATION OF HYDRODYNAMICS AND HEAT TRANSFER CHARACTERISTICS WITH BIOMASS BLENDS IN A PRESSURIZED CIRCULATING FLUIDIZED BED

A Thesis

Submitted in Partial Fulfillment of the Requirements for the Award of the Degree of

DOCTOR OF PHILOSOPHY

By

PANKAJ KALITA

CENTRE FOR ENERGY
INDIAN INSTITUTE OF TECHNOLOGY GUWAHATI
GUWAHATI – 781039, INDIA

APRIL 2013

This thesis is dedicated to my father

Late Jogen Chandra Kalita

DECLARATION

I hereby certify that the information presented in this thesis is entirely my own account of my research and contains as its main content work expect where otherwise stated, which has not previously been submitted for a degree or diploma at this institute or any tertiary educational institution.

Pankaj Kalita
Regn No. 09615101
Centre for Energy
Indian Institute of Technology Guwahati
Guwahati – 781039, India
April 2013.

CERTIFICATE

It is certified that the work contained in the thesis entitled **Investigation of Hydrodynamics and Heat Transfer Characteristics with Biomass Blends in a Pressurized Circulating Fluidized Bed** by **Pankaj Kalita (Regn No. 09615101)**, a student in the Centre for Energy, Indian Institute of Technology Guwahati, India, for the award of the degree of **Doctor of Philosophy** has been carried out under our supervision and this work has not been submitted elsewhere for the degree.

Dr. Pinakeswar Mahanta
Professor
Department of Mechanical Engineering
Indian Institute of Technology Guwahati
Guwahati – 781039, India

Dr. Ujjwal K. Saha
Professor
Department of Mechanical Engineering
Indian Institute of Technology Guwahati
Guwahati – 781039, India

ABSTRACT

Pressurized circulating fluidized bed (PCFB) is gaining popularity among the scientific community in utilizing low grade fuel for the combustion and gasification applications due to its in-built capability of capturing of sulphur and NOx. Compactness, high heat release rate and less amount of sorbent requirement makes the PCFB system more attractive. However, the complexity in hydrodynamics and heat transfer phenomena associated with bed geometry, flow parameters as well as type of fuels etc., demands for extensive research so as to open an avenue for designing of a PCFB system.

In the present investigation, two PCFB units (one cold bed and the other being hot bed) of similar dimensions have been designed and fabricated in order to investigate the hydrodynamics and heat transfer characteristics experimentally. The bed hydrodynamics along the height of the riser was investigated in the cold bed unit. The effect of superficial velocity, solid inventory, particle size and operating pressures were investigated on bed voidage and suspension density. A heat transfer probe was installed at the upper splash region of the riser to investigate the wall-to-bed heat transfer coefficient along the height of the probe. The radial variation of heat transfer coefficient was investigated at a height of 1.57 m from the distributor. The hydrodynamics and heat transfer characteristics for different blending ratios of sawdust with sand and different weight composition ratios were also investigated at different operating conditions. The hot PCFB unit has been developed to investigate the effect of temperature and pressure on bed-to-wall heat transfer and quality of product gas at different biomass blending ratios. Gas composition was evaluated with the help of a gas chromatography and a flue gas analyser. Two heat transfer probes were installed at the upper splash region of the riser to investigate the heat transfer coefficient. The heat transfer coefficient was calculated without and with twisted tapes at different solid inventories and the performance was compared. Results obtained in the present investigation were found to be well comparable with the published results.

The blending of biomass used for the above investigation in the PCFB units has been characterized to understand the change of thermal property with the increase of rate of heating. To investigate the effect of heating rates on the degradation of biomass the experiments were performed at three different heating rates of 10, 30 and 80 °C/min while performing thermogravimetric (TG) analysis. The degradation of mass with temperature was validated numerically. The kinetic parameters of biomass were evaluated for both first and second reaction zones. The thermal response of biomass undergoing decomposition has also been modelled by using one dimensional (1-D) transient thermal model. The model was tested by using transient conduction Heisler chart. This study is important to understand the requirement of optimum fluidizing air for a combustor and to maintain a temperature required for gasification when it operates below sub stoichiometric condition.

ACKNOWLEDGEMENT

I wish to express my profound sense of gratitude to Professor Pinakeswar Mahanta, and Professor Ujjwal K. Saha for their invaluable guidance and inspiration in bringing out this work to the present shape.

I would like to thank my doctoral committee members, Professor P. S. Robi, Dr. Niranjan Sahoo, and Dr. Bishnupada Mandal for their valuable suggestions and encouragement at different stages of research.

I would like to thank Professor A. K. Ghoshal, Head, Centre for Energy, Indian Institute of Technology Guwahati for his valuable help and guidance. I would also like to thank Professor U. S. Dixit, Department of Mechanical Engineering, IIT Guwahati and Professor Anupam Dewan, Department of Applied Mechanics, IIT Delhi for their constant encouragement and suggestions throughout my higher education.

I would like to acknowledge Central Power Research Institute, Bangalore for providing the financial support and Indian Institute of Technology Guwahati for providing necessary infrastructure to carrying out the research. I would also like to thank the University of Nottingham, United Kingdom for selecting me as one of the Indian Distinguished Visiting Fellows during my PhD for pursuing research for the period of three months.

I wish to express thanks to Sri Mrinal Sarma, Sri Dilip Chetri, Sri Dhaneshwar Khaklari, Sri Dipankar Kalita, Sri Mridul Deka, Sri Bhaskar Bharadwaj, Sri Biren Barman, Sri Tapan Das, Sri Krishna Das and other staff members of Central Workshop for helping me in various stages of fabrication of the experimental setups and during experimentation. Without their timely support, this work could not have been accomplished.

I would also like to thank Dr. Karuna Kalita, for his help, suggestions and encouragement throughout my academic life.

I am very much thankful to my colleagues Mrs. Lepakshi Barbora, Sri Dhiren Huzuri, Mrs. Gitanjali Hazarika, Miss. Amrita Difuza, Miss. Madhuri Das, Miss. Dipti Yadav, Sri Dibjyoti Sahoo, Sri Jonmani Kalita, Sri Utsab Guharoy, Sri Sanjib Sarma, Sri Rituraj Saikia and all the other friends working in I.I.T. Guwahati for their encouragement and help.

Grateful thanks to my mother, uncles, sisters, brothers and other family members and friends for their constant encouragement and moral support.

Author

CONTENTS

NOMENCLATURE

A : Pre-exponential factor (min^{-1})

A_B : Cross sectional area of the bed (m^2)

A_D : Cross sectional area of downcomer (m^2)

A_{htp} : Surface area of heat transfer probe (m^2)

A_{ts} : Tube surface area (m^2)

Ar : Archimedes number (or Ga, Galileo number)

B : Weight composition of biomass particles

B/S : Biomass (sawdust) to sand ratio

C_p : Specific heat (kJ/kg °C)

C_{pg} : Specific heat of gas (J/kg °C)

C_1 : Correlation constant

C_2 : Correlation constant

d_p : Particle diameter (mm)

d_p^* : Non-dimensional particle diameter

Δd_B : Error in measuring diameter of the riser (m)

Δd_D : Error in measuring diameter of the down comer (m)

E : Activation energy (kJ mol^{-1})

F_o : Froude number (Non dimensional time)

g : Acceleration due to gravity (m/s^2)

G_s : Solid circulation rate ($kgm^{-2}s^{-1}$)

h : Heat transfer coefficient (W/m^2-K)

H : Enthalpy (J/kg)

H_B : Height of the bed (m)

H_g : Enthalpy of gas (J/kg)

Δh : difference of height in manometric fluid of water column (cm)

I : Supply current (amp)

K : Thermal conductivity (W/m °C)

L : Material thickness (m)

ΔL : Error in measuring height of the heat transfer probe (m)

ΔL_a : Error in measuring solid accumulation height (m)

L_a : Solid accumulation height (m)

L_m : Difference between two consecutive pressure taps (m)

m : Mass of the sample at time "t" (kg)

M : Mass of the bed material (kg)

m_a : mass flow rate through the Orifice plate (kg/s)

m_o : Initial mass of sample (kg)

m_f : Final mass of sample at the end of the reaction (kg)

$\dot{m}_g$: Mass flux of gas (kg $m^{-2}s^{-1}$)

$\dot{m}_w$: Mass flow rate of water (kg/s)

n : Order of reaction

Nu : Nusselt number

p : Temperature divisions

ΔP : Difference in height of manometric fluid (water) of water (cm)

q : Heat supplied (Watt)

Q : Rate of heat transfer (Watt)

Q_i : Heat of decomposition (J/kg)

Δq : Error in measuring heat supplied (Watt)

R : Universal gas constant (kJ mol^{-1} K^{-1})

Re : Reynolds number

Re_{mf} : Particle Reynolds number under minimum fluidizing condition, $Re_{mf} = d_p u_{mf} \rho_g / \mu$

S : Weight composition of sand particles (g)

t : Time (s)

Δt : Error in measuring time (stop watch) (s)

T : Temperature (°C)

T_b : Bulk Temperature (°C)

ΔT_b : Error in measuring bed temperature (°C)

T_{bi} : Bed temperature in (°C)

T_I : Initial temperature (°C)

T_k : Sink temperature (°C)

T_r : Radiation source temperature (°C)

ΔT_S : Error in measuring surface temperature (°C)

T_{bs} : Bulk surface temperature (°C)

T_{ts} : Tube surface temperature (°C)

T_∞ : Environmental temperature (°C)

$T_{w,in}$: Water inlet temperature (°C)

$T_{w,out}$: Water outlet temperature (°C)

U_{G_s} : Overall uncertainty in calculating solid circulation rate

u_g : Actual fluidizing velocity (m/s)

U_g^* : Non dimensional fluidizing velocity

U_h : Overall uncertainty in calculating heat transfer coefficient

u_{mf} : Minimum fluidization velocity (m/s)

U_{sup} : Superficial velocity (m/s)

u_t : Terminal velocity of particle (m/s)

u_t^* : Non-dimensional terminal settling velocity

V : Supply voltage (volt)

W : Solid inventory (g)

x : Spatial variables (m)

Y Scaling parameter

α : Thermal diffusivity (m^2/s)

α_m : Absorptive of the material

β : Heating rate (K/min)

ε : Bed voidage

ε_m : Emissivity of the material

ε_{mf} : Bed voidage at minimum fluidization

ε_r : Radiation source emissivity

ρ : Density of rice husk (kg/m^3)

ρ_b : Bulk density (kg/m^3)

ρ_0 : Initial density (kg/m^3)

ρ_g : Gas density (kg/m^3)

ρ_s : Solid density (kg/m^3)

ρ_{sus} : Suspension density (kg/m^3)

$\Delta\rho_S$: Error in measuring solid density (kg/m^3)

ϕ_s : Spherocity of solid

σ : Stefan-Boltzman constant (5.67×10^{-8} W/m^2-K^4)

μ : Viscosity of gas (kg/ms)

ABBREVIATION

ACFB	:	Atmospheric Circulating Fluidized Bed
BFB	:	Bubbling Fluidized Bed
Ca:S	:	Calcium to Sulphur Ratio
CFB	:	Circulating Fluidized Bed
DSC	:	Differential Scanning Calorimetry
DTA	:	Differential Thermal Analysis
DTG	:	Differential Thermogravymetric
ER	:	Equivalence Ratio
FC	:	Fixed Carbon
GC	:	Gas Chromatography
ID	:	Internal Diameter
IGCC	:	Integrated Coal Gasification Combined Cycle
LHV	:	Lower Heating Value
MNRE	:	Ministry of New and Renewable Energy
OTU	:	Once-Through Unit
PBFB	:	Pressurized Bubbling Fluidized Bed
PCFB	:	Pressurized Circulating Fluidized Bed
PDE	:	Partial Differential Equation
TG	:	Thermogravimetric
TGA	:	Thermogravimetric Analysis
VM	:	Volatile Matter

LIST OF FIGURES

LIST OF TABLES

Chapter –1

INTRODUCTION

1.1 Motivation

In the recent past, more emphasis is being given to produce clean energy from biomass and other renewable sources due to rise in crude oil price and greenhouse gas emission. In order to utilize the available carbon neutral environmentally benign resources effectively, various technologies and processes have been developed around the world (Werther, 2009; Basu, 2006; Anthony, 1995). The co-firing of biomass with coal at low percentages in the thermal power plant avoids the characteristic operating problems of biomass combustion such as ash sintering and fouling of heat exchanger surfaces, and also significantly reduces the emission of pollutants (Werther, 2009). Hence, biomass fuel could substitute more expensive coal and contribute in lowering CO_2 emission. In India, the estimated annual biomass production is 200 million tons, which (unlike coal) is distributed almost evenly in the country. This is equivalent of 20 GW of installed capacity. In addition, agro-residues and woody bio-residues from wastelands (estimated at 60 million hectares) could add another 100–300 million tons, which amount to 45 GW of installed capacity. However, the total installed capacity of biomass-based power generation (inclusive of bagasse and non-bagasse cogeneration and biomass gasifiers; as of September 2007) is 838 MW (Singh, 2007). This capacity is mainly through cogeneration (692.3 MW through bagasse fired boilers), which is an inefficient method of utilization of the biomass energy. The circulating fluidized bed (CFB) technology is one of the efficient technologies where low grade biomass fuels can be burnt effectively with lower level of NOx and SOx (Anthony, 1995; Basu and Cheng, 1996). Further, this technology can be utilized for both combustion and gasification applications. However, the high volatile content and low char inventory of biomass fuels increase requirements for control of various process parameters. Particularity, in the case of large scale CFB multi-fuel operation, the effects of fuel quality and mixing ratio of the fuels with respect to the CFB combustion process must be well known and taken into account during both boiler design and control of process parameters. In addition, the hydrodynamics of gas-solid distribution in a CFB furnace have significant effects on boiler performance; for instance on combustion, heat transfer, emission formation and on boiler control. Many researchers have reviewed the bed

hydrodynamics and heat transfer at atmospheric conditions (Basu, 2006, Basu and Nag, 1996, Basu and Nag, 1987, Grace, 1986). The accuracy of heat transfer and boiler performance can be increased if the hydrodynamics of solid material (ash, sand, limestone and char) can be predicted under varying fuel mixture feeding. A host of researchers have demonstrated the dependence of various factors such as superficial velocity, solid circulation rate, solid inventory, and particle size distribution on the performance of a pressurized circulating fluidized bed (PCFB) unit. Change of any of these parameters influences the bed hydrodynamics such as bed voidage, suspension density etc. and this causes a change in the heat transfer along the bed height. Only limited information was found on the study of hydrodynamic and heat transfer characteristics in PCFBs with biomass blend despite having features like compactness, good heat transfer characteristics, fuel flexibility, and combustion efficiency suitable for steam generation, gasification and combined cycle power generation. Further, no single universal approach for designing a fluidized bed reactor system is found in the open literature. It is understood that, the fluidized bed reactor system design relies heavily on correlations, engineering models, and plant observations. The computational fluid dynamic approach may offer viable and attractive options over the traditional approaches; however, challenges remain in considering reactive flow that involves the incorporation of reaction kinetics, heat and mass transfer properties into fluid dynamic calculation. Continued research efforts are necessary toward the development of an advanced fluidized bed processes to deal with the abundantly available reactive biomass fuels. Moreover, extent of heat transfer in the upper splash region, where most of the superheater tubes are installed plays a key role in the overall efficiency of a CFB unit. Usually heat transfer coefficient is decreasing from the bottom to the top of a CFB riser. Hence, the study of heat transfer and its enhancement at the upper splash region of a PCFB is important.

The most of the literatures found in open source are based on investigation of the effect of equivalence ratio (ER), bed temperature, feeding rate etc. on the gas composition, carbon conversion efficiency and cold gas efficiency in atmospheric CFB. The ability of fluidized beds to conduct the gasification process has been confirmed by many researchers as well as from several successful operating industrial plants in developed countries. However, more research is required for extensive and flourishing progress in this area. Very few information of the quality of gas production under operating pressures has been reported. Studies on blending of biomass with bed material and its effect on gas composition in PCFB was rarely found in the open literature. Hence, more studies are required in order to understand the complex hydrodynamics of an efficient pressurized CFB gasification unit.

In view of this, the present contribution is focused to investigate thoroughly the effect of various operating parameters on hydrodynamic characteristics, heat transfer behavior and reaction kinetics in order to utilize the correct strategy in both PCFB combustion and gasification application with various mixtures of biomass.

1.2 Background of fluidization bed technology

There are various attractions to generate power from biomass derived fuels such as coal, biomass etc. through Fluidized Bed Technology. It is a compact, cheap and efficient method of using low grade coals which are either difficult to be used or not possible to use in conventional processes. Fritz Winkler from Germany was the first to obtain a patent for a fluidized bed hot gas generators in 1921. Fluidized bed processes came into wide use in the petroleum industry in 1940's. These processes are also used extensively in the chemical and metallurgical fields.

The world's first commercial CFB boiler went into service at Pihlava, Finland, in 1979 manufactured by Ahlstrom (Finland) to convert an oil-fired unit into a circulating fluidized bed boiler producing 20 tones/h of steam from wood waste. Another CFB boiler of larger capacity of 90 tones/h unit became operational in Kauttua, Finland, in 1981 which was designed to burn various fuels such as coal, peat and wood wastes. After the successful operation of these two projects many companies installed varied capacities of CFB units around the globe. Some of the notable installation are the 110 MW Colorado Rte'sNucla Plant (Pyropower), 125 MWe unit at Emile Huchet, Sweden (SteirIndustrie), 150 MWe unit at Texas, New Mexico power plant (CE) and 165 MW, Point Aconi in Nova Scotia State, Canada coal fired CFB unit. Today there are a number of CFB plants operating all over the world and size of the plant installations are increasing. The world's largest CFB power plant (Lagisza) of capacity 460 MWe began commercial operation in 2009, that marked the beginning of a new era in the evolution of this technology. This is also the world's first once-through unit (OTU) supercritical CFB boiler [Kunii and Levenspiel (1991), Chattopadhyay (2007), Basu (2006)].

Along with the commercial CFB units, various laboratory and pilot CFB units are developed to investigate and optimize the operating parameters for higher efficiencies at lower emission level. Continued research and development in the field of fluidization has led towards the development of pressurized bubbling fluidized bed (PBFB), pressurized circulating fluidized bed (PCFB) as well as integrated gasification and combined cycle (IGCC) with higher

thermal efficiency and lower emission. The pressurized circulating fluidized bed (PCFB) technology may be the most promising alternative for effective and efficient utilization of various grades of coal and biomass in various applications. Because it operates at gas densities an order of magnitude higher than conventional units, the PCFB displays a markedly different flow behavior than the atmospheric circulating fluidized bed (ACFB). In particular, due to its large relative ''slip'' velocities between solids and gases enhance the role of gas inertia and the PCFB exhibits a shorter acceleration region than the ACFB. Similarly, because of higher fluid densities, fluidization tends to stabilize and the pressurized riser features a more homogeneous and steady suspension (Louge *et al.*, 1999).

Ahlstrom developed the first pilot plant PCFB of capacity 10 MW_{th} at Karhula, Finland in 1989 suitable for various types of coal. The PCFB technology seemed to be the most promising alternative for meeting the objectives of future coal-firing applications. The PCFB could produce 10-15% higher net plant efficiency at a lower cost with significant reduction in emission level in comparison to the conventional pulverized coal fired technology. In comparison to PBFB and IGCC technology, the PCFB has very high efficiency, very low emissions and compact, besides reduces the erosion of reaction walls which is a usual problem for ACFB unit. The PCFB technology has a much lower capital cost, operating cost, and resulting cost of electricity and hence a shorter payback.

Due to the multiple advantages CFB technology such multi-fuel flexibility, compactness, uniform temperature throughout, etc. CFB gasification has also been developed side-by-side with the CFB boiler technology. The first commercial atmospheric gasifier was installed in 1983 in Jacobstad, Finland. In 1991, Foster Wheeler supplied a PCFB gasification system to a 17 MWth biomass-fired IGCC demonstration project at Varnamo Sweden, which is the first biomass-fired IGCC plant in the world. The commercial gasifiers developed by FW have used wood waste, biomass, tires, plastics, peat, cardboard, paper waste, and bark for the paper and power industries for gasification.

The potential of fluidized bed technology appears to be almost unlimited. As the technology refinement opens up new vistas, PCFB power generation holds a greater promise to feed the power hungry world in a most cost effective and environment friendly way (Chattopadhyay, 2007). However, further research is needed in order to meet challenges like utilization of abundantly available biomass resources as feedstock and understanding of reaction kinetics, hydrodynamics and heat transfer characteristics in PCFB.

1.3 Aim and objective of the present work

The aim of the present investigation is to optimize the biomass blend for better performance in gas-solid interactions, heat transfer characteristics and gasification product yield in a PCFB.

The following objectives are addressed in the present investigation

- Investigation of thermal analysis and characterization of biomass
- Study of bed hydrodynamics along the riser and heat transfer characteristics along the upper splash region of the riser under varied range of operating conditions with biomass blends in pressurized circulating fluidized beds
- Investigation of product gas composition of gasification at different blending of biomass in sand
- Enhancement of heat transfer coefficient at the upper splash region of a hot PCFB unit with passive heat transfer devices under varied operating conditions

1.4 Outline of the thesis

This thesis comprises of eight Chapters. Chapter 1 introduces the motivation, background and objectives of the present work. Chapter 2 reports the detailed review of literature on the various aspects of CFB hydrodynamics, heat transfer, kinetic modeling etc. for combustion and gasification applications. The description of the experimental setups along with the procedures is presented in Chapter 3. In Chapter 4, biomass characterization, reaction kinetics and formulation of 1D heat conduction model is discussed. Results of the reaction kinetics and modeling are outlined in Chapter 5. The results of the cold bed study are discussed in Chapter 6. Chapter 7 reports the experimental results of the hot bed study. Product gas analysis of gasification and the performance of the biomass feeding system are also discussed in this Chapter. Chapter 8 summarizes the research findings and scope for future work. The design of orifice plate, distributor plate, cyclone separator, procedure for measurement of particle size, calibration of thermocouple, design calculation of CFB gasification, uncertainty analysis in measuring heat transfer coefficient and solid circulation rate, experimental data at varied blending of biomass, Heisler chart and values of reaction kinetic parameters for five different biomass are presented in the appendices (Appendix I through XII).

Chapter – 2

LITERATURE REVIEW

2.1 Introduction

This chapter reports the review of literature on various aspects of bed hydrodynamics, heat transfer characteristics and gasification in circulating fluidized bed (CFB) units. The effect of various operating parameters on bed hydrodynamics and heat transfer characteristic are also discussed. Review on reaction kinetics, and various parameters influencing the biomass gasification in CFB system are also addressed. Summary of the literature review and the scope of the present research are presented at the end of the chapter.

2.2 Bed hydrodynamics and heat transfer phenomena in CFB

Many researchers have reviewed the bed hydrodynamics [Basu (2006), Yates (1996), Grace (1986), Kunii and Levenspiel (1991)] and heat transfer characteristics of circulating fluidized bed [Basu (2006), Basu and Nag (1996), Basu and Nag (1987), Werther (2009), Basu (1990), Anthony (1995), Basu and Cheng (1996), Gupta and Nag (2002)]. The hydrodynamic condition influences the parameters like auxiliary power consumption, heat absorption, temperature distribution, combustion condition, bed inventory and erosion. The mechanism of heat transfer in a fluidized bed is very complicated and is quite different from the usual system as it involves a large number of variables and heavily depends on bed hydrodynamics. Thus, a good understanding of local and overall hydrodynamics under different operating condition in a CFB unit is very important in order to model the heat transfer characteristics in a physically realistic manner and for a rational design. In the following subsections, the various parameters influencing the hydrodynamic behavior and its effect on heat transfer characteristics are discussed.

2.2.1 Bed hydrodynamics

For a specific design of a fluidized bed the bed hydrodynamic studies are very essential as these would provide information on basic flow patterns, mixing, particle attrition behavior, and heat

and mass transfer characteristics. In a typical CFB boiler or gasifier, the solids are in the turbulent fluidized bed regime in the lower furnace, fast regime in the upper furnace, swirling flow in the cyclone, moving bed in the standpipe, bubbling bed in the loop-seal and pneumatic transport in the back pass.

Glicksman (1988) stated that the important hydrodynamic factors in a CFB are the fraction of wall covered by particles and gas, i.e. voidage phenomena and average contact time of particles at the wall. Work of Weinstein *et al.* (1983) has confirmed the existence of core-annulus structure of the dense phase of fast fluidized bed. In simple terms, there exists a relatively dilute upflow core in which solid particles are entrained upward by a high velocity gas stream and a much denser annulus layer near the column wall in which solid particles congregate and fall as dense structures similar to waves of strands or streamers as shown in Fig.2.1. As heat transfer surfaces are commonly located at the column wall for most CFB applications, the influence of down flowing wall layer on heat transfer is significant. The velocity of descent of strands in the wall layer, the duration of their stay at the wall and the time fraction of wall coverage are all important hydrodynamic parameters that affect the heat transfer between the gas solids suspension and the wall. The following subsection describes the effect of various operating parameters on bed hydrodynamics i.e. on bed voidage, suspension density, and fluidization velocity.

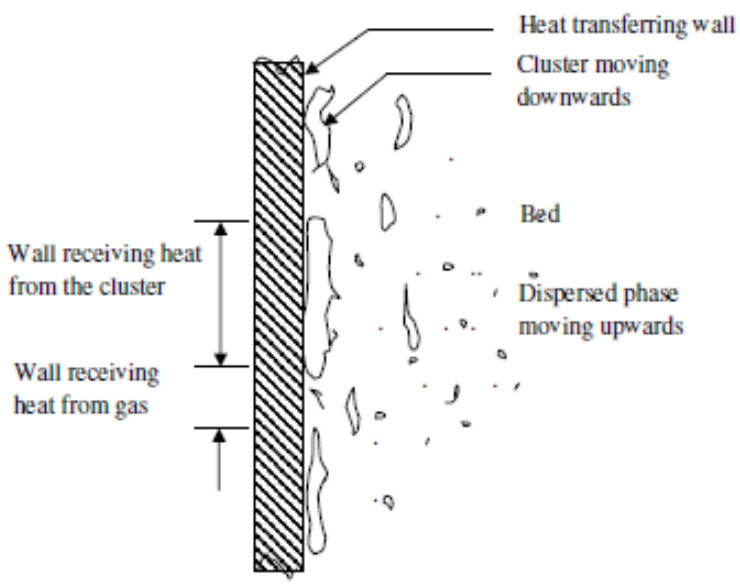

Fig.2.1 Cluster renewal heat transfer mechanism (Basu, 2006)

2.2.2 Effect of operating parameters on bed hydrodynamics

2.2.2.1 Bed Voidage

The bed voidage (ε) is the volume fraction of space occupied by the gas. The bed voidage can be determined experimentally by a number of methods, for instance, by measuring the bulk density and relating it to gas and particle densities.

$$\rho_b = \varepsilon \times \rho_g + (1-\varepsilon) \times \rho_s \tag{2.1}$$

$$\text{or, } \varepsilon = \frac{\rho_s - \rho_b}{\rho_s - \rho_g} \approx 1 - \frac{\rho_b}{\rho_s} = 1 - \frac{M}{A_B H_B \rho_s}$$

The bed voidage can also be calculated by measuring pressure drops in U-tube manometer along the riser height. Other techniques for measuring voidage in fluidized beds involve the use of capacitance probes, optical fibres, X-ray or γ-ray attenuation and capacitance tomographic imaging [Yates (1997), Louge *et al.* (1999), Sidorenko and Rhodes (2004)]. The local voidage, and the gas and solid velocities change continuously from the axis to the wall as reported by many researchers [Hartge *et al.* (1988), Horio *et al.* (1988), Yates (1997), Li *et al.* (2010)]. The voidage is the highest along the axis of the riser column and the lowest in the wall as observed by Tang and Engstrom (1987), Horio (1988), and Li *et al.* (2010). The radial voidage distribution is much flatter in the upper section of the bed, as well as at the lower circulation rates. In case of fast fluidized beds, there is a gas-solid boundary layer, where the solid generally moves downward. This is investigated by Tang and Engstrom (1987), and Schaub (1989) in both large commercial boilers as well as laboratory units.

The axial variation of voidage is typically a flattened 'S' profile as shown in Fig.2.2. At the bottom of the riser solid fraction varies from 0.2 to 0.4, whereby it decreases and these remains almost constant throughout the height of the riser. The lower portions of the bed may be called as dense phase which is generally in bubbling or turbulent mode of fluidization. Above this, the upper entrained region where the solid fraction decreases progressively to about 0.02-0.05, is called as lean phase, and this is generally the fast fluidization mode. The area averaged voidage along the axis of the riser may also be found from the static pressure drop data and its dependence on the local heat transfer coefficient may be found out. Gupta and Nag (2002) investigated that with the increase in superficial velocity, the bed voidage increases in the bottom

portion and decreases in the top region as more solids are lifted up due to more drag force. The concentration of sand particles is more in the riser column for higher bed inventory, and hence, the bed voidage is lower.

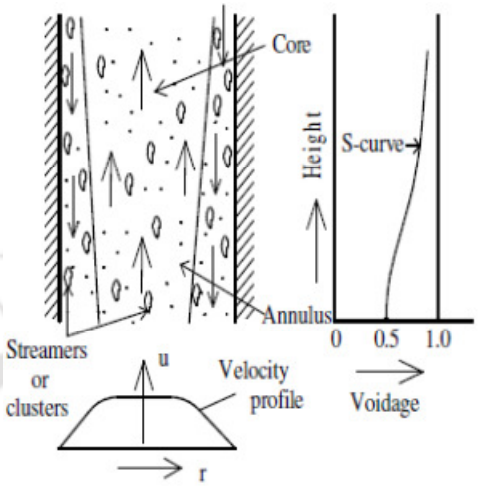

Fig.2.2 Axial variation of voidage ("S" Profile) (Nag, 2001)

Knowlton (1977) studied the effect of pressure on bed expansion for widely sized solids with average sizes of approximately 250 µm. He found no clear correlation between pressure increase and bed expansion. Sobereiro and Monteiro (1982) investigated the hydrodynamic behavior of group B powders for pressure up to 35 bar. This work suggested that ε_{mf} is independent of pressure. King and Harrison (1982), who worked with group A and group B particles, report similar trends as observed by Jacob and Weimer for group A powders. Bouratona *et al.* (1993) suggested that for large particle (≥1.51 mm), the voidage can be determined by a single non-dimensional parameter Y, as given by,

$$Y = \frac{\rho_g u_g^3}{g\mu} \tag{2.2}$$

The use of Y as a scaling parameter successfully regroups the expansion data from high pressure experiments, but fails to regroup the atmospheric one. Gupta and Nag (2002) observed that the axial bed voidage along the height of the bed is observed to be less in the bottom zone and is high in the top zone. Axial bed voidage increases at the bottom zone and decreases at the top zone with an increase in operating pressure. Shen *et al.* (1991) experimentally investigated the effects of bed voidage in a PCFB unit and found similar observation of Gupta and Nag (2002).

2.2.2.2 Suspension density

The amount of solids density at a particular section of the bed may be defined as suspension density. Mathematically, it can be expressed as,

$$\rho_{sus} = (1-\varepsilon)\rho_s + \varepsilon\rho_g \tag{2.3}$$

It is reported that, the particle size and the solid inventory have substantial practical influence on the suspension density profile in a CFB furnace (Basu, 2006). It is claimed that with the decrease in particle size, the suspension density increases. Yue *et al.* (2005) suggested that by changing the bed inventory, one can influence the suspension density. Suspension density along the height of a CFB boiler varies exponentially as it does in the freeboard region of a bubbling fluidized bed [Li and Kwauk (1980), and Kunii and Levenspiel (1991)]. However, Brereton and Stromberg (1986), and Andersson and Leckner (1992) found the profile to be better represented by a power-law equation. The solid holdup in a packed state is typically in the range of 0.45-0.65 and decreases with increasing gas velocity as confirmed from the research findings of Jiang *et al.* (2003) (Fig.2.3).

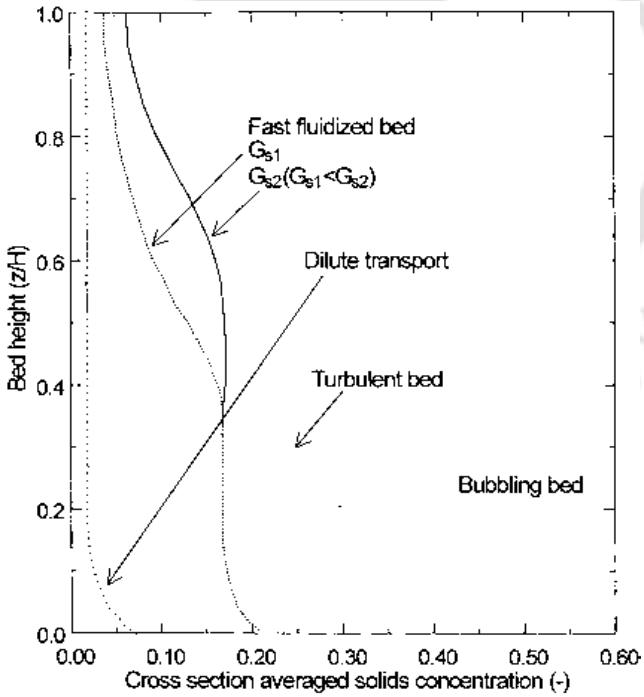

Fig.2.3 Typical axial profile of solids concentration in various fluidization regimes (Jiang *et al.,* 2003)

2.2.2.3 Minimum fluidization velocity

Minimum fluidization velocity is the basic information required for the design and development of a fluidized bed. Many researchers have studied how an increased pressure affects the minimum fluidization velocity. They have experimentally found that the effect of pressure on the minimum fluidization velocity depends on the particle size. The results of their experiments show a clear decrease in the minimum fluidization velocity with increasing pressure for particles larger than 100 µm (Geldart B and D materials) [Wen and Yu (1966a), Knowlton (1977), Saxena and Vogel (1977), King and Harrison (1982), Chitester *et al.* (1984), Nakamura *et al.* (1985), Chiba *et al.* (1986), Bouratona *et al.* (1993), Marzocchella and Salatino (2000), Vogt (2001)]. Other experiments showed that for fine Geldart A particles (less than 100 µm), the minimum fluidization velocity remains unaffected by pressure [Knowlton (1977), King and Harrison (1982), Sobreiro and Monteiro (1982), Chitester (1984)]. To estimate the effect of pressure on minimum fluidization velocity, Ergun (1952) has developed an expression of the form,

$$\frac{1.75\left(1-\varepsilon_{mf}\right)}{\phi\varepsilon_{mf}^3}\left(\frac{d_p u_{mf}\rho_g}{\mu}\right)^2+150\frac{1-\varepsilon_{mf}}{\phi_s^2\varepsilon_{mf}^3}\left(\frac{d_p u_{mf}\rho_g}{\mu}\right)=\frac{g d_p^3\rho_g\left(\rho_p-\rho_g\right)}{\mu^2} \tag{2.4}$$

$$\text{Or, } \frac{1.75}{\phi\varepsilon_{mf}^3}\left(\mathrm{Re}_{mf}\right)^2+150\frac{1-\varepsilon_{mf}}{\phi_s^2\varepsilon_{mf}^3}\left(\mathrm{Re}_{mf}\right)=\frac{g d_p^3\rho_g\left(\rho_p-\rho_g\right)}{\mu^2}$$

As observed in the Eq. (2.4), for the laminar flow region (for $\mathrm{Re}_{mf}<2$) and small/light particles with $d_p<100\mu m$ the viscous loss is dominant compared to the kinetic loss; and the minimum fluidization velocity (u_{mf}) is inversely proportional to the gas viscosity (Second left term of Eq. (2.4)). The minimum fluidization velocity (u_{mf}) is therefore expected to decrease with temperature, since μ increases with temperature and because there is no dependence on density, pressure should have no significant effect.

$$u_{mf}\propto\frac{d_p^2\left(\rho_p-\rho_g\right)}{\mu^2} \tag{2.5}$$

For larger/denser particles and turbulent flow ($\mathrm{Re}_{mf}>1000$), where the kinetic loss predominates, the minimum fluidization velocity is inversely proportional to the square root of the gas density or pressure, and therefore, it decreases with pressure.

$$u_{mf} \propto \sqrt{\frac{d_p\left(\rho_p-\rho_g\right)}{\rho_g}} \tag{2.6}$$

Equation (2.4) may be rewritten as,

$$\frac{g d_p^3 \rho_g\left(\rho_p-\rho_g\right)}{\mu^2}=\frac{1.75}{\phi \varepsilon_{mf}^3}\left(\mathrm{Re}_{mf}\right)^2+150\frac{1-\varepsilon_{mf}}{\phi_s^2 \varepsilon_{mf}^3}\left(\mathrm{Re}_{mf}\right)$$

$$or,\ Ar=\frac{1.75}{\phi \varepsilon_{mf}^3}\left(\mathrm{Re}_{mf}\right)^2+150\frac{1-\varepsilon_{mf}}{\phi_s^2 \varepsilon_{mf}^3}\left(\mathrm{Re}_{mf}\right) \tag{2.7}$$

Various correlations has been developed to calculate particle Reynolds number (Re_{mf}) at onset of fluidization based on shape, size and pressure. The generic expression of the particle Reynolds number (Re_{mf}) at onset of fluidization, is given by,

$$\mathrm{Re}_{mf}=\sqrt{C_1^2+C_2 Ar}-C_1 \tag{2.8}$$

where

$$Ar=\frac{d_p^3 g \rho_g\left(\rho_p-\rho_g\right)}{\mu^2} \tag{2.9}$$

As reported, Ergun Eq. (2.4) gave a closer fit for spherical particles and Wen and Yu (1966a) correlation was in better agreement for irregular solids. Table-2.1 provides the comparison of correlation constants C_1 and C_2 developed by various researchers for prediction of the minimum fluidization velocity at elevated pressures.

Table-2.1 Comparison of correlation constants

Correlation	**Pressure range**	**Bed Material**	**Constant** C_1	**Constant** C_2	$\frac{1-\varepsilon_{mf}}{\phi_s^2 \varepsilon_{mf}^3}$	$\frac{1}{\phi_s \varepsilon_{mf}^3}$
Wen and Yu (1966a)	Atmospheric pressure	Fine powders	33.70	0.0408	11	14
Saxena and Vogel (1977)	179-834 kPa	Core dolomite particles	25.28	0.0571	---	---
Borodulya *et al.* (1982)	8000 kPa	Quartz and glass ballotini	16.00	0.0370	---	---
Chitester *et al.* (1984)	2169, 4238 and 6306 kPa	Ballotini particles	28.70	0.0494	7.94	11.57
Nakamura *et al.* (1985)	4900 kPa	Geldart B and D Glass beads	33.95	0.0465	---	---
Basu (2006)	High pressure	---	25.25	0.0651	5.19	8.81

Effect of pressure and temperature on gas solid fluidization in both bubbling and circulating fluidized bed was studied by Yates (1996) for Geldart A and Geldart B particles. As observed, the minimum fluidization velocity, the bubbling velocity and the terminal velocity were found to decrease with an increase of operating pressure. Due to increase in gas density with pressure, high pressure may cause the appearance of homogenous fluidization conditions in systems that fluidize heterogeneously at atmospheric pressure. Sidorenko and Rhodes (2003) also reviewed the effect of pressure on gas-solid fluidized bed behavior and observed similar findings reported by Yates (1996).

2.3 Effect of operating parameters on heat transfer

The heat-transfer coefficient in a CFB riser increases from the bottom to the top as investigated by many researchers [Grace (1986), Basu and Nag (1987), Basu and Nag (1996), Basu (2006)] and it is influenced by a number of factors, including air flow, solid circulation rate, solid inventory, and particle size distribution [Anthony (1995), Basu and Cheng (1996), Gupta and Nag (2002), Basu (2006), Werther (2009)]. As observed, most of the research findings are related to the CFB unit operated under atmospheric pressure. Very few information on bed hydrodynamics and heat transfer characteristics on PCFB reactors have been found in the open literature [Shen *et al.* (1991), Molerus (1993), Wirth (1995), Reddy and Basu (2001), Gupta and Nag (2002)]. The effect of various operating parameters on heat transfer in both cold and hot CFB units are reviewed and reported in the following subsections.

Mahanta (1992) studied the effect of superficial velocity, bed inventory, solid circulation rate, suspension density and heat flux input on the heat transfer coefficient along the riser height. He has done experiment on a cold CFB riser of bed cross section 102 mm x 102 mm and height of 5.25 m. He also studied effect of these parameters on the average heat transfer coefficient along the bed cross section in the upper region of the riser. A decrease in heat transfer coefficient along the height of the riser has been observed.

Kolar and Sundaresan (2002) and Sundaresan and Kolar (2002) reported heat transfer from surface to tubes suspended in the core of a CFB furnace to the bed. They have proposed an empirical correlation model to predict the particle Nusselt number.

Meena (2004) reported the wall-to-bed heat transfer characteristics at the upper splash region of an atmospheric CFB riser of bed cross section 0.102 m x 0.102 m and height of 2 m. Study of heat transfer in the cyclone separator was also reported.

Singh and Sharma (2008) have conducted experiments at the lower splash region of the riser of bed cross section 0.15 m x 0.15 m to investigate hydrodynamic and wall-to-bed heat transfer characteristics. The effect of superficial velocity of air, effect of sand inventory on heat transfer characteristics was studied.

Praghanmor (2009) has carried out a comprehensive study on the effect of operating parameters like superficial velocity of air, and sand inventory on wall to bed heat transfer characterises at the lower splash region of a riser bed cross section 0.2 m x 0.2 m and 0.25 m x 0.25 m and also simulated the hydrodynamic characteristics of the riser of cross section 0.15 m x 0.15 m and height of 2.85 m using fluent 6.3.26. Shankarrao (2011) worked on the same setup and developed correlations for different region of the riser for a scale up of the beds. He has also studied the heat transfer in cyclone separators and observed a decreasing trend of heat transfer coefficient from the top to the bottom of the cyclone.

2.3.1 Effect of suspension density on heat transfer

The suspension density at any particular cross section of a CFB unit plays a major role in heat transfer (Basu, 2006). Experimental findings gathered in laboratory units by different investigators show an increase in heat transfer coefficients with an increase in suspension density. This was expected because the thermal capacity of solids was much higher than that of the gas. Thus, the heat transfer through the particles contributed more than that across the fluid boundary layer. The heat transfer coefficient was found to vary as square root of the cross-section average suspension density (Glicksman, 1988). Divilio and Boyd (1994) presented an overview of the effect of suspension density on the heat transfer using the data from laboratory, pilot plants, and operating plants, and found, the suspension density to vary with the height of the riser. As the riser gets taller, the solid suspension density decreases further, resulting in lower heat transfer coefficients. Using the data generated from the experiments of cold beds, they developed the following correlation.

$$h = 23.2 \times \rho_b^{0.55} \tag{2.10}$$

The following correlation was developed by Werdermann and Werther (1993) by considering their results for convective heat transfer on vertical walls

$$Nu = 7.46 \times 10^{-4} \times \mathrm{Re}^{0.757} \times \rho_b^{0.562} \tag{2.11}$$

Gupta and Nag (2002) studied the bed to wall heat transfer behavior in a 37.5 mm ID and 1940 mm height PCFB riser where the heat transfer coefficient was found increasing with an increasing operating pressure as well as with an increase in gas superficial velocity. It was also observed that, with the increase in pressure, the bed voidage increased in the bottom zone of the riser and decreased in the top zone, thereby increasing the suspension density at the top zone. Shen *et al.* (1991) suggested that when the system pressure is high, the contribution of the heat transfer due to the gas phase will also rise.

The suspension density plays a key role on heat transfer and hence on the performance of a PCFB unit. Both experimental and modeling work have been attempted to investigate the effect of suspension density on heat transfer coefficient [Basu and Nag (1987), Basu (1990), Tsukada (1994), Basu and Nag (1996), Yates (1996), Basu and Cheng (1996), Reddy and Basu (2001), Winaya and Basu (2001), Gupta and Nag (2002), Kolar and Sundaresan (2002)]. The heat transfer to the walls of a CFB is due to the conduction from clusters of particles falling along the wall, thermal radiation and convection to uncovered surface area. As reported, the bed-to-wall convective heat transfer coefficient increases with increasing system pressure, bed temperature and bed suspension density but not with particle size [Basu and Nag (1987), and Basu and Cheng (1996)].

2.3.2 Effect of particle size on heat transfer

As reported (Basu, 2006), the particle size and the solid inventory have substantial practical influence on the suspension density profile, which in turn, influence the heat transfer coefficient in a CFB furnace. It is also observed that once the particle size of the circulating solids reduces, the bed temperature is reduced due to an increased heat transfer. It is claimed that with the decrease in particle size, the suspension density increases, which in turn, increases the heat transfer.

Basu and Nag (1987) investigated that the smaller diameter particles yield higher heat transfer coefficients than larger ones. Higher heat transfer coefficients for smaller particles were

observed by several investigators [Gupta and Nag (2002), Basu and Cheng (1996), Basu and Nag (1996), Basu and Nag (1987)] in the case of short heat transfer sections located on adiabatic walls where the clusters would have a brief time of residence on the heat transferring surface. As the particle size decreases, the particle convective component of heat transfer from the clusters to the wall is enhanced due to the increase in surface area of particles per unit volume. When the heat-transfer surface is long, the first layer of particles in contact with the wall has adequate time to cool down. Thus, the thermal resistance of these particles plays an insignificant role. For the long surfaces of commercial boilers, the effect of particle size on the total heat transfer coefficient is found to be less significant (Basu, 2006).

The use of Geldart's particle sizes (Geldart A: 30-100 μm and Geldart B: 100-1000 μm) in PCFB unit has been reported as bed material in various literatures [Basu and Nag (1987), Basu and Cheng (1996), Winaya and Basu (2001), Gupta and Nag (2002), Kolar and Sundaresan (2002)]. The effect of particle size on heat transfer coefficient is not distinct in a PCFB. As observed, the increase of heat transfer coefficient with particle size is not encouraging [Basu and Nag (1987), and Basu and Cheng (1996)]. Within their range of experimental conditions, finer particles resulted a higher heat transfer coefficient for a given suspension density (Basu and Cheng, 1996). Reddy and Basu (2001) considered two particle sizes (234 μm and 489 μm) and investigated the effect of pressure on heat transfer. As observed, both particle sizes demonstrated the dominating effect of system pressure on heat transfer coefficient. A direct effect of particle size is evident with short heat transfer surfaces, but is not significant with long surfaces similar to those used in commercial boilers (Basu and Nag, 1996). The type of particle used in various literatures with properties and size of experimental setup is shown in Table-2.2. In most of the hot bed studies [Basu and Nag (1987), Basu and Cheng (1996), Winaya and Basu (2001), Gupta and Nag (2002)], experiments were carried out at different pressures ranging from 1-6 bar, and temperature up to 1123 K. Heating was done by electrical resistance heaters and Inconal 600 was used as construction material to have good mechanical strength and resistance to corrosion characteristics. In case of cold bed study, Plexiglas [Kolar and Sundaresan (2002) and Gungor and Eskin (2007)] column are used as riser fabrication material.

Table-2.2 Lab scale setup geometries, material properties and operating parameters

Investigator (s)	Set up size (riser diameter / cross-section / and height)	Bed material	Properties of bed material			Operating parameters		
			Mean Particle size d mm	ρ kg/m^3	ρ_{bulk} kg/m^3	u_{mf} m/s	u_t m/s	ϕ_s
Basu and Nag (1987)	ID: 102 mm	Sand	0.227	2650	---	0.054	1.88	---
	H: 5500 m		0.087	2650	---	0.008	0.72	---
Basu and Chang (1996)	ID: 52.5 mm	Sand	0.232	2818	1400	0.27	2.56	0.66
	H: 2020 mm		0.507	2730	1422	0.043	1.29	0.62
Reddy and Basu (2001)	ID: 52.4 mm	Sand	0.234					
	H: 2020 mm					---		
Winaya and Basu (2001)	ID: 52.5 mm	Sand	0.245	2581	1291	0.054	1.87	---
	H: 2020 mm							
Gupta and Nag (2002)	ID: 37.5 mm	Sand	0.264			---		
	H: 1940 mm							
Kolar and Sundaresan (2002)	CS: 100 mm x 100 mm, H: 5500 mm	Sand	0.363			---		
Gungor and Eskin (2007)	ID: 50- 418 mm	Sand	0.067	1398	---	---	---	---
	H: 5000 mm		0.520	2620	---	---	---	---

2.3.3 Effect of superficial velocity on heat transfer

To operate the bed under a pre-determined superficial gas velocity, the suspension density could be changed by adjusting the loop-seal control valve. Experimental data show that the heat transfer coefficients at different superficial velocities are very close to each other. However, it is said that the situation may be different at high pressure and low suspension density. In such conditions the contribution of the gas phase will be more important and therefore, the effect of superficial gas velocity may become prominent. Except for a very dilute bed, the superficial gas velocity does not have any great influence on the heat transfer coefficient [Wu *et al.* (1987), and Ebert *et al.* (1993)]. It is a result of a relatively low contribution of the gas convection component. In some situations, the heat transfer coefficient at constant circulation rate even decreases with the increase of superficial velocity [Nag and Ali (1990), Mahalingam and Kolar (1991), and Ebert *et al.* (1993)] due to the resulting decrease in the suspension density. Divillo and Boyd (1994) observed a major effect of superficial velocity but a minor effect of suspension

density on the heat flux. Gupta and Nag (2002) found that the heat transfer coefficient increases with the increase in superficial velocity.

2.3.4 Effect of pressure on heat transfer

Gupta and Nag (2002) studied the bed to wall heat transfer behavior in a 37.5 mm ID and 1940 mm height PCFB riser and observed that the heat transfer coefficient is increasing with increasing operating pressure as well as increase in gas superficial velocity. The increase in gas density with increasing pressure is the primary reason for enhancement of the convective heat transfer. The thermal conductivity of the clusters also increases with the pressure, contributing further to an improved thermal contact between the clusters and wall. With the increase in pressure, bed voidage is increases in the bottom zone of the riser and decreases in the top zone and hence suspension density increases at the top zone. Shen *et al.* (1991) carried out test on a 6 m high and 80 mm ID tube PCFB cold test rig and suggested that with the increase in operating pressure, there is a tendency of shift from aggressive fluidization to dispersion fluidization, which may decrease solid concentration near the wall. This may result in opposite effect of pressure on the heat transfer. Reddy and Basu (2001) developed a heat transfer model to predict heat transfer in a pressurized circulating fluidized bed furnace. They found that with increase in pressure heat transfer coefficient is increasing as gas density and cluster thermal conductivity increases with pressure. They also observed that both minimum fluidization velocity and particle terminal velocity decreases with pressure. The model predictions are validated against the experimental data obtained from a PCFB riser of 52.4 mm in diameter and 2020 mm high and they have found the same observation as reported by Shen *et al.* (1991), Molerus (1993), and Wirth (1995). Basu and Nag, (1996), Nag and Gupta (1999), Noymer and Glicksman (1998), Wen and Miller (1961) developed heat transfer models independently to predict heat transfer coefficient. Among the developed models, the model developed by Reddy and Basu (2001) is found to be suitable for estimation of heat transfer coefficient in pressurized CFB. Gungor and Eskin (2007) developed a two dimensional model considering the hydrodynamic behavior of CFB to investigate the effect of superficial velocity on bed hydrodynamics. Gupta and Nag (2002) observed that the axial bed voidage along the height of the bed is lesser in the bottom zone and is higher in the top zone. Richtberg *et al.* (2005) conducted some experimental investigations in a 0.19 m diameter and 9 m high pilot scale PCFB unit in order to characterize the flow patterns in a PCFB. The obtained

information is used to develop an easy correlation for the prediction of internal solids reflux in a riser reactor as a function of solids/gas density ratios and the dimensionless superficial gas velocity. Wiman and Almstedt (1997) measured hydrodynamics, local tube erosion and local instantaneous bed-to-tube heat transfer experimentally in a cold pressurized fluidized bed, with two horizontal tube banks having different tube packing's. They observed that, an increased pressure causes a transition towards dispersedly bubbling, or turbulent, bed behavior and reduces the erosion significantly. Averaged heat transfer coefficient is reported to be higher for the sparse tube bank than for the dense tube bank. Puchner *et al.* (2009) studied the variation of bed material and operating parameter for a pressurized biomass fluidized bed process. Yates (1996) reviewed the effect of pressure and temperature on fluidized bed and emphasized that more effort needs to be devoted to CFB's as there are many gaps in understanding the flow regime that exist in these system. He also specifically pointed out the need for development of a mechanistic model in order to study the sintering and agglomeration in fluidized beds.

2.3.5 Effect of bed temperature on heat transfer

The overall heat transfer coefficient increases linearly with bed temperature due to increase in thermal conductivity of fluidizing gas and higher radiation at higher temperatures (Basu, 2006). The high temperature reduces the thermal resistance of the first layer of particles as well as that of rest of the clusters. Basu and Nag (1996) found that the heat transfer to the wall is proportional to bed temperature to the power of 1.5. The solid clusters sliding down the wall experience unsteady-state heat conduction to the wall. The clusters cool down while losing heat to the wall through conduction and radiation. Consequently, the effect of bed temperature on the total heat transfer is more pronounced in shorter heat transferring surfaces. The effect of bed temperature on heat transfer coefficient also studied in a 125 MW_e boiler and they have correlated their data in the following form (Basu *et al.*, 1999),

$$h = k \times (\Delta p)^{\alpha} \left(T_f\right)^{\beta} \tag{2.12}$$

where Δp is the pressure drop across the entire furnace (a measure of the suspension density), T_f is the temperature of the furnace and k, α, β are empirical constants.

Ali (1991) studied the temperature profile along the height of the riser in a hot atmospheric CFB unit of bed cross section 102 mm x 102 mm and height of 5.25 m. In case of pressurized bed, the

heat transfer coefficients, measured at 300 kPa, against bed suspension densities for two temperatures 750 °C and 250 °C (Basu, 2006). A higher bed temperature results in a higher heat transfer coefficient.

2.3.6 Effect of other operating parameters on heat transfer

Winaya and Basu (2001) studied the effect of CO_2 addition in PCFB. They found that the heat transfer coefficient increases with increase in both system pressure and bed temperature due to increased contribution of gas convection and radiation and volumetric concentration of CO_2 in the PCFB riser. They also observed that the moderate increase of heat transfer coefficient with limestone addition due to increase in CO_2 concentration through the calcinations of $CaCO_3$. Reddy and Basu (2002) investigated the effect of CO_2 concentration and system pressure on radiation heat transfer through a bed to wall heat transfer mechanistic model. As observed, the bed to wall radiation heat transfer increases slightly with system pressure and the variation in CO_2 concentration during combustion in the PCFB combustor does not influence the bed to wall radiation heat transfer coefficient significantly. Tsukada *et al.* (1994) studied the effect of pressure on transport velocity in a CFB and found that the core diameter at transport velocity is 80 % of the bed diameter and thickness of the annulus was slightly decreasing with the operating pressure. It is also reported that the fluidizing velocities are appreciably lower and heat transfer coefficient is significantly higher in PFBC than in atmospheric units. As the PCFB technology is new and the cost involved in conducting the experiments is high at high pressure hence the published literature related to experimental study is very less. Most of the work reported in literature is on the investigation heat transfer by using mathematical model. Some of the reported work in this direction in discussed in Table-2.3.

Although much work has been done on the investigation of bed voidage profile, solid circulation rate and heat transfer at varied system pressure both in bubbling and circulating fluidized bed, there is no specific information about the investigation of hydrodynamics and heat transfer characteristics at varied percentage mixing of biomass in sand has been reported.

Table-2.3 Effect of various operating parameters on heat transfer

Investigator (s)	Experimental variables	Observations
Basu and Nag (1987)	• Heat transfer coefficient was measured for different superficial velocities and solid circulation rates. • Effect of suspension density, superficial velocity, circulation rate, particle size, temperature on heat transfer coefficient was studied. • Model was validated experimentally.	• Heat transfer in a circulating fluidized bed combustor can be predicted by cluster renewal model. • Bed to wall heat transfer coefficient increases with increasing suspension density; but it decreases as fluidization velocity increases while keeping the recycle rate constant. • Within the present range of experimental conditions finer particles resulted in a higher heat transfer coefficient for a given suspension density. • A higher heat transfer at higher bed temperature is predicted by the cluster renewal model due to the effect of radiation as well as increased thermal conductivity of the gas film at elevated temperature.
Basu (1990)	• Heat transfer to the wall of a fast fluidized bed has been measured for 4 different particle sizes, two sizes of heat transfer probes and several temperatures from 30-900 °C.	• The local heat transfer coefficient is higher at the wall than at the centre of the bed.
Basu and Chang (1996)	• Studied the effect of pressure on heat transfer, bed suspension density, particle size and superficial velocity. • Pressure variation studied from 100 kPa to 600 kPa. • Result of cluster renewal model was validated by experiment. • The entire test rig was maintained in a temperature controlled electric furnace. • Two measuring devices were used to measure the pressure drop along the bed (i) a Dura block:~ Solid Plastic Stationary Gage; (ii) a Model 700D5"24V4 Pressure Transducer.	• Maximum fall velocity of cluster was found to be 1.26 m/s. • Most particles were separated in the primary cyclone and recycled to the bed through the standpipe and the loopseal. • The bed-to-wall convective heat transfer coefficient increases with increasing system pressures and bed suspension density but not with particle size. • The effect of superficial velocity on heat transfer coefficient was reported to be negligible.

Investigator (s)	Experimental variables	Observations
Yates (1996)	• Reviewed the effect of temperature and pressure on gas solid fluidization especially on Geldart A and B particles. • Heat transfer in both bubbling and circulating fluidized bed and scaling was also studied.	• With the increase in pressure, the enhanced bed-to-surface heat transfer coefficients in beds of Group A powders is due to the suppression of bubbles while in beds of Group B materials the enhancement is through an increase in the gas convective component of the heat transfer coefficient.
Basu and Nag (1996)	• Studied the heat transfer to the wall of CFB at atmospheric pressure. • Reviewed the hydrodynamics condition in furnace. • Studied the lab and commercial scale experimental observations. • Effect of operating parameters such as suspension density, bed temperature, fluidization velocity, particle size, vertical length of heat transfer surface was reviewed. • Mechanistic models of heat transfer were reviewed.	• Suspension density is the most significant factor influencing heat transfer in a CFB furnace. • Direct effect of particle size is evident with short heat transfer surfaces, but is not significant with long surfaces similar to those used in commercial boilers. • Heat transfer coefficient 100-200 W/m^2-K varies with suspension density. • Mechanistic models can be used prediction of heat transfer coefficient.
Winaya and Basu (2001)	• Effect of pressure and carbon dioxide concentration on bed to wall heat transfer in PCFB combustor. • Effect of superficial velocity (1, 3, 5 m/s) and Ca/S ratio (1.6, 2, 2.5, 3) was investigated. • Pressure and temperature was varied from 100 kPa to 600 kPa. • Heating of the setup was done by electrical means and maintained at 925-1125 K.	• Heat transfer coefficient increases with both system pressure and bed temperature due to increased contribution of gas convection and radiation. • Heat transfer coefficient increases with volumetric concentration of CO_2 in the PCFB riser. • Average bed densities at constant inventory are observed to be 11.1 kg/m^3 at 2 bar, 16.19 kg/m^3 at 4 bar and 19.21 kg/m^3 at 6 bar.
Reddy and Basu (2001)	• The model takes into account the effect of pressure on cluster density, cluster thermal conductivity and particle convection heat transfer coefficient. • Effect of pressure, temperature and hydrodynamic parameters on bed-to-wall heat transfer coefficient was investigated. • Pressure and temperature was varied from 100 kPa to 600 kPa and 350-650 °C, respectively.	• Heat transfer coefficient increases with system pressure. • The increase in suspension density results in increase in heat transfer coefficient. • Heat transfer coefficient increase with bed temperature.

Investigator (s)	Experimental variables	Observations
Gupta and Nag (2002)	• Effect of pressure and other relevant operating parameters were investigated experimentally. • Superficial velocities were varied from: 0.25-1.25 m/s. • Bed inventories considered are 1, 1.25 and 1.5 kg. • Pressure variation studied from 2 to 6 bar.	• The axial bed voidage along the height of the bed is observed to be less in the bottom zone and is high in the top zone. It is also observed that the bed voidage increases in the bottom zone and decreases in the top zone with increase in operating pressure. • The heat transfer coefficient is found to be increasing with the increase in operating pressure as well as increase in gas superficial velocity. Also increases monotonically with the increase in bed temperature
Kolar and Sundaresan (2002)	• Studied the heat transfer characteristics at an axial copper tube of 6.9 mm OD and 0.6 m height in a CFB riser. • Tube was located axially at distances of 0.97 m, 1.62 m, 3.0 m and 4.0 m from the distributor plate. • Fluidizing air velocity varied from 4.5 – 7.3 m/s. • Solid circulation flux varied from 21 to 72 $kg.m^{-2}\ s^{-1}$.	• Heat transfer coefficient varied from 58-101 W/m^2-K and showed a decrease trend from the riser bottom to the riser exit. • Heat transfer coefficient decreases with increase of fluidizing velocity and increases with suspension density. • Suspension density is not an independent parameter but a derived one depend upon the combination of particle size, fluidizing velocity and the solids recycle rate for a given bed material, bed geometry and the bed holdup.
Reddy and Basu (2002)	• Effect of CO_2 concentration and system pressure on radiation heat transfer was investigated by using a mechanistic model. • Pressure variation studied from 100 kPa to 600 kPa. • The entire test rig was maintained at a constant temperature of 1123 K.	• For the CO_2 released during combustion in the PCFB combustor, the gas partial pressure increases. • The bed to wall radiation heat transfer increases slightly with system pressure. • The variation in CO_2 concentration during combustion in the PCFB combustor does not influence the bed to wall radiation heat transfer coefficient significantly.

2.3.7 Mechanistic model for prediction of heat transfer coefficient

Various models have been developed in order to predict the heat transfer coefficient for design of CFB unit. Some of the works related to the development of models for prediction of heat transfer coefficient are discussed in the following paragraphs.

Based on the experimental investigation of Mickley and Trilling (1949), Wen and Miller (1961), Kiang *et al.* (1976), and Fraley *et al.* (1983), the data computed from the theoretical model proposed by Grace (1986) summarized that the bed density has a major influence on the heat transfer. This inference Subbarao and Basu (1986) and subsequently suggested a theoretical model of heat transfer based on the packet theory of Mickley and Fairbanks (1955).

Basu and Nag (1987) have proposed a model to predict the heat transfer in a circulating fluidized bed. To verify the model, experiments were conducted in a 102 mm diameter and 5.5 m high Plexiglas column, in which the heat transfer coefficient was measured for different superficial velocities, solid circulation rates and at two particle sizes. The bed to wall heat transfer was measured by a carbon steel probe (length 100 mm and diameter 50 mm), flushed with the wall and installed at 2.1 m above the distributor plate. Four iron constantan thermocouples were installed at uniform intervals of 20 mm along its length for temperature measurement. It was insulated against any heat loss so as to achieve one-dimensional heat conduction and thereby a linear temperature variation along the centre line. One face of the probe was flush with the bed wall, while the other face was in contact with a chamber through which boiling water from a constant head water tank was circulated. The bed temperature was measured by other sets of thermocouple and finally calculated the heat transfer coefficient. The local voidage was estimated by measuring the pressure drop across the probe.

Basu *et al.* (1996) proposed a mechanistic model by modifying their earlier model for CFB (Basu *et al.* 1990). This model does not account for the effect of system pressure on parameters like fractional wall coverage by clusters, cluster solid fraction and on cluster and particle convection heat transfer coefficients. The effect of gas gap thickness between cluster and heat transfer surface is also not accounted by Basu *et al.* (1996). Nag and Gupta (1999) proposed a heat transfer model for pressurized CFB unit, the effect of gas density and cross-

sectional average volumetric solids concentration on cluster and particle heat transfer coefficients are not considered. Also, they did not use the available information on cluster velocity and residence time. Noymer and Glickmsman (1998), Nag and Gupta used the correlation of Wen and Miller (1961) to estimate gas convection heat transfer from bed to the heat transfer surface without accounting for the effect of system pressure and gas density on gas convection heat transfer coefficient.

Shi *et al.* (1998) performed series of experiments in a semi-industrial scale CFB unit at ambient temperatures to investigate wall-to-bed heat transfer coefficients, for different solids like FCC, glass beads and at different velocities. Their experiments have been shown a significant influence of solids concentration and solids movement near the heat transfer surface on the wall-to-bed heat transfer coefficient. They proposed a model to describe the wall-to-bed heat transfer that is applicable over the entire range of possible local solid concentrations occurring in CFB systems.

Reddy and Basu (2001) developed a mechanistic model based on the cluster renewal approach to predict bed to wall heat transfer coefficient in a pressurized CFB furnace. Experiments were carried out in a CFB unit of riser ID 52.4 mm and a height of 2020 mm. They have concluded that the proposed model can adequately explain the heat transfer behaviour of a PCFB once the effect of system pressure on thermophysical properties and the cluster residence time was accounted. Experiments were carried out to validate the model predictions of the effect of system pressure and bed temperature on particle, gas and total heat transfer coefficients and found that the model predictions were in good agreement with experimental data of own experiment and other investigators.

2.3.8 Enhancement of heat transfer coefficient

If the area of the furnace wall can be increased through the use of fins projecting into the furnace, it may be possible to provide a much greater heat absorption in the furnace wall (Basu *et al.*, 1999). This may allow the boiler furnace to be more compact or even less tall. A typical fin arrangement is shown in the Fig.2.4.

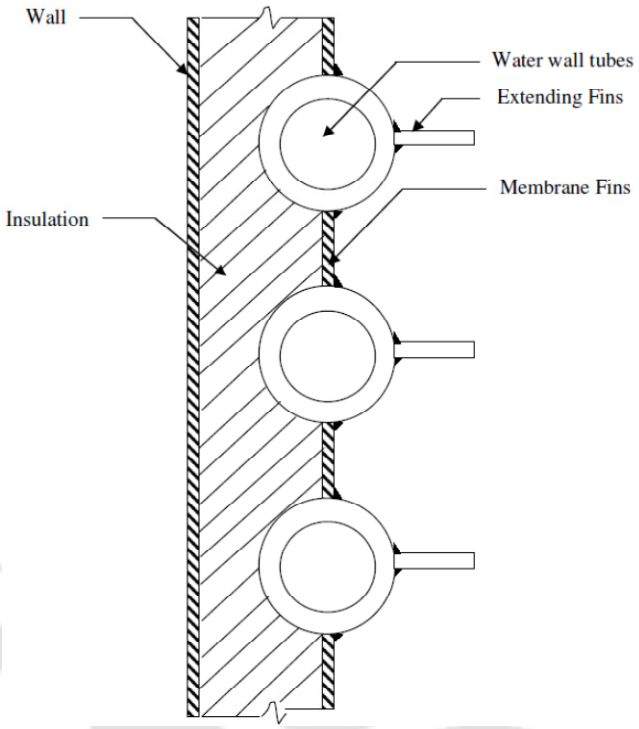

Fig.2.4 Typical of fin arrangement (Basu, 2006)

Ali (1991) studied the bed-to-wall heat transfer in a hot CFB unit of bed cross section 102 mm x 102 mm and height of 5.25 m and also investigated the effects fins of rectangular and pin shapes on heat transfer under different operating conditions. He had used LPG for heating the CFB unit. He also developed a theoretical model to predict the heat transfer coefficient under the similar operating conditions and compared the results. As reviewed by Basu and Nag (1996) heat transfer from bed to wall has been investigated by a number of researchers [Basu and Cheng (2000), Reddy and Nag (1998), Lockhart *et al.* (1995), Molerus (1993), Nag *et al.* (1995), Basu and Ngo (1993)]. Most of the researches were conducted experiment on conventional membrane tubes, and few studies were found to enhance the heat transfer coefficient by using membrane tubes with longitudinal fins on the tube crest [Basu and Ngo (1993), Reddy and Nag (1998), Basu and Cheng (1996)]. Chinsuwan and Dutta (2009) studied heat transfer for the membrane tube with two longitudinal fins and the comparison of heat transfer behaviors between longitudinal finned tubes and membrane tubes in a cold model riser of cross-section 100 mm x 100 mm and height 4.8 m. They compared the performance of different configuration at a superficial velocity of 8 m/s at bed temperature of 75 °C. The use of passive heat transfer mechanism at the upper splash region of the CFB riser was not found in the open literature.

2.4 Review on biomass feeding system

Feeding of loose biomass into the CFB reactor is one of the critical operations. Difficulties in feeding of loose biomass often impede smooth operation. The biomass properties such as particle size, size distribution, shape, particle surface (e.g., smooth, rough or sharp edges), density, moisture content, compressibility and other fuel properties (e.g., strength of large particles, consolidation over time) can all affect the ability to feed the material [Dai and Grace (2008), and Zhang *et al.* (2011)]. Several kinds of feeders and their combinations have been reported, in particular hopper or lock hopper systems, screw feeders, rotary valves, piston feeders and pneumatic feeders. For continuous operations they can also be combined rather than be separate. These feeders have been developed for a variety of solids, but they have limitations in handling certain types of biomass and/or in feeding to pressurized reactors. Biomass screw feeders operate in a manner similar to piston feeders, but have a somewhat lower pressurization range (0.5 MPa). Hopper–screw feeders are widely used in biomass energy processes. The flow patterns developed by screw feeders connected to hoppers have been studied extensively and discussed by Dai and Grace (2008). Dai and Grace (2008) developed a model for biomass screw feeding for the torque requirement of a screw feeder by considering the bulk solid mechanics of a material element within a pocket. Screw or piston operated plug feeders, common in feeding coal, have also been tested with biomass [Carl and Aimo (1993), Cummera and Brown (2002), Drift *et al.* (2004), Karel *et al.* (2009), Zhao *et al.* (2010), Zhang *et al.* (2011)]. Lack of flow is a common and serious solids handling problem. Flow stoppage may be caused by a bridge or "rathole" in the hopper, or by blockage or slippage in the screw itself. The various aspect such as flow mechanics, design, and the flow patterns developed by screw feeders coupled to a hopper have been studied extensively by various investigators [Carl and Aimo (1993), Cummera and Brown (2002), Drift *et al.* (2004), Dai and Grace (2008), Karel *et al.* (2009), Qin and Li (2010), Zhao *et al.* (2010), Zhang *et al.* (2011)]. Zhang *et al.* (2011) developed an automatic shake mechanism in a screw feeder hoper in order to provide continuous flow of sawdust which removes the bridge formation problem. Li *et al.* (2002) mentioned that, the amount of biomass like rice husk required to generate 1kW-hr of energy is about 2.2 kg. Although, much work has been done on various type of hoppers and its modifications, all the work attributed to industrial scale where energy consumption is very high. Therefore, there is urgent need of development of an energy efficient biomass feeding system for lab scale pressurized CFB unit. The study

and evaluation of the working range of biomass particle size, and its hydrodynamic behaviour at different velocities is also very important for characterization of the feeding system.

2.5 Review on reaction kinetics and thermal analysis

The knowledge of properties and behaviour of biomass with time and temperature in a CFB reactor is very essential for designing an efficient gasification unit. The design of fluidized bed reactor requires understanding of reaction chemistry such as reaction kinetics, conversion or yield, thermodynamics and process parameters (e.g. operating temperature and pressure as well as heat of reaction) which affects the reaction. The effective heat and mass transfer properties of fluidized beds provide the possibility of using various types of biomass wastes with different compositions and heating values (Yassin *et al.*, 2009). Table 2.4 depicts the ultimate and proximate analysis of various lignocellulosic biomass.

Table-2.4 The proximate and ultimate analysis of various lignocellulosic biomass

Biomass type	Ultimate analysis (db, % w/w)					Proximate analysis (% w/w)				LHV
	C	H	O	N	S	ASH	VM	FC	M	(MJ/kg)
Wood sawdust (Cao *et al.*, 2006)	46.2	5.1	35.4	1.5	0.06	1.3	70.4	17.9	10.4	18.81
Rice husk (Ve´lez et al., 2009)	45.8	6.0	47.9	0.3	---	0.8	73.8	13.1	12.3	13.36
Rice straw (Li *et al.*, 2009)	38.61	4.28	37.16	1.08	0.65	12.64	65.23	16.55	5.58	14.40
Pine sawdust (Lv *et al.*, 2004)	50.54	7.08	41.11	0.15	0.57	0.55	82.29	17.16	DB	20.54
Spruce wood pellet (Miccio *et al.*, 2009)	49.30	5.9	44.4	0.1	---	0.3	74.2	17.1	8.4	18.5
Coffee husk (Ve´lez *et al.*, 2009)	46.80	4.9	47.1	0.6	0.6	1.0	74.3	14.3	10.4	16.54
Jute stick (Asadullah *et al.*, 2004)	49.79	6.02	41.37	0.19	0.05	0.62	76-78	21.4-23.4	DB	19.66
Sugar cane bagasse (Asadullah *et al.*, 2004)	48.58	5.97	38.94	0.2	0.05	1.26	67-70	28.74-30.74	DB	19.05
Wheat straw (Oesch, 1996)	46.1	5.6	41.7	0.5	0.08	6.1	75.8	18.1		17.20
Cotton stem (Guo *et al.*, 2001)	42.8	5.3	38.5	1.0	0.2	4.3	72.3	15.5	7.9	15.20
Straw (Shen *et al.*, 2008)	36.57	4.91	40.7	0.57	0.14	8.61	64.98	17.91	8.5	14.60
Camphor wood (Zhou *et al.*, 2009)	43.43	4.84	38.53	0.32	0.1	0.49	72.47	14.75	12.29	17.48
Beech wood (Radmanesh *et al.*, 2006)	48.27	6.36	45.2	0.14	---	0.8	81	18	DB	19.20

VM: Volatile matter, FC: Fixed Carbon, M: Moisture, DB:Dry basis

Thermal analysis has been widely used in pyrolysis research [Suneerat *et al.* (2004), Niksa and Lau (1993), Lazaro *et al.* (1998), Cucoci *et al.* (2009), Sommariva *et al.* (2009)]. Thermogravimetric analysis (TGA), differential thermal analysis (DTA), differential

scanning calorimetry (DSC) or a combination of the same is used for the pyrolysis of the biomass containing cellulose, hemicelluloses and lignin [Sommariva *et al.* (2009), Alèn *et al.*(1996), Mansaray and Ghaly (1999)]. As reported [Kaupp (1984), Boateng *et al.* (1992), Bridgwater (1995), Mansaray and Ghaly (1997)] wide variation of experimental conditions such as rate of heating, medium of heating etc. have been applied in TGA.

Suneerat *et al.* (2004) developed a two-stage pyrolysis model with consideration of (a) single, irreversible, first order processes and (b) multiple parallel, independent, irreversible, first-order reactions with a Gaussian distribution of activation energies. Both the models were based on the assumption that pyrolysis reaction consists of two stages. Result of their investigation suggests that the values calculated using the multiple reaction models are more realistic than those calculated with the single-reaction model.

Niksa and Lau (1993) had reported significant influence of the pre-exponential factors with variation of heating rates. They observed an increase of pre-exponential factor by six for every order of magnitude increase in heating rate. Affect of activation energy on heating rate was reported by them to be insignificant. However, Lazaro *et al.* (1998) had reported increase in activation energy with increase in temperature leading to higher gas yield for high rank coals.

Cuoci *et al.* (2009) developed a mathematical model for design and operation of gasification and combustion unit for solid fuels and waste such as coal, biomass, plastic and refused derived fuel.

Sommariva *et al.* (2090) developed a multistep kinetic model which gives the detail information on the residual char as well as on the speciation of released gas and tar component.

Open flame combustion of ligno-cellulosic fuels occurs when the volatile gaseous products from the thermal degradation ignite in the surrounding air. The heat released from combustion causes the ignition of adjacent unburned fuel. Thus the analysis of the thermal degradation of ligno-cellulosic fuels is decisive for fire modeling as well as fuel hazard studies [Sommariva *et al.* (2009), Alèn *et al.* (1996), Balbi (1999)].

As reported in [Bining and Jenkins (1992), Ergudenler and Ghaly (1992), Koufopanos *et al.* (1989), Shamsuddin and Williams (1992), Williams and Besler (1994), Varhegyi (1994), Cozzani (1997)] the heating rate, the type of biomass tested and the atmosphere in which thermal degradation takes place, have significant effects on the thermal degradation rates and therefore the activation energies. It is also observed that the researcher assumed first order reactions [Bining and Jenkins (1992), Koufopanos *et al.* (1989), Cozzani (1997), Nasser (1985), Agrawal (1988), Teng *et al.* (1997)] in most of the kinetic studies. Ramiah (1970) has also reported the evaluation of kinetic parameters for thermal decomposition of cellulose with the assumption that the decomposition follows a first order mechanism. Antal *et al.* (1995) has reported the evaluation of energy of activation and pre-exponential factor assuming first order mechanism. Duvvuri *et al.* (1975) and Bingyan *et al.* (1992) reported order of reactions in the range of 1.2-1.4 for cellulose and 0.6-0.8 for wood, respectively. Hornof *et al.*, (1977) studied the effect of lignin content on the thermal degradation of wood pulp and found that the reactions above 330 °C are mostly dominated by the decomposition of lignin, which is the case in the second reaction zone. They also observed significant decrease in the degradation rate and activation energy with increasing lignin content above 330 °C. The thermal degradation characteristics of lignocellulose materials are strongly influenced by their chemical composition (cellulose, hemicellulose and lignin contents) [Antal *et al.* (1995), Liou *et al.* (1997), Qu *et al.* (2011)]. Although the thermal degradation of some lignocellulose materials such as wood and their components have been studied extensively, the exact mechanism and kinetics of the reactions occurring are not yet completely clear. As reported by various authors [Bining and Jenkins (1992), Ergudenler and Ghaly (1992), Antal *et al.* (1995)] the large variations of biomass characteristics is mostly due to the differences in the methods, heating rate and atmosphere used as well as differences in the chemical compositions. Therefore, in order to provide reliable kinetic data, it is necessary to conduct extensive thermogravimetric analysis under conditions resembling to those encountered in combustion and/or gasification situations.

Sharma *et al.* (2006) focused on modelling of volatile composition. There are large numbers of other papers on modelling of pyroysis which focus mainly on the rate of evaluation of volatiles during pyrolysis [Gronli and Melaaen (2000), Zaror and Pyle (1982), Srivastava *et al.* (1996), Larfeldt *et al.* (2000), Di (1993), Green *et al.* (1997), Simmons and Lee (1985), Di (1998)]. Di (1998) presented a comparative evaluation of various mechanisms that exist for kinetics of pyrolysis and also emphasized the need of mathematical models for optimal design and

operation of industrial units of gasification processes. The first mathematical model to predict the thermal response of a decomposing material was proposed by Bamford *et al.* (1946) which consist of the 1D transient heat conduction equation with an additional term associated with the thermal decomposition. In this model, constant thermal properties and first order decomposition reaction were assumed. In the model developed by Panton and Rittmann (1969) variable thermal and physical properties were considered during decomposition. Later, Kanury (1969) and Munson and Spindler (1961) proposed models which not only accounted for the variable properties of the material, but included the effects of gas flow through the char structure and the temperature dependent heat of gasification. All of these models utilized a first order kinetic rate equation to calculate the material decomposition resulting from pyrolysis reactions. Buragohaign *et al.* (2010) developed a model in order to investigate the product gas composition and heating value at various operating parameters. Sheth *et al.* (2010) developed a combined transport and kinetic model in order to design pyrolysis/gasification reactor by considering kinetics of chemical reactions, transport of volatiles produced, heat and mass transfer between solid and gaseous phase and pyrolysis reaction. No literature has been reported on investigation of transient temperature variation during decomposition of biomass like rice husk, sawdust etc.

Mansaray and Ghaly (1999) determine the kinetic parameters (activation energy, pre-exponential factor and order of reaction) of rice husks in oxygen atmosphere using thermogravimetric analysis. For determination of kinetic parameters from TGA data, they have used the following rate expression,

$$\frac{dX}{dt} = -Ae^{-\left(\frac{E}{RT}\right)}X^n \tag{2.13}$$

Kalita (2009) studied the thermogravimetric (TG) analysis followed by the study of the DTG curves of various lingo-cellulosic materials. A sample TG and DTG curve of the sawdust at a heating rate of 10 $^{\circ}$C min^{-1} are shown in Figs.2.5 and 2.6.

The predicted thermogravimetric curve of sawdust is in good agreement with the experimental curves in the both first and second reaction zone (Figs.2.7). They have also investigated the average variation of predicted and experimental results at the end of the reaction and it was reported to be 0.5 %.

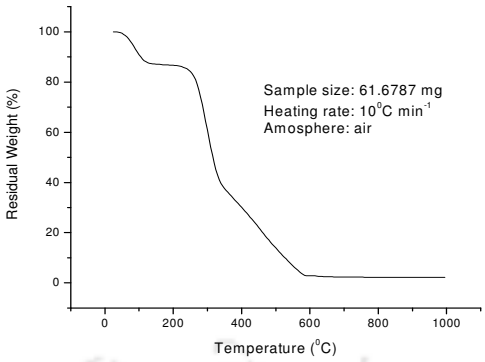

Fig.2.5 TG curves of sawdust (Kalita, 2009)

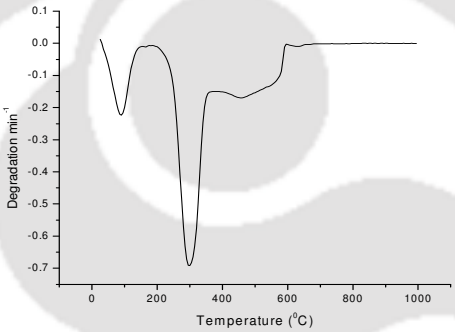

Fig.2.6 DTG curves of sawdust (Kalita, 2009)

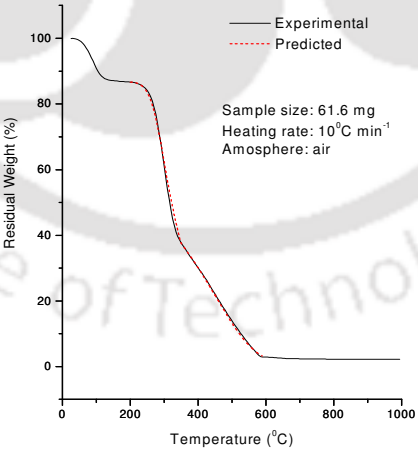

Fig.2.7 Predicted and experimental results for sawdust (Kalita, 2009)

Various efforts have been made to convert low density biomasses into higher value fuels through combustion and/or gasification processes [Mansaray and Ghaly (1999), Kaupp (1984),

Boateng *et al.* (1992), Bridgwater (1995), Mansaray and Ghaly (1997)]. Even though much work has been done on the evaluation of kinetic parameters at different heating rates, very limited information is available on the study on thermal response of biomass while heating. Further, the development of technically and economically feasible systems for the conversion of low density biomass to energy by thermo chemical conversion processes requires a fundamental understanding of its thermal properties and reaction kinetics. Moreover, effect of various operating parameters on the CFB gasifier performance is also requires extensive study.

2.6 Review on various parameters influencing the performance of biomass gasification

Biomass gasification is a versatile thermochemical conversion process which produces a gas mixture of CH_4, CO and H_2, the proportions being determined by the use of air, oxygen or steam as the gasification medium, with a concomitant range of calorific values (CVs), low (4–6 MJ/m^3), medium (12–18 MJ/m^3) and high (40 MJ/m^3). The various factors such as biomass composition, equivalence ratio, operating temperature and pressure, suspension density, gasifying agent, bed material etc. influencing the performance of a CFB gasifier. This has been reviewed in the following subsections along with the thermochemical processes involved in the gasification, product of gasification and challenges in mixing of biomass and coal (due to fibre nature of biomass and the large difference in gasification temperature). Co-gasification of coal with various types of biomass blend improves the biomass gasification by reducing the tar content in the product gas. Besides, the ash presents in biomass catalyses the gasification of coal.

2.6.1 Gasification processes

Gasification takes place at high temperature (500-1000°C) in the presence of a gasifying agent such as air, oxygen, steam, nitrogen, carbon dioxide or combination of these. Heat is supplied to the gasifier either directly or indirectly. In the presence of an oxidizing agent or gasifying agent at high temperature, the large polymeric molecule of biomass decompose into lighter molecules and finally, producesgases like CO, H_2, CH_4 and lighter hydrocarbons, ash, char, tar and minor contaminants. Char and tar are the result of incomplete conversion of biomass. The main chemical reactions that occur in the gasifier are summarized below:

$$CH_xO_y(\text{Biomass}) + O_2(21\%\ \text{of air}) + H_2O(\text{steam}) \\ = CH_4 + CO + CO_2 + H_2 + H_2O(\text{unreacted steam}) + C(\text{char}) + \text{tar} \quad (2.14)$$

Oxidation: $C + O_2 \leftrightarrow CO_2,\ \Delta H = +408.8$ kJ/mol (2.15)

Partial oxidation: $2C + O_2 \leftrightarrow 2CO, \Delta H = +246.4$ kJ/mol (2.16)

Steam forming: $CH_4 + H_2O \leftrightarrow CO_2 + 3H_2, \Delta H = -206$ kJ/mol (2.17)

$CH_4 + 2H_2O \leftrightarrow CO_2 + 4H_2, \Delta H = -165$ kJ/mol

Water-gas: $C + H_2O \leftrightarrow CO + H_2, \Delta H = -131$ kJ/mol (2.18)

Boudourd: $C + CO_2 \leftrightarrow 2CO, \Delta H = -172$ kJ/mol (2.19)

Water-gas shift reaction: $CO + H_2O \leftrightarrow CO_2 + H_2,\ \Delta H = -41.98$ kJ/mol (2.20)

$C + 2H_2O \leftrightarrow CO_2 + 2H_2, \Delta H = +100$ kJ/mol (2.21)

Equation (2.14) represents the overall reaction in an air and/or steam gasifier, which proceeds with multiple reactions and pathways. Equations 2.15 through 2.21 are the usual reactions involved during gasification. Equations 2.17 through 2.20 occur when steam is available during gasification. Many researchers [Kalita (2009), Mansaray and Ghaly (1997)] have studied the degradation kinetics of various biomass feedstocks (rice husk, sawdust, bamboo dust, pine chips, wheat straw, rapseed straw, pigeon pea stalk, etc.) using thermogravimetric analyses (TGA). TGA provides the weight loss of any material with change in temperature at different heating rates. The weight loss (or thermal degradation) in a nitrogen atmosphere occurred in mainly three stages; with the first stage being dehydration (below 125 °C), the second stage being active pyrolysis (125–500 °C) and the third stage being passive pyrolysis above 500 °C. The dehydration reflects loss of water, the active pyrolysis reflects the loss of the hemicellulose, cellulose and part of lignin, and the passive pyrolysis reflects the slow and continuous loss of residual lignin. The temperature ranges of these stages and the kinetic parameters of the degradations depend primarily on the rate of heat transfer, the composition of the biomass, and the degree of the oxidizing environment [Kalita (2009), Mansaray and Ghaly (1997), Kumar *et al.* (2008), Varhegyi *et al.* (1997), Biagini *et al.* (2006)].

2.6.2 Gasification types

Depending on the type of bed and flow, the gasifier may be classified into two categories such as fixed bed and fluidized bed. Fixed bed gasifiers (updraft and downdraft) constitute first generation of commercial gasifiers. The major advantage of this design was its simplicity and flexibility to handle variety of feedstock, high carbon conversion and low exit gas

temperature. High tar yield and gas channelling leading to oxygen breakthrough and dangerous situations were the major drawbacks. Fluidized bed processes have advantages of excellent gas-solid mixing and uniform temperature within the bed. Presence of dense suspension provides a large thermal inventory for flash pyrolysis of solid fuel particles. In CFB reactors, a cyclone or other type of separator is used for solid capture and recycle in order to extend the solid residence time in the reaction zone. CFB gasifiers operate in either turbulent fluidization or fast fluidization regime. These features not only improve carbon conversion but also reduce tar yields. Kumabe *et al.* (2007) used a down-draft gasifier for gasification of Japanese cedar and Mulia coal and Kezhong *et al.* (2010) used a fluidized bed reactor for gasification of bituminous coal with pine dust and rice straw. Temperature variation among reactors can cause different compositions of syngas. Vélez *et al.* (2009) gasified mixtures of biomass (sawdust, rice husk, and coffee husk) and coal in a fluidized bed gasifier at 1000 °C and observed two operational problems. The first problem was de-fluidization of the fluidized bed gasifier caused due to agglomeration of low melting point ash present in the biomass. The second problem was clogging of the downstream pipes due to excessive tar accumulation. Collot *et al.* (1999) studied co-gasification and co-pyrolysis of birch wood and coal in a fixed bed, as well as fluidized bed gasifiers. They observed a major difference in tar content of product gas between fixed bed and fluidized bed reactors. Tar content was found to be 4.0 to 6.0 % (by weight) in fluidized bed reactor whereas in the case of fixed bed reactortar yields ranging from 25.5 to 26.1 % (by weight) for co-gasification of coal and silver birch wood mixtures (1:1 ratio by wt) at 1000 °C temperature, 20 bar pressure, and 60 second holding time.

2.6.3 Gasification in circulating fluidized beds

The high stream velocity and recirculation in CFBs provide appropriate mixing and contact time which boosts the heat and mass transfer characteristics within the gasifier. As a result, a suitable environment is created for gasification and the quality of the producer gas is improved [Basu (2006), Natarajan (1998)]. Another advantage of CFB over BFB is the prolonged catalytic activity. In BFBs, fouling which is caused by deposition of carbon on the catalyst surface causes a rapid loss of catalytic activity. The prolonged catalytic activity would eliminate deposition of carbon on the catalyst surface of CFBs. This is due to the burning of deposited carbon in the circulation process. Besides, the circulation of the bed

materials which acts as a heat carrier compensates the heat consumed in the endothermic reactions involved in gasification process [Shen *et al.* (2008), and Corella *et al.* (2007)]. Numerous approaches have been found in the literature on simulation and modeling of CFBs that aim at the optimization of the operating parameters as well as their design and scale-up [Murakami *et al.* (2007), Xiao *et al.* (2010), Pfeifer *et al.* (2009), Corella *et al.* (2007), Kaushal *et al.* (2008), Corella *et al.* (2005), Sanz *et al.* (2006), Doherty *et al.* (2008), Nikoo *et al.* (2008), Sadaka *et al.* (2002)].

Bingyan *et al.* (1994) studied the effect of ER on the composition of the producer gas in an atmospheric CFB gasifier of bed internal diameter 410 mm and height of 410 mm. They used air as gasifying media and wood powder as feed which was maintained at 210 kg/h. The bed temperature and equivalence ratio was varied from 650-1042 °C and 0.17-0.28, respectively. Their experiments revealed, an optimum value of ER (= 0.25) and bed temperature (= 974 °C) at which the % gas composition (CO: 16.7; H_2: 16.32; CO_2: 15.6; CH_4: 6.9; N_2: 43.25; C_nH_m: 1.0) and lower hearing value (= 7.2 MJ/m^3) becomes maximum.

The effects of bed temperature and catalyst on the composition and heating value of the producer gas was investigated by Li *et al.* (2002) in an atmospheric CFB gasifier run on sawdust of bed ID: 0.1 m and height of 6.5 m. Experiments were carried out at by varying the bed temperature from 700 to 850 °C at a constant feeding rate of 41 kg/hr and they have found that bed temperature of 800 °C was optimum at which % gas composition (CO: 17.9; H_2: 7.3; CO_2: 16.3; CH_4: 3.2; N2: 55.4) and LHV (4.6 MJ/m^3) maximum. They have also measured tar yield and carbon conversion and found to be 2.35 g/m^3 and 94.9 %, respectively.

Zhou *et al.* (2009) investigated the effect of ER and fluidization velocity in an internal circulating fluidized bed gasifier in which rice husk and sawdust were used as feedstock and air was used as fluidizing media. The ER of rice husk and sawdust was maintained in the range of 0.22-0.26 and 0.17-0.24, respectively. The lower heating value of rice husk and sawdust was found to be 5 and 6.5 MJ/m^3 at the ER of 0.28 and 0.25, respectively.

Drift *et al.* (2001) evaluated the performance of the CFB gasifier using several feedstock under air atmosphere. Experiments were performed at a constant ER of 0.37 and bed temperature of 800-860 °C and reported 92 % carbon conversion and heavy tars of 270 mg/m^3.

Hallgren *et al.* (1993) studied the influences of various fluidization velocities on the total gas production and fuel/air consumption in a PCFB unit of riser dia 40.9 mm and height of 3 meter (Fig. 2.8). They conducted experiments at 950 ºC and at the pressure interval of 0.4-2.0 MPa.

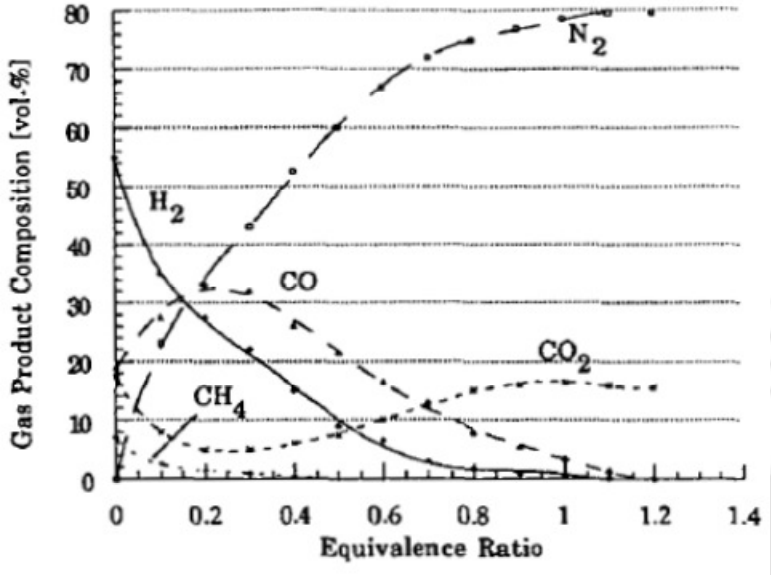

Fig.2.8 Gas product composition for adiabatic air/biomass conversion versus the air to fuel ratio at 0.1 MPa Hallgren *et al.* (1993)

Buragohain *et al.* (2013) mentioned two approaches of modelling of gasification process to estimate the quality and quantity of gas produced from biomass gasification unit. The first approach is based on kinetics where kinetics of the gasification reactions is taken into account with proper frequency factor, activation energy and order of reaction. The second approach is based on thermodynamic equilibrium where different algorithms are used to estimate the composition of producer gas obtained from biomass gasification under equilibrium conditions.

Liu and Gibbs (2003) have given following expression for the devolatilization time (in second) of biomass particles: $t_d = \frac{27.443 \times d_p^{1.662}}{(T-613)^{0.508}}$ where d_p is the biomass particle size in mm, and T is the temperature in K.

Wu *et al.* (2009) reported the performance analysis of a 1-MW-scale biomass gasification and electric power generation system and evaluated the optimal operating parameters when wood

powder was used as feed under air environment. The optimum parameters were T = 780 °C, ER = 0.26, for a safe, continuous, and steady production of fuel gas with LHV = 5.8 MJ/m^3. They also observed that, the fluctuation of pressure inside the gasifier found to decrease with the use of sand bed.

Buragohain *et al.* (2013) extensively studied the comparative evaluation of kinetic, equilibrium and semi-equilibrium models for biomass gasification process and demonstrated that the kinetic models could provide a more realistic picture.

2.6.4 Effect of operating parameters on gasification

There are various factors which influence the co-gasification process and the composition of the product gas. These factors include properties and types of biomass, types of gasifier, gasification temperature, flow rates of coal-biomass mixtures and oxidizing agents (air and/or steam), type and amount of catalysts, and proportion of biomass in the coal-biomass mixture, and the properties and type of biomass [Kumabe *et al.* (2007), Kezhong *et al.* (2010), and Pinto *et al.* (2003)]. In the following subsections some of the important parameters are discussed.

2.6.4.1 Type of biomass and feeding

Ligno-cellulosic biomass is mainly composed of several chemical constituents such as cellulose and hemicellulose (60-80 % dry basis), lignin (10-25 %), and some extractives and minerals (Kalita *et al.*, 2009). This biomass differs greatly in their physical, chemical and morphological properties which affect the characteristics of the gasification process (Moilanen, 2009). Besides, the choice of a biomass significantly depends on its heating value (Nemtsov and Zabaniotou, 2008). Biomass wastes with high heating value contribute to more energy recovery and better system performance in terms of efficiency and economy. However, effective heat and mass transfer properties of fluidized beds provide the possibility of using various types of biomass wastes with different compositions and heating values (Yassin *et al.*, 2009).

The study of co-firing of biomass with coal has been reported [Corella *et al.* (2004), Kumabe *et al.* (2007), Skoulou *et al.* (2008), Vélez *et al.* (2009), Kezhong *et al.* (2010)]. Kezhong *et al.* (2010) used pine sawdust and rice straw, along with coal and studied the gas composition

at different blending ratios. They have observed that, when 20% of each biomass (oven dried for 20 hours at 90 ^{o}C) with 80 % coal was gasified, H_2 composition in syngas gas increased from 17.66 % for pine sawdust to that of 21.96 % for rice straw. Three different types of biomass viz., rice husk, sawdust and coffee husk were used by Vélez *et al.* (2009) in their experiment and found that a mixture of 6 % of coffee husk with sub-bituminous coal produced 14 %, 8 % and 8.2 % of H_2, CO_2 and CO, respectively. A mixture of sawdust with coal produced syngas composition of 10.7 %, 10 % and 11.8 % H_2, CO_2 and CO, respectively and a mixture of coal and 6 % of rice husk produced syngas composition containing 11.4 % of H_2, 9.3 % of CO_2 and 6.0 % of CO. These results suggest that the type of biomass selected during the co-gasification influences the product gas composition.

Pan *et al.* (2000) reported that, besides proportion of biomass, co-gasification also depends on the type of coal used in the mixtures. In the study conducted by Vélez *et al.* (2009) the mixtures of 6 and 15 % raw biomass (sawdust, rice husk, and coffee husk) with sub-bituminous coal, were gasified in preheated steam and air. The authors found that the high proportion of biomass in the mixture increased hydrogen content in the product gas (up to 15 %) but significantly decreased the energy efficiency of the process. In a fluidized bed co-gasification of pine wood, two types of coals (low-grade coal and refuse coal) was studied by Pan *et al.* (2000). It has been reported that a minimum of 20 % pine chip (by weight) for the low grade coal and 40 % pine chip (by weight) for the refuse coal were recommended for co-gasification.

Kumabe *et al.* (2007) observed that by varying the ratio of coal to biomass for the gasification, the extent of the water gas shift reaction was maximal at the ratio of 0.5 which they attributed to the synergy between the coal and biomass (Corella *et al.*, 2004). They observed with an increase in biomass ratio, CO_2 yield increases, while char, tar and H_2 decreases, and hydrocarbons remains unchanged. Gasification of coal with biomass reduces problems associated with high ash and sulfur contents of the coal (Skoulou *et al.*, 2008). Overfeeding of biomass can lead to plugging and reduced conversion efficiencies whereas starve-feeding results in a lesser gas yield. Hence, an optimum biomass flow rate is desired for the gasification system to maximize energy efficiency. Optimum biomass flow rate depends primarily on the design of the gasifier and the properties of the biomass [Corella *et al.* (2004), Kumabe *et al.* (2007), Skoulou *et al.* (2008), Vélez *et al.* (2009), Kezhong *et al.* (2010)].

2.6.4.2 Ash content

In the fluidized bed biomass gasification, the presence of ash is not favorable as the low melting point of ash present in woody biomass leads to agglomeration which causes de-fluidization problems (Vélez *et al.,* 2009). The ash caused sintering, deposition, and corrosion of the gasifier construction metal. McKendry (2002) reported that, biomass containing alkali oxides and salts with ash content above 5 % causes clinkering/slugging problems. On the other hand, gasification was improved by adding wood waste with a low-grade coal, having an ash content of 32 %. The improvement was due to the high volatiles, the low ash content and the low sulfur in biomass which counterbalanced the negative effects of the high sulfur present in the coal (Pinto *et al.*, 2003). It is very important to study the melting of biomass ash, its chemistry within the gasification bed (no bed, silica/sand, or calcium bed), and the fate of alkali metals when using fluidized bed gasifiers.

2.6.4.3 Effect of gasifying agent

Fluidized bed biomass gasification has been performed using various gasifying agents such as air, steam, oxygen-steam, air-steam, O_2-enriched air and oxygen-air-steam (Rapagna *et al.*, 2008). The technology of biomass air gasification boosts the feasibility of the gasification process and has been developed for industrial application. However, it generates a producer gas highly diluted by nitrogen with LHV of 4–6 MJ/m^3 and H_2 content of 8–14 vol.% which seems to be useful for electricity production or heat generation [Gil *et al.* (1997), and Campoy *et al.* (2009)]. Biomass O_2-enriched air gasification provides a gas with medium heating value but, it requires oxygen production equipment which increases the cost of gasification process. Biomass steam gasification is capable of producing a fuel gas with heating value of 10–16 MJ/m^3 and H_2 content of 30–60 vol.% (Shen *et al.*, 2008). However, endothermic reactions involved in this process reduce the bed temperature and additional equipment and energy are required to increase the temperature to above 700 °C (Umeki *et al.*, 2010). In steam-oxygen gasification, the necessary heat is provided through partial oxidation reactions. The produced gas has a high H_2 content and the problem of dilution with nitrogen is avoided but the high cost of pure O_2 makes the process unfavorable for industrial applications (Campoy *et al.*, 2009).

2.6.4.4 Equivalence ratio

Equivalence ratio (ER) is one of the most important operating parameters involved in air biomass gasification. It is defined as the actual air to biomass weight ratio divided by stoichiometric air to biomass weight ratio needed for a complete combustion (Narvaez *et al.*, 1996). Effect of equivalence ratio on product gas composition was studied by Narvaez *et al.* (1996), Mansaray and Ghaly (1999), Lv *et al.* (2004), Skoulou *et al.* (2008). As reported, both the higher and lower values of ER are not good for CFB gasification. There is an optimum range of ER at which the calorific value of product gas is maximum and it is also dependent on the gasifying medium. At high ER, excess air supply into the gasifier improves the char burning to produce CO_2 instead of combustible gases such as CO, H_2, CH_4 and C_nH_m. This results in a decrease of the LHV of producer gas because it hinders the production of CH_4 and other light hydrocarbons which have relatively large heating values. Besides, at high ER, nitrogen provided by air dilutes the producer gas, which in turn, results in its low energy content (Mansaray and Ghaly, 1999). As reported, biomass gasification is also not favorable at lower ER as it lowers the reaction temperature (Lv *et al.*, 2004). Therefore, there is an optimum value for ER in biomass gasification that exists in the range of 0.2-0.4 which again differs according to various operating parameters (Narvaez *et al.*, 1996). Yassin *et al.* (2009) reviewed the effect of various parameters on ER.

2.6.4.5 Effect of bed materials

Bed materials in fluidized bed gasifiers act as heat transfer medium but their major role involves in tar cracking which avoids complicated downstream tar removal process (Lu *et al.*, 2008). The presence of catalyst in the bed material during biomass gasification promotes several chemical reactions which influences the composition and heating value of the producer gas. Generally, three main groups of catalysts are used to remove tar from the producer gas viz., (1) natural catalysts such as dolomite and olivine; (2) alkali-based catalysts such as (Li, Na, K, Rb, Cs and Fr) and (3) metal-based catalyst such as nickel catalysts [Wang *et al.* (2008), and Weerachanchai *et al.* (2009)]. Dolomite is the most commonly used catalyst which effectively removes heavy hydrocarbons from the gas stream (Weerachanchai *et al.*, 2009). It also decreases agglomeration in a fluidized bed while using biomass with high alkali content. Li *et al.* (2002) investigated the effect of bed material on tar removal efficiency in a CFB. They used silica sand and a commercial Ni-alumina catalyst as bed

material. At a bed temperature of 800 °C, the amount of tar got reduced from 0.4 g/m^3 to 0.15 mg/m^3, when silica sand was replaced by Ni-alumina catalyst.

2.6.4.6 Effect of temperature

Bed temperature is one of the most important operating parameters which affect both the heating value and the product gas composition. Based on Le Chatelier's principle, the effect of temperature on producer gas composition depends on the thermodynamic behavior of the reactions. High temperatures improve product formation in endothermic reactions whereas they favor reactants in exothermic reactions. The main reactions that occur during gasification has already been summarized in the subsection 2.6.1 (gasification process) [Li *et al.* (2009), and Weerachanchai *et al.* (2009)].

Skoulou (2008) reported that increasing the gasification temperature reduces the gas heating value. The necessary heat for gasification is provided by combustion enthalpy of the biomass, therefore, high temperature improves biomass combustion which consequently results in more CO_2 and N_2 production and low heating value (Wu *et al.*, 2009). The research findings of Pinto *et al.*, (2003), Lv *et al.* (2004), Chaiprasert and Vitidsant (2009) indicate that, high bed temperatures improve carbon conversion and steam cracking, and reforming of tars which results a lesser char and tar formation and high gas yields.The carbon conversion efficiency and gas yield is reported to be enhanced from 78.17 to 92.59 % and 1.43 to 2.53 m^3/kg with the increase in temperature. Narvaez *et al.* (1996) investigated the effect of bed temperature (700–850 °C) on composition, tar content and LHV of the producer gas. They reported that in the studied temperature range, the H_2 content increased from 5 to 10 %, CO increased from 12 to 18 %, CO_2 decreased from 15.7 to 14 % and CH_4, and C_nH_m contents were found nearly constant. It was also observed that as the temperature increased, the tar content of the producer gas gradually reduced due to tar cracking and steam reforming reactions at high temperatures. Further, the LHV of the producer gas was found to increase marginally due to the increase of H_2 and CO content. In another set of experiments conducted by Pinto *et al.* (2003), cogasification of coal and biomass in the bed temperature range of 750–890 °C was studied. It was observed that increasing the temperature led to an increase of about 70 % in H_2 concentration, whereas a decrease of around 30 % was obtained in CH_4 concentration. It was also found that the char formation was reduced by 9 % at high temperatures. The reduction in char yield confirmed improved carbon conversion while

increasing bed temperature. Wu *et al.* (2009) investigated rice husk gasification at 700–800 °C. It was observed that as the temperature was raised from 700 to 800 °C, H_2 concentration increase from 5.37 to 7.46 %, CO reduced from 20.62 to 16.53 %, CH_4 concentration varied from 5.79 to 4.79 % and CO_2 increased slightly from 15.52 to 16.08 %. The gas LHV also reduced from 6.47 to 5.54 MJ/m^3 as the temperature was elevated from 700 to 800 °C. Kumar *et al.* (2009) also studied the effect of gasification temperature in the range of 650–850 °C. They obtained a maximum carbon conversion of 82% and an energy efficiency of 96 % at 850 °C. It was also found that increasing the bed temperature from 650 to 850 °C improved H_2 concentrations from 4 to 15 %.

Pan *et al.* (2000) maintained the average temperature between 840 to 910 °C during the co-gasification experiments. High temperature in the reduction zone (above 850 °C to 900 °C) reduces the tar content in the product gas; however, this high temperature in the combustion zone might causes sintering problems and de-fluidization of the bed [Pan *et al.* (1999), Lv *et al.* (2004), and Kumar *et al.* (2009)]. Vélez *et al.* (2009) maintained the maximum gasification temperature below 1000 °C to avoid sintering. Pinto *et al.* (2003) observed that methane and hydrocarbons were decreased by 30 and 63 %, respectively, while H_2 concentration increased by 70 %, when temperature was increased from 750 °C to 890 °C. In the steam flow rate of 5 kg/h and a gasification temperature at 890 °C, H_2 (39.8 %), CO (17.3 %), CO_2 (20.4 %), CH_4 (14.9 %) and CnHm 7.6 % (v/v) were produced. Pinto and his colleagues recommended that a temperature range of 850 to 900 °C should be used for co-gasification of coal and pine. The temperature profile inside the directly-heated co-gasification reactor is also influenced by the proportion of biomass in the coal-biomass mixtures. Pan *et al.* (2000) observed that an average temperature drop by 60 °C (approx.) in the fluidized bed gasifier when the proportion of pine chip was increased from 20 to 100 % in the mixtures. Hence, the temperature profile was found to be specific to a particular coal-biomass mixture and the type of biomass.

2.7 Summary of the literature review

As observed in the open literature, CFB systems have been proved useful, reliable, and cost-effective, suitable to many industrial applications. Host of research is available on various aspects of CFB hydrodynamic, heat transfer and gasification characteristics. However, no single universal approach for designing a fluidized bed reactor system is found in the open literature. It is understood that the fluidized bed reactor system design relies heavily on

correlations, engineering models, and plant observations. The computational fluid dynamics approach may offer viable and attractive options over the traditional approaches; however, challenges remain in considering reactive flow that involves the incorporation of kinetics, heat, and mass transfer properties into fluid dynamic calculations. Continued research efforts are therefore necessary toward the development of an advanced fluidized bed processes to deal with the abundantly available reactive biomass fuels. It is reported that, the design of such a boiler is largely based on bed hydrodynamics and heat transfer (Gupta and Nag, 2002). Many researchers have studied the bed hydrodynamics and heat transfer at atmospheric conditions [Grace (1986), Basu and Nag (1987), Basu and Nag (1996), Basu (2006)]. Use of fins has been reported [Ali (1991), Basu and Nag (1996), Basu (2006), Chinsuwan and Dutta (2009)] to enhance the heat transfer coefficient in atmospheric CFB. Both circular and rectangular CFB risers have been reported in the in the laboratory scale studies. The research findings of Gupta and Nag (2002), Basu and Cheng (1996), and Basu (2006) had shown the dependence of various factors such as superficial velocity, solid circulation rate, solid inventory, and particle size distribution on the performance of pressurized CFB units. The change of any of these parameters influences the bed hydrodynamics such as bed voidage, suspension density etc. and this causes a change in the heat transfer along the bed height. Very limited information is found on the study of hydrodynamic and heat transfer characteristics in PCFB reactors despite having very good characteristics features like compactness, good heat transfer characteristics, fuel flexibility, and combustion efficiency suitable for steam generation, gasification and combined cycle power generation [Anthony (1995), Basu and Cheng (1996), Basu and Nag (1996), Gupta and Nag (2002)]. The use of heat transfer augmentation techniques was not found in PCFB. Besides, hydrodynamic and heat transfer behavior dealing with various blending of biomass in sand in a PCFB is scarce. Further, a thorough study on effect of various operating parameters on hydrodynamic characteristics, heat transfer behavior and reaction kinetics is very essential in order to bring further refinement in the current reactor models and their implementation in future power plants.

So far, numerous studies have been made on gasification of lignocellulosic biomass using CFB. The equivalence ratio and bed temperature are the two crucial parameters which determine the quality of gasification in a CFB. It was seen that, more than 95 % of the published research on CFB was primarily on atmospheric CFB and in most of the studies, the effect of ER, bed temperature, feeding rate etc. on the gas composition, carbon conversion

efficiency and cold gas efficiency were investigated. The ability of fluidized beds to conduct the gasification process has been confirmed by many researchers as well as several successful operating industrial plants in developed countries. However, more research is required to see extensive and flourishing progress in this area. Information on the quality of gas production on operating pressures has been scarce in open literature. Similarly, studies on blending of biomass with bed material and its effect on gas composition in a pressurized CFB is also scarce. Thus, there is a need to carry out further studies in order to understand the complex phenomena occurring in a pressurized CFB gasification unit.

2.8 Scope for research

In view of the above, an attempt has been made to investigate the effect of various operating parameters on hydrodynamics, heat transfer and gasification characteristics in a PCFB with various proportions of biomass. In order to achieve this following activities are proposed

(1) Investigation of thermal analysis and characterization of biomass
(2) Study of bed hydrodynamics along the riser and heat transfer characteristics along the upper splash region of the riser under varied range of operating conditions with biomass blends in pressurized circulating fluidized beds
(3) Investigation of product gas composition of gasification at different blending of biomass in sand
(4) Enhancement of heat transfer coefficient at the upper splash region of a hot PCFB unit with passive heat transfer devices under varied operating conditions

The next chapter addresses the details of the experimental setups and procedures of the present investigations.

Chapter – 3

EXPERIMENTAL SETUP AND PROCEDURE

3.1 Introduction

This chapter describes the PCFB experimental setup and its operational procedures to investigate the bed hydrodynamics, heat transfer characteristics and gasification performance. Two units of PCFB (one cold bed and one hot bed) of similar dimensions have been developed. The bed hydrodynamics along the riser height and wall-to-bed heat transfer characteristics were investigated in the cold PCFB unit, whereas bed-to-wall heat transfer coefficient and gasification study was investigated in the hot PCFB unit. The heat transfer probes used for calculation of heat transfer coefficient at the upper splash region of the riser for both cold and hot CFB units are also discussed and presented. The development of a novel feeding system used for feeding of loose biomass into the CFB units has also been outlined. The various components of the CFB units such as riser, distributor plate and cyclone separator have been designed as per the procedure described by the hydrodynamics of fluidization. Individual design procedure and calculations for air mass flow measurement (orifice plate), distributor plate and cyclone separator are presented in the appendices-I through III.

3.2 Description of cold bed unit

3.2.1 Setup description

The schematic diagram and the photograph of the cold PCFB setup are shown in Figs.3.1 and 3.2, respectively. The PCFB unit comprises of a riser, a transparent downcomer, and a cyclone separator. The riser is made of stainless steel of ID 54 mm, height of 2000 mm and thickness of 3 mm. The PCFB unit contains a mild steel cyclone separator of barrel diameter 80 mm and height 160 mm. Entrained solids are recovered in a cyclone separator and are then sent to the bottom of the riser column through a transparent return leg of ID 24.5 m. Air is supplied to the CFB unit through the bottom of the riser by a high pressure centrifugal blower (Model No.: 710, motor capacity: 20 HP) and a compressor (Make: Ingersoll Rand (IR), Model No.: S-01480). The air flow rate is measured by a standard orifice meter (BS 1042)

and is regulated by an air control valve and a bypass arrangement. The air passes through a porous distributor plate (straight hole) of 16.8 % opening area which is fixed at the bottom of the riser column. Figure 3.3 shows the photograph of the orifice plate, while Fig.3.4 shows the photograph of distributor plate used for this experimental setup. The detailed design of the orifice plate and distributor plate is presented in the appendices-I and II, respectively. The design of the cyclone separator is presented in the appendix-III. Static pressures are measured and bed voidage are calculated along the riser height at 6 (six) different locations such as 120 mm, 192.5 mm, 370 mm, 495 mm, 970 mm and 1570 mm above the distributor plate. Suspension densities at those points have also been calculated. Fine wire mesh (Mesh size of 200 μm) and cigarette filters are used at the pressure taping ends to minimize the pressure fluctuations and to avoid the escape of sand particles from the column. Pressure drops are measured with U-tube water filled manometer fabricated for this purpose.

3.2.2 Heat transfer probe

The heat transfer probe is located at a height of 1300 mm above the distributor plate i.e. at the upper splash region of the riser. Internal diameter and height of the heat transfer probe are 54 mm and 500 mm respectively (Fig.3.5). Necessary thermocouples are facilitated to measure the surface and bed temperatures. The thermocouples are located at a distance of 1400, 1500, 1600, 1700 and 1800 mm from the distributor plate. Besides, thermocouples are also installed to measure the radial temperature variations in the bed at *d/D* of 0.2, 0.3, 0.4, 0.6 and 0.8 (Fig.3.6) at a height of 1.57 m from the distributor plate. A heater coil (rated power of 1000 Watt and resistance of 46 Ohms) of the required length is wrapped uniformly around the probe. Adequate electrical and thermal insulation are provided. Mica sheet of 1 mm thickness is used as electrical insulation over which heater coil is warped. For thermal insulation, ceramic wool and ceramic rope are used around the probe. The axial heat loss by conduction is also prevented by providing ceramic wool insulation in between the joints. Both surface and bed temperatures are measured with copper-constantan thermocouples which are connected to Agilent 34972 LXI data acquisition/ switch unit for display. Local sand having mean particle diameters (d_p) of 278, 307 and 469 μm, and density of 2300 kg/m^3 is used as the bed material in the study. The procedure for the calculation of mean particle size of sand and biomass is presented in the appendix-IV.

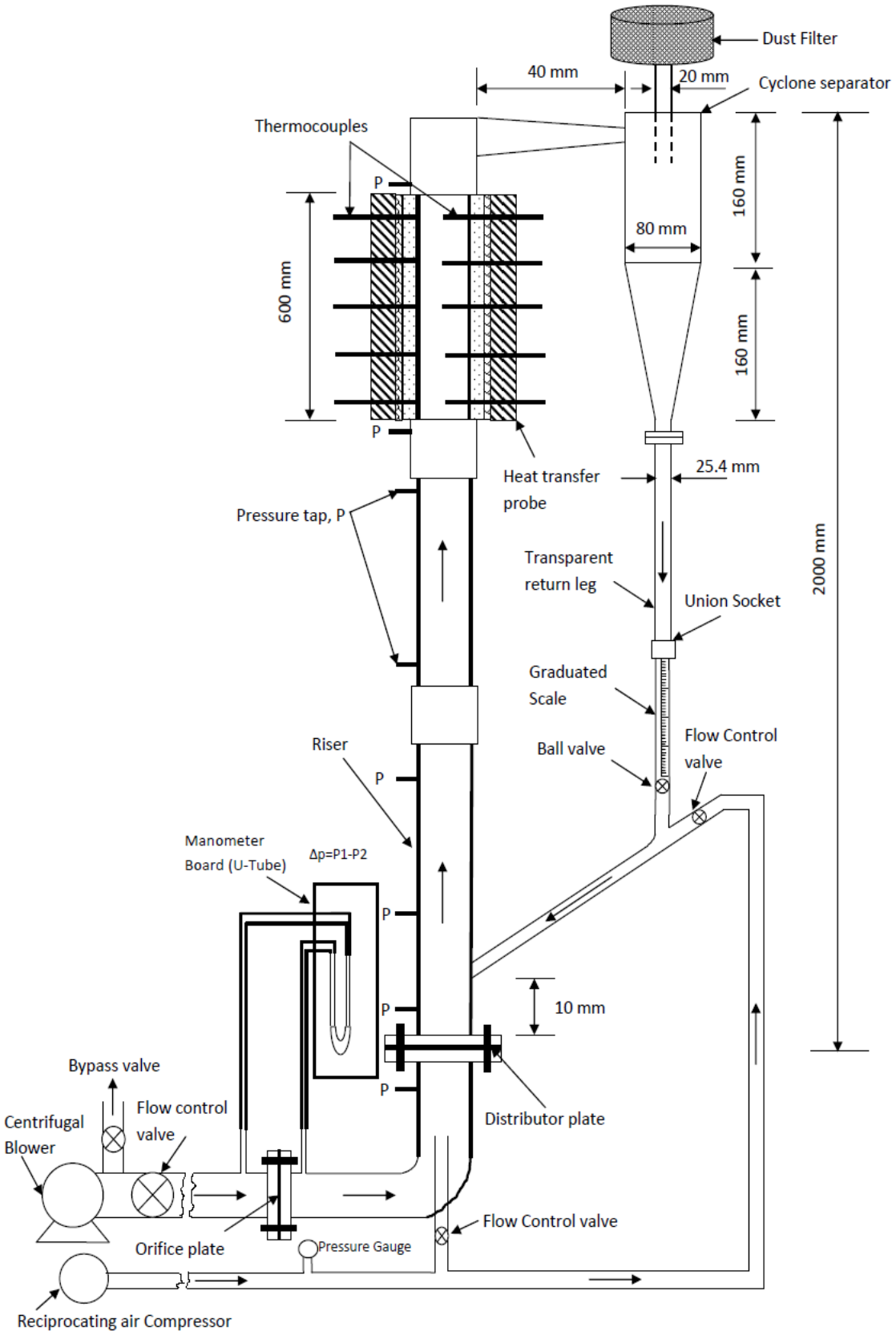

Fig.3.1 Schematic of cold CFB experimental setup

Fig.3.2 Photograph of the cold PCFB experimental setup

F

Fig.3.3 Orifice plate, D-D/2 pressure tapings connected with manometer board

Fig.3.4 Straight hole type distributor plate

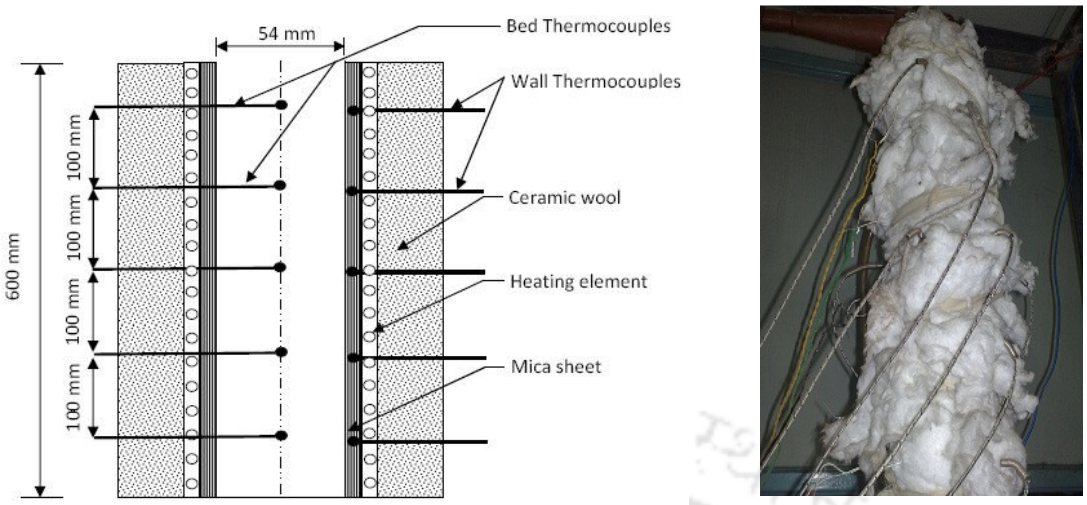

Fig.3.5 Schematic of heat transfer probe

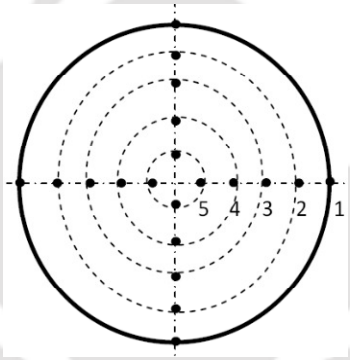

Fig.3.6 Location of thermocouples for radial temperature measurement

3.2.3 Experimental procedure

A measured quantity of inventory (dust free sand particles after cleaning and drying) is fed into the unit through the top of the cyclone separator. This sand particles are rests on the ball valve of the transparent return leg (downcomer) till the valve open. Heating of test section is done by a heater coil-auto transformer assembly. The heat transfer probe is heated by providing a known heat flux before the start of experiment. The thermocouples meant for the measurement of bed and wall temperatures are connected to a data acquisition system and these are calibrated before use. The calibration of thermocouple is presented in the appendix-V. Pressure drops along the riser are measured by using U-tube water manometer. High precision pressure gauge (Swagelok make) is used for the measurement of the compressor delivery pressure. Blower delivery air flow is controlled by a gate valve installed along the flow, and the flow rate is calculated by measuring the orifice pressure drop (*D* and *D/2* tapings) in the U-tube water manometer. The orifice plate is installed at 6.5 meters away from

the exit of the blower (Fig.3.1). Finally, the superficial velocity (U_{sup}), defined as the volume flow rate of air per unit cross-section of the bed, is calculated by using the measured orifice pressure drop (Eq.3.1).

In each experiment, controlled amount of air is supplied from the blower at a required superficial velocity to the CFB loop. Compressed air is supplied from the compressor at a required pressure to the riser bottom. For each operating conditions, about 60 minutes time is required to attain the thermal and hydrodynamic equilibrium. For thermal and hydrodynamic equilibrium, temperature rise, and circulation rate are monitored. Once the equilibrium condition is reached, experimental data such as temperature, pressure drop and circulation rate are recorded. The same procedure is followed with every change in operating parameters. In the experimentation, the time taken to accumulate a fixed quantity of solids is measured by closing the ball valve located at the transparent return leg (Fig.3.1). A stop watch is used to measure the time of accumulation and the solid accumulation is observed from the graduated scale located just above the ball valve. Once these two parameters are measured, the solid circulation rate is calculated by using Eq. (3.5). Transportation velocity, terminal velocity and fast fluidization velocity are also investigated and presented in the Table 3.1 along with the properties of sand. Emptying time and floating point determination method is used for measurement of transportation velocity. Experiments have been performed at a constant heat flux of 830 W/m^2 and at three superficial velocities such as 6, 7 and 8 m/s. In each superficial velocity, experiments have been conducted at three different system pressures of 1, 3 and 5 bar. Finally, bed hydrodynamics (bed voidage, suspension density and solid circulation rate) and heat transfer characteristics (axial and radial) have been investigated for three different particle sizes of 278, 307 and 479 µm and five different inventories of 400, 500, 600, 800, and 1000 g. The axial and radial variation of heat transfer coefficient with six proportions blending of sawdust in sand such as 2.5 %, 5.0%, 7.5 %, 12.5%, 15.0 % and 20.0 % have also been studied and compared. Comparisons have also been made at two different weight composition ratios i.e. weight of sawdust to 400 g sand and weight of sawdust to 600 g of sand. The percentage blending of sawdust is always kept constant irrespective of weight compositions. Average particle size of sawdust used for the experiments is calculated to be 407 µm. All the experiments have been repeated thrice in order to establish the repeatability.

3.2.4 Working formula

The *superficial velocity* (U_{sup}) can be expressed as,

$$U_{sup} = \frac{m_a}{\rho_g \times A_B} \tag{3.1}$$

where m_a is the mass flow rate through the orifice plate in kg/s, ρ_g is the density of air in kg/m^3 and A_B is the cross-sectional area of the bed in m^2.

Once the pressure drop through the orifice is measured by a U-tube water manometer, the superficial velocity (m/s) may be calculated by using the following relation,

$$U_{sup} = \frac{m_a}{\rho_g \times A_B} = 4.844 \times \sqrt{\Delta P} \tag{3.2}$$

where ΔP is the difference in height of manometric fluid (water) in cm of water measured across the orifice plate.

The *voidage* (ε) is defined as the volume fraction of the bed occupied by air bubbles. This may be calculated by using the following expression,

$$\varepsilon = 1 - \frac{10 \times \Delta h}{\rho_s \times L_m} \tag{3.3}$$

where Δh is the difference of height in manometric fluid measured in cm of water column, L_m is the difference between two consecutive pressure taps across which pressure drops measured in m, and ρ_s is the density of sand in kg/m^3.

The *suspension density* of the bed (ρ_{sus}) can be evaluated by the relation as suggested by Kunni and Levenspiel (1991)

$$\rho_{sus} = \rho_s (1 - \varepsilon) + \varepsilon \rho_g \tag{3.4}$$

where ε is the voidage and ρ_g is the density of air in kg/m^3.

The *solid circulation rate* or *solid mass flux* (G_s) is calculated from,

$$G_s = \frac{\rho_s \times L_a \times A_D \times (1 - \varepsilon_{mf})}{A_B t} \tag{3.5}$$

where

ε_{mf} : Bed voidage at minimum fluidization

L_a : Solid accumulation height in m

A_B : Cross sectional area of the bed in m^2

A_D : Cross sectional area of downcomer in m^2

t : Time to accumulate particular height after closing ball valve in sec

G_s : Solid circulation rate in $kgm^{-2}s^{-1}$

The *wall-to-bed heat transfer coefficient* (h_i) at any location along the riser height '*i*' is estimated from the measured local surface to bed temperatures as given below

$$h_i = \frac{q}{A_{htp}(T_{bs} - T_{bi})} = \frac{V \times I}{A_{htp}(T_{bs} - T_{bi})} \tag{3.6}$$

where V, I, A_{htp}, T_{bs} and T_{bi} are the voltage supply, current supply, heat transfer probe surface area, bulk surface temperatures and bed temperatures, respectively.

Table-3.1 Properties of sand particles

Name of the properties	Values
Mean diameter (μm)	307
True density (kg/m^3)	2300
Bulk density (kg/m^3)	1690
Spherocity, ϕ_s	0.95
Minimum fluidization velocity, (m/s)	0.0841
Terminal velocity, (m/s)	2.296

3.3 Description of hot bed unit

3.3.1 Setup description

The schematic diagram and the photograph of the hot PCFB setup are shown in Figs.3.7 and 3.8. The PCFB unit comprises of a riser, a transparent quartz downcomer, a cyclone separator and a dust filter. The riser is made of stainless steel of ID 54 mm, height of 2000 mm and thickness of 3 mm. The riser comprises of six of sections of height 600 mm, 200 mm, 400 mm, 200 mm, 400 mm and 200 mm (starting from the lower splash region of the riser). These

sections are connected by joining one above the other with the help of a flange. A metallic gasket of thickness 3 mm placed in between the flange in order to minimize leakage in between the joints. A KANTHAL heating element of capacity 3500 W (resistance of 14 Ohms) is installed at the lower section of the riser. This is wrapped over a ceramic tube of OD 24 mm. Required voltage and current are supplied to the heating element through auto-transformer-ammeter-thermocouple (Chromel-alumel)-controller assembly to heat the unit to a predefined temperature. Figure 3.9 shows the electrical circuit diagram for controlling of temperature. Adequate electrical and thermal insulation are provided. For thermal insulation, ceramic wool and ceramic rope are used around the riser. The axial heat loss by conduction is also prevented by providing insulating gasket in between the flanges in the joints. The PCFB unit contains a mild steel cyclone separator of barrel diameter 80 mm and height 160 mm. Entrained solids are recovered in a cyclone separator and are then transported to the bottom of the riser column through a return leg of ID 24.5 mm. The other experimental facility for delivering air and the type of distributor plate used are described under the section 3.2.1. Both surface and bed temperatures are measured with chromel-alumel thermocouples and these have been calibrated before use. Calibration chart is also used to verify the temperature readings. A total of 22 K-type thermocouples are used to measure temperature at various locations of the CFB unit. Out of 22 thermocouples, 7 are used to measure the bed temperature along the height of the riser, 10 are used to measure the radial temperature, and 5 are used to measure the inside temperature of cyclone along the height. These thermocouples are connected to an Agilent 34972 LXI data acquisition/ switch unit for the display of temperature reading. Finally, the measured data are recorded in a computer for further analysis. Dial gauges (4 nos.) are used to measure the pressure drop along the height of the CFB riser. Fine metallic wire mesh of size 200 μm is used at the pressure taping ends to minimize the pressure fluctuations.

The heat transfer coefficients with and without twisted tape inserts at the upper splash region of the riser have been calculated and compared. The temperature profiles along the riser height have also been recorded with the variation solid inventory and biomass blending. Finally, product gas composition is investigated by using a precision gas chromatograph (Make: Thermo Fisher, Model: CERES800) and a flue gas analyzer (Make: Testo, Model: 350 XL).

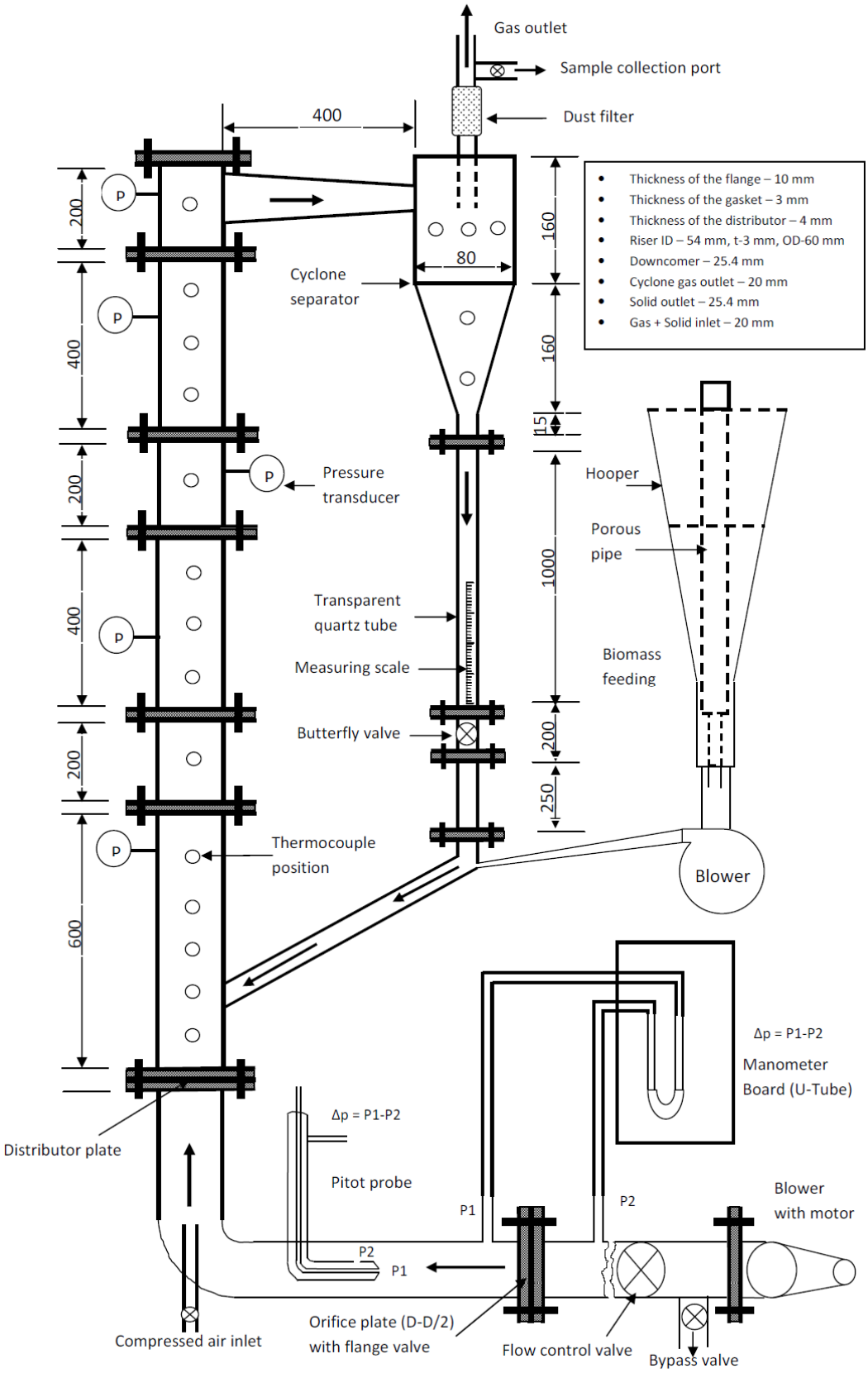

Fig.3.7 Schematics of hot PCFB with feeding system

Fig.3.8 Photograph of cold and hot PCFB units

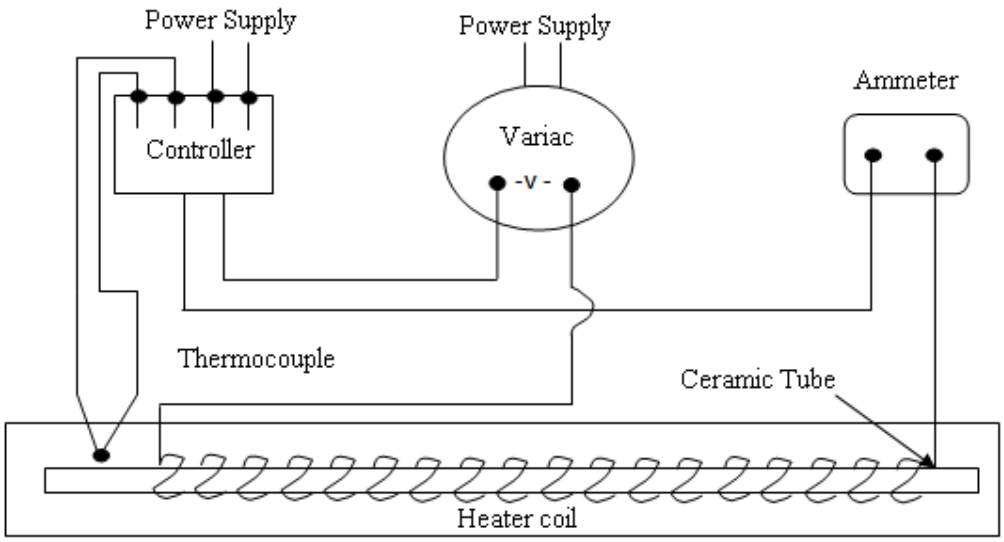

Fig.3.9 Heater coil assembly

3.3.2 Heat transfer probes

Three heat transfer probes of height 400 mm were fabricated and installed at the upper splash region of the riser at a height of 1400 mm above the distributor plate. The internal diameters of all the probes are same as the diameter of the riser i.e. 54 mm. The configurations of the three probes are shown in the Figs.3.10-3.12. Probe-1 is a plain tube, probe-2 has three copper tubes without twisted tapes and probe-3 has three copper tubes with twisted tapes of twist ratio 4 in between the tubes. The outer diameter and length of the copper tubes are 10 mm and 300 mm, respectively. The tubes are welded on a copper strip which connects all the tubes to hold the tube assembly (Figs.3.11 and 3.12). A controlled flow rate of water (200 ml/min) was allowed to flow through the middle tube of the heat transfer probes 2 and 3. Static constant head is maintained at the water reservoir from which water is allowed to flow to the heat transfer probes. The inlet and outlet temperatures of the water flowing through the copper tubes have been measured by using two different thermometers. In each probe, adequate provisions for measurement of bed and surface temperatures were provided. Finally, the heat transfer coefficient was calculated by using the value of heat flow and surface area of the tube. The equations (Eqs.3.7 to 3.10) used for the calculation of heat transfer coefficient are presented below. Ceramic wool and ceramic rope is used around the probe for thermal insulation. The axial heat loss by conduction is also prevented by providing ceramic wool insulation in between the joints.

Assuming a constant water specific heat capacity and steady state conditions, heat transfer (Q) from the bed to the tubes can be determined from the total heat gained by water as;

$$Q = \dot{m}_w \times C_p \times \left(T_{w,\text{out}} - T_{w,\text{in}}\right) \tag{3.7}$$

where $\dot{m}_w$, C_p, $T_{w,\text{in}}$,and $T_{w,\text{out}}$ are water mass flow rate, specific heat capacity of water, outlet and inlet water temperatures, respectively.

From the energy balance between total heat gained by water and the heat transfer from the bed to the tube, the average heat transfer coefficient (h) can be determined by using the following expression;

$$h = \frac{Q}{T_{\text{b}} - T_{\text{ts}}} = \frac{\dot{m}_w \times C_p \times \left(T_{w,\text{out}} - T_{w,\text{in}}\right)}{A_{\text{ts}}\left(T_{\text{b}} - T_{\text{ts}}\right)} \tag{3.8}$$

Where ts = tube surface

The bulk bed temperature may be calculated as,

$$T_b = \frac{T_{b1} \times 0.15 + T_{b2} \times 0.15}{0.3} \tag{3.9}$$

The tube surface temperature may be calculated as,

$$T_{ts} = \frac{T_{ts1} + T_{ts2} + T_{ts3}}{3} \tag{3.10}$$

3.3.3 Experimental procedure

The experimental procedure described for the cold CFB unit has been followed for the hot bed also. The primary difference in operation is that, the bed is heated by using a heater coil, controller, auto-transformer and thermocouple assembly internally. At the beginning of the experiments, blower is turned on to circulate air around the CFB loop. The temperature of the air passing through the CFB loop is monitored before the heater turn on. After 15 minutes of continuous running of air through the loop i.e. after attaining thermal equilibrium, the current is supplied to the heater installed at the lower splash region of the riser. The required temperature is set at the controller. Once the required temperature is achieved, a measured quantity of inventory is fed into the unit with the help of a feeding system designed for the purpose. This is attached just below the butterfly valve of the return leg (downcomer). The thermocouples meant for the measurement of bed and wall temperatures are connected to a data acquisition system. The similar equipment and measuring devices used in the cold CFB

unit for supplying air and measuring air flow has been used in the hot CFB unit. Finally, the superficial velocity is calculated by using the measured orifice pressure drop. In each experiment, controlled amount of air is supplied from the blower at a required superficial velocity to the CFB loop. Compressed air is supplied from the compressor at a required pressure to the riser bottom. Once the equilibrium condition is reached, experimental data such as bed temperature, surface temperature and pressure drop are recorded in a data sheet. Same procedure is followed with every change in operating parameters. Experiments were performed at a superficial velocity of 7 m/s and at three different temperatures such as, 300, 400, and 450 °C. In each temperature, experiments were conducted at three different system pressures of 1, 3 and 5 bar. Extensive experiments were carried out to investigate the bed temperature along the height of a CFB riser at different operating pressures, temperatures, biomass blending ratios and solid inventories. Product gas composition were investigated at two different biomass blending ratios such as 12.5 % and 20.0 % and two different weight compositions (400 and 600 g of sand with biomass: percentage blending is fixed irrespective of biomass blending). The heat transfer coefficient with and without twisted tape inserts at the upper splash region of the CFB at three different inventories of sand such as 400, 600 and 800 g have also been studied and compared. Average particle size of sand and sawdust used for the experiment are calculated to be 307 and 407 µm, respectively. All the experiments were repeated thrice in order to establish the repeatability.

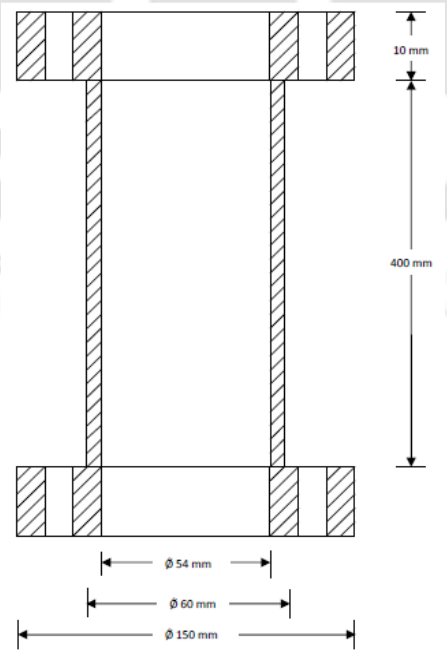

Fig.3.10 Heat transfer probe-1 (plain tube)

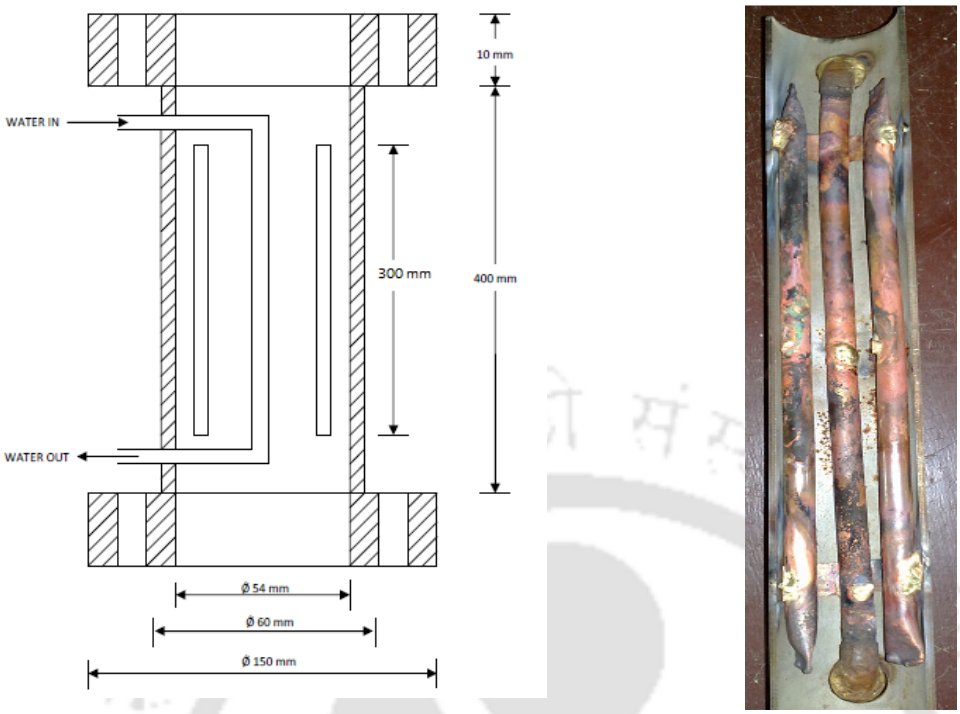

Fig.3.11 Heat transfer probe-2 (without twisted tape)

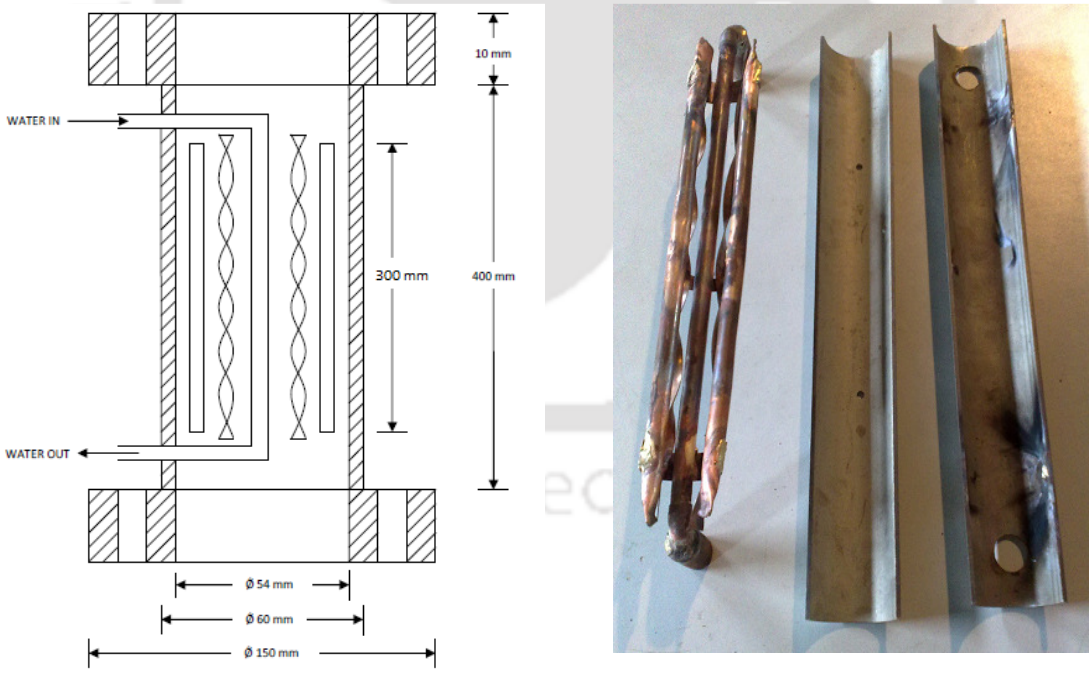

Fig.3.12 Heat transfer probe-3 (with twisted tape)

3.4 Biomass feeding system and its experimental procedure

The purpose of this study is to develop a simple, low cost, energy efficient and a reliable feeding system to supply biomass continuously to a CFB unit without flow blockage and bridge formation. The novel feeding system comprises of a hopper, an aeration pipe, a flexing hose pipe, a feed control valve, a blower, an auto-transformer and a delivery pipe. The schematic diagrams of the hopper and the porous rod are shown in Figs.3.13 and 3.14. The photograph of the setup is shown in the Fig.3.15. The inlet and outlet inner diameters of the cone hopper are 30 cm to 3 cm respectively, and the height of the cone hopper is 70 cm. A mild steel pipe of ID 3.0 cm and length of 15 cm is welded at the smaller diameter end of the cone. The outer diameter and length of the porous pipe are 3 cm and 80 cm, respectively. A small pipe of ID 0.5 cm and the length of 6 cm are welded at one end of the porous pipe. Necessary hanging support is provided inside the cone. The holes of 3 mm diameter were drilled on the pipe installed at the core. The total number of holes drilled on the pipe is 64. The holes were spaced at 3 cm intervals along the axis. The diameter, number of holes and spacing between the holes were decided based on the experimental investigation with different particle sizes of biomass and its hydrodynamics. An auto-transformer is connected to the blower in order to regulate the delivery speed and hence the flow. The flow of biomass with voltage supply has been calibrated and presented in appendix-VI. The flow of the blower is regulated by operating the auto-transformer at varied voltage. For each operation, a known quantity of biomass is fed into the hopper and rested on the neck of the cone hopper till the porous pipe is lifted up to a certain height and after the blower is turned on. The control of required feed rate of biomass is regulated by supplying voltage through an auto-transformer. Once the required air flow is achieved, biomass is allowed to flow into the CFB unit by lifting the porous pipe upto a certain height. The blower became operational only if the power supply was above 50 V and the flow is initiated at this voltage. The experiments were carried out at four different inventories of sawdust such as 250, 500, 750 and 1000 g and at three different particle size of average mean diameter 527, 732 and 853 µm. Sieve analysis were carried out to investigate the average particle size of sawdust. In each experiment, time taken to discharge a known biomass inventory completely at a particular supply voltage has been recorded. The hydrodynamics of the sawdust is also investigated. The moisture content of the biomass used for the experiment has been measured and it is found to be 3.0 %. The property of the sawdust used in the present study is shown in Table-3.2.

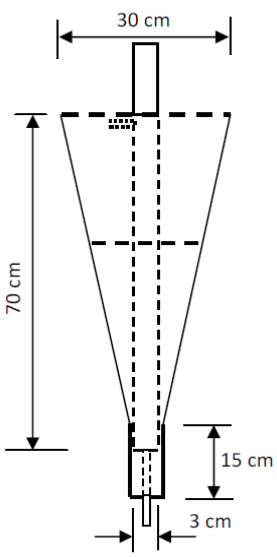

Fig.3.13 The cone hopper with dimensions

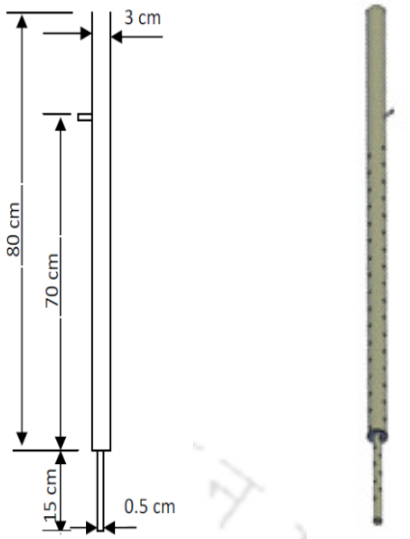

Fig.3.14 The porous pipe with dimensions

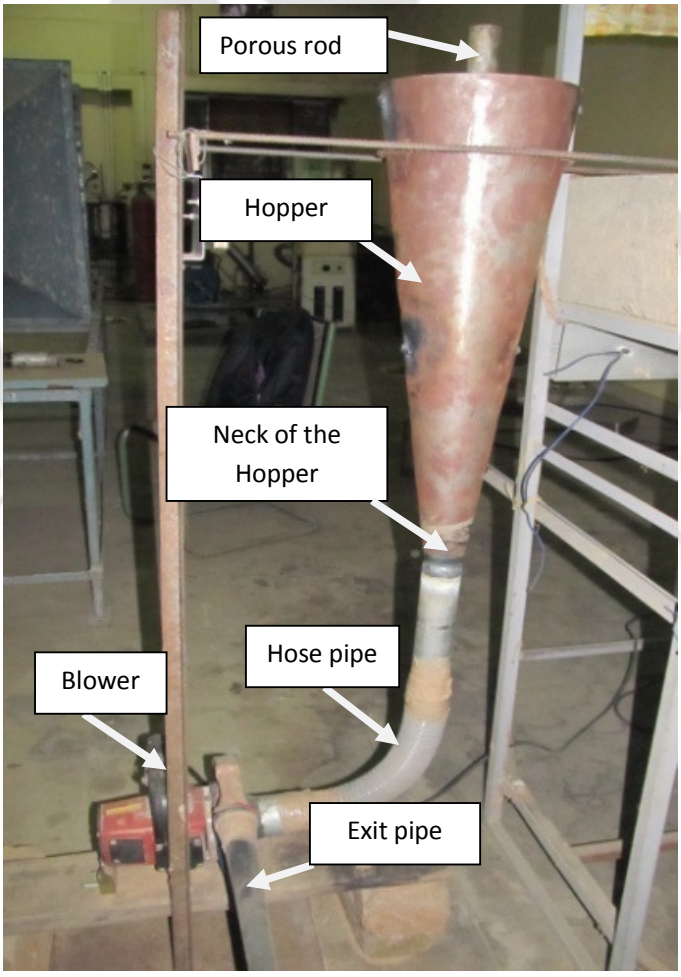

Fig.3.15 Snapshot of biomass feeding experimental setup

Table-3.2 Properties of sawdust

Properties	Weight %
Volatile matter	77.0
Fixed carbon	19.9
Ash	0.7
Moisture	2.6
HHV (kJ/kg)	19891
Carbon (C)	48.5
Hydrogen (H)	6.4
Nitrogen (N)	0.1
Suplhur (S)	0.3
Oxygen (O)	44.6

3.5 Experimental procedure for gasification study

The gasification study is carried out in the hot CFB unit. As described earlier, the biomass is fed into the riser at a height of 10 cm from the distributor plate. The air entering through the distributor plate is heated up with the help of a heating element installed in the lower splash region of the riser. The sand of mean particle size 307 µm is used as bed material. Initially, hot air-sand mixture is circulated in the CFB loop to establish uniform temperature in the riser. The velocity of air through the riser is adjusted so as to give a turbulent mode of fluidization for sand, while a pneumatic conveyance mode for biomass particles. Under these fluidization conditions, the bed of sand and biomass expands. The dry biomass of medium particle size of 420-921 µm, enters the riser and gets mixed with hot sand in turbulent motion. Both gas-particle and particle-particle heat transfer rates are high and hence biomass particles reach the temperature of sand bed and get pyrolyzed almost instantly. The pyrolysis time for sawdust, calculated based on the expression developed by Liu and Gibbs (2003), is found to be 0.494 sec. This is sufficiently small to justify the assumption of instantaneous de-volatilization of biomass particles. The product of pyrolysis i.e. char (which is carbon rich solid fraction), tar (which is essentially heavy hydrocarbons) and light gases disengage and emerge out of the turbulent sand bed, and flows along the riser in a gasification medium; and finally exits at the top to enter a cyclone separator. Various species in the gas undergo reactions (both homogenous and heterogeneous) during their flow through the riser. The cyclone separator separates the solids from the exhaust gas i.e. char particles along with some

sand particles that get elutriated, and returned them to the riser bottom. The gas exiting from the cyclone separator consists of fine dust particles which are separated by a dust filter. The cleaned hot gas is then cooled by using a condenser and finally, the gas sample was collected for gas chromatography analysis.

The experiments were carried out to investigate the temperature profile along the riser height. The product gas composition at the biomass to sand blending ratio of 12.5 % and 20.0 % were also investigated. All the experiments were done at three different operating pressures of 1, 3 and 5 bar and at an equivalence ratio (ER) of 0.27. The ER of 0.27 was selected because this value was found to be very close to the optimum ER (= 0.26) for a continuous and stable release of product gas (Wu *et al.*, 2009). A precision gas chromatograph (Make: Thermo Fisher, Model: CERES800) and a precision flue gas analyzer (Make: Testo, Model: 350 XL) was used for measurement of product gas. The design calculation of the CFB gasification which is based on thermodynamic and hydrodynamics of gas-solid fluidization has been presented in the appendix-VII.

3.6 Summary of the chapter

In this chapter, development of two units of pressurized circulating fluidized bed (PCFB) (one of the two units is cold bed and the other being hot bed) and its experimentation have been discussed. The results of the experiments carried out as per the experimental procedure are presented in the chapter 6 and 7. The specifications of the equipment used in the experiment are presented in the appendix-XII. In the next two chapters (4 and 5) the formulation and results of the reaction kinetic study and thermal analysis of biomass used for feedstock of both the PCFB units have been presented.

Chapter – 4

FORMULATION FOR CHARACTERIZATION AND THERMAL ANALYSIS OF BIOMASS

4.1 Introduction

In this study, the influence of heating rate on the degradation of rice husk, rice straw, water hyacinth, sawdust and tea waste is investigated by simultaneous therogravimetric (TG) analysis and differential scanning calorimetry (DSC). These five varieties of biomass have been selected because of their availability and tremendous potential as feedstock for circulating fluidized bed gasification. Experiments have been carried out at three heating rates of 10, 30 and 80 °C/min and the kinetic parameters (pre-exponential factor, activation energy and order of reaction) are evaluated for both first and second reactions zones which are categorized based on the degradation of cellulose, hemicelluloses and lignin content in the biomass. Mass degradation with temperature is validated numerically. The thermal response of biomass undergoing decomposition has also been modelled by using one dimensional (1-D) transient thermal model with nth order approximation for the rate of decomposition. Kinetic parameters, heat of decomposition and thermal properties are taken as input to the model. The model is tested by using transient conduction chart (called Heisler Chart). The data for specific heat and thermal conductivity of the biomass are taken from literature, while the values of heat of decomposition and kinetic parameters are taken from experiment.

4.2 Evaluation of reaction kinetics

Therogravimetric analysis of all the biomass fuels has been carried out at three heating rates viz 10, 30 and 80 °C/min in an air atmosphere. The initial sizes of the rice husk samples are taken to be 10.068 mg, 8.822 mg and 4.791 mg for heating rates of 10, 30 and 80 °C/min, respectively. The experiments were performed under air atmosphere in a METTLER Thermogravimetric analyzer. The air flow rate into the TGA was maintained at 200 ml/min for all the three heating

rates. TG data was used to evaluate the kinetic parameters such as activation energy, pre-exponential factor and order of reaction. The advantage of determining kinetic parameters from TG is that only a single sample and considerably fewer data are required for calculating the kinetics over an entire range in a continuous manner.

Samples of various types of fuels are collected locally for the study. The collected biomass samples were stored in air tight plastic containers until TG analysis were performed. The procedure described by Ergudenler and Ghaly (1992) has been followed for the TG analysis.

The determination of kinetic parameters from TG data was based on the following Arrhenius rate expression (Ergudenler and Ghaly, 1992).

$$\frac{dX}{dt} = -Ae^{-\left(\frac{E}{RT}\right)}X^n \tag{4.1}$$

where

X : Non dimensional mass of sample undergoing reaction

t : Time (min)

A : Pre-exponential or frequency factor (min^{-1})

E : Activation energy of the decomposition reaction (kJ mol^{-1})

R : Universal gas constant (kJ mol^{-1} K^{-1})

T : Absolute temperature (K)

n : Order of reaction (-)

Kinetic parameters were determined from typical curves of TG data over the entire temperature range in a continuous manner [Goldfarb *et al.* (1968), and Duvvuri *et al.* (1975)]. The value of A, E and n were calculated by using a multiple linear regression. As proposed by the above authors, the linearized form of the Arrhenius equation is as follows

$$y = B + Cx + Dz \tag{4.2}$$

The parameters y, x, z, B, C and D in Eq. (4.2) are defined as follows:

$y = \ln\{[-1/(m_\circ - m_f)][dm/dt]\}$

$x = 1/(RT)$

$z = \ln[(m - m_f)/(m_\circ - m_f)]$

$B \quad = \ln A$

$C \quad = -E$

$D \quad = n$

$m \quad =$ weight of sample at time 't'

$m_{\circ} \quad =$ initial weight of sample

$m_f \quad =$ final weight of sample remaining at the end of the reaction

A code has been written in MATLAB(R) to solve the multiple linear regression. The multiple linear regression method used in the present study is found to be accurate and has the precision of order 10^{-2}. To validate the experimental results, numerical Fourth Order Runge-Kutta method was used. In this analysis, the rate expression is integrated numerically for two reaction zones separately over the given temperature ranges. The simplified form of the rate expression (Eq.4.1) for Fourth Order Runge-Kutta is as follows

$$\frac{dX}{dt} = -Ae^{-\left(\frac{E}{RT}\right)}X^n$$

$$\Rightarrow \frac{dX}{dT}\left(\frac{dT}{dt}\right) = -Ae^{-\left(\frac{E}{RT}\right)}X^n$$

$$\Rightarrow \frac{dX}{dT} = -\frac{1}{\beta}Ae^{-\left(\frac{E}{RT}\right)}X^n = f(X,T) \qquad (4.3)$$

where $\beta = \frac{dT}{dt}$ =Heating rate

In the present case, the temperature range is divided into 'p' parts with the interval 'h'. By integrating equation (4.3) :

$$X(T_{p+1}) - X(T_p) = \int_{T_p}^{T_{p+1}} \left(\frac{dX}{dT}\right) dT = \int_{T_p}^{T_{p+1}} X'(T) dT \qquad (4.4)$$

The values of X were found out at regular interval of temperature at two different temperature zones of all the samples. Ode 45 in MATLAB(R) was used to calculate the value of X.

4.3 Model formulation and description

The following non linear partial differential equation (PDE) gives the energy conservation for 1D heat transfer undergoing thermal decomposition;

$$\frac{\partial}{\partial t}[\rho h] = \frac{\partial}{\partial x}\left[K\frac{\partial T}{\partial x}\right] - \frac{\partial}{\partial x}\left[\dot{m}_g h_g\right] - Q_i\frac{\partial \rho}{\partial t} \tag{4.5}$$

where

h = Enthalpy (J/kg)

h_g = Enthalpy of gas (J/kg)

k = Thermal conductivity (W/m °C)

$\dot{m}_g$ = Mass flux of gas (kg $m^{-2}s^{-1}$)

Q_i = Heat of combustion (J/kg)

T = Temperature ($^{\circ}$C)

t = Time (s)

x = Spatial variables (m)

ρ = Density (kg/m^3)

The rate of change of internal energy per unit volume is represented by the term on the left hand side of equation (4.5). The first term on the right hand side of the above equation represents the conduction flux. The convection energy is given by the second term. The last term of the equation represents the rate of heat generation or consumption resulting from the decomposition.

The rate of decomposition is given by an nth order kinetic rate equation of the form

$$\frac{\partial m}{\partial t} = -A_i m_0\left[\left(m - m_f\right)/m_0\right]^n \exp\left(\frac{-E_i}{RT_k}\right) \tag{4.6}$$

where

A_i = Pre-exponential factor (min^{-1})

E_i = Activation energy (J/g-mol)

m = Mass (kg)

m_o = Initial mass (kg)

m_f = Final mass (kg)

n_i = Order of reaction

R = Universal gas constant (J/g-mol-K)

T_k = Temperature (K)

Assuming no expansion of the solid material, Eq.(4.6) also yields the rate of change of density in Eq.(4.5). If the accumulation of gas is ignored, the conservation of mass may be written as

$$\frac{\partial \dot{m}_g}{\partial x} = -\frac{\partial \rho}{\partial t} \tag{4.7}$$

The mass flux, $\dot{m}_g$ at any spatial location and time may be calculated by integrating Eq.(4.7), which is

$$\text{or, } \dot{m}_g = \int_l^x \frac{\partial \rho}{\partial t} dx \tag{4.8}$$

where

l = Material thickness in m

Equation (4.5) implies

$$\rho C_p \frac{\partial T}{\partial t} + h\frac{\partial \rho}{\partial t} = K\frac{\partial^2 T}{\partial x^2} + \frac{\partial K}{\partial x} \times \frac{\partial T}{\partial x} - \dot{m}_g C_{pg} \frac{\partial T}{\partial x} + h_g \frac{\partial \dot{m}_g}{\partial x} - Q_i \frac{\partial \rho}{\partial t} \tag{4.9}$$

Substituting the expression $\frac{\partial \dot{m}_g}{\partial x} = -\frac{\partial \rho}{\partial t}$ in equation (4.9) and rearranging, we have

$$\rho C_p \frac{\partial T}{\partial t} = K\frac{\partial^2 T}{\partial x^2} + \frac{\partial K}{\partial x} \times \frac{\partial T}{\partial x} - \dot{m}_g C_{pg} \frac{\partial T}{\partial x} + h_g \frac{\partial \rho}{\partial t} - Q_i \frac{\partial \rho}{\partial t} - h\frac{\partial \rho}{\partial t} \tag{4.9}$$

$$\rho C_p \frac{\partial T}{\partial t} = K\frac{\partial^2 T}{\partial x^2} + \frac{\partial K}{\partial x} \times \frac{\partial T}{\partial x} - \dot{m}_g C_{pg} \frac{\partial T}{\partial x} - \left(Q_i + h - h_g\right)\frac{\partial \rho}{\partial t} \tag{4.10}$$

where

C_p = Specific heat (J/kg °C)

C_{pg} = Specific heat of gas (J/kg °C)

h_g = Enthalpy of gas (J/kg)

h = Enthalpy of solid (J/kg)

In the above expression the contribution of $\left(h - h_g\right)$ is very low as compared to the values of Q_i. Besides, it is difficult to investigate the values of both gas and solid enthalpies with increase in temperature. The values of heat of decomposition, Q_i at different temperatures are taken from the TGA experiments. Hence, the governing energy equation reduces to:

$$\rho C_p \frac{\partial T}{\partial t} = K\frac{\partial^2 T}{\partial x^2} + \frac{\partial K}{\partial x} \times \frac{\partial T}{\partial x} - \dot{m}_g C_{pg} \frac{\partial T}{\partial x} - Q_i \frac{\partial \rho}{\partial t} \tag{4.11}$$

Equation (4.5), (4.6) and (4.7) form a set of non-linear PDE which must be solved simultaneously for m, $\dot{m}_g$ and T respectively. Figure 4.1 shows the schematic to represent the boundary condition, flow direction and energy interactions.

The following boundary and initial condition were applied,

$$-K\frac{\partial T}{\partial x} = f(T) \text{ for } x = 0, \quad t > 0 \tag{4.12}$$

$$\frac{\partial T}{\partial x} = 0, \ \dot{m}_g = 0 \text{ for } x = l, \ t > 0 \tag{4.13}$$

$$T = T_I, \ \rho = \rho_o, \ \dot{m}_g = 0 \text{ for } 0 \le x \le l, t = 0 \tag{4.14}$$

where

T_I = Initial temperature (°C)

ρ_0 = Initial density (Kg/m^3)

The function $f(T)$ is defined as

$$f(T) = \bar{h}\left(T_\infty - T\right) + \sigma\left(\varepsilon_r d_m T_r^4 - \varepsilon_m T_k^4\right) \text{ for } x = 0, \quad t > 0 \tag{4.15}$$

where

T_∞ = Environmental temperature (°C)

T_r = Radiation source temperature (°C)

$\bar{h}$ = Convection heat transfer coefficient (W/m^2 °C)

ε_r = Radiation source emissivity

ε_m = Emissivity of the material

α_m = Absorptive of the material

σ = Stefan-Boltzman constant (5.78x10^{-8} W/m^2-K^4)

In the above analysis, the following assumptions were made,

(a) Variation of thermal conductivity with time is neglected

(b) Variation of specific heat with time is neglected

(c) Specific heat of rice husk and the gas generated from rice husk is considered to be same

(d) Radiation heat transfer is not considered

(e) No thermochemical expansion

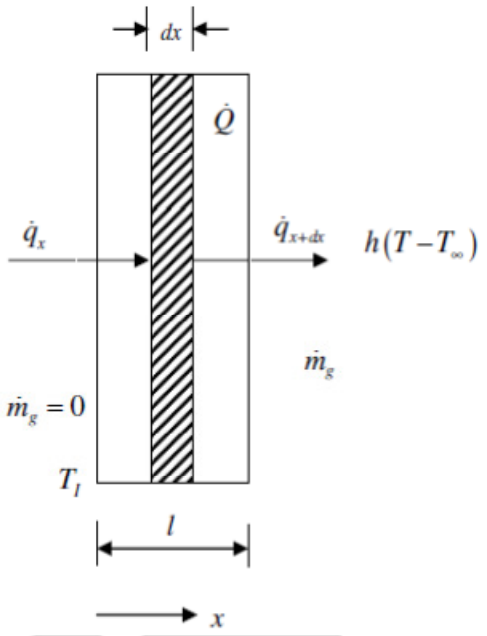

Fig.4.1 Schematic of the sample with boundary condition

The equations (4.5), (4.6) and (4.7) were solved using a straightforward explicit finite difference scheme. The time derivative terms were represented by the forward differences and the special variables by the central and the mass flux term was represented by the backward differences. The formulations are presented in the following sub sections. The solution was carried out on a digital computer. Equation (4.5) implies,

$$\rho C_p \frac{\partial T}{\partial t} = K \frac{\partial^2 T}{\partial x^2} + \frac{\partial K}{\partial x} \times \frac{\partial T}{\partial x} - \dot{m}_g C_{pg} \frac{\partial T}{\partial x} - Q_i \frac{\partial \rho}{\partial t} \tag{4.16}$$

$$\frac{\partial T}{\partial t} = \frac{K}{\rho C_p} \frac{\partial^2 T}{\partial x^2} + \frac{1}{\rho C_p} \frac{\partial K}{\partial x} \times \frac{\partial T}{\partial x} - \frac{\dot{m}_g C_{pg}}{\rho C_p} \frac{\partial T}{\partial x} - \frac{Q_i}{\rho C_p} \frac{\partial \rho}{\partial t}$$

$$\frac{T_i^{n+1} - T_i^n}{\Delta t} = \frac{K}{\rho C_p} \left[\frac{T_{i+1}^n - 2T_i^n + T_{i-1}^n}{(\Delta x)^2} \right] + \cancel{\frac{1}{\rho C_p} \frac{\partial K}{\partial x} \times \frac{\partial T}{\partial x}} - \frac{\dot{m}_g C_{pg}}{\rho C_p} \left[\frac{T_i^n - T_{i-1}^n}{\Delta x} \right] - \frac{Q_i}{\rho C_p} \frac{\partial \rho}{\partial t}$$

$$T_i^{n+1} = T_i^n + \Delta t \frac{K}{\rho C_p} \left[\frac{T_{i+1}^n - 2T_i^n + T_{i-1}^n}{(\Delta x)^2} \right] - \frac{\dot{m}_g C_{pg}}{\rho C_p} \Delta t \left[\frac{T_i^n - T_{i-1}^n}{\Delta x} \right] - \Delta t \frac{Q_i}{\rho C_p} \frac{\partial \rho}{\partial t}$$

$$T_i^{n+1} = T_i^n + \Delta t \frac{K}{\rho C_p}\left[\frac{T_{i+1}^n - 2T_i^n + T_{i-1}^n}{(\Delta x)^2}\right] - \frac{\dot{m}_g C_{pg}}{\rho C_p}\Delta t\left[\frac{T_i^n - T_{i-1}^n}{\Delta x}\right] - \Delta t \frac{Q_i}{\rho C_p}\frac{\partial \rho}{\partial t}$$

$$T_i^{n+1} = T_i^n + C\left(T_{i+1}^n - 2T_i^n + T_{i-1}^n\right) - \left[\int_l^x \frac{\partial \rho}{\partial t} dx\right]\frac{C_{pg}}{\rho C_p}\frac{\Delta t}{\Delta x}\left[T_i^n - T_{i-1}^n\right] - \Delta t \frac{Q_i}{\rho C_p}\frac{\partial \rho}{\partial t}$$

$$T_i^{n+1} = T_i^n + C\left(T_{i+1}^n - 2T_i^n + T_{i-1}^n\right) - \left[\int_0^l \frac{\partial X}{\partial t} dx\right]\frac{C_{pg}\rho_0}{\rho C_p}\frac{\Delta t}{\Delta x}\left[T_i^n - T_{i-1}^n\right] - \Delta t \frac{Q_i \rho_0}{\rho C_p}\frac{\partial X}{\partial t}$$

$$T_i^{n+1} = T_i^n + C\left(T_{i+1}^n - 2T_i^n + T_{i-1}^n\right) - U \times D\left[T_i^n - T_{i-1}^n\right] - \Delta t \frac{Q_i \rho_0}{\rho C_p}\frac{\partial X}{\partial t}$$

where

$$C = \frac{K}{\rho C_p} \times \frac{\Delta t}{(\Delta x)^2}$$

$$D = \frac{C_{pg}\rho_0}{\rho C_p}\frac{\Delta t}{\Delta x} \text{ for present case, } D = \frac{\Delta t}{\Delta x}$$

$$U = \left[\int_0^l \frac{\partial X}{\partial t} dx\right] = \frac{\partial X}{\partial t} \times l$$

$$X = -8\times10^{-7} \times t^6 + 5\times10^{-5} \times t^5 - 0.001 \times t^4 + 0.008 \times t^3 - 0.031 \times t^2 + 0.029 \times t + 0.987$$

$$\frac{\partial X}{\partial t} = -48\times10^{-7} \times t^5 + 25\times10^{-5} \times t^4 - 4\times10^{-3} \times t^3 + 0.024 \times t^2 - 0.62 \times t + 0.029$$

$$T_i^{n+1} = T_i^n + C\left(T_{i+1}^n - 2T_i^n + T_{i-1}^n\right) - U \times D\left[T_i^n - T_{i-1}^n\right] - \Delta t \frac{Q_i \rho_0}{\rho C_p}\frac{\partial X}{\partial t}$$

$$T_i^{n+1} = CT_{i+1}^n + (1 - 2\times C - U \times D)T_i^n + (C + U \times D)T_{i-1}^n - \Delta t \frac{\rho_0}{\rho C_p}\frac{\partial X}{\partial t} Q_i$$

$$\cong T_i^{n+1} = CT_{i+1}^n + \left(1 - 2\times C - U \times D \times \frac{1}{60}\right)T_i^n + \left(C + U \times D \times \frac{1}{60}\right)T_{i-1}^n - \frac{\Delta t}{C_p} \times \frac{1}{60} \times \frac{\partial X}{\partial t} Q_i$$

In terms of heat transfer coefficient

$$T_i^{n+1} = T_i^n + C\left(T_{i+1}^n - 2T_i^n + T_{i-1}^n\right) - U \times \Delta t \times \frac{C_{pg}\rho_0}{\rho C_p}\left[-\frac{h}{k}(T_\infty - T)\right] - \Delta t \frac{Q_i \rho_0}{\rho C_p}\frac{\partial X}{\partial t} \quad (4.15)$$

$$T_i^{n+1} = CT_{i+1}^n + (1 - 2\times C)T_i^n + CT_{i-1}^n + U \times \Delta t \times \frac{C_{pg}\rho_0}{\rho C_p}\left[\frac{h}{k}(T_\infty - T)\right] - \Delta t \frac{\rho_0}{\rho C_p}\frac{\partial X}{\partial t} Q_i$$

$$\cong T_i^{n+1} = CT_{i+1}^n + (1 - 2\times C)T_i^n + CT_{i-1}^n + U\left(= \frac{\partial X}{\partial t} \times l\right) \times \Delta t \times \frac{1}{60}\left[\frac{h}{k}(T_\infty - T)\right] - \frac{\Delta t}{C_p} \times \frac{1}{60}\frac{\partial X}{\partial t} Q_i$$

Both the density and its rate of change are calculated by the kinetic rate equation. The model is extremely sensitive to these values. This is expected since the rate of energy consumption or addition resulting from the decomposition is proportional to $\partial\rho/\partial t$. Additionally, the thermal and transport properties of the materials are the functions of the stage of decomposition. The combination of these effects can significantly alter the predicted thermal response of the material. It is therefore necessary to model the rate decomposition as accurately as possible.

4.4 Summary of the chapter

Formulation for multivariable regression analysis from Arrhenius equation, Runge-Kutta Method for numerical analysis and one dimensional (1-D) transient thermal model with nth order approximation for the rate of decomposition have been discussed in this chapter. Excel spreadsheet was used for regression analysis and MATLAB$^{(R)}$ platform was used for coding and other numerical calculations. The results of the formulation and procedure described in this chapter have been discussed in the next chapter. The Heisler chart and sample calculation for transient temperature measurement are presented in the appendix-VIII.

Chapter – 5

RESULTS AND DISCUSSION - REACTION KINETICS AND THERMAL ANALYSIS OF BIOMASS

5.1 Introduction

Based on the formulation described in the chapter 4, the results of both experimental and numerical investigation on the reaction kinetics, thermal degradation, 1D heat equation and their validation has been presented in this chapter. The properties of biomass used for gas solid fluidization are also evaluated and discussed. Knowledge of these information's are required for design of an efficient device suitable for biomass combustion and gasification.

5.2 Experiments

Kinetic parameters of both first and second reaction zones of rice husk and sawdust are evaluated by using multi variable regression analysis. These kinetic parameters are utilized in the numerical technique in order to predict the mass degradation with temperature in both the reaction zones at three heating rates viz.10, 30 and 80 °C/min, respectively. The predicted degradation results are well comparable with the experimental results in both the reaction zones for all the three heating rates. A transient one dimensional heat conduction model has been formulated to study the transient response with and without considering the heat of formation. Kinetic parameters, properties of biomass, temperature range for both the reaction zones are used as input to the model. Model results agree well with the results obtained by using Heisler Chart without considering heat of formation.

5.3 Characterization and thermal analysis of biomass

This study involves characterisation of two different locally available biomasses such as rice husk and sawdust. Both the thermogravimetric (TG) analysis and differential scanning calorimetry (DSC) are used to study the influence of heating rate on the degradation of rice husk and sawdust. Experiments are carried out at three different heating rates such as 10, 30 and 80

°C/min, respectively. The kinetic parameters viz. pre-exponential factor, activation energy and order of reaction are evaluated for both first and second reaction zones which are categorized based on the degradation of cellulose, hemicelluloses and lignin content present in the biomass. The thermal analysis biomass has also been investigated.

TG and DTG curves of the rice husk at three heating rates such as 10, 30 and 80 °C/min, respectively are shown in Figs.5.1 through 5.3. The comparison of mass degradation of rice husk and sawdust at three different heating rates are shown in Figs. 5.4 and 5.5. From these figures, it is observed that the mass degradation patterns are found to be similar for all the cases and the maximum moisture removal takes place at about 80 °C. The moisture loss took place up to 200 °C followed by pyrolysis. Major weight loss due to the degradation of volatiles starts at around 180-205 °C for all the three heating rates. Up to 400 °C, weight loss is about 85 % of the total volatile matter. After rapid pyrolysis, relatively slow pyrolysis occurred over 400 °C. Finally, char is formed with the removal of most volatile matters. The weight fraction of the char to the total weights of the raw rice husk and sawdust are found to be 23 % and 26 % respectively, which is comparable to the results of the proximate analysis of the biomass. As reported [Myung *et al.* (2004), Lee *et al.* (2004), and Park *et al.* (2006)] hemicellulose, cellulose and lignin are decomposed at 150-300 °C, 275-300 °C and 250-500 °C, respectively. In the present study, TG and DTG curves divided into two regions. The first weight loss occurs due to the fast successive decomposition of hemicellulose and cellulose at 200-400 °C which is referred to as the active pyrolysis zone, and the second weight loss causes by the lignin decomposition. For all the three cases, the mass degradation patterns are found to be similar.

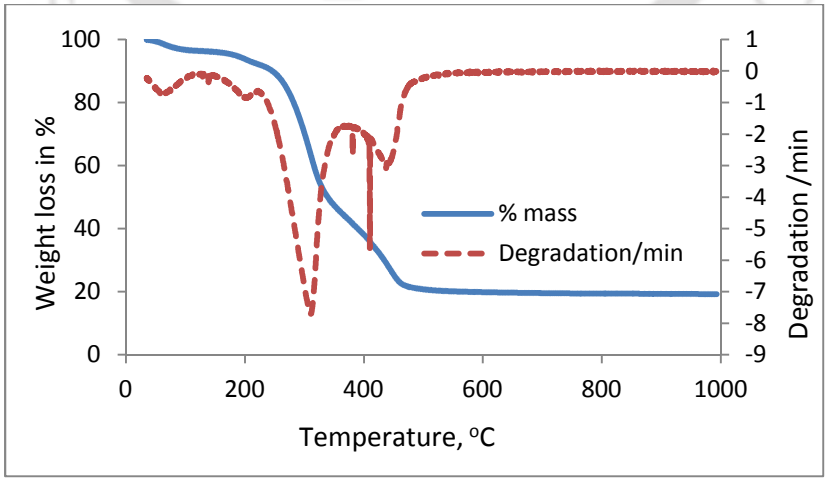

Fig.5.1 TG and DTG curve at 10 °C/min

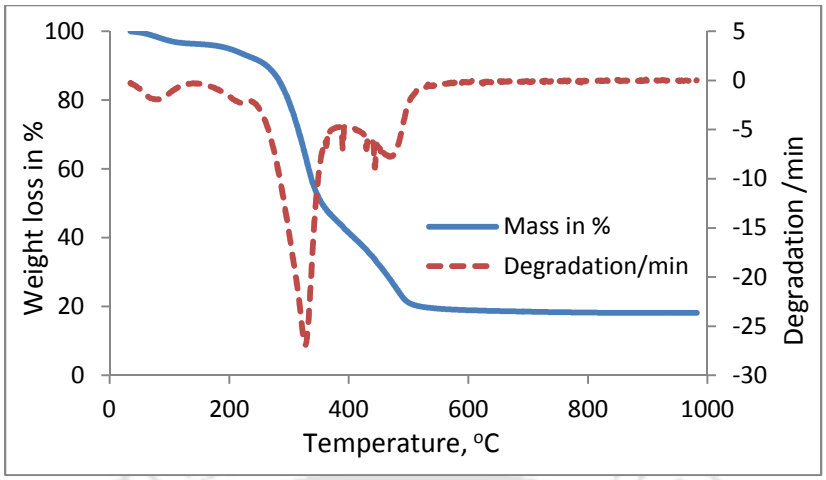

Fig.5.2 TG and DTG curve at 30 °C/min

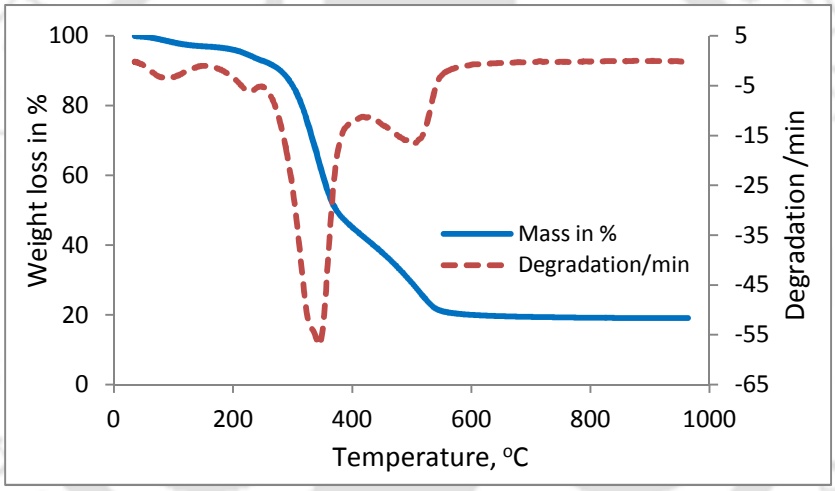

Fig.5.3 TG and DTG curves at 80 °C/min

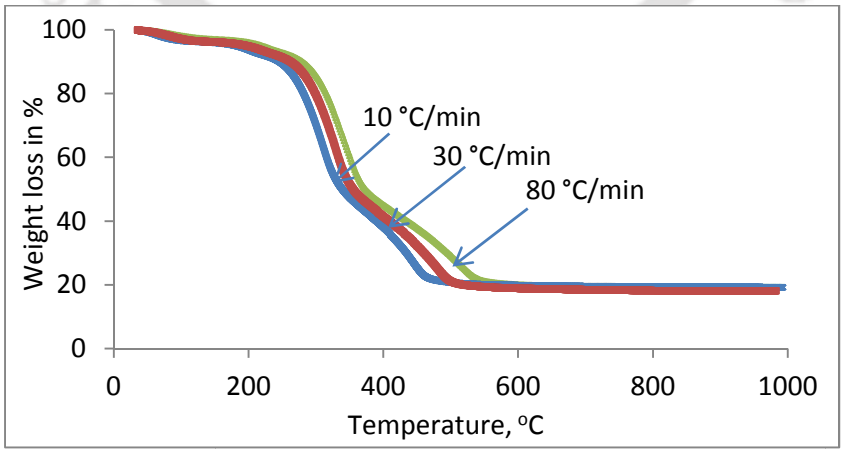

Fig.5.4 Comparison of mass degradation of rice husk

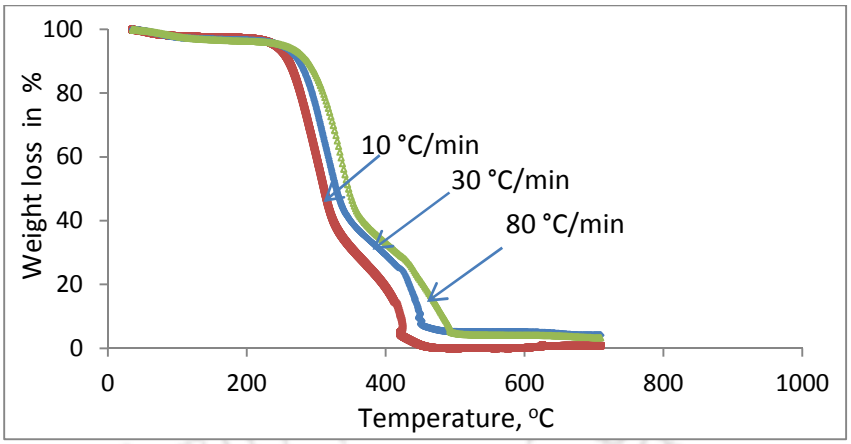

Fig.5.5 Comparison of mass degradation of sawdust

Values of the kinetic parameters evaluated for the two reaction zones are presented in the Table-5.1. In first reaction zone, a higher value of activation energy and pre-exponential factor has been found at 30 °C/min in comparison to the other two heating rates. It is also seen that, the variation of activation energy is not so significant as compared to pre-exponential factor in the case of rice husk. This observation is similar to the findings made by Niksa and Lau (1993). The value of pre-exponential factor is found to be higher at 30 °C/min than the other two heating rates in the case of second reaction zone. The order of reaction in the first reaction zone is found to be in the range of 0.360-0.518. Whereas, these values in the second reaction zone is found to be varies from 0.619 to 0.676 which is slightly higher than that of first reaction zone in case of rice husk. As depicted from the table, the values of kinetic parameters are higher in the case of sawdust as compared to rice husk.

Table-5.1 Kinetic parameters for biomass

Heating rate (°C/min)	**Kinetic parameters for rice husk**					
	First reaction zone			**Second reaction zone**		
	A **(min^{-1})**	***E*** **(kJmol^{-1})**	***n***	***A*** **(min^{-1})**	***E*** **(kJmol^{-1})**	***n***
10	12180	54.113	0.485	929.60	50.265	0.619
30	74120	58.839	0.518	1009.00	45.937	0.656
80	30570	51.917	0.360	339.52	37.053	0.676
	Kinetic parameters for sawdust					
10	3.948×10^{9}	111.827	0.751	712.200	47.534	0.699
30	8.050×10^{8}	100.467	0.906	2.655×10^{7}	101.463	0.780
80	1.540×10^{10}	112.025	0.684	159.530	31.269	0.170

A detail comparison of values of activation energy, pre-exponential factor and order of reaction of rice husk with the published results [Mansaray and Ghaly (1999), Ozawa (1965), Coats and Redfern (1964)] is presented in Table-5.2. As observed in the table, the kinetic parameters of first reaction zone in the present work are found to be lower than that of the other three finding, however activation energy and order of reaction found in the second reaction zone is found to be higher than the reported literature. The value of pre-exponential factor in the second reaction zone found in the present investigation is close to the other three reported findings. It is also seen that, the TGA of the reported literature were carried out at different environmental conditions viz. nitrogen, air and pure oxygen. These variations of the values of the kinematic parameters may be attributed to the different environmental conditions used in TGA experiments, quality of rice husk sample, sample size and rate of heating. The proximate and ultimate analysis of rice husk and sawdust is presented in Table-5.3. Table-5.4 presents the data of cellulose, hemicelluloses and lignin content of rice husk.

Table-5.2 Comparison of kinetic parameters of rice husk

Biomass	**Particulars**	**First reaction zone**				**Second reaction zone**			
		Ozawa, 1965	**Coats-Redfern, 1964**	**Mansaray and Ghaly, 1999**	**Present result**	**Ozawa, 1965**	**Coats-Redfern, 1964**	**Mansaray and Ghaly, 1999**	**Present result**
Rice husk	Activation energy, E (kJ mol^{-1})	82.9	77.4	142.7	58.839	38.5	28.1	14.3	45.937
	Pre-exponential factor, A (min^{-1})	3.72 x 10^8	5.6 x 10^7	1.18 x 10^{14}	7.412 x 10^4	2.58 x 10^5	4.8 x 10^3	0.13 x 10^2	1.009 x10^3
	Order of reaction, n	---	---	0.7	0.518	---	---	0.2	0.656
	Heating rate	30 K/min	30 K/min	20 K/min	30 °C/min	30 K/min	30 K/min	20 K/min	30 °C/min
	Atmosphere used	N_2	N_2	Pure oxygen	air	N2	N2	Pure oxygen	air

Table-5.3 Proximate and ultimate analysis of biomass

Biomass	**Ultimate analysis (in %)**						**Proximate analysis in (%)**		
	C	**H**	**N**	**S**	**O**	**Cl**	**VM**	**FC**	**Ash**
Rice husk	35.10	4.80	0.29	<0.02	35.90	0.16	60.30	17.00	22.70
Sawdust	48.5	6.4	0.1	0.3	44.6	---	77.0	19.9	0.7

Table-5.4 Cellulose, hemicellulose and lignin content of rice husk (dry basis in %)

Cellulose	Hemicellulose	Lignin
31.3	24.3	14.3

5.4 Prediction of TG curves

Degradation of mass with temperature obtained from TG curve is validated numerically. In order to predict the TG curve, the kinetic parameters of both first and second reaction zones evaluated by using multiple regression analysis. 4th order Runge-Kutta in MATLAB® software was used to predict the TG curve. The comparison of experimental and numerical curves at 10, 30 and 80 °C/min for rice husk and sawdust are shown in Figs.5.6 through 5.8 and Figs.5.9 through 5.11, respectively. Similar patterns of both predicted and experimental curves have been found in all the heating rates for both the biomasses. It is also observed that, at lower heating rate (Figs.5.6 and 5.9) difference in weight loss with respect to temperature is higher between the experimental and predicted results. However, at higher heating rate, predicted results are very close to the experimental results in both first and second reaction zones.

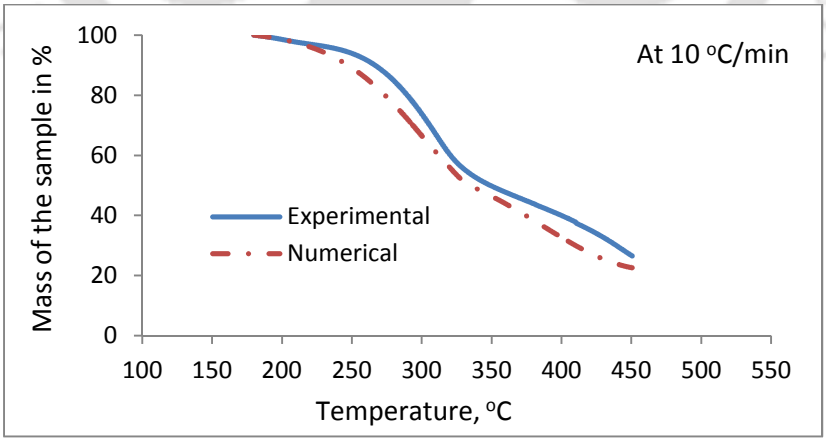

Fig.5.6 Comparison of experimental and numerical results at 10 °C/min (rice husk)

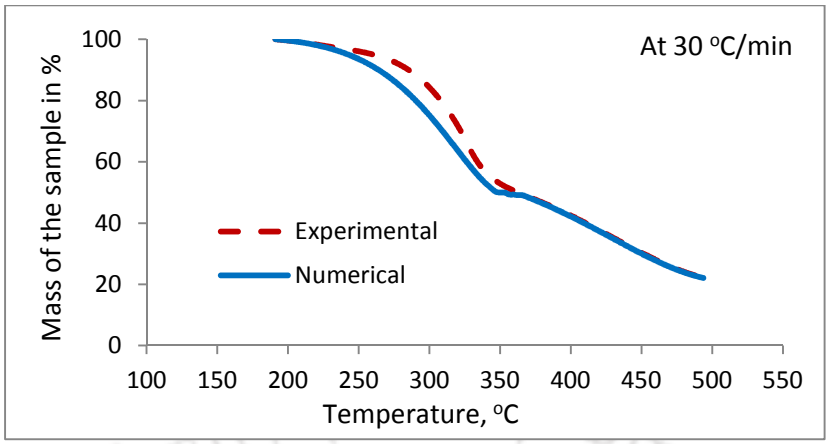

Fig.5.7 Comparison of experimental and numerical results at 30 °C/min (rice husk)

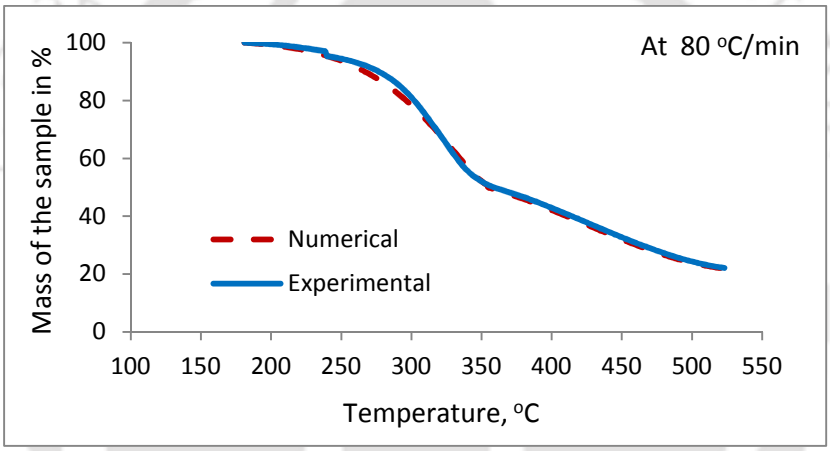

Fig.5.8 Comparison of experimental and numerical results at 80 °C/min (rice husk)

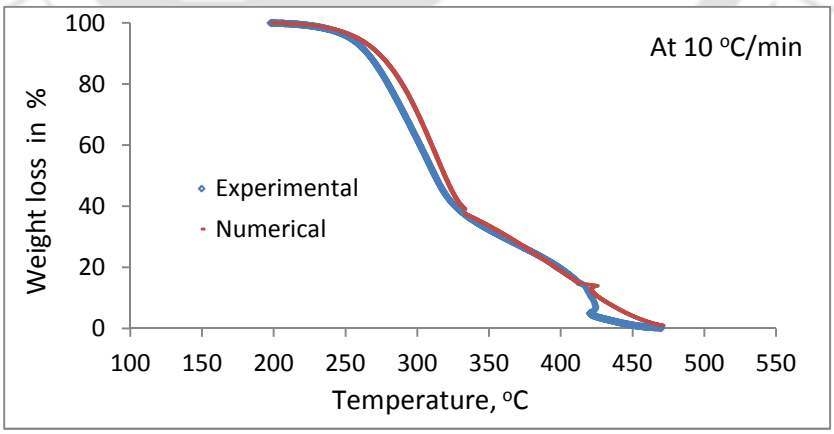

Fig.5.9 Comparison of experimental and numerical results at 10 °C/min (sawdust)

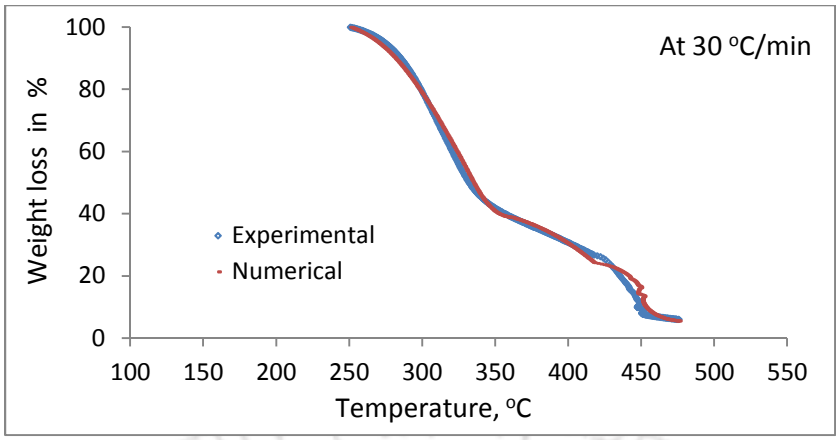

Fig.5.10 Comparison of experimental and numerical results at 30 °C/min (sawdust)

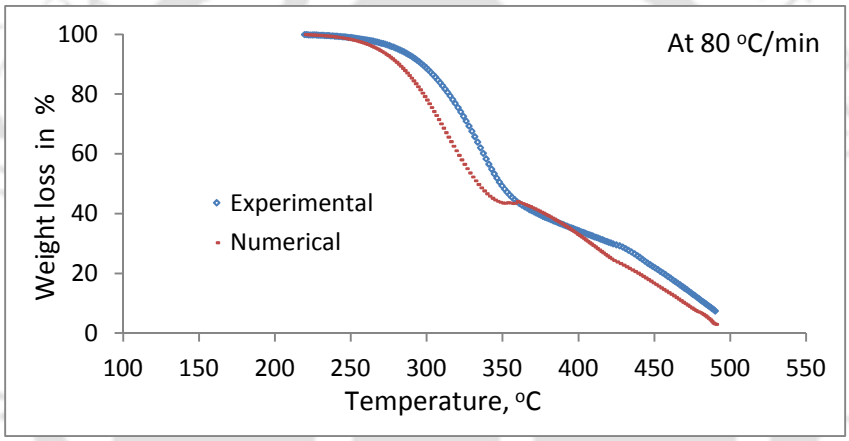

Fig.5.11 Comparison of experimental and numerical results at 80 °C/min (sawdust)

5.5 Transient thermal model and its prediction

The thermal response of rice husk undergoing decomposition has also been modelled by using an one dimensional (1-D) transient thermal model with an nth order approximation for the rate of decomposition. The kinetic parameters and the heat of decomposition for both the reaction zones and thermal properties are taken as input to the model. The model was tested by measuring the transient temperature profiles during decomposition using Heisler chart. The specific heat and thermal conductivity of the biomass were taken from literature [Mishra *et al.* (1986), and Jha and Singh (2007)] and the values of heat of decomposition and kinetic parameters were taken from in-house experimental. Table-5.5 presents the thermodynamic properties used in the model as well as while using Heisler chart. In the present case, the length of the sample is considered to

be 10 mm and temperature is predicted throughout the length. The sketch of the measuring arrangement of temperature profile along the length of the rice husk sample is presented in the Fig.5.12. The boundary conditions applied at x = 0 and x = L are also shown in the figure. Figures 5.13 and 5.14 show the transient temperature distribution during pyrolysis and gasification along the length of the sample at heat transfer coefficient 20 W/m^2-K without considering heat of formation. Figure 5.13 shows the temperature distribution at 20 discrete x/L values, while Fig.5.14 presents the temperature distribution at time 10s, 100s and up to 1500 seconds in steps of 100 seconds. As seen from the figures, no significant variation of temperature with time has been observed after 1000 seconds. As Fourier number is a function of thermal diffusivity, time and the length of the specimen, the results of the model are validated by using Heisler chart at different Fourier number (non-dimensional time), which is presented in Fig.5.15. Transient temperatures were evaluated at eight values of Fourier number i.e. at eight different times such as 10, 25, 60, 120, 240, 480, 600 and 960 seconds, respectively. As seen from the figure, Hesiler results give accurate prediction to the model results.

Table-5.5 Thermodynamic properties of rice husk

[Mishra *et al.* (1986), and Jha and Singh (2007)]

True Density, ρ (kg/m^3)	Specific heat, C_p (kJ/kg °C)	Thermal conductivity, K, (W/m °C)	Thermal diffusivity, $\alpha = \frac{K}{\rho C_p}$ (m^2/s)
1030.93	1.69071	0.0523	3.0×10^{-8}

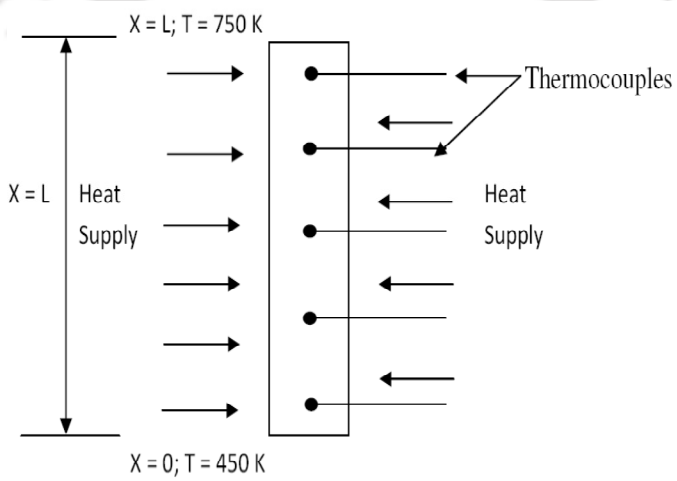

Fig.5.12 Sketch of the numerical sample with boundary condition

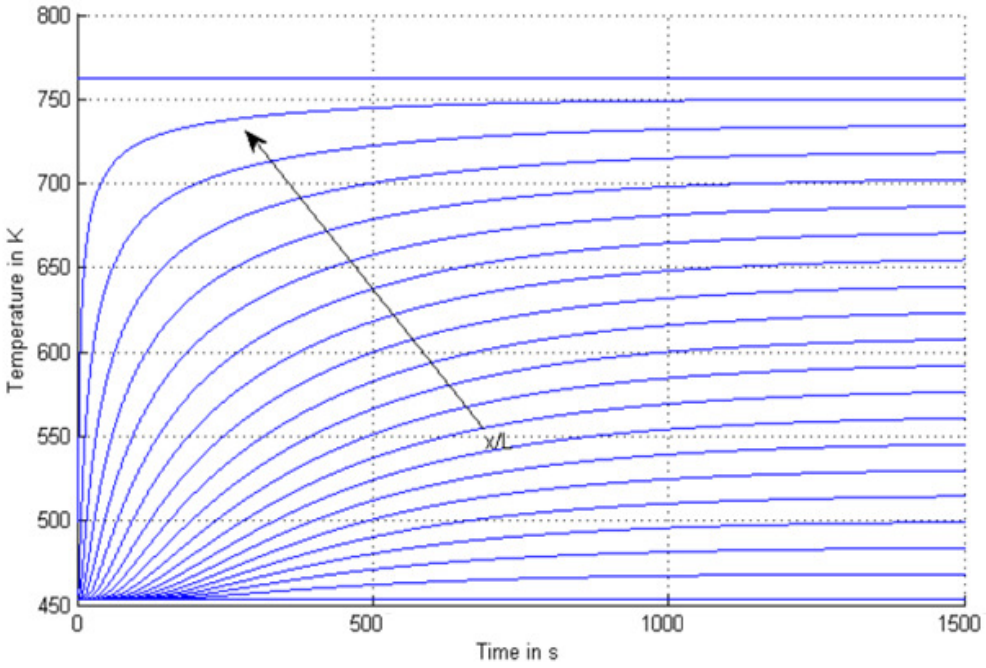

Fig.5.13 Variation of temperature with time at 20 W/m^2-K without heat of formation

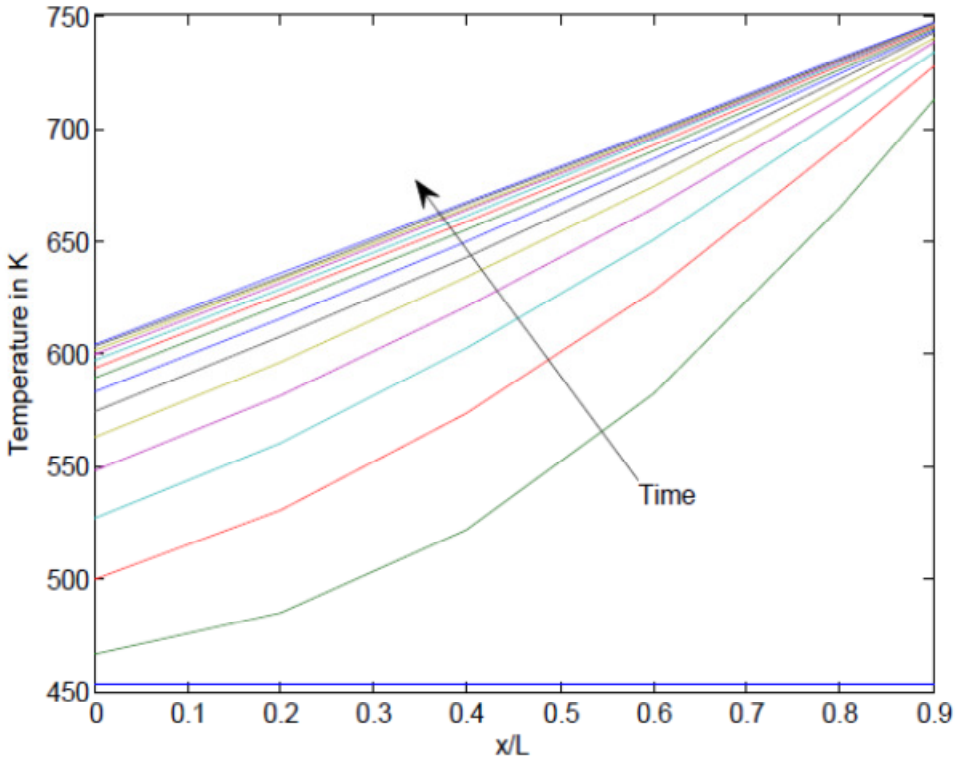

Fig.5.14 Temperature distributions along the length at 20 W/m^2-K

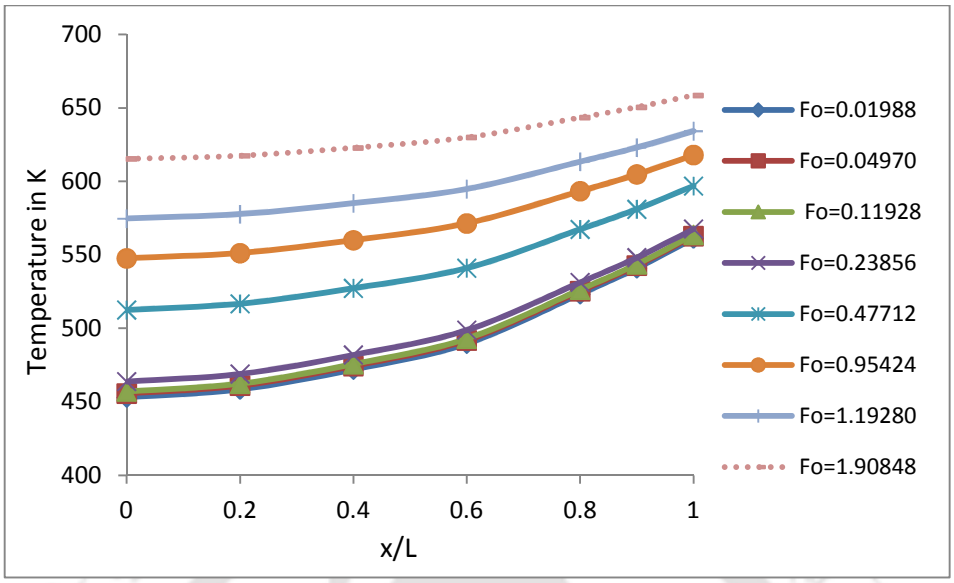

Fig.5.15 Temperature distributions at varied time interval at heat transfer coefficient 20 w/m^2-K

Figures 5.16-5.19 show the transient temperature distribution during pyrolysis and gasification along the length of the sample at heat transfer coefficient 20 W/m^2-K by considering heat of formation. Different variation of temperature has been found when heat of formation is considered (Figs.5.16, 5.18, 5.19). This variation may be because of endothermic and exothermic reactions taking place during pyrolysis and gasification processes. The positive and negative values of heat of formation during these processes makes the temperature profile different from the profile observed without considering heat of formation. Figure 5.16 shows the temperature distribution at 20 discrete x/L values (between 0 to 1). Figure 5.17 shows the variation of temperature along the length of the sample up to 430 seconds from the start of pyrolysis. As seen in the figure, the temperature increases with time up to 430 seconds. With further increase of time step, the temperature variation shows different patterns (Figs.5.18 and 5.19) because of exothermic and endothermic chemical reactions taking place during gasification. Similar temperature variations were observed at the centre of the specimen for both the models i.e. model with and without considering heat of formation.

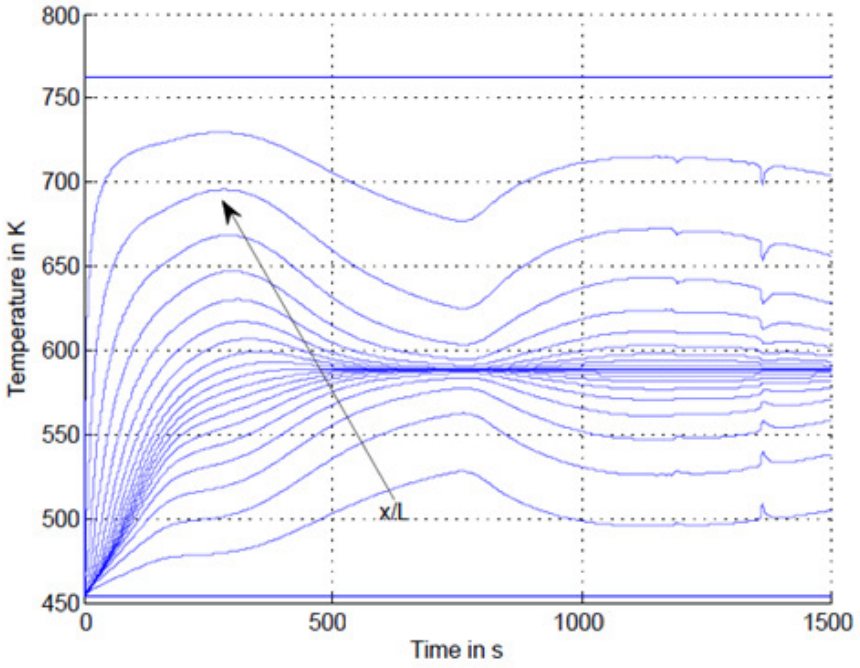

Fig.5.16 Variation of temperature with time at 20 W/m^2-K with heat of formation

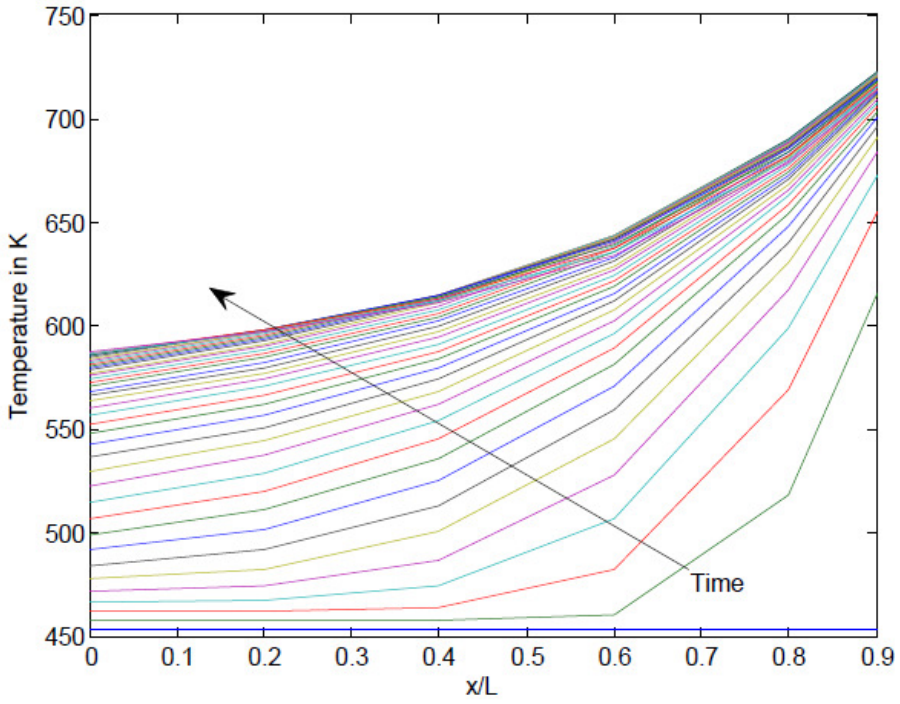

Fig.5.17 Variation of temperature along the length of the sample up to 430 seconds

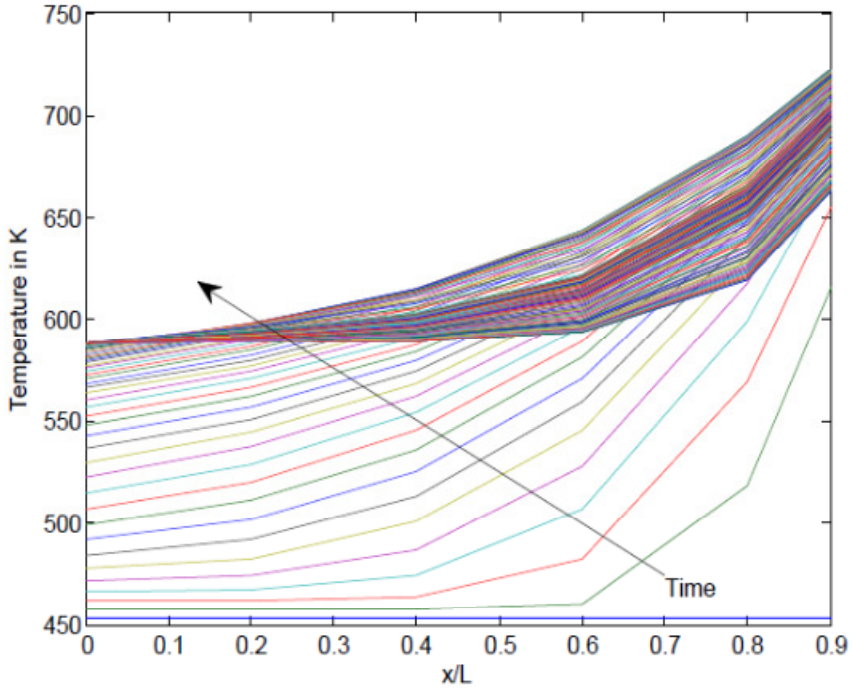

Fig.5.18 Variation of temperature along the length of the sample

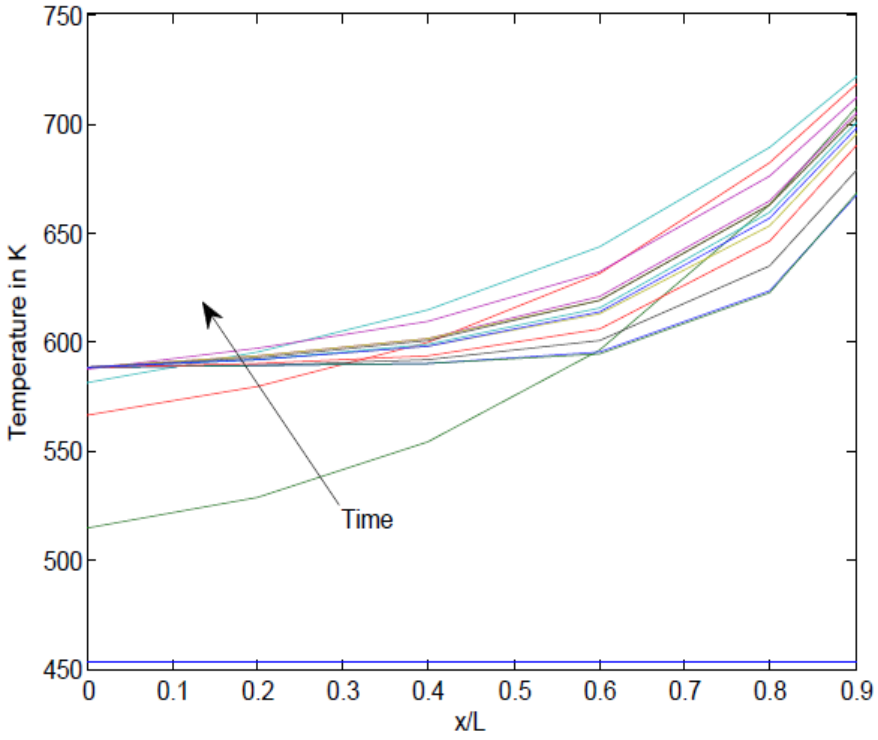

Fig.5.19 Selected temperature profiles along the length of the sample

5.6 Characteristics of other biomass

Similar studies were carried out for other three different types of biomass namely rice straw, water hyacinth and tea waste. The kinetic parameters were evaluated based of the TG analysis by using multi-variable regression analysis. The result of the analysis with temperature ranges of both active pyrolysis zone (first reaction zone) and second reaction zone are presented in appendix-IX.

5.7 Summary of the chapter

This chapter reports the thermogravimetric (TG) analysis and DTG of five different biomass samples evaluated at three different heating rates of 10, 30 and 80 °C/min. From the analysis, it has been found that, the major weight loss due to the degradation of volatiles starts at around 180-205 $^{\circ}$C for all the three heating rates. Up to 400 $^{\circ}$C, weight loss is about 85 % of the total volatile matter. After rapid pyrolysis, relatively slow pyrolysis occurred over 400 $^{\circ}$C. Finally char is formed with the removal of most of the volatile matters. At higher heating rate, predicted results are found to be very close to the experimental results in both first and second reaction zones. Kinetic parameters of all the biomass samples are also evaluated. These values are presented in the appendix-IX. The rice husk is used as a representative biomass fuel for TG and thermal analysis which is presented in this chapter. As sawdust is used as blending fuel when studying the hydrodynamic and heat transfer characteristics in the CFB units, hence the TGA curves along with the numerical validation of sawdust is presented along with rice husk. In the next chapter results of the experiments carried out in the cold CFB unit has been presented and discussed.

Chapter – 6

RESULTS AND DISCUSSION - COLD CFB BED UNIT

6.1 Introduction

This chapter reports the results of the experiments carried out to investigate the bed hydrodynamics along the height of the riser and heat transfer coefficient at the upper splash region of the riser at different operating conditions. The effect of operating parameters such as solid inventory, superficial velocity, and operating pressure were studied in separate subsections. The study of bed hydrodynamics and heat transfer characteristics at different biomass blending ratios and weight compositions are also presented. Some of the significant results are compared with the earlier published results.

6.2 Experiments on cold CFB unit

In the chapter, the effects of various parameters such as superficial velocity, particle size, solid inventory, and operating pressure on bed hydrodynamics and heat transfer in a pressurized circulating fluidized bed (PCFB) has been studied. Three particle sizes of sand having mean particle diameter of 278, 307 and 469 μm are considered. Experiments have been conducted at five different solid inventories such as 400, 500, 600, 800, and 1000 g, and at three different operating pressures of 1, 3 and 5 bar. All the above studies have been made at three different superficial velocities of 6, 7 and 8 m/s. In some of the investigations, experiments were also performed at a superficial velocity of 5 m/s. The hydrodynamic along the riser height and heat transfer characteristics along the heat transfer probe at various proportion of blending of biomass such as sawdust with sand have also been investigated. These experiments have been conducted at the sawdust blending of 2.5 %, 5.0 %, 7.5 %, 12.5 %, 15.0 % and 20.0 % in sand and at two different weight composition ratios. Effects of solid circulation rate have also been studied. Particle size of biomass considered in the present study is 407 μm. The overall uncertainties in calculating heat transfer coefficient and solid circulation rate are found to be ± 3.90 % and ± 5.32 %, respectively.

6.3 Investigation of bed hydrodynamics

Static pressures and hence bed voidage were measured along the riser height at 6 (six) different locations such as 120 mm, 192.5 mm, 370 mm, 495 mm, 970 mm and 1570 mm above the distributor plate. Suspension densities at those points were also calculated. Effect of particle size, superficial velocity, solid and biomass inventory and operating pressure on bed voidage and suspension density have also been studied and discussed.

6.3.1 Variation of bed voidage profile with pressure, inventory and particle size

The variation of bed voidage along the height of the PCFB riser operating at three different operating pressures and at four different inventories of 400 g, 600 g, 800 g and 1000 g without blending of biomass are shown in Figs.6.1 through 6.4. In all the cases, the S-shaped bed voidage profile has been observed. The S-shaped profile of bed voidage in the CFB riser is due the particle diffusion in the axial direction as explained by Kwauk *et al.* (1986) and also the gas velocity near the wall is considerably lower than that in the core of the bed as demonstrated by Gupta and Nag (2002), and Basu (2006). It is also observed that, as the operating pressure and solid inventory increase, the bed voidage decreases at all the measured points and this is more significant at the top of the riser exit. The bed voidage is observed to be lowest ($\varepsilon = 0.55$ and at about 370 mm from the distributor plate) at the solid inventory of 600 g and at the operating pressure of 5 bar. At higher pressure, the drag force on the particles increases which results in increase in particle concentration at the upper splash region of the riser, hence the bed voidage decreases at the exit of the riser with increase in pressure. The uncertainty in calculating bed voidage at different inventories and operating pressures are tabulated in the appendix-X.

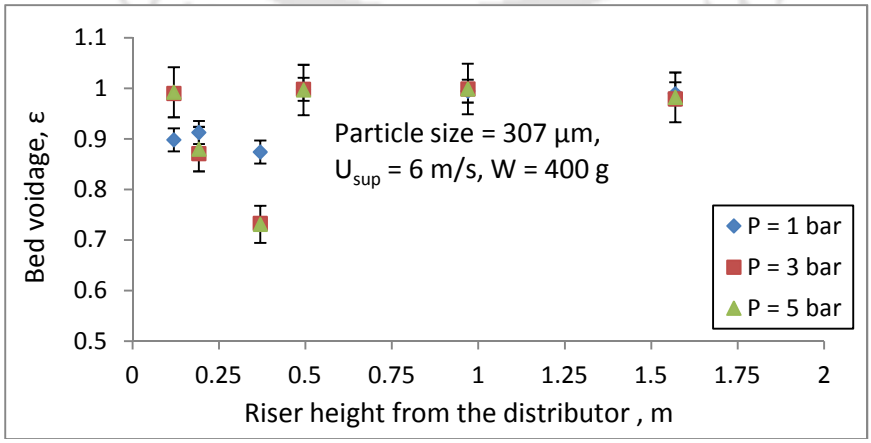

Fig. 6.1 Variation of bed voidage with operating pressure at W = 400 g

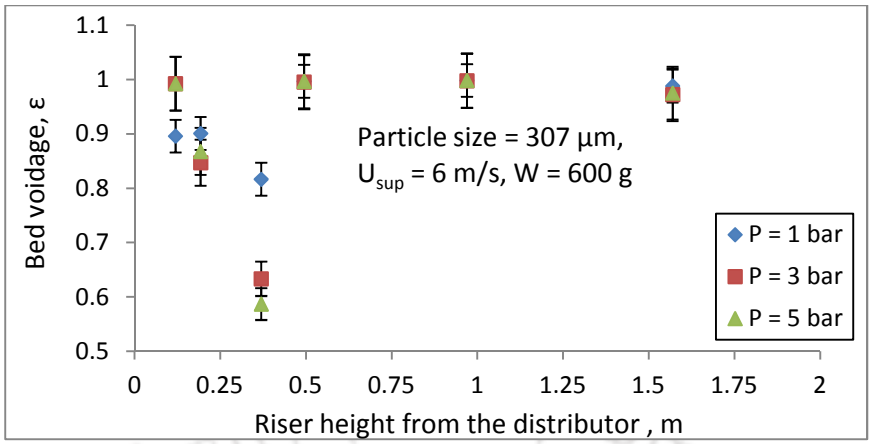

Fig.6.2 Variation of bed voidage with operating pressure at W = 600 g

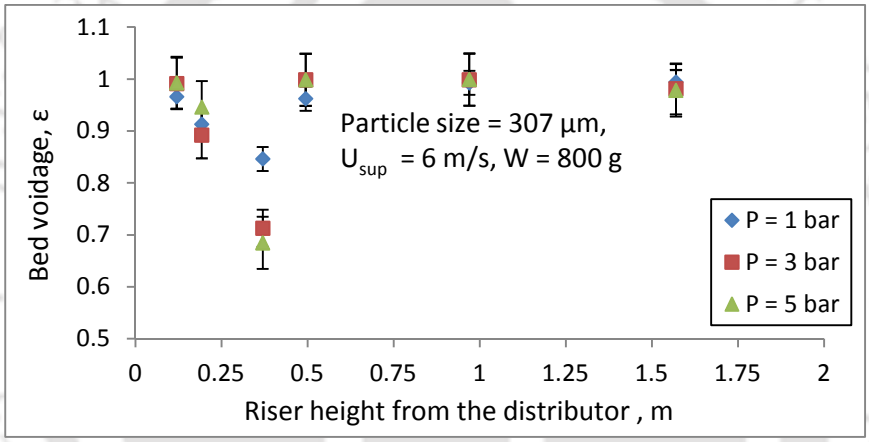

Fig.6.3 Variation of bed voidage with operating pressure at W = 800 g

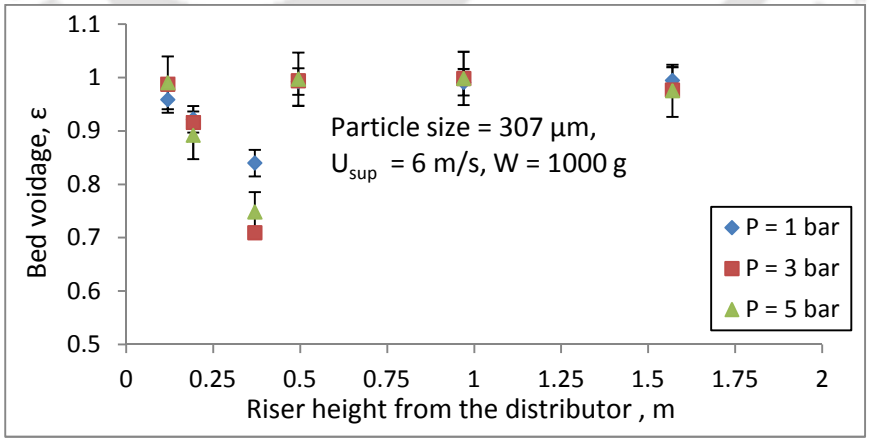

Fig.6.4 Variation of bed voidage with operating pressure at W = 1000 g

The comparison of bed voidage along the height of the riser with system pressure at four different percentages blending of biomass in sand at U_{sup} = 6 m/s are shown in Figs.6.5 through 6.8. Standard errors are also shown to represent the uncertainties of the data point in the same figures by error bars. In all the cases, it has been found that with an increase in pressure the bed voidage decreases. However, with an increase in percentage addition of biomass, the bed voidage increases at the bottom of the CFB riser for example, at 20.0 % biomass blend and at 0.195 m from the distributor, it is observed to be about 0.9 than 0.84 at 2.5% biomass blend. At the higher pressure, the bed appears to be homogenous, with the void of solids phase and emulsion phase becoming practically indistinguishable, and entrainment increases at the exit. This is probably the reason why bed voidage decreases at the exit of the riser with an increase in pressure.

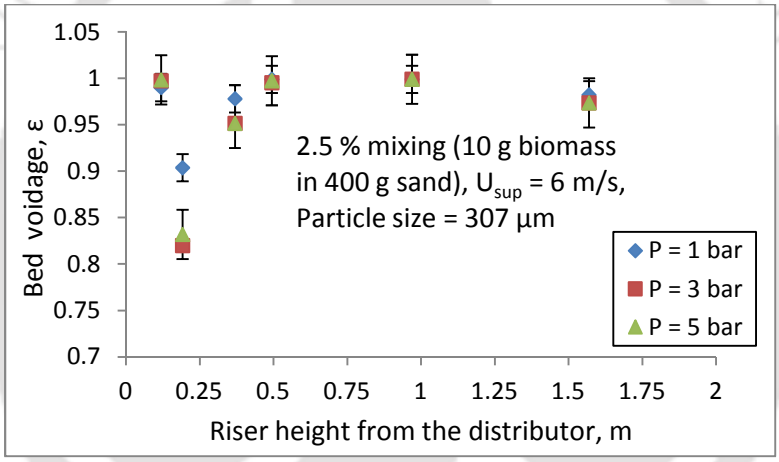

Fig.6.5 Bed voidage profile along the height of the riser with 2.5 % biomass blend

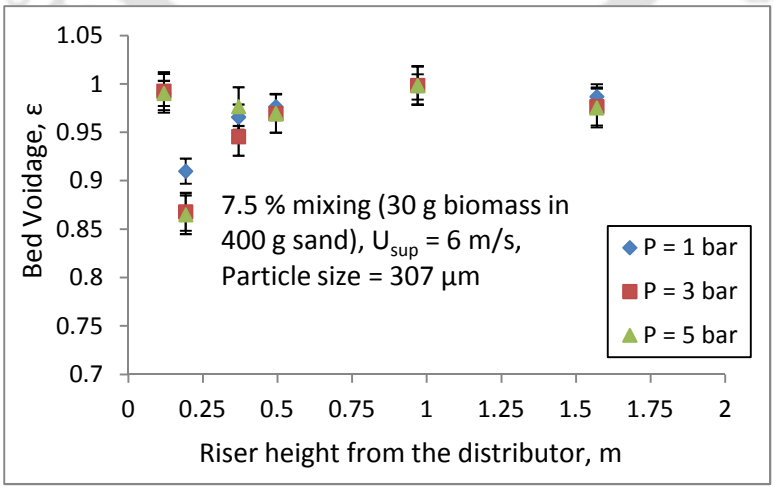

Fig.6.6 Bed voidage profile along the height of the riser with 7.5 % biomass blend

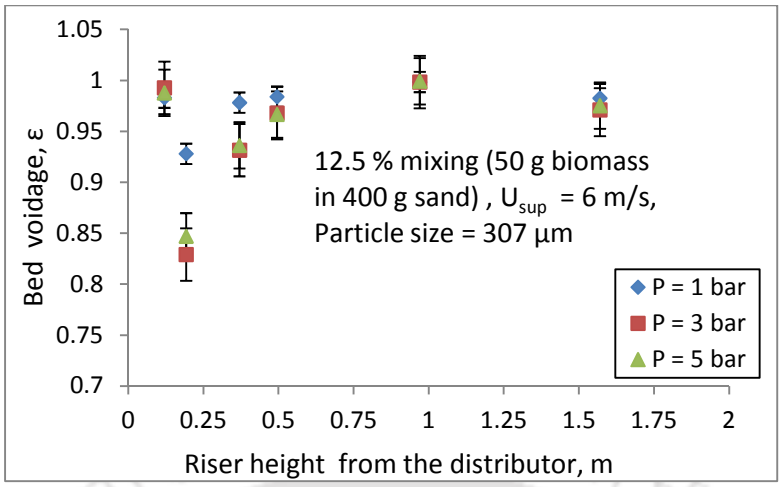

Fig.6.7 Bed voidage profile along the height of the riser with 12.5 % biomass blend

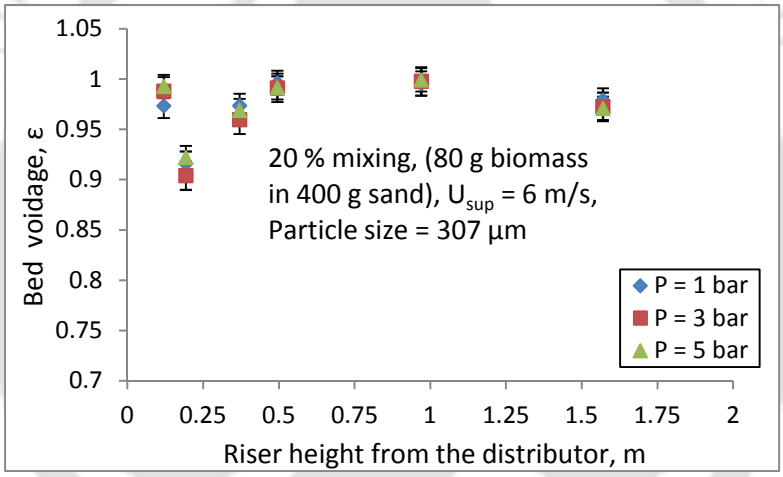

Fig.6.8 Bed voidage profile along the height of the riser with 20.0 % biomass blend

The comparison of bed voidage profile along the riser height at three different superficial velocities such as 8 , 7 and 6 m/s and at three different operating pressures 1, 3 and 5 bar in the case of 2.5 % blending of saw dust in sand are shown in Figs.6.9a, 6.9b and 6.9c respectively. Bed voidage along the height of the riser at operating pressure, P = 1 bar is found to be very close to each other at all the three superficial velocities (Fig.6.9a). As the pressure increases, the bed voidage decreases at all the measured points. It is also observed that at U_{sup} = 6 m/s, the bed voidage is found to be lowest as compared to 7 and 8 m/s at operating pressures of 3 and 5 bar (Figs.6.9b and 6.9c).

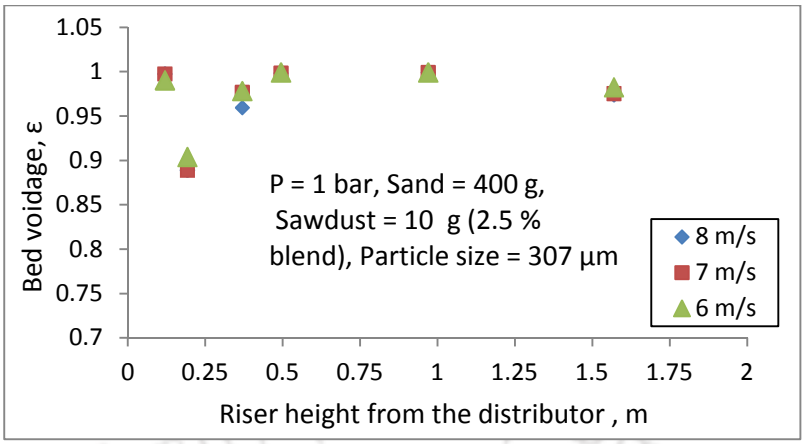

Fig.6.9a Variation of bed voidage profile at P = 1 bar and at 2.5 % biomass blend

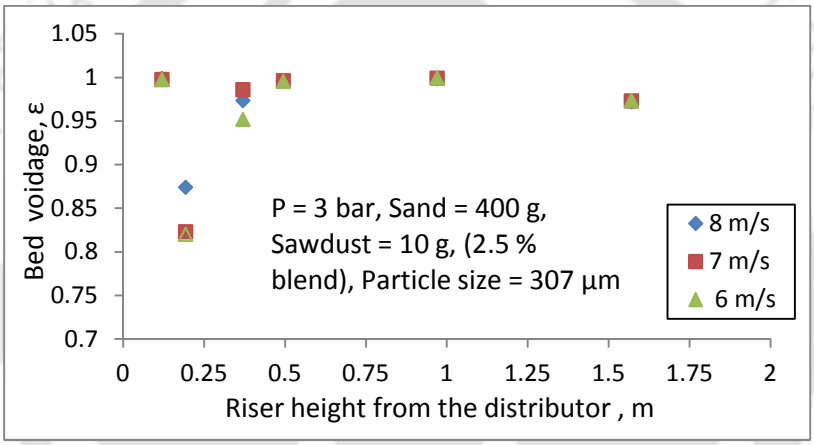

Fig.6.9b Variation of bed voidage profile at P = 3 bar and at 2.5 % biomass blend

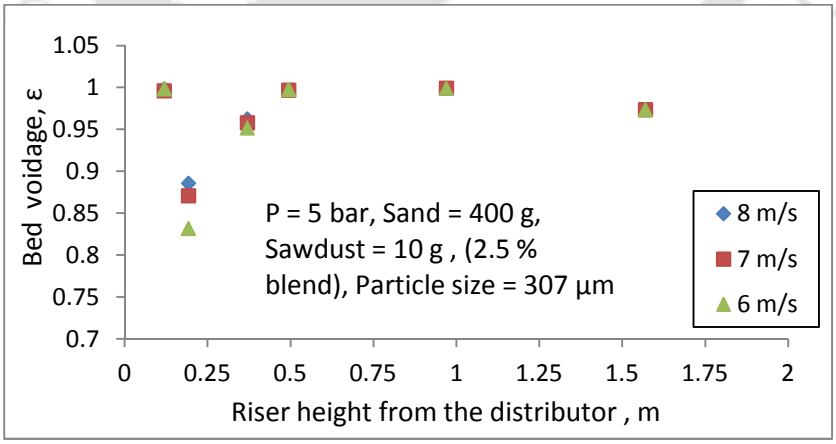

Fig.6.9c Variation of bed voidage profile at P = 5 bar and at 2.5 % biomass blend

The comparison of bed voidage profile along the riser height at three different superficial velocities such as 6 , 7 and 8 m/s and at three different operating pressures 1, 3 and 5 bar in the case of 12.5 % blending of saw dust in sand are shown in Figs.6.10a, 6.10b and 6.10c respectively. Similar variation of bed voidage along the height of the riser has been found as in the case of 2.5 % sawdust blend in sand. As the pressure increases, the bed voidage decreases at all the measured points. It is also observed that at U_{sup} = 6 m/s, the bed voidage is found to be lowest as compared to 7 and 8 m/s at operating pressures of 3 and 5 bar (Figs.6.10b and 6.10c).

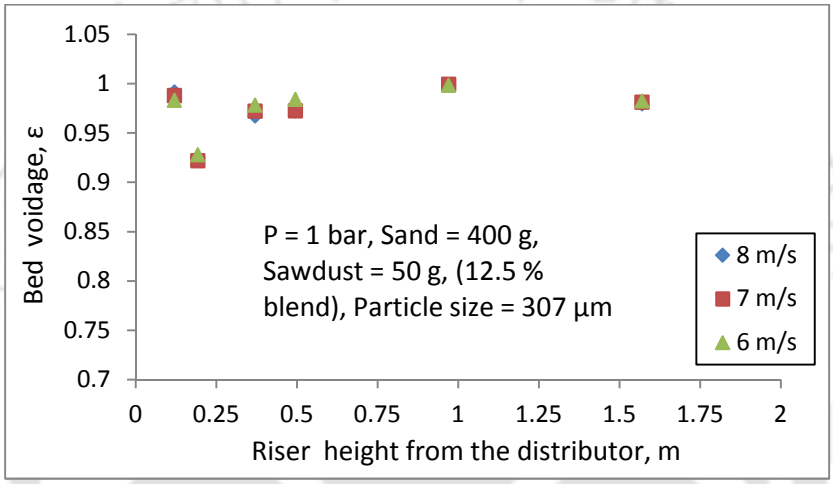

Fig.6.10a Variation of bed voidage profile at P = 1 bar and at 12.5 % biomass blend

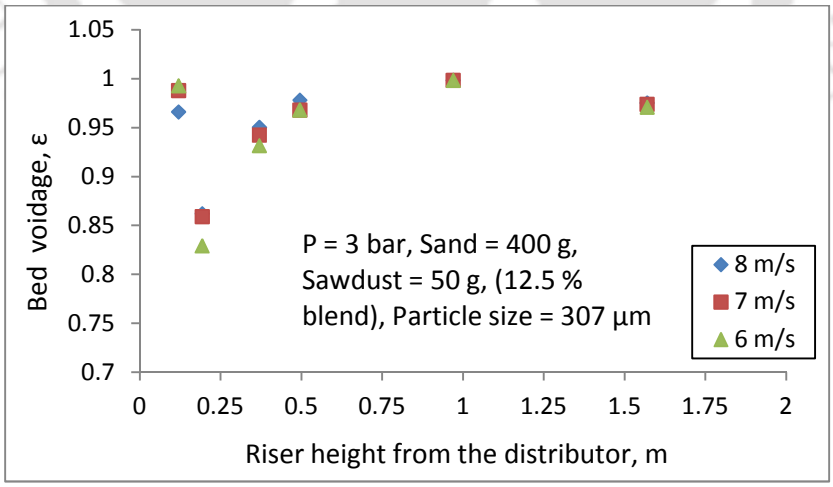

Fig.6.10b Variation of bed voidage profile at P = 3 bar and at 12.5 % biomass blend

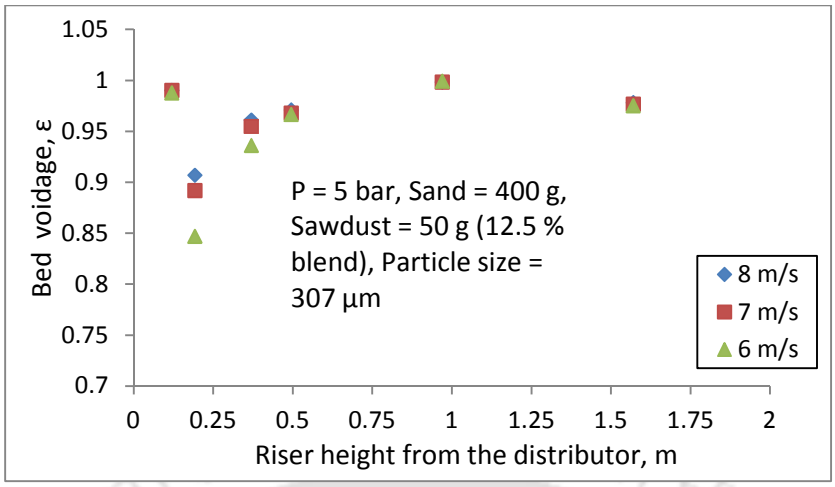

Fig.6.10c Variation of bed voidage profile at P = 5 bar and at 12.5 % biomass blend

The comparison of variation of bed voidage along the height of the riser at three different particle sizes and at two different operating pressures of 3 and 5 bar are shown in Figs.6.11 and 6.12 respectively. It has been observed that, the particle bed voidage decreases with the decrease in particle size as the concentration of particle increases at the exit of the riser.

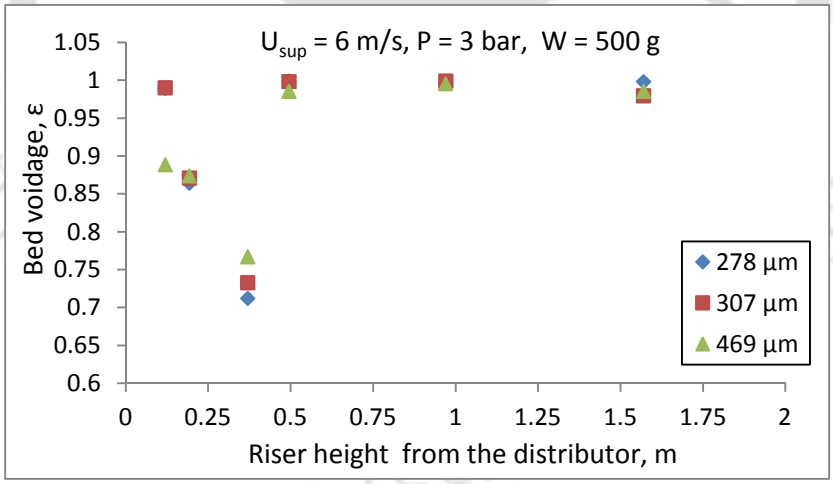

Fig.6.11 Comparison of bed voidage with particle size at P = 3 bar and W = 500 g

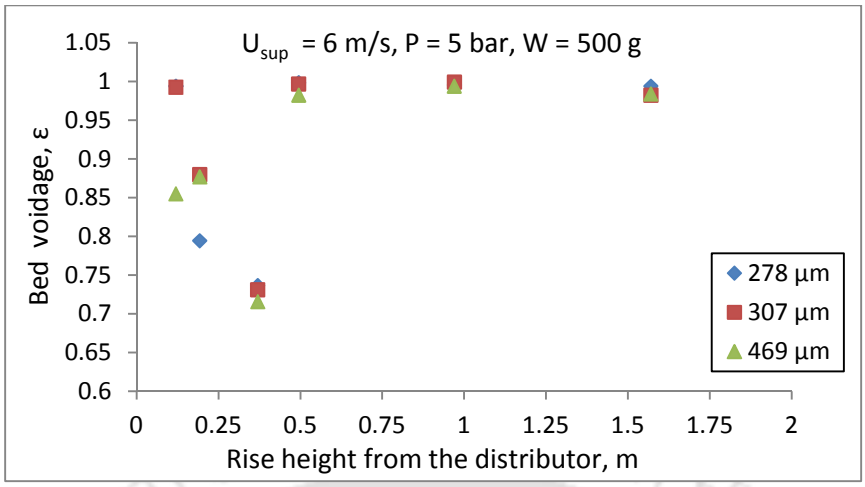

Fig.6.12 Comparison of bed voidage with particle size at P = 5 bar and W = 500 g

Figures 6.13 and 6.14 present the variation and comparison of bed voidage at operating pressures 1 and 5 bar, respectively. The comparisons were made at two different weight composition ratios and at a superficial velocity of 5 m/s. In these conditions percentage blending of biomass is maintained at 15.0 %. As seen, the bed voidage is first decreases and then increases, before it decreases at the exit of the riser which may be better represented by S-shaped bed voidage profile. With the increase of pressure, the bed voidage is found to decrease at the exit of the riser. This may be due to the increase in concentration of particles at the riser exit. This is found to be more in the case of weight composition ratio (B/S) of 90:600.

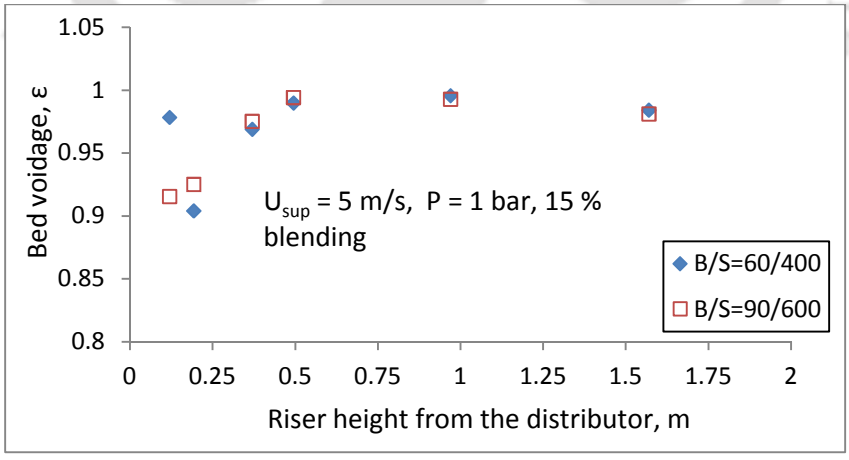

Fig.6.13 Comparison of variation of bed voidage along the height of the riser at P = 1 bar

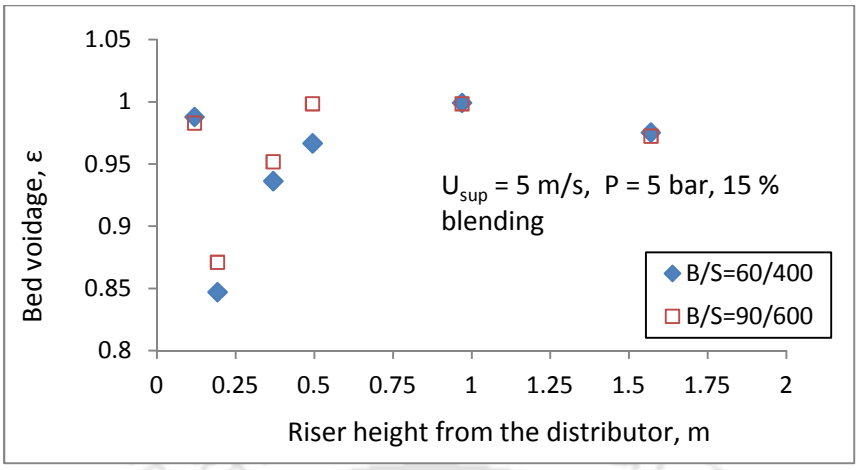

Fig.6.14 Comparison of variation of bed voidage along the height of the riser at P = 5 bar

6.3.2 Effect of operating parameters on suspension density

The comparison of suspension density along the height of the riser with solid inventory at operating pressures of 1, 3 and 5 are shown in the Figs.6.15 through 6.17. From these figures it is seen that with the increase in pressure, the suspension density increases along the height of the heat transfer probe at all the inventories. Higher concentration of sand particles at higher bed inventories and higher operating pressure may be the reason why suspension density becomes more. Similar observation has already been reported by Basu and Nag (1987), and Basu and Nag (1996).

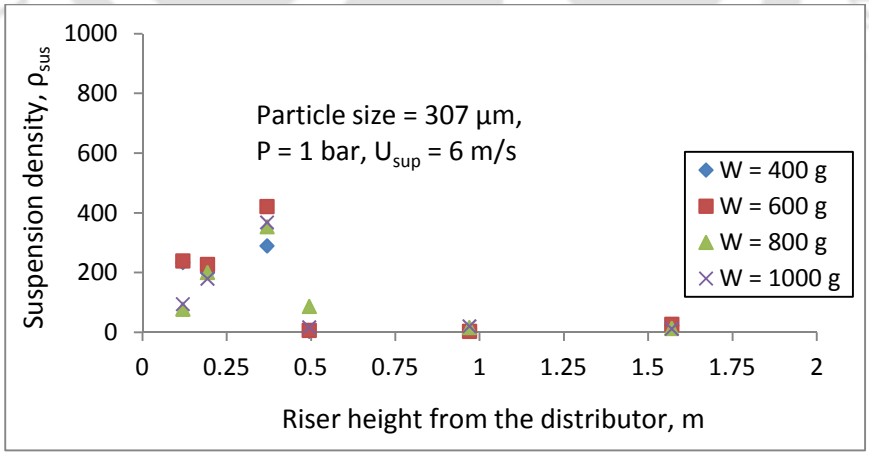

Fig.6.15 Comparison of suspension density with bed inventory at P = 1 bar

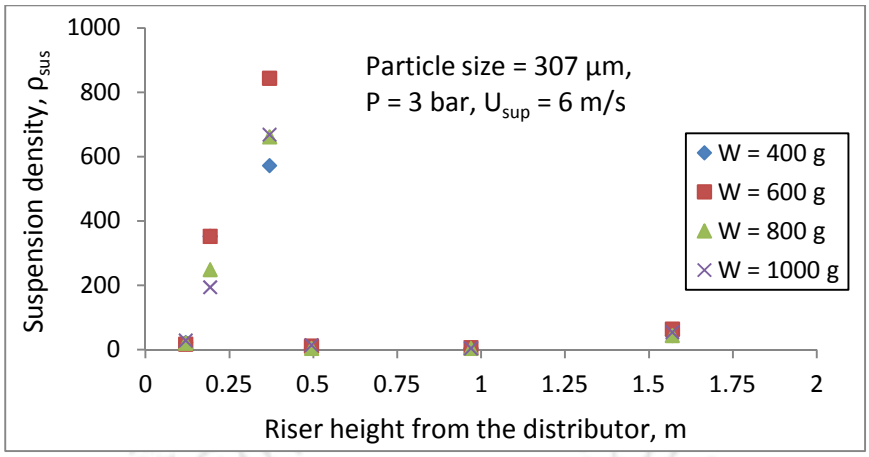

Fig.6.16 Comparison of suspension density with bed inventory at P = 3 bar

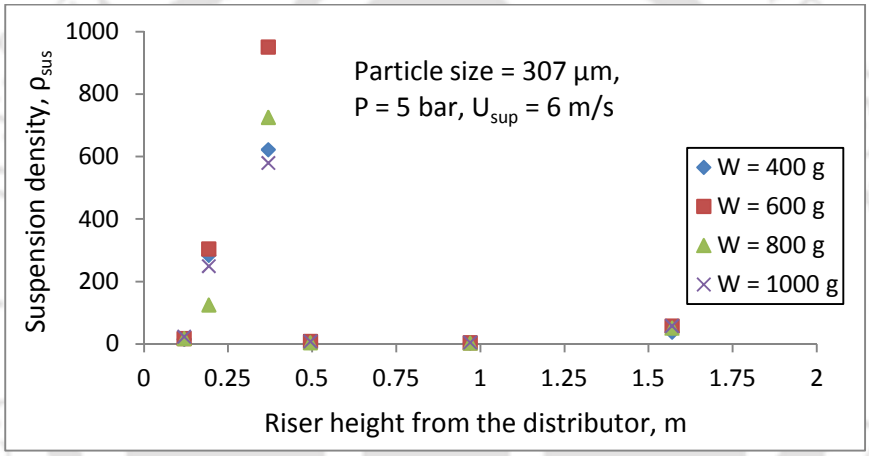

Fig.6.17 Comparison of suspension density with bed inventory at P = 5 bar

The suspension density plays a key role on the quality heat transfer along the riser of a CFB. This can be controlled by adjusting the solid circulation rate and the superficial velocity (Basu, and Cheng, 1996). The variation of bed suspension density with pressure along the bed height at U_{sup} = 6 m/s is shown in Figs.6.18 through 6.22. The suspension density increases as the pressure increases at a particular superficial velocity. As seen from the figures, suspension density is higher at the lower portion of the bed, which then, decreases upto the top middle part, and then starts increasing to the exit of the riser. As much as 480 kg/m^3 suspension density at the lower part (0.195 m from the distributor) and 44 kg/m^3 (1.57 m from the distributor) at the top of the riser has been observed at U_{sup} = 6 m/s and at P = 5 bar without mixing of biomass (Fig.6.18). As the % blending of biomass increases, the suspension density decreases to about 230 kg/m^3 at the

bottom (0.195 m from the distributor) and increases above 50 kg/m^3 at 1.57 m from the distributor under similar operating conditions at 20% biomass blend (Fig.6.22).

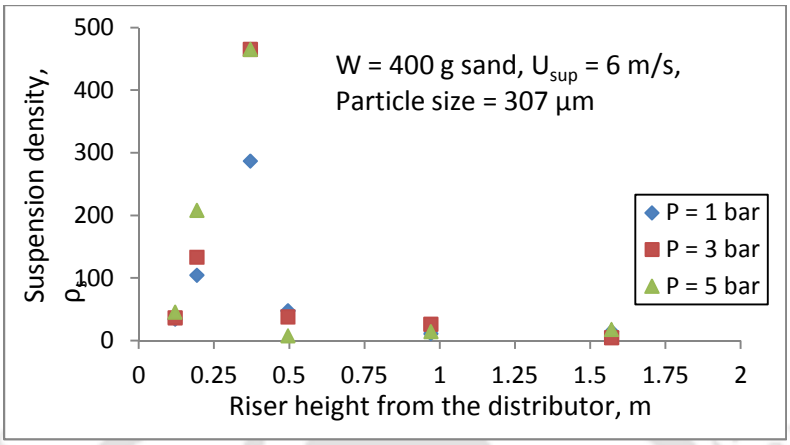

Fig.6.18 Variation of suspension density along the riser without biomass blend

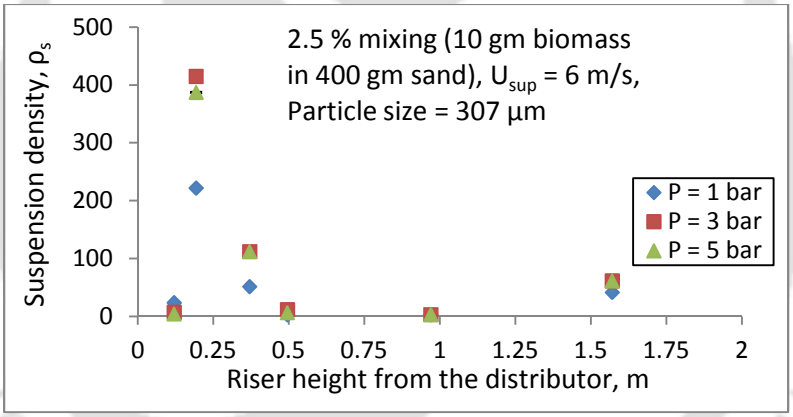

Fig.6.19 Variation of suspension density along the riser at 2.5 % biomass blend

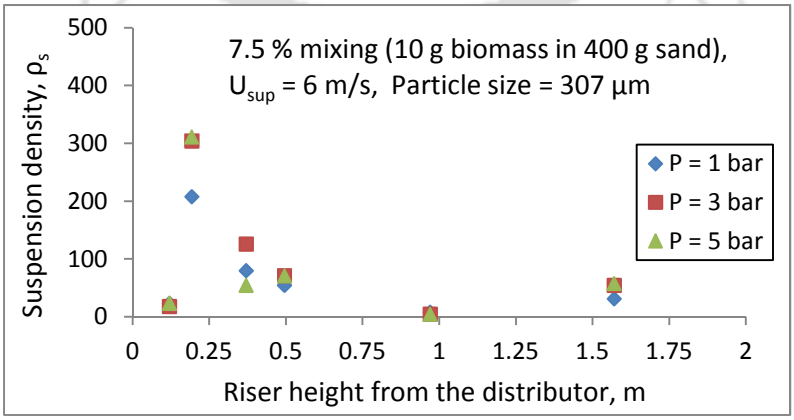

Fig.6.20 Variation of suspension density along the riser at 7.5 % biomass blend

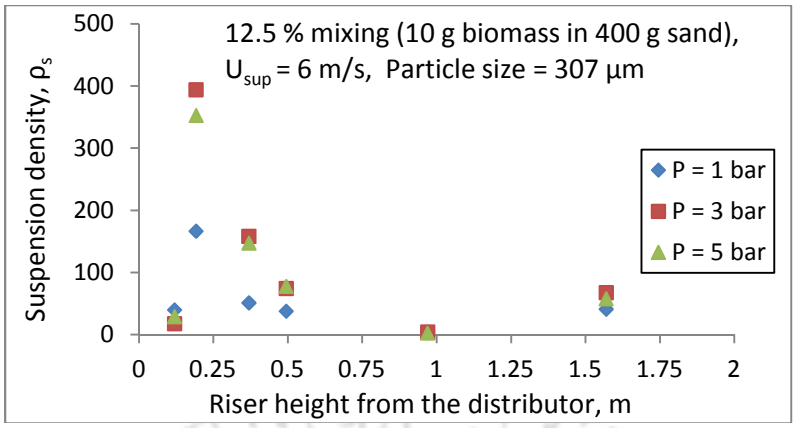

Fig.6.21 Variation of suspension density along the riser at 12.5 % biomass blend

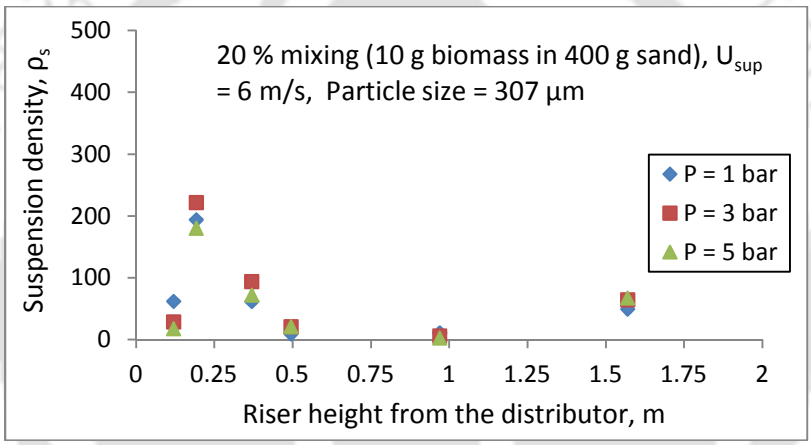

Fig.6.22 Variation of suspension density along the riser at 20 % biomass blend

The variations of suspension density with superficial velocity at 12.5 % biomass blend and at 1, 3 and 5 bar operating pressures are shown in Fig.6.23 through 6.25. As seen in Fig.6.23, the suspension density increases with an increase in superficial velocity at atmospheric pressure. At the lower portion of the riser, suspension density increases first and then decreases to the upper middle zone and thereafter increases at the top of the riser. The maximum value of about 180 kg/m^3 at the lower portion of the bed (0.1925 m from the distributor plate) and about 50 kg/m^3 (1.57 m from the distributor plate) at the top of the riser have been observed at 8 m/s. In Figs.6.24 and 6.25, it is seen that at lower superficial velocity (U_{sup} = 6 m/s), the suspension density is found to be more at operating pressures of 3 and 5 bar. The higher suspension density at the exit of the riser may be due to the significant increase of entrainment at higher operating pressures. Figure 6.26 show the comparison of variation probe average suspension density with

operating pressure at 7.5, 12.5 and 20.0 % biomass blend and at U_{sup} = 6 m/s. Standard errors are also shown at each data point to represent the experimental uncertainty. A monotonic increase of suspension density with operating pressure has been observed.

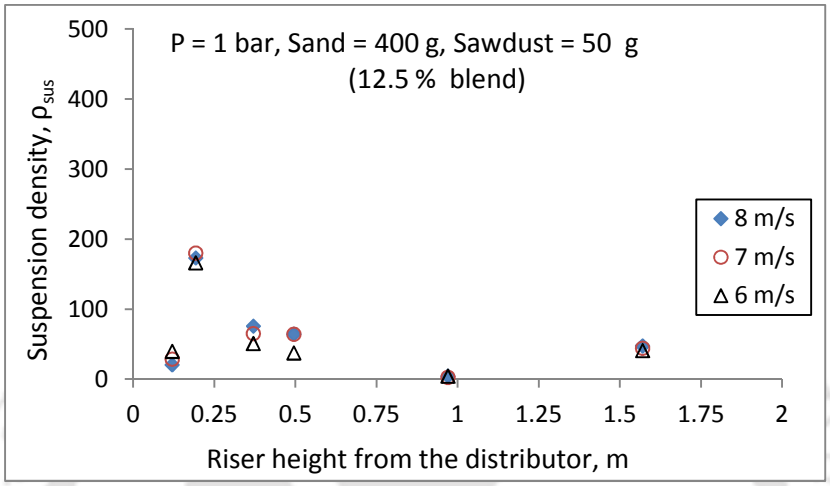

Fig.6.23 Variation of suspension density at P = 1 bar and at 12.5 % biomass blend

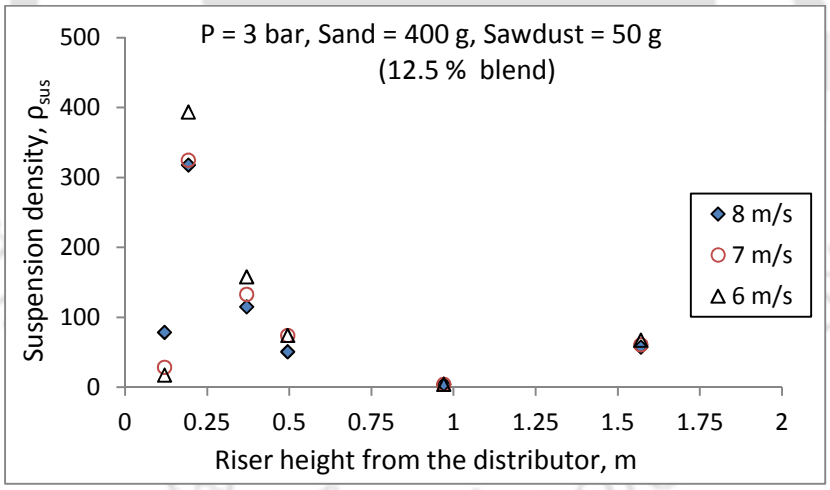

Fig.6.24 Variation of suspension density at P = 3 bar and at 12.5 % biomass blend

The comparison of variation of suspension density along the height of the riser at three different particle sizes and at two different operating pressures of 3 and 5 bar are shown in Figs.6.27 and 6.28 respectively. It has been observed that, the suspension density increases with the decrease in particle size.

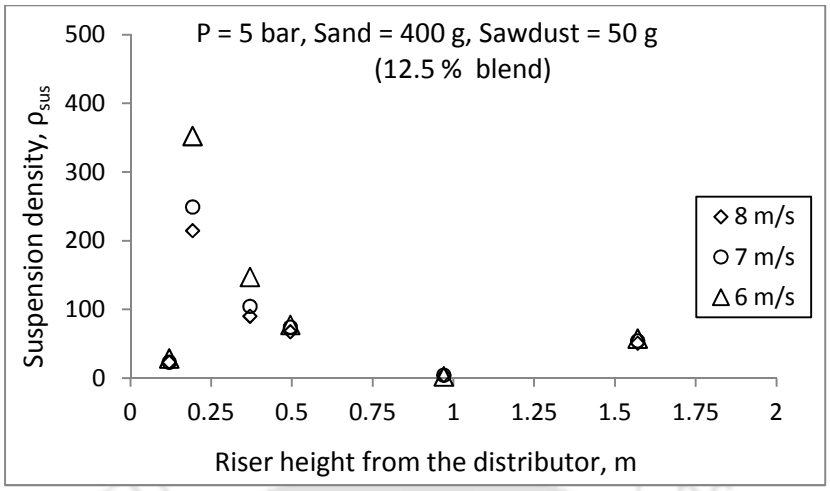

Fig.6.25 Variation of suspension density at P = 5 bar and at 12.5 % biomass blend

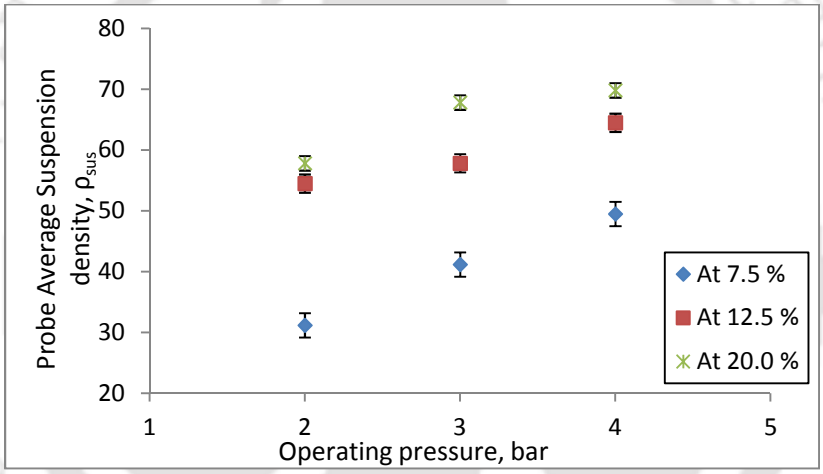

Fig.6.26 Comparison of probe average suspension density

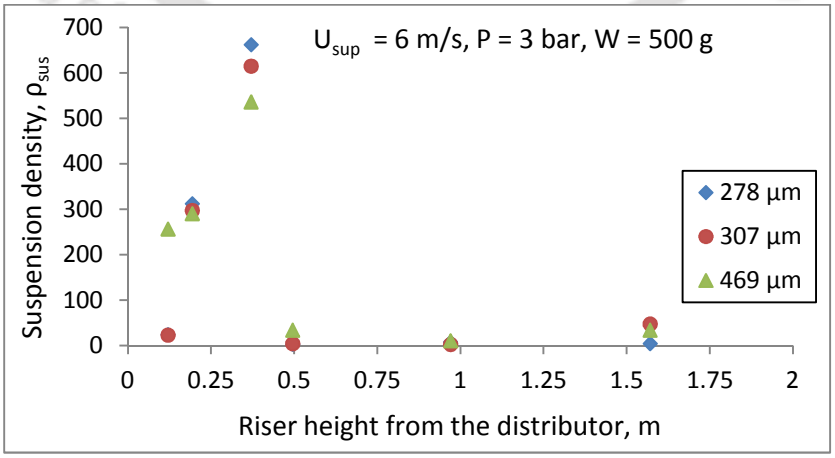

Fig.6.27 Comparison of suspension density with particle size at P = 3 bar and W = 500 g

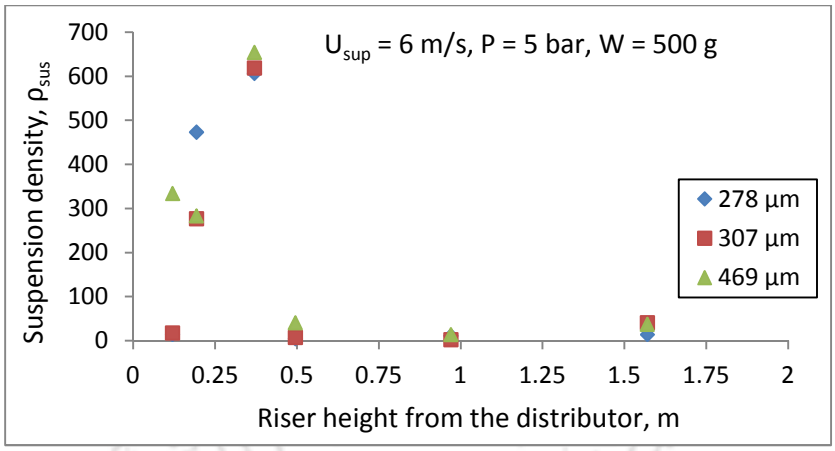

Fig.6.28 Comparison of suspension density with particle size at P = 5 bar and W = 500 g

The suspension density variation at a height of 1.57 m from the distributor with operating pressures at two different superficial velocities of 5 and 7 m/s are shown in Figs.6.29 and 6.30, respectively. The comparison is made at a percentage blending of 15 and at two different weight composition ratios. It has been found that, the suspension density increases with the increase in operating pressure in both the weight composition ratios. However, the higher value of suspension density has been observed at weight composition ratio (B/S) of 90 g: 600 g.

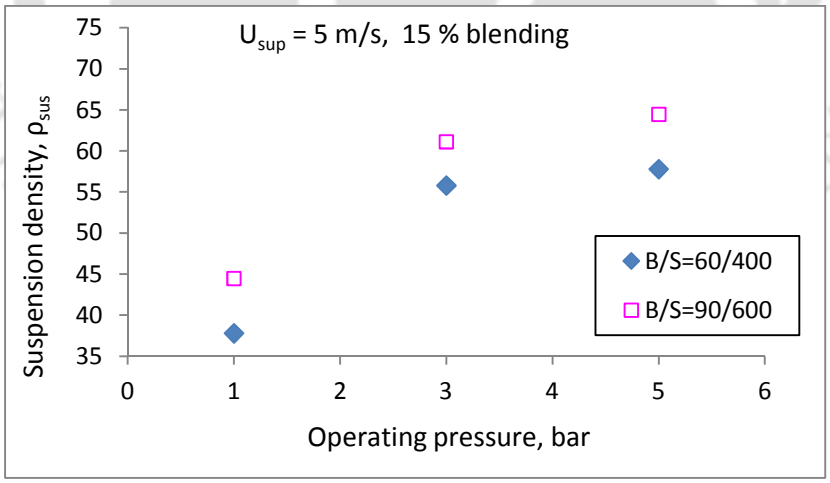

Fig.6.29 Variation of suspension density at U_{sup} = 5 m/s

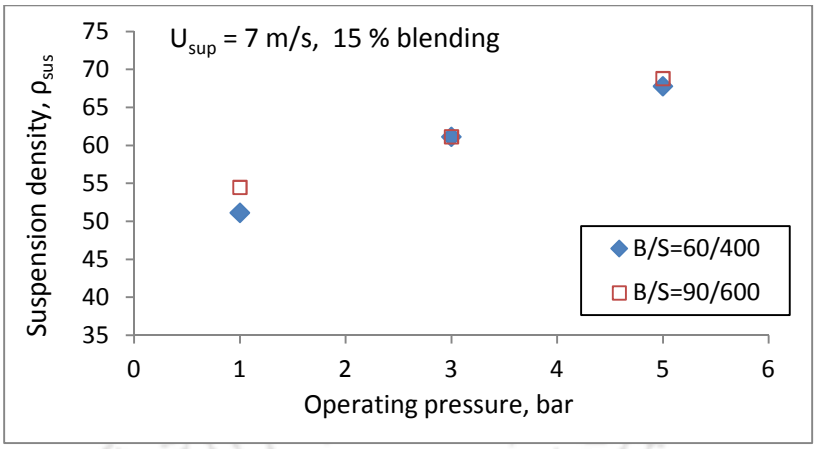

Fig.6.30 Variation of suspension density at U_{sup} = 7 m/s

6.3.3 Variation of solid circulation rate

The variation of solid circulation rate with operating pressure at four different inventories in the case of 307 µm particle size is shown in the Fig.6.31. It has been observed that the solid circulation rate increases with the increase of both operating pressure and solid inventory.

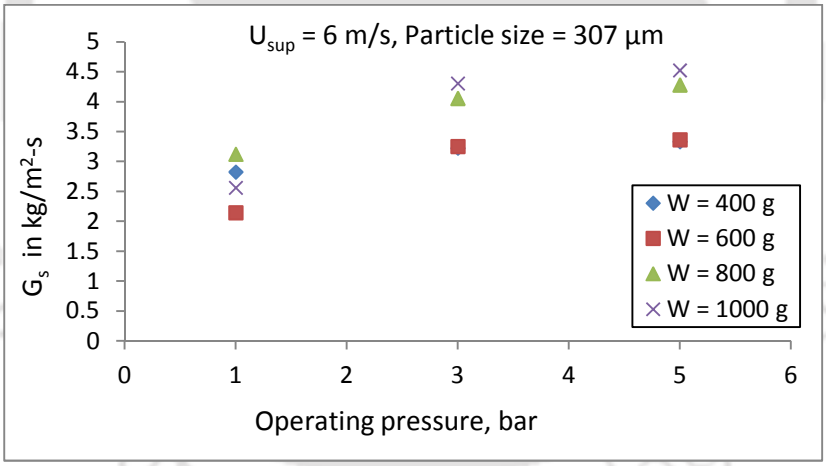

Fig.6.31 Comparison of solid circulation rate with bed inventories at varied operating pressure

6.4 Investigation of heat transfer

The wall-to-bed heat transfer coefficient along the riser height has been investigated at the upper splash region of the riser. The effects of bed voidage, suspension density, superficial velocity, solid (sand and biomass blending) inventory, particle size, solid circulation and operating pressures were studied and reported. The effects of these parameters on heat transfer coefficient along the radial direction were also studied at a height of 1.57 m from the distributor plate.

6.4.1 Effects of operating parameters on wall-to-bed heat transfer without biomass blending

The wall-to-bed heat transfer coefficient variations along the height of the heat transfer probe with operating pressures at two different inventories of 400 and 600 g are shown in Figs.6.32 and 6.33. In each plot, the superficial velocity is kept constant at 6 m/s. The heat transfer coefficient increases with an increase in operating pressure. Similar variations of heat transfer coefficient have also been observed at the inventories of 800 and 1000 g. This is more significant at the exit of the riser. This increase of heat transfer toward the riser exit may be due to (a) an increase in particle concentration because of more drag force acting on the bed material in the bottom zone with bed material being lifted to the top zone, and (b) at elevated pressure, the gas phase convective heat transfer is higher due to high density of gas.

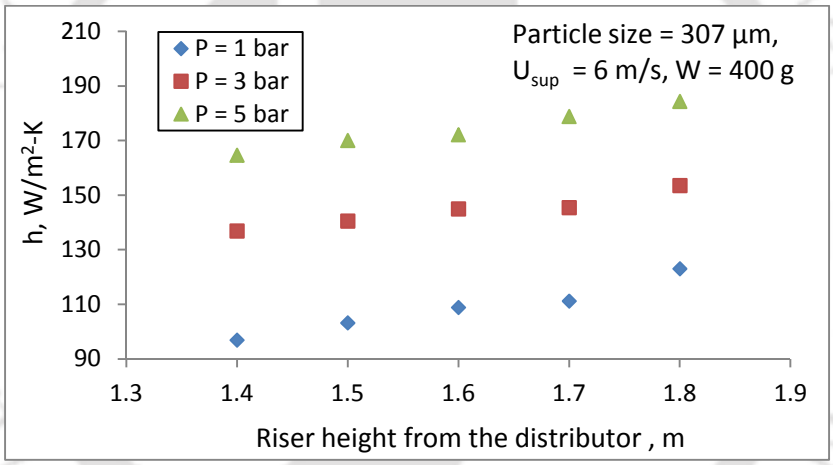

Fig.6.32 Variation of heat transfer coefficient with operating pressure at W = 400 g

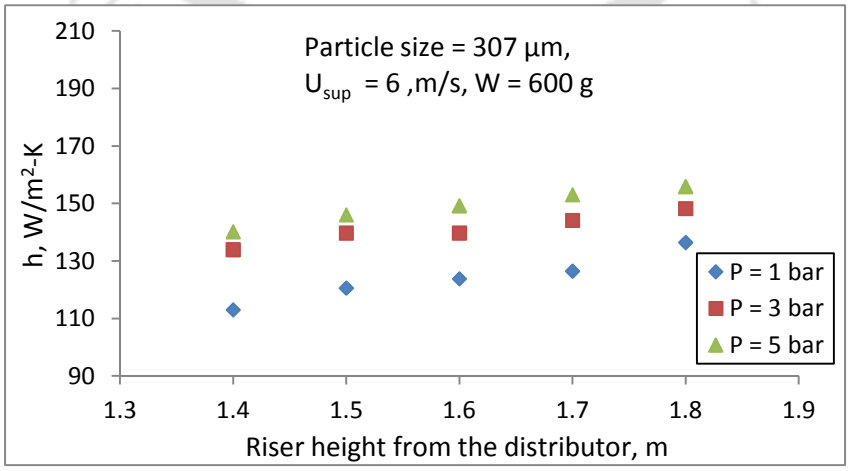

Fig.6.33 Variation of heat transfer coefficient with operating pressure at W = 600 g

The comparison of variation of wall-to-bed heat transfer coefficient along the height of the heat transfer probe at three different particle sizes and at two different operating pressures of 3 and 5 bar are shown in Figs.6.34 and 6.35. The comparisons are made at a superficial velocity of 6 m/s and at a bed inventory of 500 g. The heat transfer coefficient is found to be more in the case of smaller particles i.e. particle mean diameter of 278 µm as compared to 307 µm and 469 µm at both the operating pressures. The increase in heat transfer coefficient in the case of smaller particle size is may be due to increase in particle concentration at any particular cross-section of the bed (Fig.6.38). Shen *et al.* (1991) also observed the same phenomenon. This feature is similar to that observed in atmospheric pressure CFBs having a short heat transfer section (Basu and Cheng, 1996). When the particle size is finer, more particles will be transported to the upper riser to make the upper heat-absorbing section denser. This causes more exchange of energy due to particle-particle interactions. In the case of larger particle size, the particles remain in the lower furnace instead of rising into the upper splash region as the pressure drag force required to lift the particles becomes higher. This may be the reason why the heat transfer coefficient decreases in the upper bed when particle size increases.

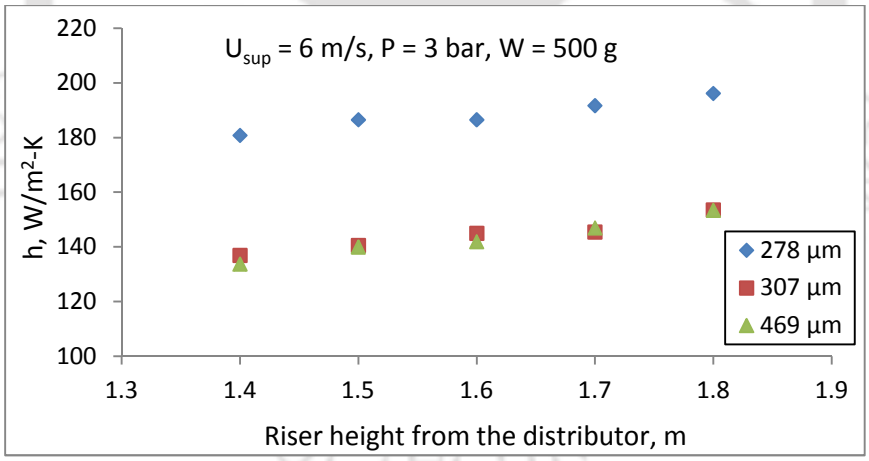

Fig.6.34 Comparison of heat transfer coefficient at P = 3 bar and W = 500 g

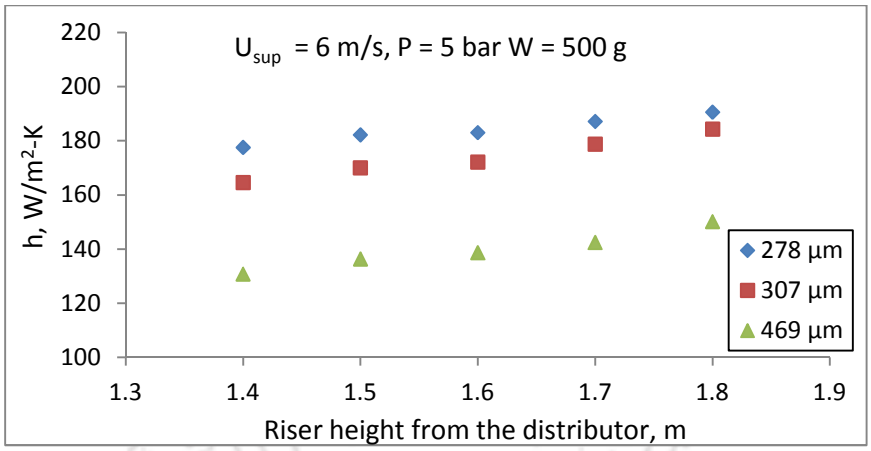

Fig.6.35 Comparison of heat transfer coefficient at P = 5 bar and W = 500 g

The comparison of variation of heat transfer coefficient along the radial direction at three different particle sizes and at two different operating pressures of 3 and 5 bar are shown in Figs.6.36 and 6.37. The comparisons are made at a superficial velocity of 6 m/s and a bed inventory of 500 g. The heat transfer coefficient decreases from the wall-to-core of the riser at both the pressures. The heat transfer coefficient is observed to be more in the case of smaller particles i.e. 278 µm at all the measured points except the point measured adjacent to the wall. At these points, the heat transfer coefficient is found to be more with particle mean diameter of 469 µm. This probably due to the presence of higher concentration of larger particle clusters near the wall of the riser.

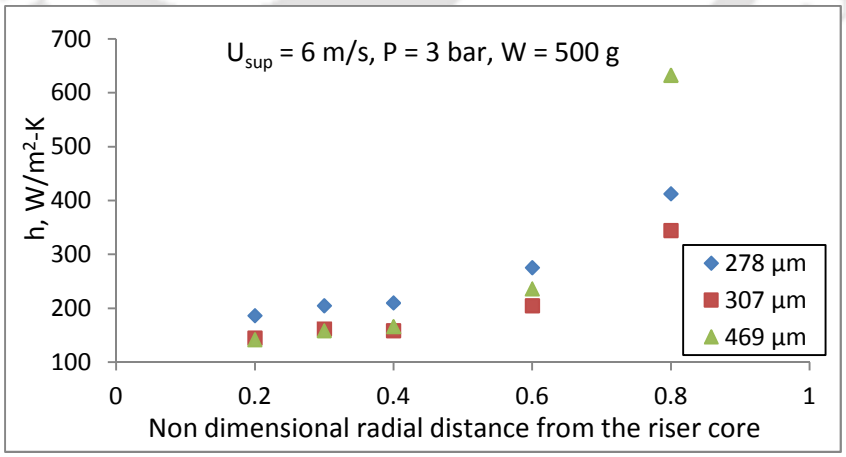

Fig.6.36 Comparison of heat transfer coefficient (radial) at P = 3 bar and W = 500 g

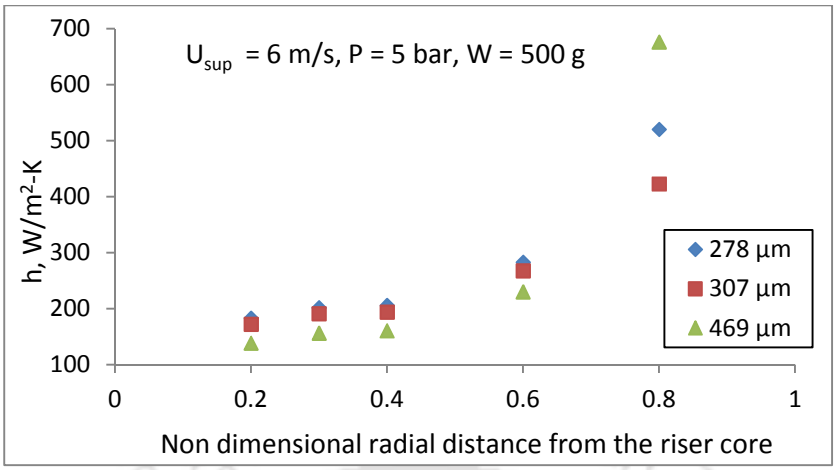

Fig.6.37 Comparison of heat transfer coefficient (radial) at P = 5 bar and W = 500 g

Figure 6.38 through 6.40 present the variation of wall-to-bed heat transfer coefficient with particle size at the operating pressures of 1, 3 and 5 bar and at superficial velocity of 6 m/s. The comparisons are made at a height of 1.57 m from the distributor at two different bed inventories such as 500 g and 1000 g. In all the three figures, it has been observed that the heat transfer coefficient is found to be more in case of smaller particle size i.e. 278 µm followed by 307 µm and 469 µm. Besides, the heat transfer coefficient increases by 1.1 times as the operating pressure increases. At higher bed inventories, the heat transfer coefficient is found to be more at all the operating pressures. The difference in the heat transfer coefficient in two bed inventories is more at P = 1 bar in the case of 307 and 469 µm particle size as compared to 278 µm. These differences in heat transfer coefficient decreases as the operating pressure increases.

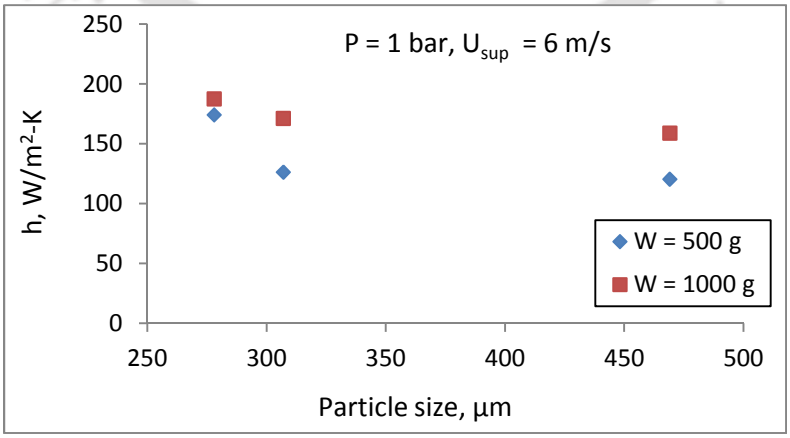

Fig.6.38 Comparison of heat transfer coefficient with bed inventory at P = 1 bar

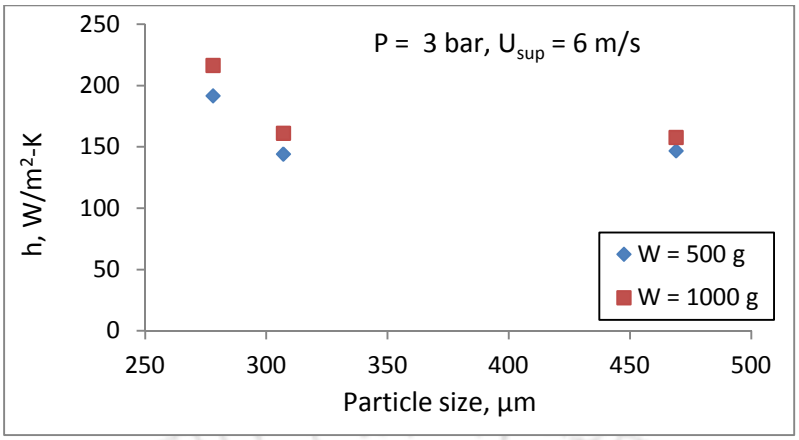

Fig.6.39 Comparison of heat transfer coefficient with bed inventory at P = 3 bar

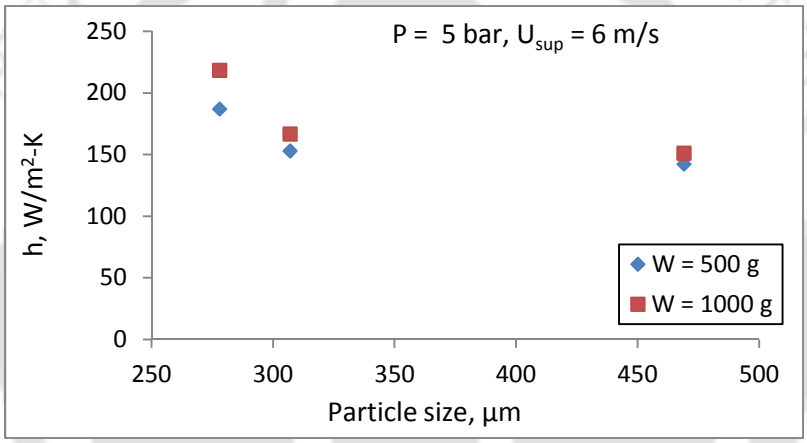

Fig.6.40 Comparison of heat transfer coefficient with bed inventory at P = 5 bar

The comparison of variation of wall-to-bed heat transfer coefficient with superficial velocity at a height of 1.57 m from the distributor for the three particle sizes at operating pressures of 1, 3 and 5 are shown in the Figs.6.41 through 6.43. At operating pressure, P = 1 bar (Fig.6.41) it has been found that, in case of smaller particles (278 µm) the heat transfer coefficient is almost constant at all the superficial velocities, whereas it first increases as superficial velocity increases and then decreases in the case of 307 µm particle size. With higher particle size, the heat transfer coefficient increases with increase in superficial velocity as the drag force increases with the increase in superficial velocity. This causes an increase in particle interactions, and hence, the energy transfer.

From Figs.6.42 and 6.43, it has been observed that, with the increase in superficial velocity, heat transfer coefficient first decreases and then it becomes independent with an increase in superficial velocity in the case of 278 µm particle size. With the particles of mean diameter of 307 µm, the heat transfer coefficient is almost independent of the superficial velocity whereas the particle having mean diameter of 469 µm, the heat transfer coefficient increases with an increase in superficial velocity. This demonstrates the accumulation of more solids at the exit of the riser as operating pressure increases. Similar variations of heat transfer coefficient have been observed in all the pressure conditions. Higher values of heat transfer coefficient have been found at higher pressures.

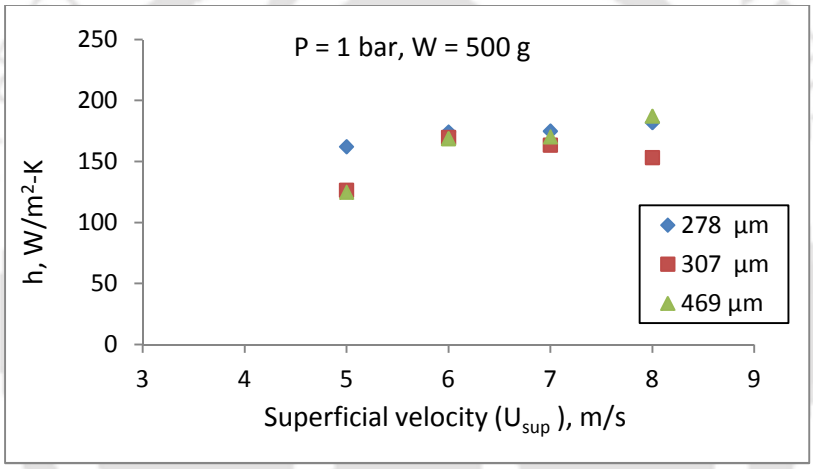

Fig.6.41 Comparison of heat transfer coefficient with superficial velocity at P = 1 bar

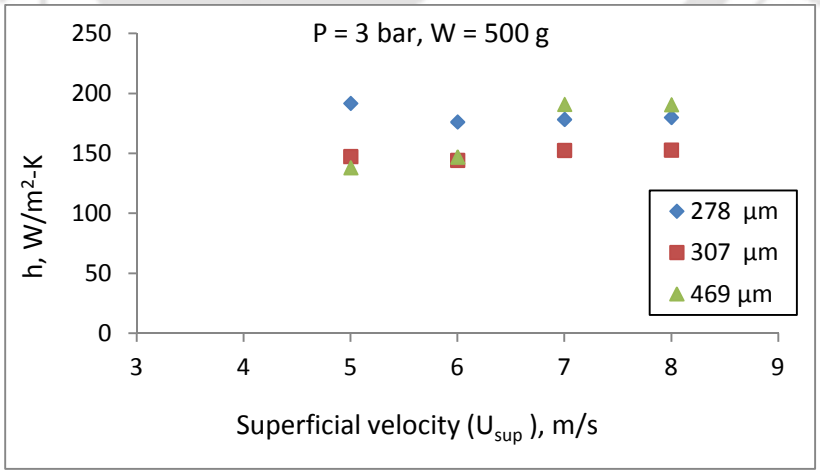

Fig.6.42 Comparison of heat transfer coefficient with superficial velocity at P = 3 bar

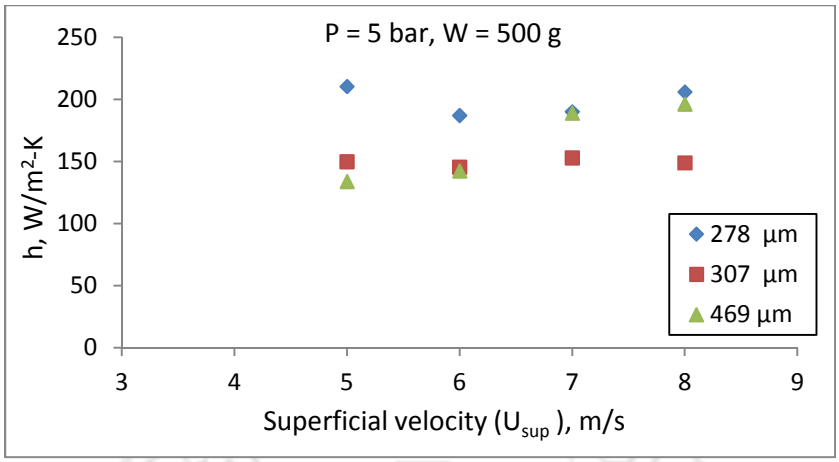

Fig.6.43 Comparison of heat transfer coefficient with superficial velocity at P = 5 bar

6.4.2 Effects of operating parameters on wall-to-bed heat transfer with biomass blending

The variation of wall-to-bed heat transfer coefficient with superficial velocity at three operating pressures (at 1, 3 and 5 bar) in the case of 2.5 % biomass blend are shown in Figs.6.44 through 6.46. At P = 1 bar, the heat transfer coefficient is found to be higher (128.38 to142.48 W/m^2-K from bottom to the top of the heat transfer probe) at higher superficial velocity (8 m/s). At U_{sup} = 6 m/s, heat transfer coefficient is found to vary from 106.73 to 120.34 W/m^2-K from the bottom to the top of the heat transfer probe. At system pressure, P = 3 bar (Fig.6.45) the heat transfer coefficient varies from 119.51 to 131.22 W/m^2-K at superficial velocity 8 m/s and at U_{sup} = 6 m/s this values falls in between 112.7 to 124.53 W/m^2-K. The values of heat transfer coefficient at U_{sup} = 7 m/s falls in between the heat transfer coefficient found at the superficial velocities of 6 and 8 m/s. This demonstrates the less dependency on superficial velocity at higher pressure. Basu and Cheng (1996) studied the influence of operating pressure and superficial velocity (3.6 to 4.8 m/s) on heat transfer and found the same variation. However, the values of heat transfer coefficient are found to be lower than the present observed values. This is probably due to lower superficial velocity.

At system pressure of 5 bar (Fig.6.46), the heat transfer coefficient is found to be more at all the superficial velocities from the bottom to the top of the heat transfer probe. Highest values of heat transfer coefficient is found at U_{sup} = 8 m/s followed by 7 m/s and 6 m/s. Similar variations of heat transfer coefficient has been observed at all the operating conditions in the case of 2.5 % biomass blend.

The variation of heat transfer coefficient with system pressure at U_{sup} = 6 m/s in the case of 2.5 % biomass blending is shown in Fig.6.47. Trade lines are also shown in the figure to represent the trends of heat transfer coefficient along the height of the heat transfer probe. It is seen that heat transfer coefficient increases with an increase in pressure. Shen *et al.* (1991) and Basu and Cheng (1996) suggested that, the contribution of the heat transfer due to gas phase will rise as the operating pressure increases. A homogenous variation of heat transfer coefficient was noticed with pressure, and the results matches well with the observations of Namkung *et al.* (1999).

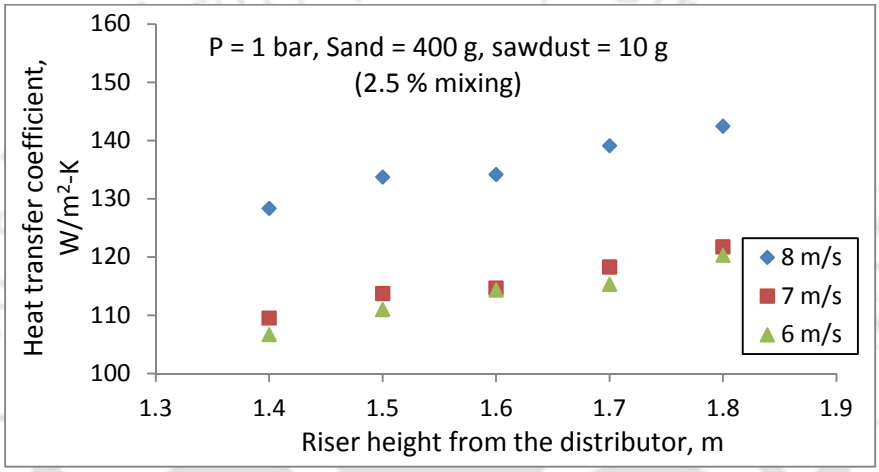

Fig.6.44 Variation of heat transfer coefficient at P = 1 bar and at 2.5 % biomass blend

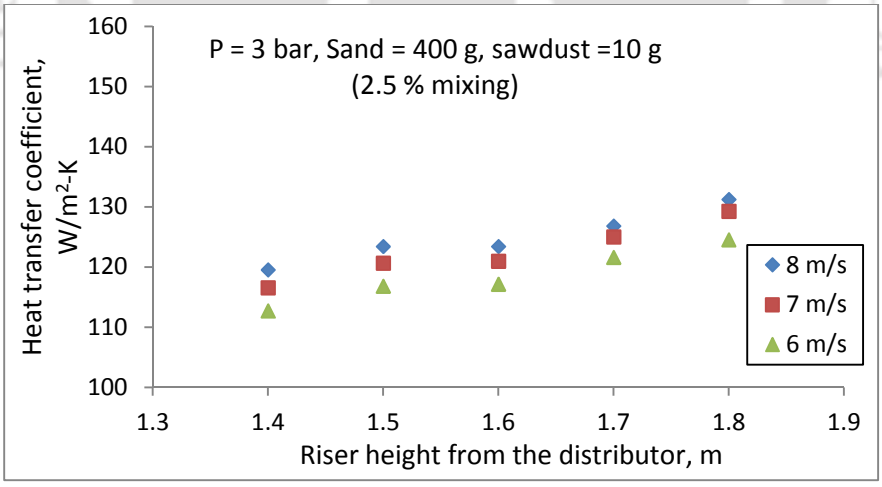

Fig.6.45 Variation of heat transfer coefficient at P = 3 bar and at 2.5 % biomass blend

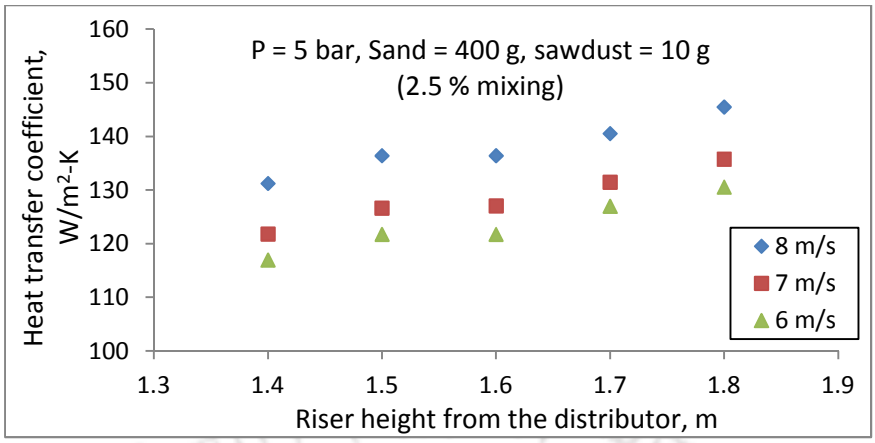

Fig.6.46 Variation of heat transfer coefficient at P = 5 bar and at 2.5 % biomass blend

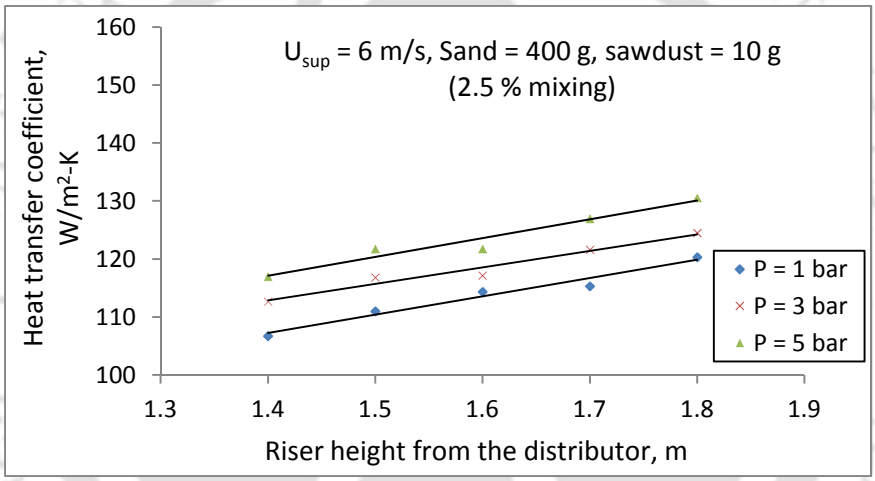

Fig.6.47 Variation of heat transfer coefficient at U_{sup} = 6 m/s and at 2.5 % biomass blend

Figure 6.48 shows the variation of wall-to-bed heat transfer coefficient with superficial velocity in the case of 12.5 % biomass blend and at 5 bar operating pressure. It is seen that with an increase in superficial velocity, the heat transfer coefficient increases. At U_{sup} = 8 m/s, the heat transfer coefficient is increasing from 129.34 W/m^2-K at the bottom to 145.17 W/m^2-K at top of the heat transfer probe. The increase in heat transfer coefficient at higher superficial velocities may due to increase intermixing of solid particles caused by enhanced turbulence. Effect of system pressure on heat transfer coefficient at superficial velocity 6 m/s in the case of 12.5 % biomass blend is shown in Fig.6.49. It has been found that with an increase in pressure, the heat transfer coefficient increases. At system pressure of P = 5 bar, the heat transfer coefficient varies from 121.19 to 139.04 W/m^2-K, followed by 116.56-130.07 W/m^2-K at 3 bar and 106.46-117.28 W/m^2-K at 1 bar along the heat transfer probe.

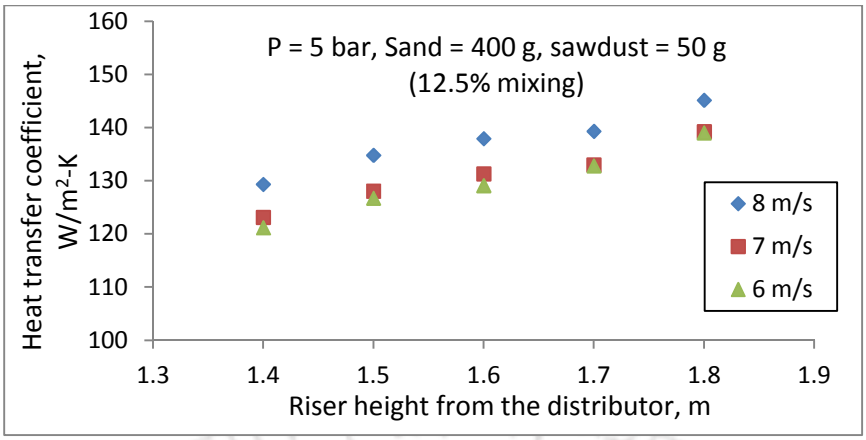

Fig.6.48 Variation of heat transfer coefficient at P = 5 bar and at 12.5 % biomass blend

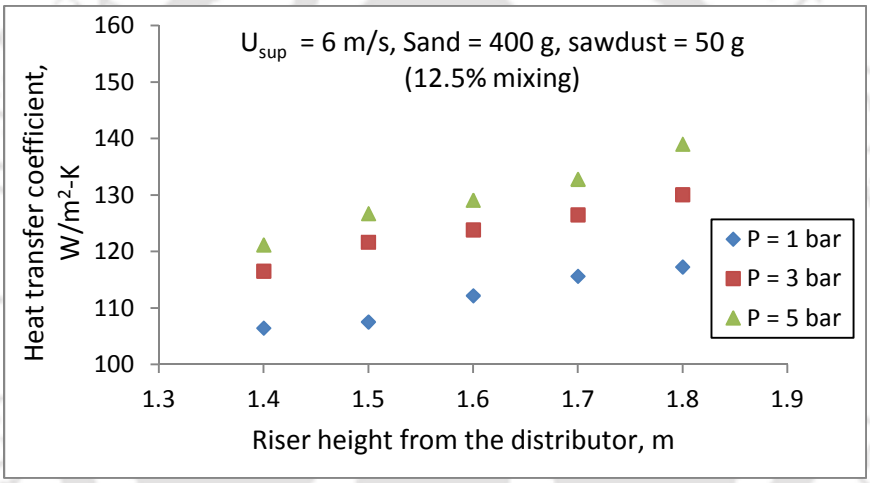

Fig.6.49 Variation of heat transfer coefficient at U_{sup} = 6 m/s and at 12.5 % biomass blend

The variation of heat transfer coefficient with pressure at four different percentage blending of biomass in sand and at U_{sup} = 6 m/s is presented in the Fig.6.50. It has been observed that the heat transfer coefficient increases with an increase in pressure at all the % mixing of biomass in sand. At 12.5 % biomass blend, the heat transfer coefficient is found to be more at all the pressure conditions and at 20 % biomass blend, the heat transfer coefficient is found to be lowest. The heat transfer coefficient increases with increase in operating pressure and with increase in % blending of biomass in sand up to 12.5 %, and then it decreases with further increase in % mixing of biomass. The increase in heat transfer coefficient at high pressure is may be due to increase in gas density and uniform mixing, which led particle-particle interactions resulting energy interactions.

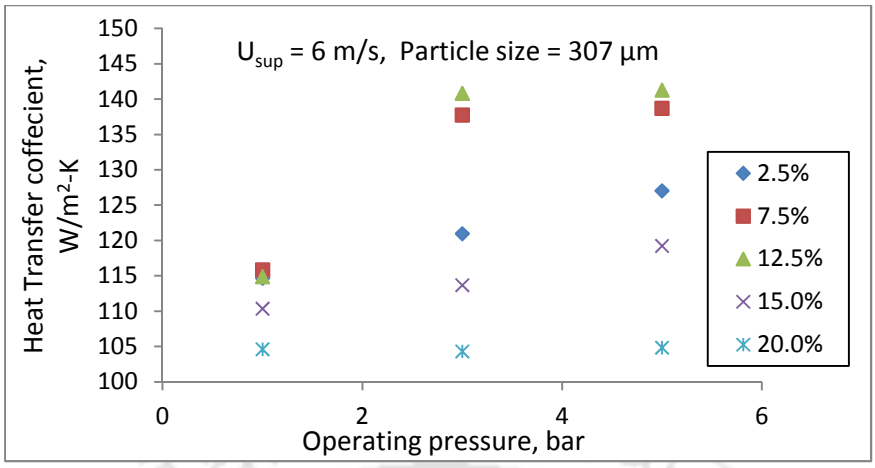

Fig.6.50 Variation of heat transfer coefficient with operating pressure at U_{sup} = 6 m/s

6.4.3 Variation of wall-to-bed heat transfer coefficient with suspension density

The variation of heat transfer coefficient with suspension density at a height of 1.57 m from the distributor plate in the case of 7.5 % and 12.5 % biomass blend is shown in Figs. 6.51 and 6.52 respectively. Both the plots were made at a constant operating velocity, U_{sup} = 6 m/s. From these figures, it has been observed that with an increase in suspension density, the heat transfer coefficient increases by 1.2 times with operating pressure. These data are comparable to the results obtained by Gupta and Nag (2002) in spite of using different setups and operating conditions.

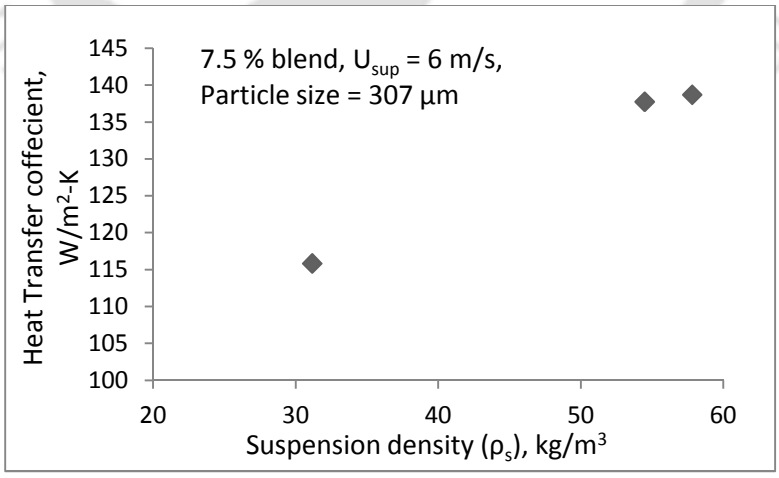

Fig.6.51 Variation of heat transfer coefficient with suspension density at U_{sup} = 6 m/s and at 7.5 % biomass blend (at 1.57 m from the distributor plate)

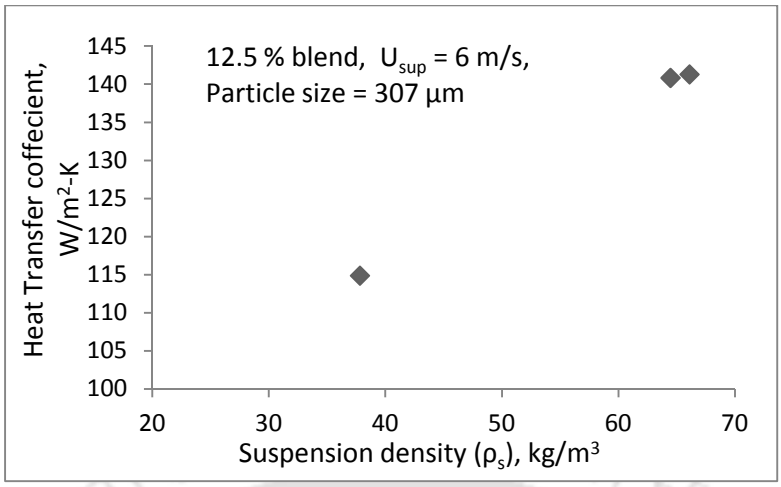

Fig.6.52 Variation of heat transfer coefficient with suspension density at U_{sup} = 6 m/s and at 12.5 % biomass blend (at 1.57 m from the distributor plate)

6.4.4 Variation of wall-to-bed heat transfer coefficient with weight composition ratio

Figures 6.53 through 6.59 present the variation of heat transfer coefficient at a height of 1.57 m from the distributor plate at 2.5 %, 7.5 %, 15.0 % and 20 % blending of sawdust in sand. The comparisons were made at two different weight composition ratios and at two different superficial velocities of 5 and 7 m/s. From these figures, it has been found that, the heat transfer coefficient increases with the increase in operating pressures. At superficial velocity of 5 m/s, the heat transfer coefficient is found to be higher (120-135 W/m^2-K) at 7.5 % blending (Fig.6.54) with weight composition ratio 30 g: 400 g as compared to the other three percentage blending. At superficial velocity of 7 m/s, the heat transfer coefficient is found to be higher (between 120-130 W/m^2-K) at 15 % blending (Fig.6.58) with weight composition ratio (B/S) of 90 g: 600 g as compared to the other three percentage blending. The heat transfer coefficient is found to be lowest (90-105 W/m^2-K) at 20 % biomass blending (Figs.6.55 and 6.59) among the other blending at both the superficial velocities i.e. at 5 and 7 m/s. This may be due to the lowest solid circulation rate observed in both the cases as compared to the other percentage blending. The values of the solid circulation rate at the superficial velocities of 5 and 7 m/s and at four different percentage blending is shown in the Table-6.1.

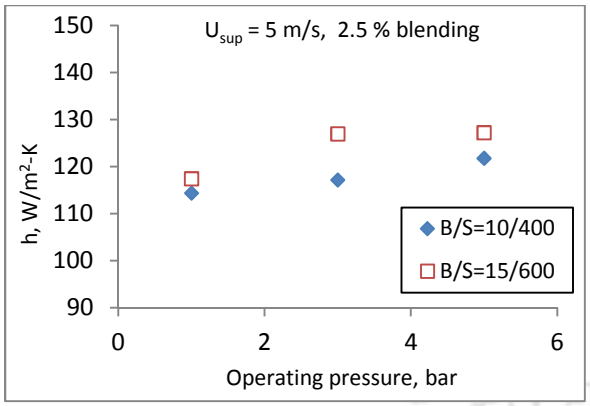

Fig.6.53 Variation of heat transfer coefficient at U_{sup} = 5 m/s and at 2.5 % blending

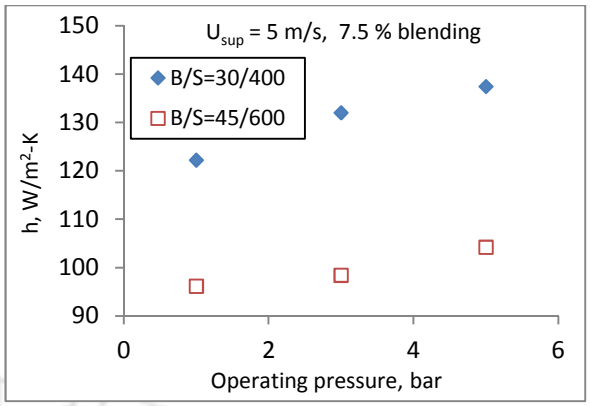

Fig.6.54 Variation of heat transfer coefficient at U_{sup} = 5 m/s and at 7.5 % blending

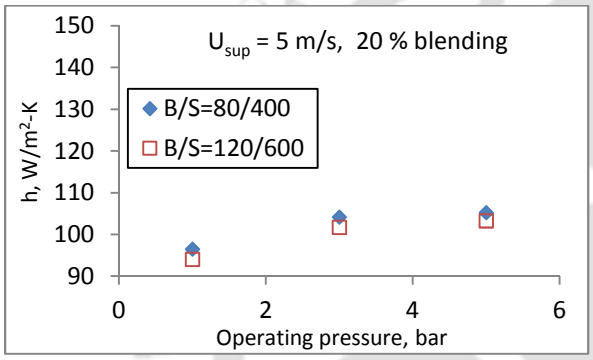

Fig.6.55 Variation of heat transfer coefficient at U_{sup} = 5 m/s and at 20.0 % blending

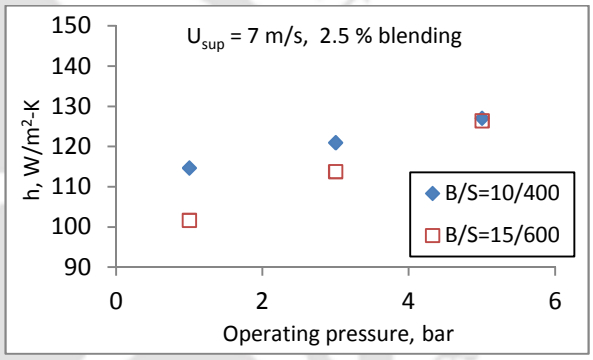

Fig.6.56 Variation of heat transfer coefficient at U_{sup} = 7 m/s and at 2.5 % blending

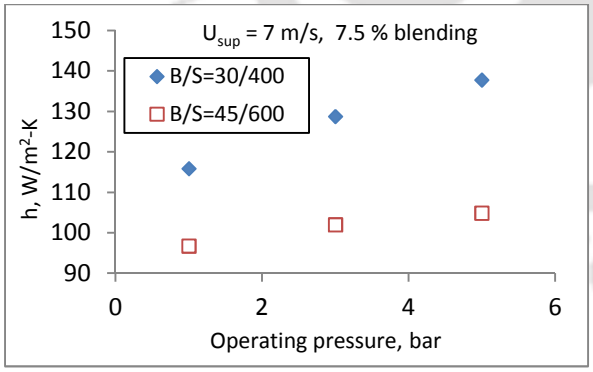

Fig.6.57 Variation of heat transfer coefficient at U_{sup} = 7 m/s and at 7.5 % blending

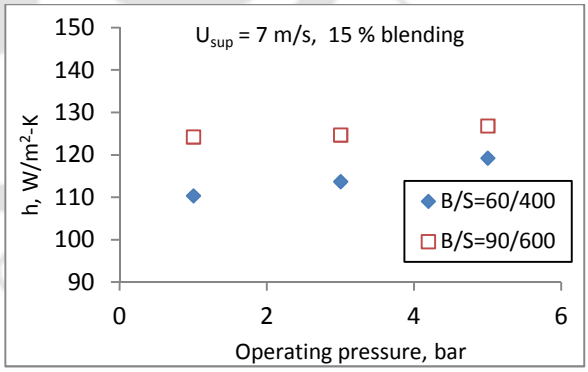

Fig.6.58 Variation of heat transfer coefficient at U_{sup} = 7 m/s and at 15.0 % blending

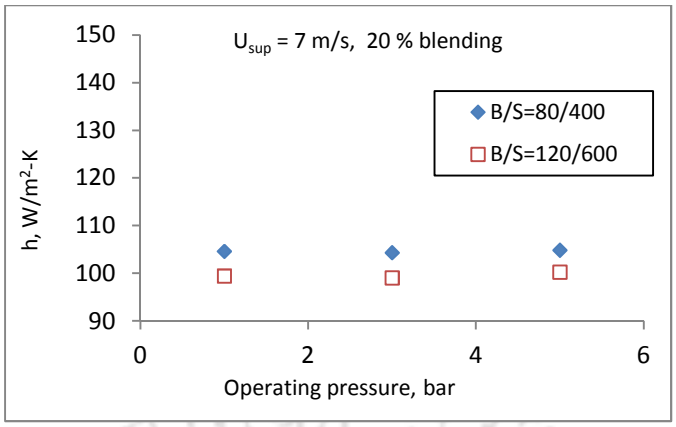

Fig.6.59 Variation of heat transfer coefficient at U_{sup} = 7 m/s and at 20.0 % blending

Figure 6.60 show the variation of heat transfer coefficient along the heat transfer probe at the operating pressure of 5 bar and at the superficial velocity of 5 m/s. It is observed that, the heat transfer coefficient increases from the bottom to the top of the heat transfer probe. This is a representative figure for percentage blending of biomass in sand at varied pressure conditions. The similar variation of heat transfer coefficient without blending of biomass is demonstrated by Gupta and Nag (2002).

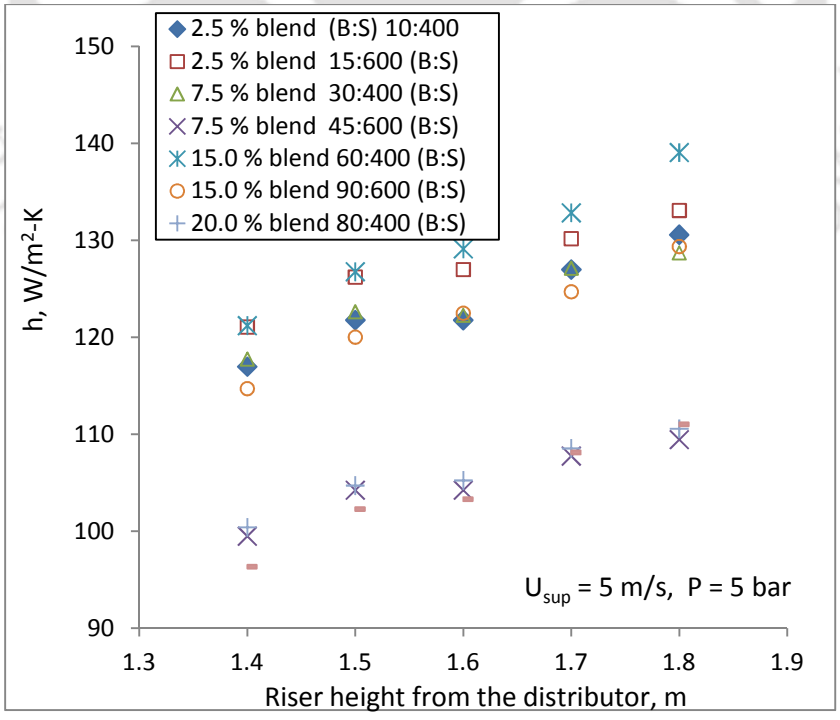

Fig.6.60 Comparison of variation of heat transfer coefficient along the heat transfer probe

Table-6.1 Solid circulation rate, G_s (kg $m^{-2}s^{-1}$) data with pressure

P, bar	2.5 % blend (B/S) 10:400	2.5 % blend (B/S) 15:600	7.5 % blend (B/S) 30:400	7.5 % blend (B/S) 45:600	15.0 % blend (B/S) 60:400	15.0 % blend (B/S) 90:600	20.0 % blend (B/S) 80:400	20.0 % blend (B/S) 120: 600
				U_{sup} = 5 m/s				
1	0.816	1.381	0.946	1.072	0.773	0.912	0.205	0.0817
3	1.164	1.086	1.623	0.753	1.094	1.762	0.926	0.1388
5	0.952	1.455	1.798	1.350	1.637	1.327	0.989	0.3033
				U_{sup} = 7 m/s				
1	1.296	1.406	1.565	1.261	1.137	1.451	1.064	0.1921
3	1.275	1.123	2.089	1.205	1.434	1.861	1.352	0.2609
5	1.093	1.455	2.012	1.260	1.389	1.650	1.332	0.3533

Figures 6.61 through 6.63 present the variation of heat transfer coefficient along the heat transfer probe at three different operating pressures of 1, 3 and 5 bar respectively. The comparisons were made at four different blending of biomass (sawdust) in sand with two different sets of weight compositions. In all the three figures, similar variations of heat transfer coefficient have been observed i.e. heat transfer coefficient increasing toward the riser exit. Lowest values of the heat transfer coefficient along the heat transfer probe have been found at 20 % sawdust blending in sand in both the weight compositions at all the three operating pressures. This may be due to the lower solid circulation rate (0.0817 kg m^{-2} s^{-1} for P = 1 bar, 0.1388 kg m^{-2} s^{-1} for P = 3 bar and 0.3033 kg m^{-2} s^{-1} for P = 5 bar) at this condition, which results lower suspension density at the riser exit. As the operating pressure changes, the heat transfer coefficient associated with the percentage blending of biomass in sand and weight composition also changes. At P = 1 bar and P = 3 bar, the heat transfer coefficient is found to be higher at 7.5 % sawdust blending with weight composition ratio of 30 g: 400 g followed by 2.5 % with weight composition ratio of 15 g: 600 g respectively. At these conditions, solid circulation rates are found to be 0.946 and 1.276 kg m^{-2} s^{-1}, respectively. At operating pressure of 5 bar, the heat transfer coefficient is found to be higher as compared to the other two operating pressures and the maximum values of heat transfer coefficient is found at 15.0 % sawdust blend at a weight composition ratio of 60 g: 400 g. The corresponding solid circulation rate is 1.637 kg m^{-2} s^{-1}. Moreover, at this condition very close variations of heat transfer coefficient has been observed at the blending ratios of 2.5 %, 7.5 % and 15.0 % at both the weight composition ratios. The heat transfer coefficient varies from 85.18 to 147.75 W/m^2-K in the entire range of biomass blending. More uniform and higher heat transfer has been observed as the operating pressure increases. Based on the requirement and

operating conditions the optimum weight composition may be maintained for maximum heat transfer and gas yield.

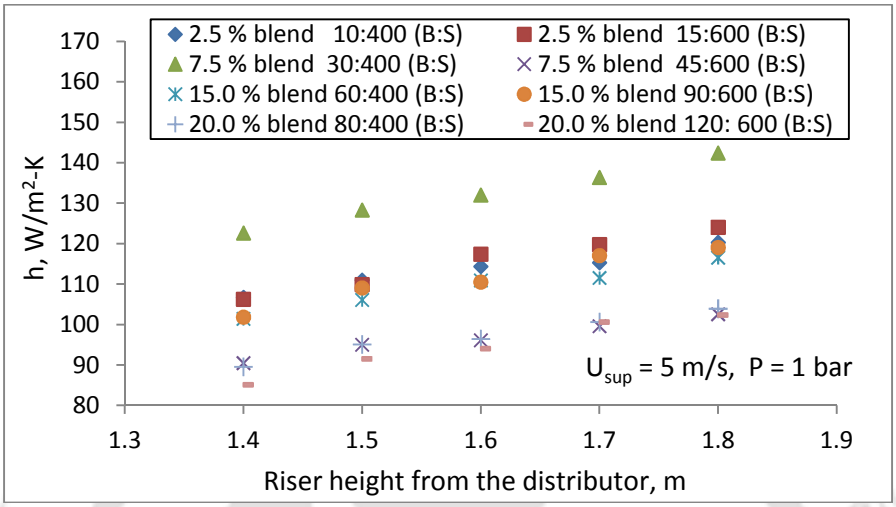

Fig.6.61 Variation of heat transfer coefficient at P = 1 bar

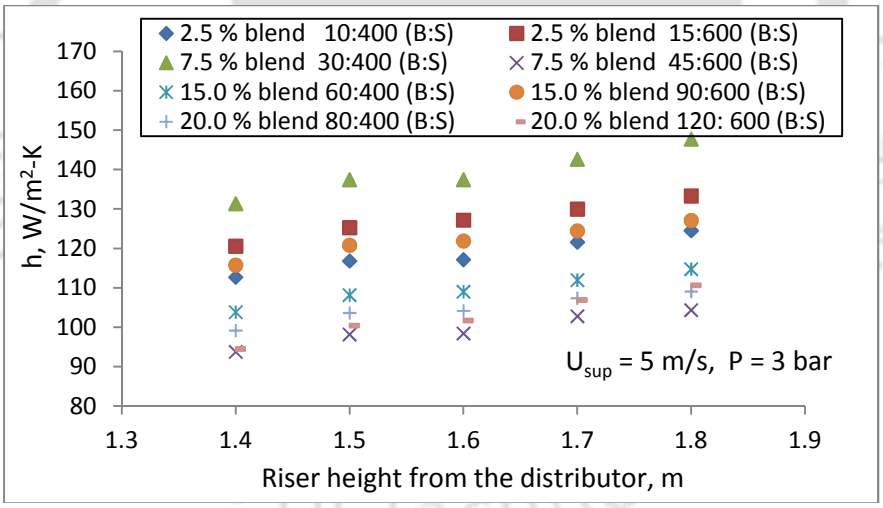

Fig.6.62 Variation of heat transfer coefficient at P = 3 bar

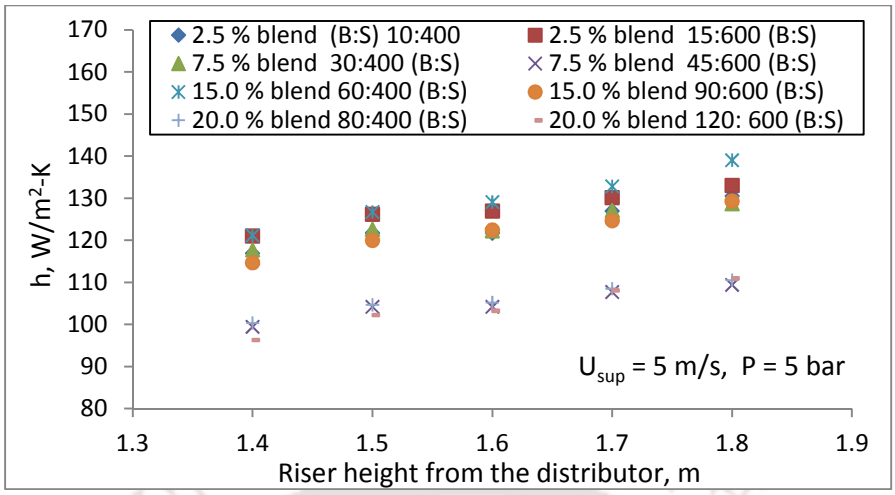

Fig.6.63 Variation of heat transfer coefficient at P = 5 bar

6.4.5 Variation of heat transfer coefficient along the radial direction without biomass blending

Figures 6.64 through 6.67 present the variation of heat transfer coefficient along the radial direction with operating pressures at four different inventories keeping the superficial velocity (6 m/s) and particle size (307 µm) constant. As observed, the heat transfer coefficient decreases from the wall-to-the core of the riser and it increases with increase in operating pressure. This is probably due to the decrease in particle concentration from the wall to the core of the CFB riser. The higher heat transfer coefficient may be attributed to the higher concentrations of solids clusters sliding down the wall.

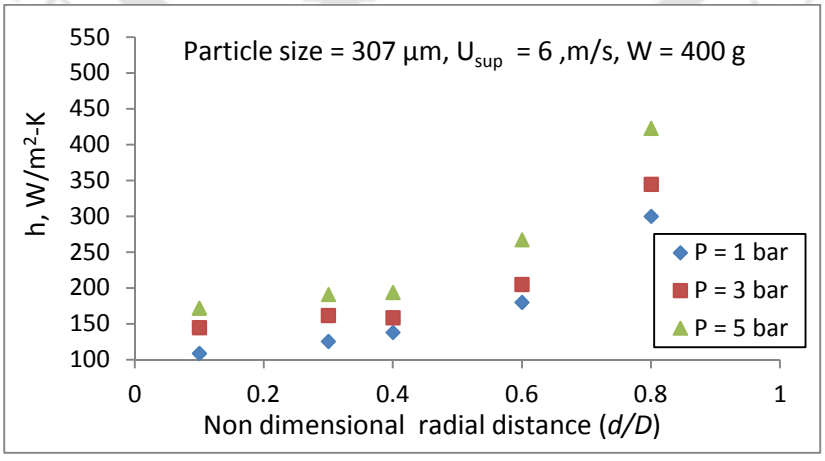

Fig.6.64 Radial variation of heat transfer coefficient with pressure at W = 400 g

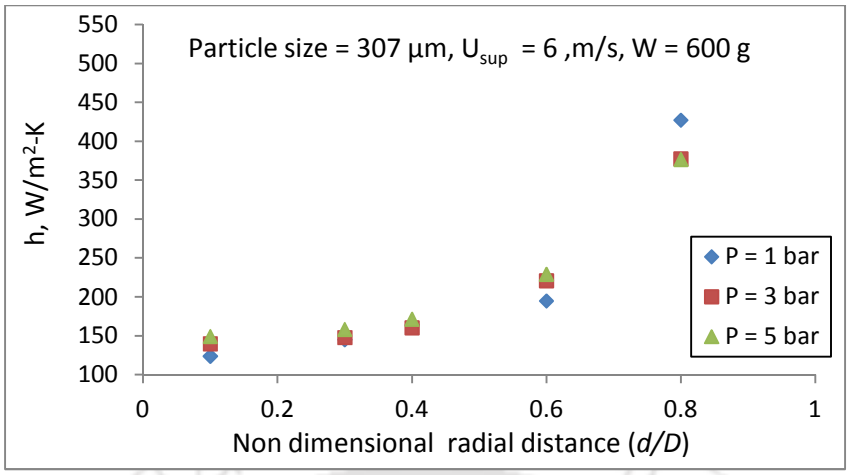

Fig.6.65 Radial variation of heat transfer coefficient with pressure at W = 600 g

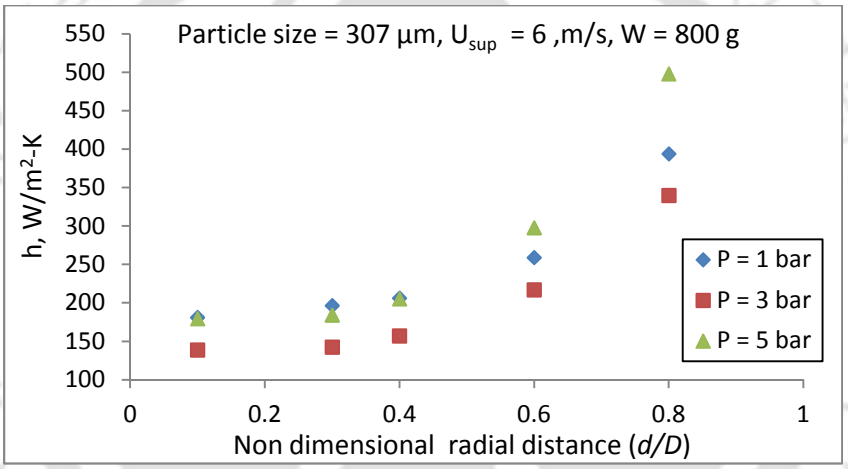

Fig.6.66 Radial variation of heat transfer coefficient with pressure at W = 800 g

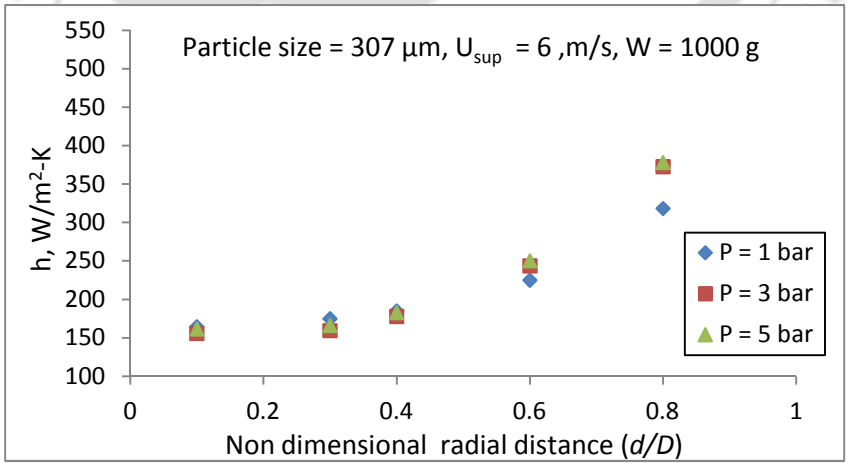

Fig.6.67 Radial variation of heat transfer coefficient with pressure at W = 1000 g

6.4.6 Variation of heat transfer coefficient along the radial direction with biomass blending

The radial variation of heat transfer coefficient at a height of 1.57 meter from the distributor and at three superficial velocities and at 5 bar operating pressure is shown in Fig.6.68. The heat transfer coefficient decreases from the wall to the core of the riser. Similar profiles have been found in all the percentage blending considered in the present study. The near wall and core heat transfer coefficient is observed to be 425.4 W/m^2-K and 129.1 W/m^2-K respectively at 12.5 % biomass blending. The heat transfer coefficient also increases with an increase in system pressure, which is demonstrated in Fig.6.69.

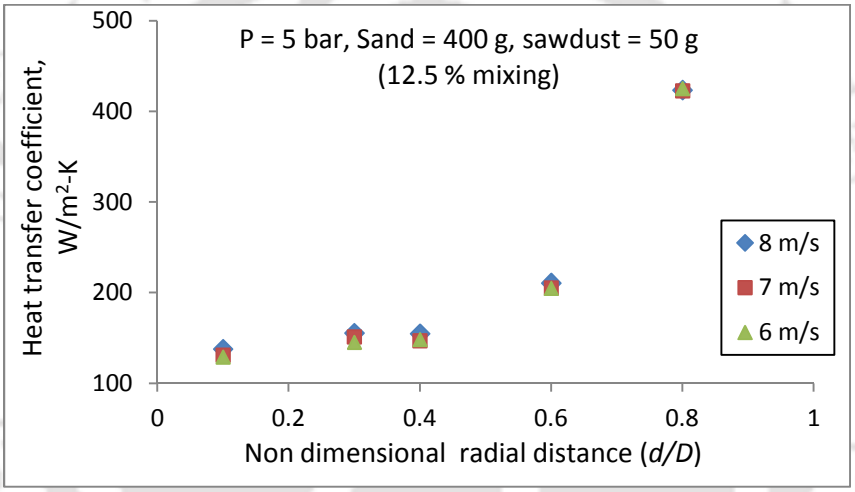

Fig.6.68 Radial variation of heat transfer coefficient at 12.5 % biomass blend

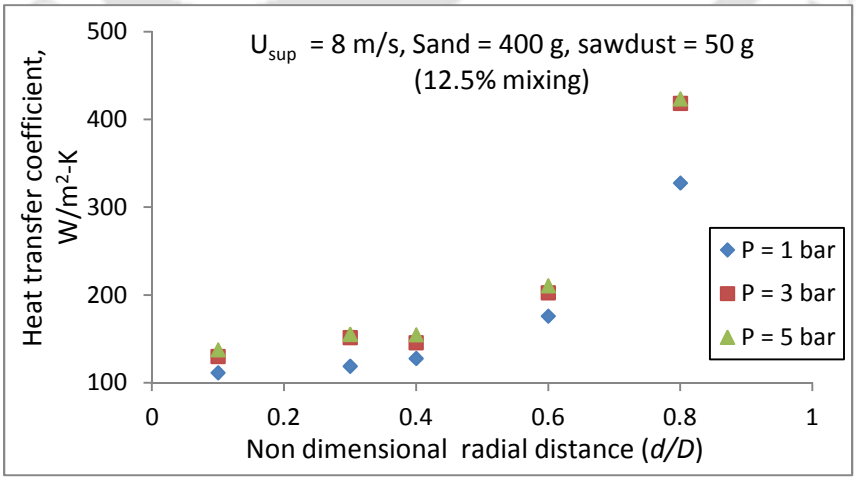

Fig.6.69 Radial variation of heat transfer coefficient with operating pressure

The comparison of radial variation of heat transfer coefficient at two different superficial velocities is presented in Figs.6.70 through 6.72. These plots have been made at a distance of 1.57 m from the height of the distributor and at 2.5 %, 15.0 % and 20.0 % sawdust blending. From these figures, it has been observed that, the heat transfer coefficient decreases from the wall to the core of the riser. This may be due to decrease in particle concentration from the wall to the core of the riser. It is also seen that with the increase in pressure, heat transfer coefficient increases. This may be due to the increase in particle concentration with increase in pressure. At 20 % biomass blending, heat transfer coefficient near to the wall of the riser is found be highest and at the core it is found to be lowest. This is probably due to the diffusion of particles from the core to the wall of the riser.

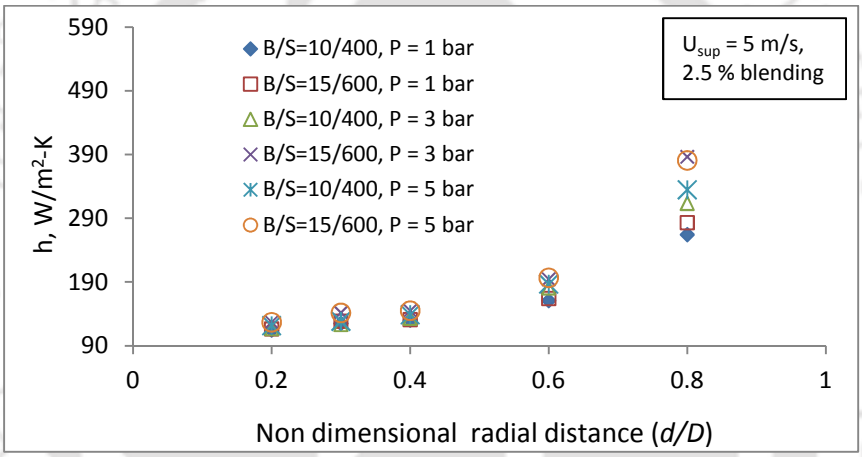

Fig.6.70 Comparison of radial variation of heat transfer coefficient at 2.5 % blending

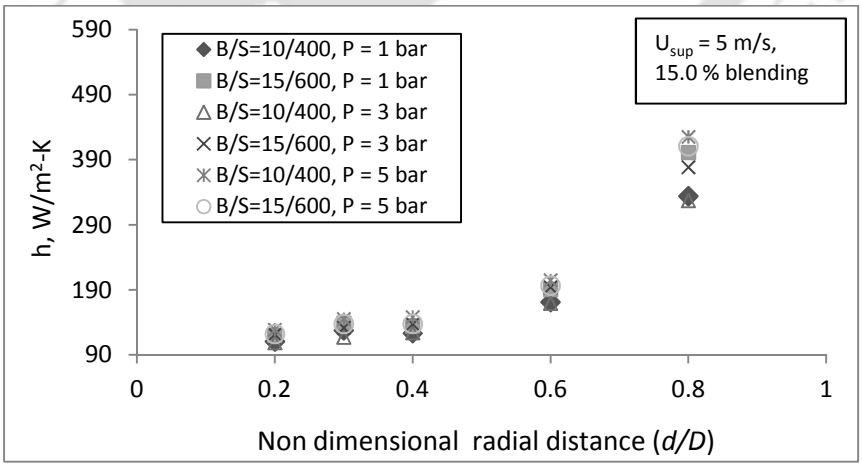

Fig.6.71 Comparison of radial variation of heat transfer coefficient at 15.0 % blending and at U_{sup} = 5 m/s

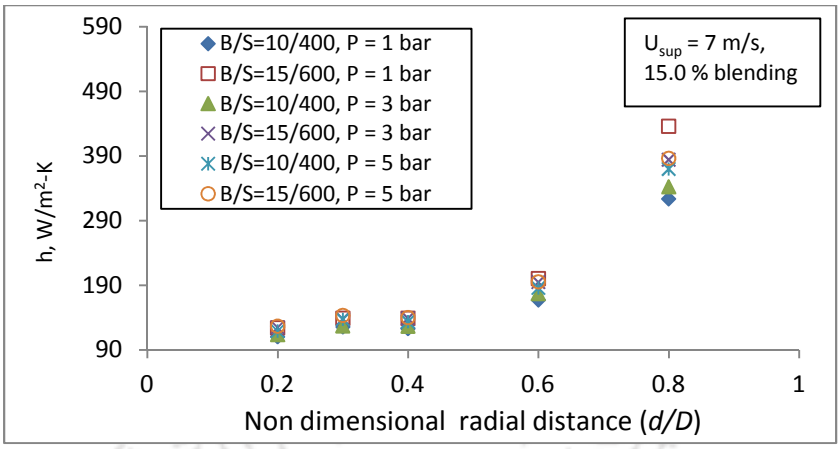

Fig.6.72 Comparison of radial variation of heat transfer coefficient at 15.0 % blending and at U_{sup} = 7 m/s

6.4.7 Effect of solid circulation rate on heat transfer

The solid circulation rate also increases with an increase in pressure at all the percentage blending of biomass in sand as shown in Fig.6.73. However, this is found to be more in the case of 7.5 % and 12.5 % in comparison to 2.5 % and 20.0 % biomass blend. This may be due to the proper mixing of biomass with sand. The lowest values of solid circulation rate have been observed in the case of 20 % biomass blend at all the system pressures. As the % blending of biomass increases, the riser volume occupied by biomass also increases (as the bulk density of biomass is much lower) this contributes to the increase in resultant weight. As a result of which time taken to occupy the predefined distance by the solids after closing the ball valve is more, and hence the recirculation rate is lesser. Lower values of solids recirculation rate in the case of 2.5 % biomass blend is may be due to lower percentage of biomass present. Due to the proper mixing of sawdust in the case of 7.5 % and 12.5 % blending of sawdust in sand solid circulation rate is found to be higher. In both the cases, the biomass mixes well with the sand, and hence, improves the solid circulation rate. Result of this uniform mixing and optimum recirculation enhances the heat transfer characteristics in both the mixing conditions. At these two % blending, an uniform increase in suspension density has also been observed with the increase in pressure (Figs.6.20 and 6.21).

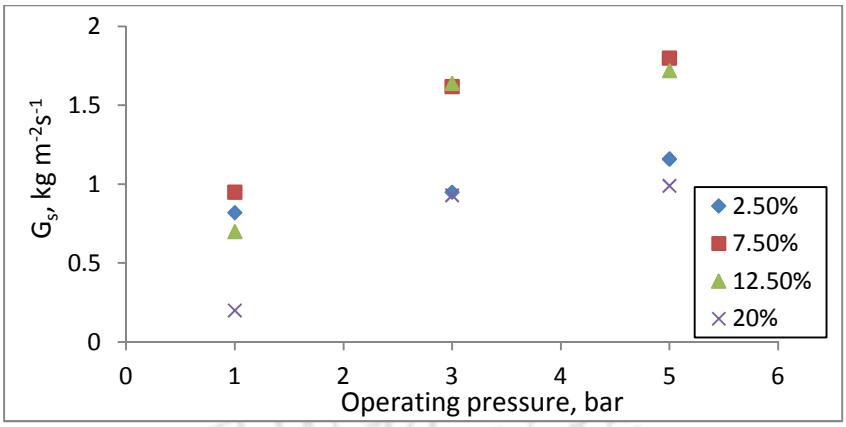

Fig.6.73 Variation solid circulation rate with operating pressure

6.5 Comparison of experimental results

Figure 6.74 presents the variation of heat transfer coefficient with suspension density of the present investigation along with the published data [Basu and Nag (1987), Nag and Moral (1990), Gupta and Nag (2002)]. For the cases, it is seen that the heat transfer coefficient increases with the increase in suspension density. This is due to the increase in energy transfer through particle to particle interactions as concentration of particles increases. It is also noticed that the present heat transfer coefficient data with suspension density are comparable to the published results despite varying experimental conditions (operating parameters and geometry of the setup). The heat transfer coefficient with % blending of biomass could not have been compared with the published literature because of unavailable published data. However, in case of bubbling bed, it was reported that 12 % biomass blending in sand was found to be optimum for maximum heat transfer and proper gasification (Oka and Oka, 2004).

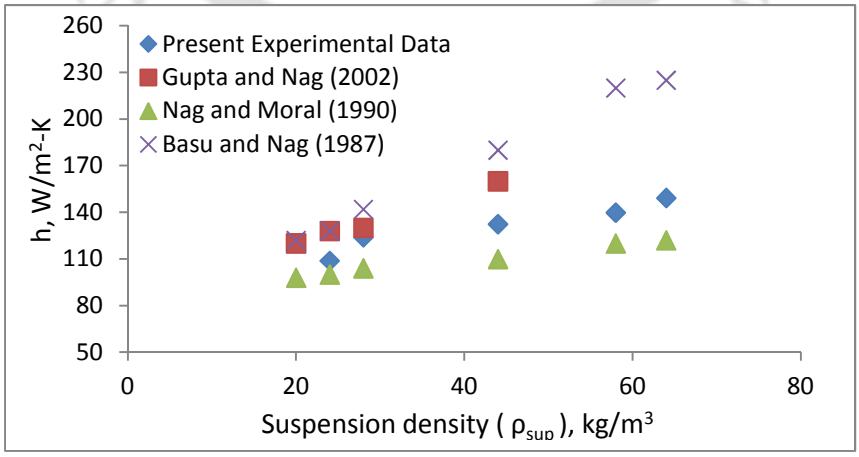

Fig.6.74 Comparison of heat transfer coefficient

6.6 Uncertainty analysis

In the present experimentations, various measuring devices were used. The individual accuracies of measuring devices based on the specification provided by the manufacturer and accuracies of fabricated units (observed during the experiment) are given in the Table-6.2.

Table-6.2 Accuracies of measured parameters

Parameters	Accuracy
Thermocouple sensor	± 0.5 °C
Auto-transformer	± 1 V
Ammeter	± 0.1 A
Manometer	± 0.5 mm
Stopwatch	± 0.2 s
Solid density	± 5 kg/m^3
Diameter	± 0.005 m
Height	± 0.001 m
Weight	± 2 g
Orifice pressure drop	± 0.5 mm

By considering the individual uncertainties of measuring devices, the overall uncertainties of solid circulation rate and heat transfer coefficient were carried out with respect to the equations (3.5) and (3.6) described under the subsection 3.2.4 of chapter 3. The procedure described in (Holman, 2007) was followed for the analysis of overall uncertainties. The overall uncertainties of solid circulation rate and heat transfer coefficient were found to be ± 5.32 % and ± 3.90 % respectively. The detail calculations of overall uncertainty are presented in the appendix-X.

6.7 Summary of the chapter

Series of experiments were carried out in order to investigate the various operating parameters on bed hydrodynamics and wall-to-bed heat transfer at the upper splash region of the riser. The flattened S-shaped bed voidage has been observed from the bottom to the top in all the cases and with the increase in pressure, bed voidage increase at the bottom and decreases at the top. The heat transfer coefficient increases from the bottom to the top of the heat transfer probe and it increases with the increase in pressure. It is also found that, 12.5 % biomass blending is found to be optimum for hydrodynamic and heat transfer point of view. The experimental values at varied percentage blending of biomass are presented in the appendix-XI. Next chapter presents the results of the experiment carried out in the hot PCFB.

Chapter – 7

RESULTS AND DISCUSSION - HOT CFB UNIT

7.1 Introduction

This chapter reports the results of the experiments carried out on the hot PCFB unit. The effect of operating pressures and biomass blending ratios on heat transfer characteristics and temperature along the riser height were studied and compared with the published results. The effect of twisted tape inserts on bed-to-wall heat transfer coefficient was studied at the upper splash region of the riser. A set of experiments were also carried out to investigate the quality of product gas generated during PCFB gasification operation at two different percentage biomass to sand blending ratios of 12.5 % and 20.0 % and at an equivalence ratio of 0.27. The quality of product gas composition was studied with the help a gas chromatography and a flue gas analyser at three different operating pressures. The performance of a novel biomass feeding system employed in the PCFB unit was also evaluated.

7.2 Experiments on hot bed study

In each experiment, the superficial velocity of 7 m/s was kept constant. Experiments were carried out at three different heat supplies, and hence, at three different controller temperatures. At each temperature, the effect of pressure was studied at three different operating pressures of 1, 3 and 5 bar. At each pressure condition, bed temperature distributions along the height of the riser were investigated. The temperature distributions at two different biomass blending ratios of 12.5 % and 20.0 % and at two different weight composition ratios were investigated and compared. The product gas composition was also investigated at each pressure condition and at an equivalence ratio of 0.27 and at two different biomass blending ratios. The effect of twisted tape inserts on heat transfer at the upper splash region of the riser was studied at three different operating pressures and at three different solid inventories of 400, 600 and 800 g. The mean particle size of sand and biomass considered in the study are 307 and 407 μm, respectively. The performance of the feeding system in terms of feeding rate with power supply has also been investigated and reported. The overall uncertainty in calculating heat transfer coefficient is found to be ± 12.3 %.

7.3 Study of temperature profile and heat transfer characteristics

7.3.1 Variation of bed temperature along the riser height

The temperature variations along the bed height at a superficial velocity of 7 m/s and at three different operating pressures for 400 g bed inventory at a certain solid circulation rate are shown in Figs.7.1-7.3. It has been found that the bed is not isothermal at all the pressures and temperatures. The maximum temperature recorded at 0.5 m above the distributor. Then it tapers off along the height of the riser. As the controller temperature increases, the temperature at all the measured point increases. Due to the proper mixing of solid particles at higher pressure a uniform variation of temperature has been observed (Fig.7.3). The temperature variation along the riser height has been compared with the earlier reported results (Ali, 1991) and presented in the Fig.7.4. A similar bed temperature variation has been observed along the height of the riser despite the different operating conditions and geometry used in the experiments.

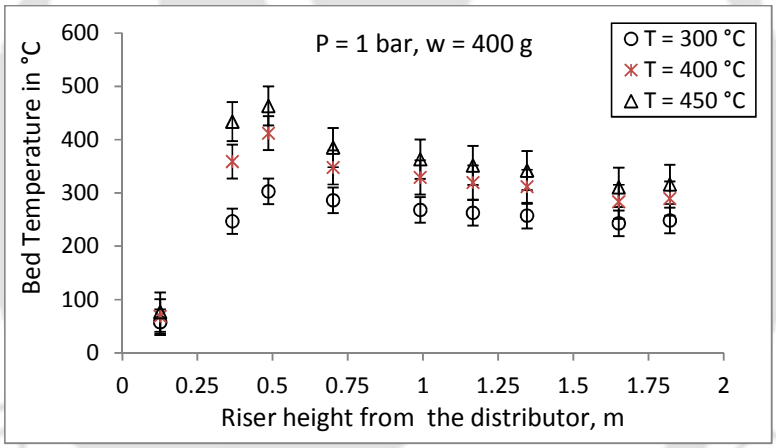

Fig.7.1 Bed temperature profile at P = 1 bar when only send is used as fluidizing media

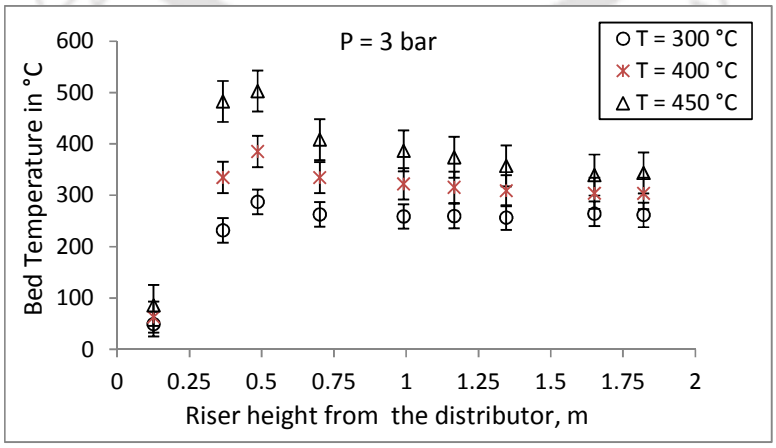

Fig.7.2 Bed temperature profile at P = 3 bar when only send is used as fluidizing media

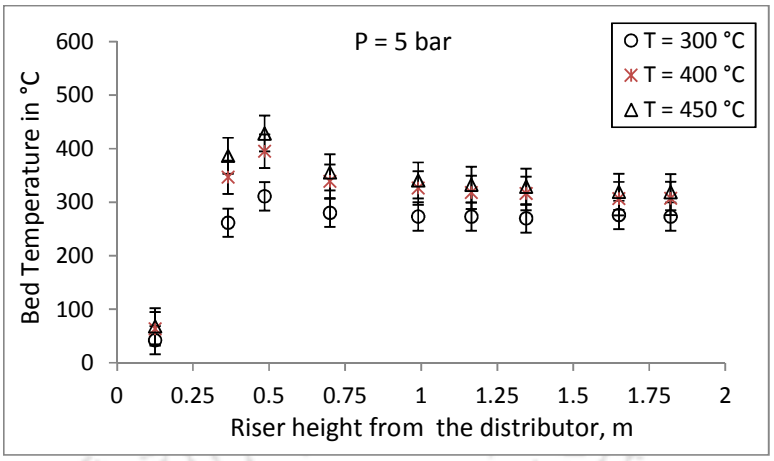

Fig.7.3 Bed temperature profile at P = 5 bar when only send is used as fluidizing media

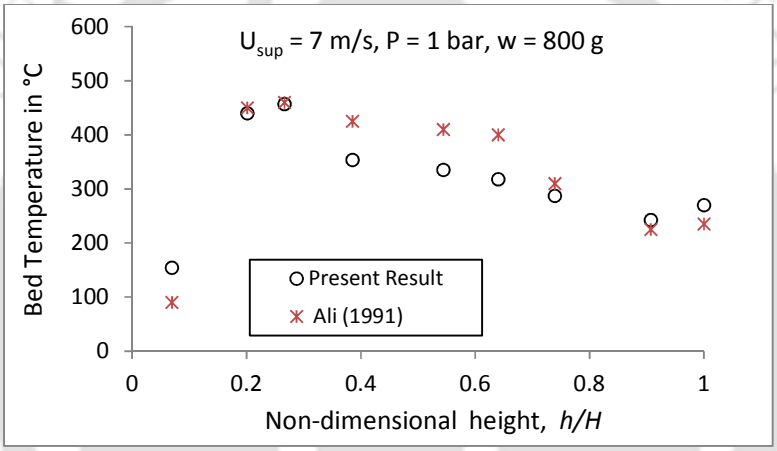

Fig.7.4 Comparison of bed temperature variation along the riser

7.3.2 Comparison of bed temperature with solid inventory along the riser height

The effect of solid inventory on bed temperature at three different operating pressures is shown in Figs.7.5 through 7.7. Similar bed temperature variations have been observed at all the operating pressures for all the three solid inventories. However, the bed temperature is found to be higher at the lower splash region for higher inventories and the temperature is very close to each other at the middle splash region of the riser. This is due to the higher solid accumulation at the lower splash region. At the upper splash region the bed temperature is higher at the lower solid inventories (400 g). This is due to the uniform mixing of solids due to more turbulence.

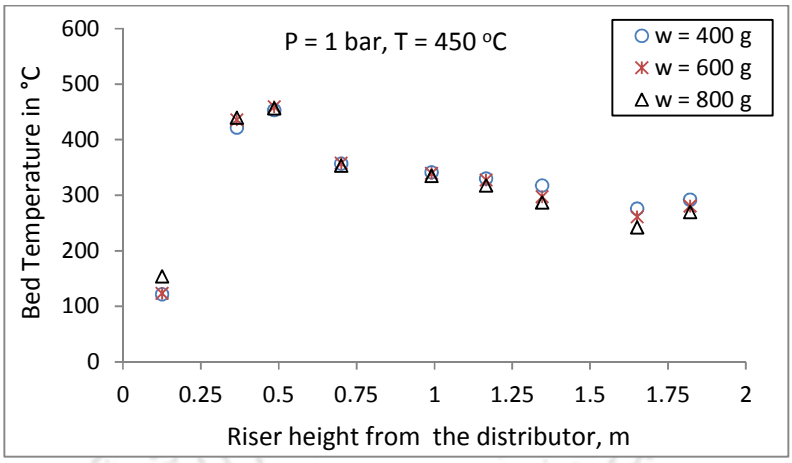

Fig.7.5 Effect of solid inventory on bed temperature at P = 1 bar

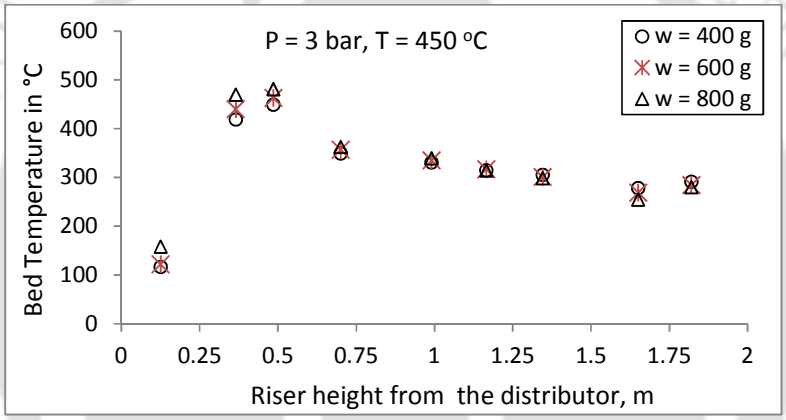

Fig.7.6 Effect of solid inventory on bed temperature at P = 3 bar

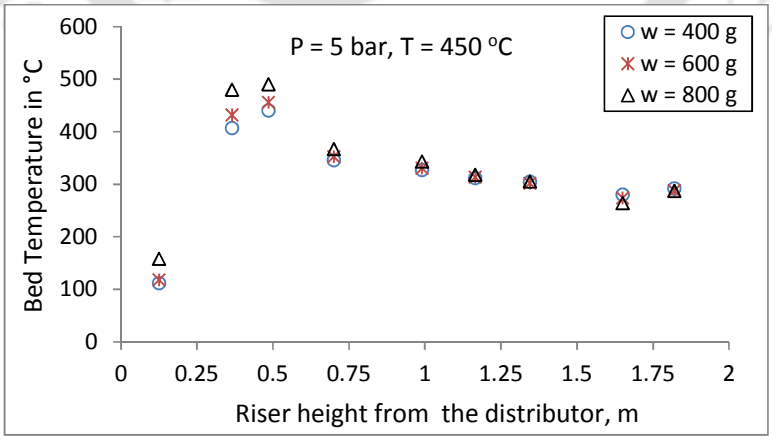

Fig.7.7 Effect of solid inventory on bed temperature at P = 5 bar

7.3.3 Comparison of bed temperature at different biomass blends

The comparison of bed temperature with operating pressures at the blending ratios of 12.5% and 20.0 % are shown in Figs.7.8 and 7.9. Based on the experience of cold bed results this two blending ratios are selected. A higher bed temperature has been observed at higher operating pressure along the height of the riser. However, very close temperature variation has been found at a blending ratio of 20.0 %. Similar bed temperature variation has been observed at different operating pressures, inventories and different biomass blending ratios as depicted from Figs.7.10 and 7.11.

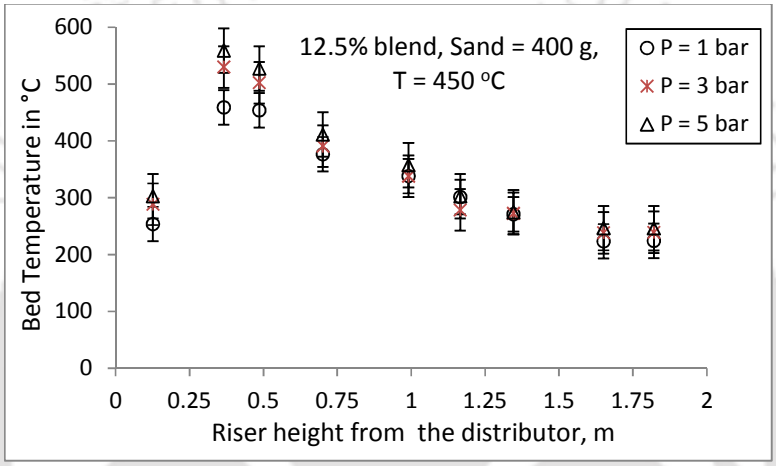

Fig.7.8 Comparison of bed temperature profiles at 12.5 % blend

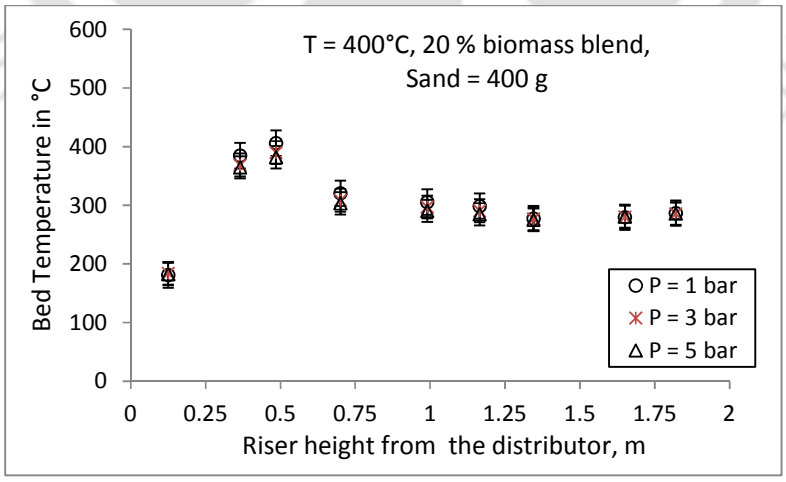

Fig.7.9 Comparison of bed temperature profiles at 20.0 % blend

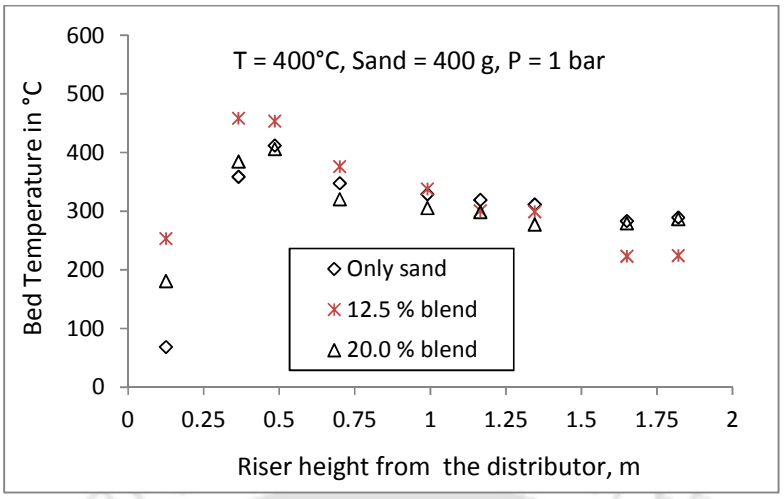

Fig.7.10 Comparison of bed temperature variation along the riser at P = 1 bar

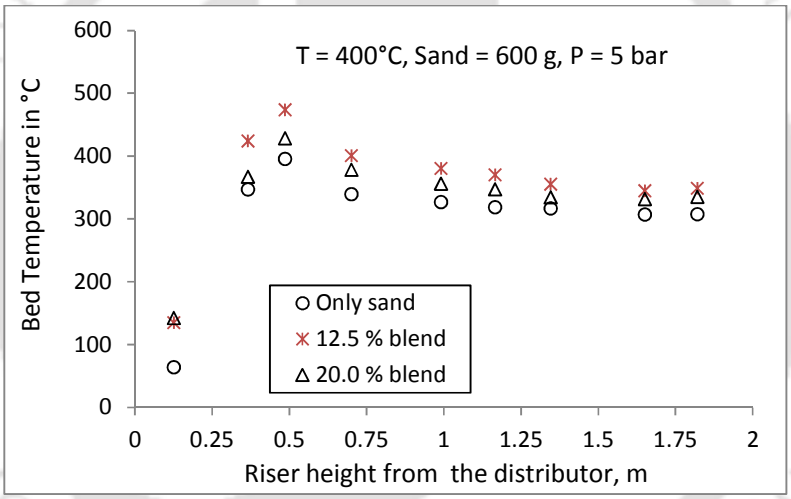

Fig.7.11 Comparison of bed temperature variation along the riser at P = 5 bar

7.3.4 Comparison of bed temperature at different weight composition ratios

Figures 7.12 through 7.17 compare the variation of bed temperature at two different weight composition ratios and at two different % blending of biomass in sand at three different operating pressures of 1, 3 and 5 bar. A similar variation of bed temperature along the height of the riser has been observed at both the % blending of biomass. More homogenous and uniform temperature distribution has been found at higher pressure and at a blending ratio of 12.5 %.

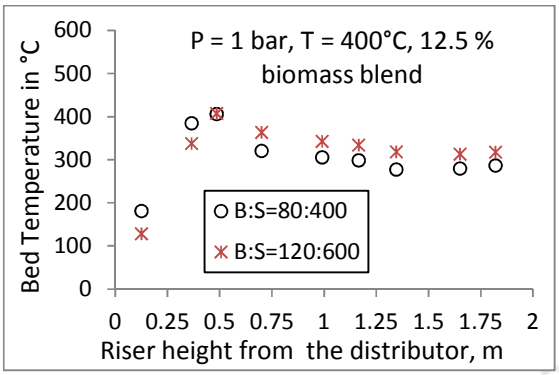

Fig.7.12 Comparison of bed temperature at P = 1 bar and at 12.5 % blend

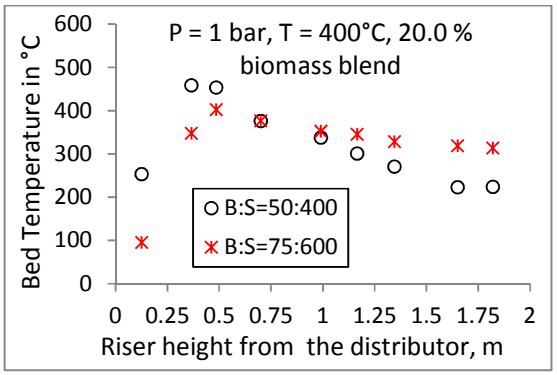

Fig.7.13 Comparison of bed temperature at P = 1 bar and at 20.0 % blend

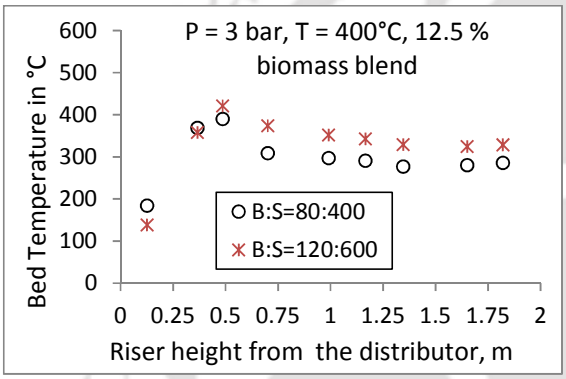

Fig.7.14 Comparison of bed temperature at P = 3 bar and at 12.5 % blend

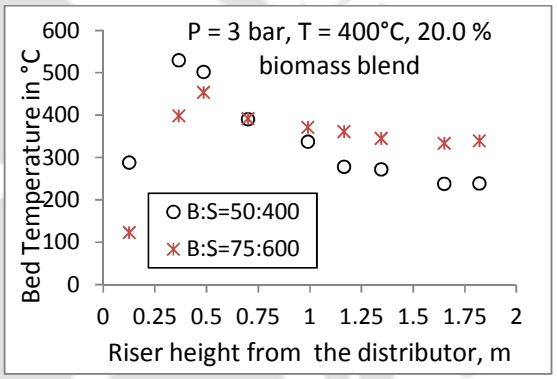

Fig.7.15 Comparison of bed temperature at P = 3 bar and at 20.0 % blend

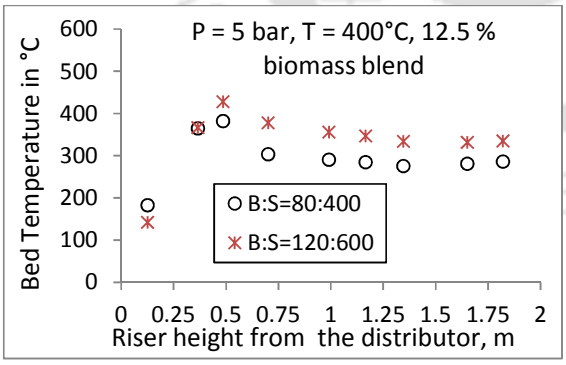

Fig.7.16 Comparison of bed temperature at P = 5 bar and at 12.5 % blend

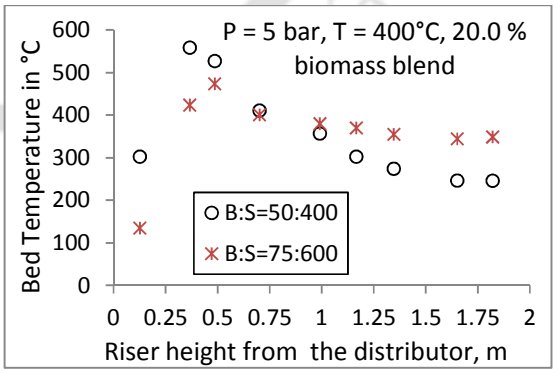

Fig.7.17 Comparison of bed temperature at P = 5 bar and at 20.0 % blend

7.3.5 Effect of twisted tape inserts

7.3.5.1 Comparison of bed temperature without and with twisted tape inserts

The comparison of bed temperature along the height of the riser without (probe-2) and with twisted tape (probe-3) for the solid inventory of 600 g at the operating pressures of 1, 3 and 5 bar are presented in Figs.7.18, 7.19 and 7.20 respectively. These three are the representative figures at the superficial velocity of 7 m/s. Similar temperature profiles have been found for the inventories of 400 and 800 g. The maximum temperature is recorded at a height of 0.5 m from the distributor and thereafter, the temperature drops before it reaches the riser top. At the top, solid concentration increases, and hence, the temperature increases. Similar trends have been observed at all the operating pressures. The lower temperature at the exit of the riser in the case of probe-2 is due to the more heat carried away by the water when twisted tape is used.

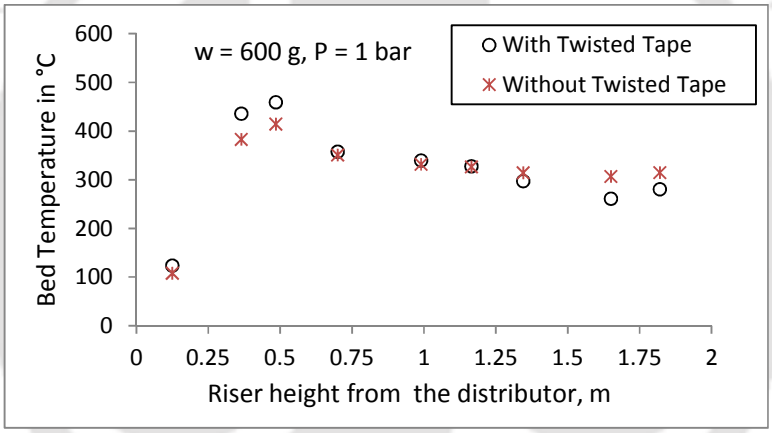

Fig.7.18 Comparison of bed temperature along the riser height at P = 1 bar

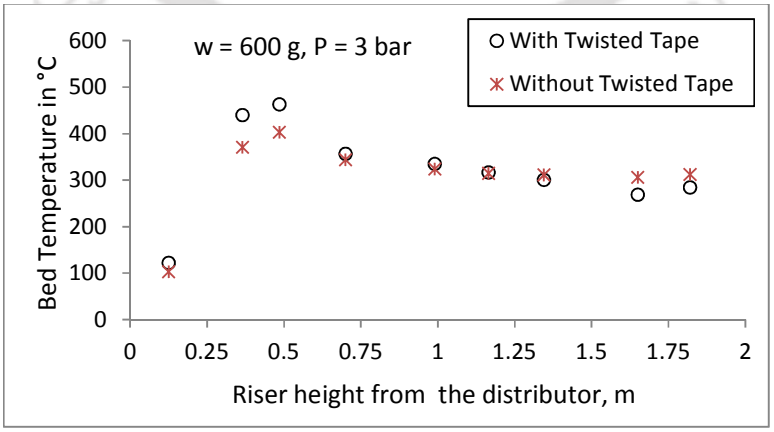

Fig.7.19 Comparison of bed temperature along the riser height at P = 3 bar

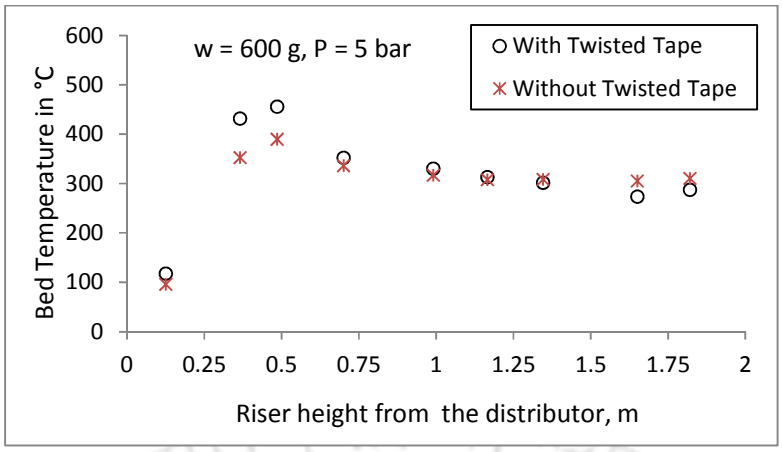

Fig.7.20 Comparison of bed temperature along the riser height at P = 5 bar

7.3.5.2 Comparison of heat transfer coefficient without and with twisted tape inserts

The comparison of probe average heat transfer coefficient without and with twisted tape inserts at three different operating pressures for the solid inventories of 400 g, 600g and 800 g are presented in Figs.7.21 through 7.23. The experiments were performed at a superficial velocity of 7 m/s. From the figures it has been observed that, the heat transfer coefficient is increasing with the increase in operating pressures. Similar trends of variation of heat transfer coefficient have been observed for all the three inventories. However, the values of probe average heat transfer coefficient are found to be higher for the solid inventory of 400 g. This is due to the higher turbulence and uniform distribution of solids throughout the riser.

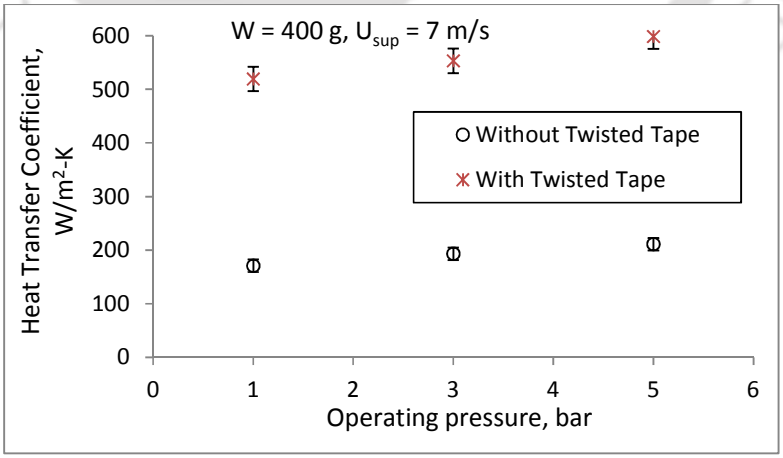

Fig.7.21 Comparison of heat transfer coefficient at the upper splash region of the riser at W = 400 g

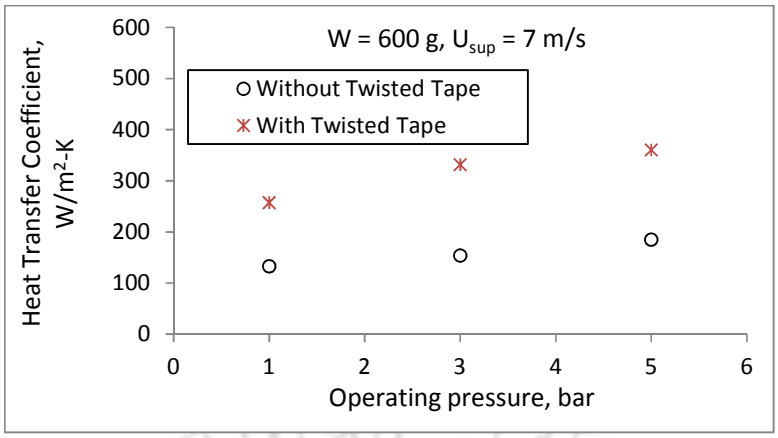

Fig.7.22 Comparison of heat transfer coefficient at the upper splash region of the riser at W = 600 g

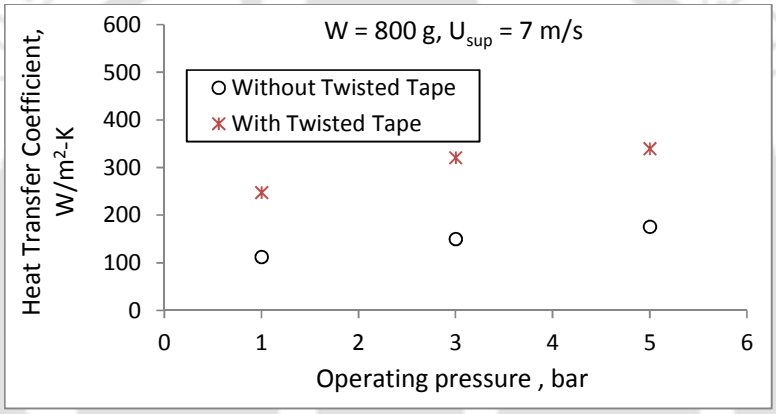

Fig.7.23 Comparison of heat transfer coefficient at the upper splash region of the riser at W = 800 g

7.4 Gas composition analysis

Based on the TGA results discussed in the chapter 5, it has been noticed that all the volatiles present in the biomass released before reaching a temperature of 500 ^{o}C. Biochar is produced after releasing the volatiles from the raw biomass. Hence, the product gas composition was investigated at a temperature of 500 ^{o}C at two different biomass blending ratios of 12.5 % and 20.0 %. The hot CFB unit could not be operated beyond 500 ^{o}C ± 30 ^{o}C due to the constraint associated with the heating element. The experiments were performed at an optimum equivalence rato of 0.27, as cited by Wu *et al.* (2009), and Zhou *et al.,* (2009). The studies were caried out at three different operating pressures. Table-7.1 compares the result of the product gas obtained at 500 ^{o}C with those obtained by Li *et al.* (2002) at 800 ^{o}C. From the table, it has been observed that, % of hydrogen is significantly higher in the present investigation.

Table-7.1 Gas composition analysis

Blending ratio	Operating pressure in bar	Current Result			Result of Li *et al.* (2002)			Bingyan *et al.* (1994)		
		Temp °C	ER	H_2 content in %	Temp °C	ER	H_2 content in %	Temp °C	ER	H_2 content in %
12.5 %	1	500 ± 30	0.27	19.036	800	0.26	7.3	924	0.25	16.32
	3	500 ± 30	0.27	14.011	---	---	---	---	---	---
	5	500 ± 30	0.27	10.108	---	---	---	---	---	---
20.0 %	1	500 ± 30	0.27	16.421	---	---	---	---	---	---
	3	500 ± 30	0.27	11.230	---	---	---	---	---	---
	5	500 ± 30	0.27	7.561	---	---	---	---	---	---

The conversion of carbon is also investigated by collecting the bottom ash and found to be in the range of 75.3-80.5 % and 70.1-77.6 % for 12.5 % and 20.0 %, respectively. The higher % H_2 and higher carbon conversion at a biomass blending ratio of 12.5 % was belived to be due to good circulation and optimum inter-mixing of biomass and sand. The gas produced in the hot CFB is cooled by using an annulus heat exchanger, before the sample is collected for gas analysis. Gas samples are collected in tedlar bags for chromatography (GC) analysis. An online flue gas analyzer is also used for gas analysis. The gas samples are analyzed at different operating pressures and at two different biomass blending ratios. CO and H_2 content found to be varied from 754 to 1213 ppm and 19.036 to 7.561 % in the entire sets of experiments. From the GC analysis, it has been noticed that, with the increase in operating pressure, the volume percentage of H_2 content decreases in both the weight composition. Due to lack of experimental facility volume percentage of CO_2 present in the product gas could not be measured. Figures 7.24 and 7.25 present the result of GC analysis at the blending ratios of 12.5% and at 1 and 5 bar operating pressures, respectively. These two are the representative curves, similar results have been found at the other blending ratios and operating pressures.

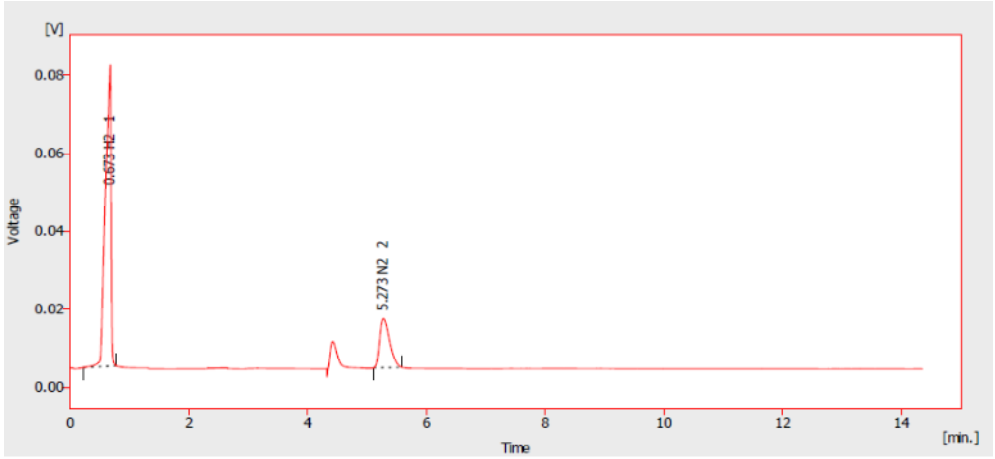

Result Table (ESTD - C:|Documents and Settings|HOME|Desktop|Pankaj|15-Oct-2012 sample 600+20 pankaj)

	Reten. Time [min]	Area [mV.s]	Response	RB	Amount [% VOL]	Amount [%]	Peak Type	Compound Name
1	0.673	506.420	506.420	A	19.036	68.4	Ordnr	H2
2	5.273	146.996	146.996	A	8.807	31.6	Ordnr	N2
	Total	653.416			27.843	100.0		

Fig.7.24 Gas chromatography result at 12.5 % blending ratio and at P = 1 bar

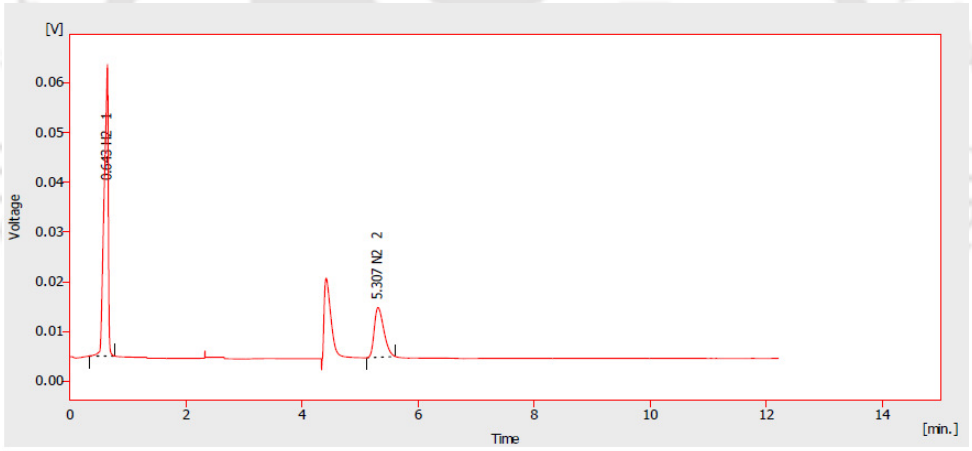

Result Table (ESTD - C:|Documents and Settings|HOME|Desktop|Pankaj|15-Oct-2012 sample 12.5+1 bar pankaj)

	Reten. Time [min]	Area [mV.s]	Response	RB	Amount [% VOL]	Amount [%]	Peak Type	Compound Name
1	0.643	285.497	285.497	A	10.732	61.0	Ordnr	H2
2	5.307	114.552	114.552	A	6.863	39.0	Ordnr	N2
	Total	400.049			17.595	100.0		

Fig.7.25 Gas chromatography result at 12.5 % blending ratio and at P = 5 bar

7.5 Performance of biomass feeding system

Figure 7.26 shows the variation and comparison of solid flow with blower exit velocity at four different inventories of 250, 500, 750 and 1000 g. The sawdust particle size of mean diameter of 732 μm has been used for this comparison. From the figure, it has been found that, with the increase in blower exit velocity the solid flow rate increases. The solid flow rate

also increases with the increase in inventory. This may be due to the increase of gravitational force with increase in weight. In all the inventories and at the sawdust particle sizes of 732 and 853 μm, no chocking has been noticed. Biomass appears to have smoothly discharged along the opening area between the pipe and the cone while there was air suction via the pipe, carrying the biomass along with it at the bottom. Unlike other models of biomass feeding systems, this apparatus avoided choking and bridge formation successfully.

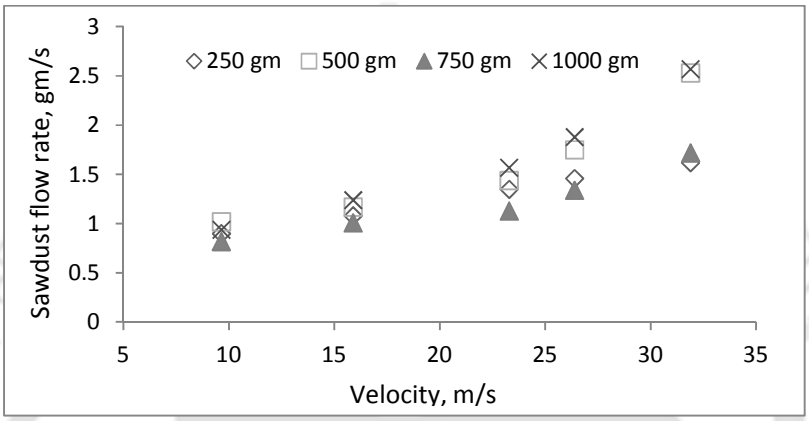

Fig.7.26 Variation of solid flow rate with blower exit velocity

The comparison of variation of biomass discharge time with blower exit velocity at four different inventories of 250, 500, 750 and 1000 g is presented in Fig.7.27. From the figure, it is noticed that, the biomass discharge time is maximum at lower blower exit velocity and it decreases with the increase in velocity. Successful continuous flow has been observed in all the inventories. In all the experiments, the voltage is varied from 50 V to 90 V. The plot explains the ability of this feeder to deliver 1 kg of biomass in about 18 min 3 s and at 55 V.

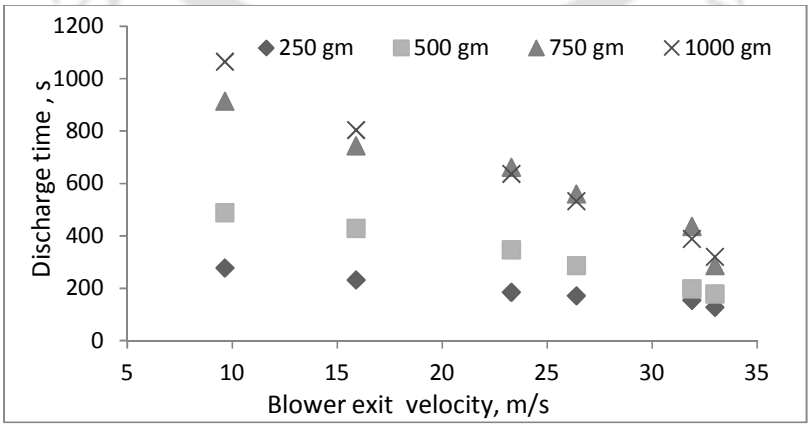

Fig.7.27 Biomass discharge time with blower exit velocity

In case of the larger particles, having particle diameter of more than 921 µm, the pipe with holes seen to provide insufficient suction and agitation. This causes feed flow intermittent as well as rat holes formation in the hopper (around the pipe), even the feeder shakes momentarily in the intervals of 5 minutes. Besides, sawdust having irregular particle shape and size, the flow through the blower is initiated only at 75 V and the solid gets discharged very quickly. The discharge time was found to be as low as 1 min 57 sec for 1 kg of biomass inventory. The snapshot of the bridge formation, formation of rat holes and shocking is shown in Fig.7.28. The physical properties such as spherocity, bulk density also affect the flow. The hydrodynamics of the flow at different velocities are also shown in Figs.7.29 through 7.31.

Fig.7.28 Snapshot of the inside of the cone feeder in intervals of 30 seconds

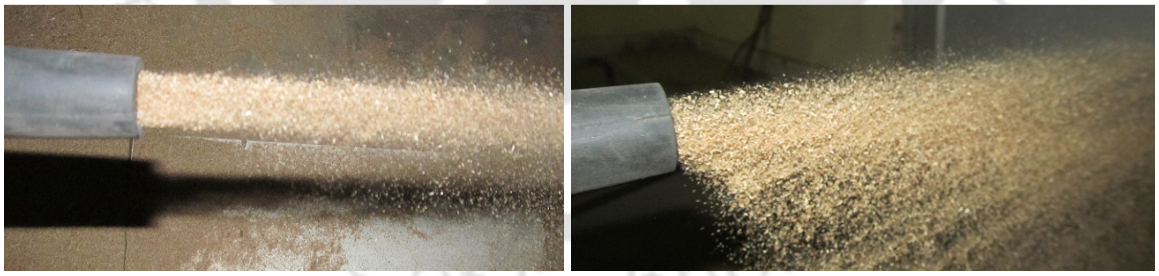

Fig.7.29 Flow of biomass for the particle size of 732 µm at high speed

Fig.7.30 Flow of biomass for the particle size of 732 µm at low speed

Fig.7.31 Flow of biomass for the particle size of 921 µm at high speed

7.6 Uncertainty analysis

In the present experimentations, various measuring devices were used. The individual accuracies of measuring devices based on the specification provided by the manufacturer and accuracies of fabricated units (observed during the experiment) are given in the Table-7.2.

Table-7.2 Accuracies of measured parameters

Parameters	Accuracy
Thermocouple sensor	± 0.5 °C
Thermometer	± 1 V
Bulk Temperature	± 0.1 °C
Mass flow rate of water	± 0.1 A
Area of the tube	± 0.5×10^{-3} m
Diameter	± 0.005 m
Height	± 0.001 m

By considering the individual uncertainties of measuring devices, the overall uncertainty of heat transfer coefficient was carried out with respect to the equation (3.8) described in the chapter 3 under the subsection 3.3 (Description of hot bed unit). The overall uncertainty of heat transfer coefficient was calculated to be ± 12.3%. The detail calculations of overall uncertainty are presented in the appendix-X.

7.7 Summary of the chapter

This chapter presents the results of the experiments carried out in the hot PCFB unit. The maximum bed temperature was observed at a height of 0.5 m from the distributor. Thereafter bed temperature decreases along the height of the riser. This has been observed in all the biomass blending ratios as well as all at different operating pressures. The bed-to-wall heat transfer coefficient found to increase significantly with the use of twisted tape at the upper splash region of the riser. This is more pronounced at higher operating pressures. The product gas composition was studied at an equivalence ratio of 0.27 and at a controlled temperature of 500 ^{o}C. It has been found that, with the increase in operating pressures hydrogen content in the product gas decreases (from 19.04 % at P = 1 bar to 10.10 % at 5 bar at biomass blending ratio of 12.5 %). Performance of a novel biomass feeding system was also investigated and was found to be very effective up to a particle size of 731 µm. The next chapter summarizes the findings of the present research and the scope of future work.

Chapter – 8

CONCLUSIONS AND FUTURE SCOPE

8.1 Summary of the investigation

In the present investigation, two units of PCFB (one cold and one hot) of similar dimensions have been developed. The bed hydrodynamics along the height of the riser have been investigated in the cold PCFB unit. The heat transfer characteristics have been investigated in both the PCFB units at the upper splash region of the riser. A novel biomass feeding system was also developed for feeding of biomass in the PCFB units and performance was analyzed. The bed hydrodynamics and heat transfer characteristics have been investigated at different operating conditions such as operating pressures, solid inventories, superficial velocities, and at different blends of biomass in sand and at two different weight compositions. The biomass used for the study has been characterized. The thermogravimetric (TG) analysis and differential scanning calorimetry (DSC) have been used to study the influence of heating rate on the degradation of biomass. The kinetic parameters viz. pre-exponential factor, activation energy and order of reaction were evaluated for both first and second reaction zones which were categorized based on the degradation of cellulose, hemicelluloses and lignin content present in the biomass. The degradation of mass with temperature obtained from TG curve was validated numerically. The thermal response of biomass undergoing decomposition has also been modelled by using one dimensional (1-D) transient thermal model with an nth order approximation for the rate of decomposition. Gasification study has been carried out at an equivalence ratio of 0.27 in the hot PCFB unit. The product gas composition has been investigated by using a gas chromatograph and a flue gas analyzer at different blending ratios of biomass and at three different operating pressures. The enhancement of heat transfer by using twisted tape inserts at the upper splash region of the riser has been studied at three different solid inventories and at three different operating pressures. The key research findings are summarized in the following subsections.

8.1.1 Results of characterization and thermal analysis of biomass

Kinetic parameters of both first and second reaction zones of locally available biomass such as rice husk and sawdust were evaluated by using multi variable regression analysis. These kinetic parameters were utilized in the numerical technique in order to predict the mass degradation with temperature in both the reaction zones at three heating rates of 10, 30 and 80 °C/min. From the TG and DTG analysis, it has been found that, the major weight loss due to the degradation of volatiles starts at around 180-205 °C for all the biomasses at three different heating rates. Up to 400 °C, weight loss is about 85 % of the total volatile matter. After a rapid pyrolysis, a relatively slow pyrolysis occurred over 400 °C. Finally, bio-char is formed with the removal of most of the volatile matters. It is also observed that, with the increase of rate of heating, the degradation temperature increases. The predicted degradation results are well comparable with the experimental data in both the reaction zones for all the three heating rates. A transient one dimensional heat conduction model was formulated to investigate the transient response without and with considering the heat of formation. Kinetic parameters, properties of biomass, temperature range for both the reaction zones are used as input to the model. Results of the model agree well with the results obtained by using Heisler Chart without considering heat of formation.

8.1.2 Results of cold bed studies

In this investigation, the effect of superficial velocity, operating pressures, particle size and solid inventory on hydrodynamics and wall-to-bed heat transfer characteristics in a PCFB unit has been studied. The experiments were carried out at four different superficial velocities such as 5, 6, 7 and 8 m/s. At each superficial velocity, the experiments were performed at three different operating pressures of 1, 3 and 5 bar. The hydrodynamics and wall-to-bed heat transfer characteristics at four different proportions blending of sawdust (2.5, 7.5, 12.5, 15.0 and 20.0 %) and at two different sets of weight (inventories) composition ratio were investigated. Effects of recirculation rate have also been studied. From the study, it has been found that flattened S-Shaped bed voidage profile appeared in all the percentage mixing of sawdust in sand at all the operating conditions. With an increase in pressure, the bed voidage increases at the lower splash region of the riser and decreases at the upper splash region. The solid circulation rate increases with an increase in operating pressures and an increase in bed inventories. The suspension

density increases with the decrease in particle size and increases with an increase in operating pressure. The suspension density is also found to increase towards the riser exit with an increase in pressure. It is also seen that with the increase in both superficial velocity and system pressure, the heat transfer coefficient increases along the height of the heat transfer probe. The heat transfer coefficient is found to be maximum (145.17 W/m^2-K) at 12.5 % biomass blending with sand and at 5 bar operating pressure and at a superficial velocity of 8 m/s. However, at this superficial velocity, the suspension density along the height of the riser is found to be higher at higher pressure except at the riser exit. The increase in suspension density results in an increase of heat transfer coefficient, which indicates a lower consumption of blower power. The radial heat transfer coefficient decreases from the wall to the bed at all the operating conditions and operating pressures. Similar profiles have been observed in all the percentage mixing of biomass in sand. The heat transfer coefficient decreases with the increase in particle size. More homogenous fluidization and uniform heat transfer coefficient has been found as the operating pressure increases. Sawdust blend in sand (7.5 – 15.0 %) is observed to be optimum for obtaining higher heat transfer coefficient at both the sets of weight compositions. Prominent results of the present investigation are comparable to the published results under similar operating conditions.

8.1.3 Results of hot bed studies

Experiments were performed at three different heat inputs, and hence, at three different controller temperatures. At each temperature, the effect of pressure was studied at three different operating pressures of 1, 3 and 5 bar. At each pressure condition, the bed temperature distributions along the height of the riser were investigated. The temperature distributions at two different biomass blending ratios of 12.5 % and 20.0 %, and at two different weight composition ratios were investigated and compared. It has been observed that, the bed temperature first increases up to a height of 0.5 m from the distributor, and then decreases along the height of the riser before it increases at the exit. The product gas composition was also investigated at each pressure condition and at an equivalence ratio of 0.27 and at two different biomass blending ratios. With an increase in operating pressure, % composition of H_2 in the product gas decreases, however, the % composition of CO increases with pressure. The effect of twisted tape inserts on heat transfer at the upper splash region of the riser was studied at three different operating

pressures and at three different solid inventories of 400, 600 and 800 g. The heat transfer coefficient at the upper splash region increases with the increase in operating pressures as well as with the used of twisted tape having twist ratio of 4.

8.1.4 Performance of biomass feeding system

Performance of a biomass feeding system has been evaluated at four different biomass inventories of 250, 500, 750 and 1000 g and at three different particle sizes of 732, 853, and 921 μm. Absolutely no choking has been observed at all the inventories having biomass particle size ≤ 853 μm. The bridge formation and shocking has been observed for the biomass particles having particle size ≥ 921 μm. The developed system is a very flexible one, depending on the requirement of the feed, the appropriate voltage may be supplied in order to control the speed and hence flow. The feeding range of the developed feeding system is found to be 1-12 kg/hr, which is capable of supplying feed to a reactor of power generating capacity of 1-5 kW-hr. The developed feeding system is very much suitable for feeding of low bulk density biomass such as sawdust having particle size ≤ 853 μm to the circulating fluidized bed unit. Feeding of biomass without porous rod has also been tried, however, a continuous flow could not have been achieved.

In conclusion, this research gives an approach for an effective utilization of biomass under specific range of operating parameters in a PCFB unit where the reaction kinetics of biomass, bed hydrodynamics, and heat transfer behaviour along the riser have been thoroughly studied. Further, the findings of the present investigation will give sufficient guidance for the design of an efficient PCFB unit suitable for combustion as well as gasification applications.

8.2 Scope for future work

In the present investigation, steady state hydrodynamics and heat transfer characteristics were investigated at different operating conditions in two PCFB units. The important research findings have already been highlighted. However, there are lots of scopes for further research which can be carried out by using the developed units. Some of the scopes and suggestions for further studies are given below.

- The result of 1-D transient heat conduction considering the heat of formation gives an understanding of thermal degradation process which will help in designing an efficient thermo-chemical conversion system. The accuracy of the model depends upon the thermal, transport and kinetic properties as well as the boundary conditions. The model could further be improved by including some of the important physical processes such as, radiation heat transfer and considering variation of thermal conductivity and specific heat with temperature.
- In order to control the load variation in different circumstances, the study of transient behaviour of the CFB boiler is very essential. The investigation of transient study of hydrodynamics and heat transfer characteristics at different proportion mixing of coal, biomass and sand at higher operating pressures may be a challenging task to understand the load characteristics. There is also scope for heat recovery from the cyclone as the gas exiting the cyclone carries a huge quantity of heat.
- The entire work may be carried out at higher pressures as it may so happen that the linear scaling laws may not be applicable for higher operating pressures.
- The correlation for calculation of heat transfer coefficient based on the experimental observation under different experimental conditions may be developed. This would be a challenging task as the heat transfer coefficient varies with operating pressure, height of the riser, solid inventory, superficial velocity, size and type of the particles etc.
- The simulations of the entire PCFB unit for the scale up of the developed units, can be carried out.
- The optimization of gasification parameters for higher carbon conversion and for higher quality gas production at varied % blending of biomass and coal can be studied.
- The combustion charactristics inside the CFB reactor such as time of combustion, number of circulations, bottom ash and fly ash losses, can also be investigated.

REFERENCES

Agrawal R.K., Kinetics of reactions involved in pyrolysis of cellulose: I. The three reaction model. Canadian Journal of Chemical Engineering. 66 (2) (1988) 403-412.

Alèn R., Kuoppala E., Oesch P., Formation of the main degradation compound groups from wood and its components during pyrolysis. Journal of Analytical and Applied Pyrolysis. 36 (2) (1996) 137-148.

Ali M.S., (1991). Some studies on hydrodynamics and heat transfer in high temperature circulating fluidized beds, PhD Thesis, Department of Mechanical Engineering, IIT Kharagpur.

Andersson B.A., and Leckner B., Experimental methods of estimating heat transfer in circulating fluidized bed. International Journal of Heat Mass Transfer, 35 (1992) 3353-3362.

Antal Jr. M.J., and Varhegyi G., Cellulose pyrolysis kinetics: The current state of knowledge. Industrial and Engineering Chemistry Research, 34 (3) (1995) 703-717.

Anthony E.J., Pressurized fluidized bed combustion, Blackie Academic & Professional, Glasgow, 1995.

Asadullah M., and Miyazawa T., Ito S., Kunimori K., Koyama S., Tomishige K., A comparison of Rh/CeO2/SiO2 catalysts with steam reforming catalysts, dolomite and inert materials as bed materials in low throughput fluidized bed gasification systems, Biomass Bioenergy. 26 (2004) 269-279.

Balbi J.H., Santoni P.A., Dupuy J.L., Dynamic modelling of fire spread across a fuel bed. International Journal of Wildland Fire. 9 (1999) 275-284.

Bamford C.H., Crank J., Malan D.H., The combustion of wood: Part-I. Cambridge Philophysical Society Proc. 42 (1946) 166.

Basu P., Combustion and Gasification in Fluidized beds, Taylor and Francis (CRC Press). UK, 2006.

Basu P., Heat transfer in high temperature fast fluidized beds, Chemical Engineering Science. 45 (10) (1990) 3123-3136.

Basu P., and Cheng L., Heat transfer in a pressurized circulating fluidized bed, International Journal of Heat and Mass Transfer. 39 (13) (1996) 2711-2722.

Basu P., and Fraser S.A., Circulating fluidized bed boiler: design and operations, Butterworth-Heinemann, Boston, MA, USA, 1991.

Basu P., Jestin L., and Kefa C., Boilers and burners, 3rd Edition, Springer, 1999.

Basu P., and Nag P.K., An investigation into heat transfer in circulating fluidized beds. International Journal of Heat and Mass Transfer. 30 (11) (1987) 2399-2409.

Basu P., and Nag P.K., Heat transfer to walls of a circulating fluidized-bed furnace. Chemical Engineering Science. 51 (1) (1996) 1-26.

Basu P., and Ngo T., Effect of some operating parameters on heat transfer to vertical fins in a circulating fluidized bed furnace, Powder Technology. 74 (1993) 249-258.

Biagini E., Barontini F., Tognotti L., Devolatilization of biomass fuels and biomass components studied by TG/FTIR technique. Industrial Engineering and Chemical Research. 45(2006) 4486-4493.

Bining A.S., and Jenkins B.M., Thermochemical reaction kinetics for rice straw from an approximate integral technique. St. Joseph, MI, ASAE Paper No. 92-6029, 1992.

Bingyan X., Zengfan L., Chungzhi W., Haitao H., Xiguang Z., Circulating fluidized bed gasifier for biomass. In: Integrated energy systems in China-The Cold Northeastern Region Experience Food and Agriculture Organization of the United Nations. Rome, Italy: Publications Division; 1994.

Bingyan X., Chuangzhi W., Zhengfen L., Xiguang Z., Kinetic study on biomass gasification. Solar Energy. 49(3) (1992) 199-204.

Boateng A.A., Walawender W.P., Fan L.T., Chee C.S., Fluidized bed steam gasification of rice hull, Bioresource Technology. 40(3) (1992) 235-239.

Borodulya, V.A., Ganzha, V.L., and Kovensky, V.I., "Gidrodynamika i teploobmen v psevdoozhizhenom sloye pod davleniem (in Russian)." Nauka i Technika, Minsk, (1982).

Bouratona, R., Molodtsof, Y., Koniuta, A., Hydrodynamic characteristics of a pressurized fluidized bed, Paper presented at 12th International Conference on Fluidized Bed Combustion, La Jolla. 1993.

Brereton C.M.H., and Stromberg L., Some aspects of fluid dynamic behavior of fast fluidized beds, in Circulating Fluidized Bed Technology (Edited by P. Basu), Pergamon Press, Toronto, 1986, pp.133-144.

Bridgwater AV., The technical and economic feasibility of biomass gasification for power generation. Fuel. 74(3) (1995) 631-653.

Buragohain B., Mahanta P., Moholkar V.S., Biomass gasification for decentralized power generation: The Indian perspective, Renewable and Sustainable Energy Reviews. 14 (2010) 73-92.

Buragohain B., Chakma S., Kumar P., Mahanta P., Moholkar S.V., Comparative evaluation of kinetic, equilibrium and semi-equilibrium models for biomass gasification, International Journal of Energy and Environment. 4 (2013) 1-33.

Buragohain B., Manhanta P., Moholkar S.V., First principles design of a circulating fluidized bed (CFB) biomass gasifier, Published in the book chapter on "New technologies for rural development having potential of commercial" (Editor: Jai Prakesh Shukla), Allied Publishers Pvt Ltd., 2009, pp.210-223.

Campoy M., Gmez-Barea A., Vidal F., Ollero P., Air–steam gasification of biomass in a fluidised bed: process optimisation by enriched air, Fuel Processing Technology. 90 (2009) 677-685.

Cao Y., Wang Y., Riley J., Pan W., A novel biomass air gasification process for producing tar-free higher heating value fuel gas, Fuel Processing Technology 87 (2006) 343-353.

Carl W., and Aimo R., Handling and feeding of biomass to pressurized reactors: safety engineering. Bioresource Technology. 46 (1/2) (1993) 77-85.

Chaiprasert P., and Vitidsant T., Promotion of coconut shell gasification by steam reforming on nickel–dolomite. American Journal of Applied Science. 6 (2) (2009) 332-336.

Chattopadhyay P., Fluidized bed boiler, Galgotia Publications Pvt. Ltd., New Delhi, 2007.

Chiba S., Kawabata J., and Chiba T., Characteristics of pressurized gas-fluidized beds, in "Encyclopedia of Fluid Mechanics", N. P. Cheremisinoff, ed., Gulf Publishing, Houston, 1986, pp.929-945.

Chinsuwan A., and Dutta A., An investigation of the heat transfer behavior of longitudinal finned membrane water wall tubes in circulating fluidized bed boilers. Powder Technology 193 (2009) 187–194.

Chitester D.C., Kornosky R.M., Fan, L.S., Danko J.P., Characteristics of fluidization at high pressure. Chemical Engineering Science. 39(2) (1984) 253-261.

Coats A.W., and Redfern J.P., Kinetic Parameters from Thermogravimetric Data. Nature (London). 201 (1964) 68-69.

Collot A.G., Zhuo Y., Dugwell D. R., Kandiyoti R., Co-pyrolysis and co-gasification of coal and biomass in bench-scale fixed-bed and fluidized bed reactors. Fuel. 78 (6) (1999) 667-679.

Corella J., Toledo J., Padilla R., Olivine or dolomite as in-bed additive in biomass gasification with air in a fluidized bed: Which is better? Energy Fuels. 18 (2004) 713-720.

Corella J., and Sanz A., Modeling circulating fluidized bed biomass gasifiers. A pseudorigorous model for stationary state. Fuel Processing Technology. 86 (2005) 1021-1053.

Corella J., Toledo J.M., Molina G., A review on dual fluidized-bed biomass gasifiers. Industrial and Engineering Chemistry Research. 46 (21) (2007) 6831-6839.

Cozzani V., Lucchesi A., Stoppato G., Maschio G., A new method to determine the composition of biomass by thermogravimetric analysis. Canadian Journal of Chemical Engineering. 75 (1) (1997) 127-133.

Cucoci A., Faravelli T., Frassoldati A., Grana R., Pierucci S., Ranzi E., Sommariva S., Mathematical modelling of gasification and combustion of solid fuels and wastes. Chemical Engineering Transactions. 18 (2009) 989-994.

Cummera K.R., and Brown R.C., Ancillary equipment for biomass gasification, Biomass and Bioenergy. 23 (2002) 113-128.

Dai J., and Grace J.R., Biomass screw feeding with tapered and extended sections. Powder Technology. 186 (1) (2008) 56-64.

Dai J., and Grace J.R., A model for biomass screw feeding, Powder Technology. 186 (1) (2008) 40-55.

Di Blasi C., Modelling and simulation of combustion process of charring and non-charring solid fuels. Progress in Energy and Combustion Science 19 (1993) 71-104.

Di Blasi C., Comparision of semi global mechanismfor primary pyrolysis of lignocellulosic fuels. Journal of Analytical and Applied Pyrolysis. 47 (1998) 43-64.

Divilio R.J., and Boyd T.J., Practical implications of the effect of solids suspension density on heat transfer in large scale CFB boilers, in Circulating Fluidized Bed Technology IV (Edited by A. Avidan), AIChE, New York, 1994, pp.334-339.

Doherty W., Reynolds A., Kennedy D., Simulation of a circulating fluidised bed biomass gasifier using ASPEN Plus: a performance analysis. In: Conference proceedings; 2008.

Drift A van der, Boerrigter H., Coda B., Cieplik M.K., Hemmes K., Entrained flow gasification of biomass Ash behaviour, feeding issues, and system analyses, April 2004, ECN-C--04-039.

Drift A Van Der, Van Doorn J., Vermeulen J.W., Ten residual biomass fuels for circulating fluidized-bed gasification. Biomass Bioenergy. 20 (2001) 45–56.

Duvvuri M.S., Muhlenkamp S.P., Iqbal K.Z., Welker J.R., The pyrolysis of natural fuels. Journal of Fire and flammability. 6 (2) (1975) 468-477.

Ebert T.A., Glicksman L.R., Lints M., Determination of particle and gas convective heat transfer component in circulating fluidized bed. Chemical Engineering Science. 48 (1993) 2179-2188.

Ergun S., Fluid flow through packed columns. Chemical Engineering Process, 48 (2) (1952) 89-94.

Ergudenler A., and Ghaly A.E., Determination of reaction kinetics of wheat straw using thermogravimetric analysis. Journal of Applied Biochemistry and Biotechnology. 34/35(1) (1992) 75-91.

Fraley L.D., Lin Y.Y., Hsiao K.H., Solbakken A., Heat transfer coefficient in circulating bed reactor. ASME 83-HT-92, 1983.

Gil J., Aznar M., Caballero M., Frances E., Corellas J., Biomass gasification in fluidized bed at pilot scale with steam–oxygen mixtures. Product distribution for very different operating conditions. Energy Fuels. 11 (6) (1997) 1109–1118.

Glicksman L., Circulating fluidized bed heat transfer, in Circulating Fluidized Bed Technology II (Edited by P. Basu and J. F. Large), Pergamon Press, Oxford, 1988, pp.13-29.

Goldfarb I.J., Guchan R., Meeks A.C., Kinetic analysis of thermogravimetry. Part II. Programmed temperatures, Report No. ARML-TR-68-181. Ohio: Air Force Laboratory, Wright-Patterson AFB, 1968.

Grace J.R., Heat transfer in circulating fluidized beds, in: P.Basu (Ed.), Circulating Fluidized Bed Technology, Pergamon, Canada, 1986, pp.63-81.

Green A.E.S., Zanardi M.A., Mullin J.P., Phenomenological models of cellulose pyrolysis. Biomass and Bioenergy. 13(1/2) (1997) 15-24.

Gronli M.G. and Melaaen M.C., Mathematical model for wood pyrolysis - Comparison of experimental measurements with model predictions. Energy & Fuels. 14 (2000) 791-800.

Gungor A., and Eskin N., Hydrodynamic modeling of a circulating fluidized bed, Powder Technology. 172 (1) (2007) 1-13.

Guo B., Li D., Cheng C., Lu Z., Shen Y., Simulation of biomass gasification with a hybrid neural network model. Bioresource Technology. 76 (2) (2001) 77–83.

Gupta A.V.S.S.K.S., and Nag P.K., Bed-to-wall heat transfer behavior in a pressurized circulating fluidized bed. International Journal of Heat and Mass Transfer. 45 (2002) 3429-3436.

Hallgren A.L., Bjerle I., Chambert L.A., PCFB Gasification of biomass, Sweden, 1993, pp.866-872.

Hartge E. U., Rensner D., Werther J., Solid concentration and velocity patterns in circulating fluidized beds, in Circulating Fluidized Bed Technology II (Edited by P. Basu and J. F. Large), Pergamon Press, Oxford, 1988, pp. 165-180.

Holman J. P., Experimental methods for engineers, 7th Edition, McGraw-Hill, 2007.

Horio M., Morishita K., Tachibana O., and Murata N., Solid distribution and movement in circulating fluidized beds, in Circulating Fluidized Bed Technology II (Edited by P. Basu and J. F. Large), Pergamon Press, Oxford, 1988, pp. 147-154.

Hornof V., Kokta B.V., Valade J.L., Fassen J.L., Effect of lignin content on thermal degradation of wood pulp. Thermochimica Acta. 19(1) (1977) 63-68.

Jha S.K., Singh A., Physical and thermal properties of untreated and chemically treated rice husk. Journal of Agricultural Engineering. 44(4) (2007) 48-53.

Jiang P., Wei F., Fan L-S., General approaches to reactor design, Taylor & Francis Group LLC, 2003.

Kalita P., (2009). Charactrization of loose biomass for gasification, M.Tech Thesis, IIT Guwahati, India.

Kalita P., Mohan G., Pradeep Kumar G., Mahanta P., Determination and comparison of kinetic parameters of low density biomass Fuels, Journal of Renewable and Sustainable Energy, 1 (023109) (2009) 1-12 doi:10.1063/1.3126936.

Kanury A.M., (1969). PhD Thesis, University of Minnesota, Minneapolis, Minnesota.

Karel S., Michael P., Miloslav H., Jiří M., Pretreatment and feeding of biomass for pressurized entrained flow gasification, Fuel Processing Technology. 90 (2009) 629-635.

Kaupp A., Gasification of rice hulls, Theory and Praxis, Friedr, Braunschweig/Wiesbaden, Germany, Vieweg & Sons, 1984.

Kaushal P., Proll T., Hofbauer H., Model for biomass char combustion in the riser of a dual fluidized bed gasification unit: Part 1—model development and sensitivity analysis. Fuel Processing Technology. 89 (7) (2008) 651-659.

Kezhong L., Zhang R., and Bi J., Experimental study on syngas production by Co- gasification of coal and biomass in fluidized bed. International journal of hydrogen energy. 35 (2010) 2722-2726.

King, D.F., and Harrison, D., The dense phase of a fluidized bed at elevated pressures, Trans. Inst. Chem. Eng. 60(1) (1982) 26-30.

Kiang, K.D., Liu, K.T., Nack, H., and Oxley, J.H., Heat transfer in fast fluidized beds, in Fluidization Technology, Ed. D. Keairns, Hemisphere publishing corporation, Washington, D.C., Vol.2, 1976, pp.471-483.

Knowlton, TM., High-pressure fluidization characteristics of several particulate solids, primarily coal and coal-derived materials, American Institute of Chemical Engineering symposium series. 73(161) (1977) 22-28.

Kolar K.A., and Sundaresan R., Heat transfer characteristics at an axial tube in a circulating fluidized bed riser. International Journal of Thermal Sciences. 41(7) (2002) 673–681.

Koufopanos C.A., Maschio G., Lucchesi A., Kinetic modeling of the pyrolysis of biomass and biomass components. Canadian Journal of Chemical Engineering. 67 (1) (1989) 75-84.

Kumabe K., Hanaoka T., Fujimoto S., Minowa T., and Sakanishi K., Co-gasification of woody biomass and coal with air and stream. Fuel. 86 (5-6) (2007) 684-689.

Kumar A., Eskridge K., Jones D., Hanna M., Steam–air fluidized bed gasification of distillers grains: effects of steam to biomass ratio, equivalence ratio and gasification temperature. Bioresource Technology. 100 (2009) 2062-2068.

Kumar A., Jones D.D., Hanna M.A., Thermochemical biomass gasification: A review of the current status of the technology. Energies 2 (3) (2009) 556-581.

Kumar A., Wang L., Dzenis Y.A., Jones D.D., Hanna M.A., Thermogravimetric characterization of corn stove as gasification and pyrolysis feedstock, Biomass Bioenergy. 32 (2008) 460–467.

Kunii D., and Levenspiel O., Fluidization engineering, Butterworth-Heinemann, USA, 1991.

Kwauk M., Ningde W., Youchu L., Bingyu C., and Zhiyuan S., Fast fluidization at ICM, In Circulating Fluidized Bed Technology-I, Basu, P., Ed., Pergamon Press, Toronto, 1986, pp.33-62.

Larfeldt J., Leckner B., and Melaaen M., Modelling and measurement of pyrolysis of large wood particles. Fuel. 79 (2000) 1637-1643.

Lazaro, M.J., Moliner, R., and Suelves, I., Non-isothermal versus isothermal technique to evaluate kinetic parameters of coal pyrolysis, Journal of Analytical and Applied Pyrolysis. 47 (2) (1998) 111-125.

Lee S.H., Choi Y.C., Lee J.G., Kim J.H., The effects of heating rate on pyrolysis of agricultural wastes. Journal of Korea Society of Waste Management. 21 (2004) 465.

Li J.J., Zhang H., Yang H.R., Wu Y.X., Lu J.F., and Yue G.X., Zhang, Hydrodynamic model with binary particle diameter to predict axial voidage profile in a CFB combustor, Proceedings of the 20th International Conference on Fluidized bed Combustion, Springer Dordrecht Heidelberg London (Tsinger University Press, Beijing), China, 2010, pp.768-773.

Li K., Zhang R., Bi J., Experimental study on syngas production by co-gasification of coal and biomass in a fluidized bed. International Journal of Hydrogen Energy. 35 (2009) 2722-2726.

Li Y., and Kwauk M., The dynamics of fast fluidization, Proceedings of the 3rd International Conference on Fluidized Bed Combustion (Edited by J. R. Grace and J. M. Matsen), Henniker, New Hampshire, August 3-8, 1980, pp. 539-544.

Li Y. X., Zhi W.C., Peng Z.S., Yong C., Design and operation of a CFB gasification and power generation system for rice husk, Biomass and Bioenergy. 23 (3) (2002) 181-187.

Liou T.H., Chang F.W., Lo J.J., Pyrolysis kinetics of acid-leached rice husk. Industrial and Engineering Chemistry Research. 36(2) (1997) 568-571.

Liu H., and Gibbs B.M., Modeling of NH_3 and HCN emissions from biomass circulating fluidized bed gasifiers, Fuel. 82 (2003) 1591-1604.

Lockhart C., Zhu J., Brereton C.M.H., Lim C.J., Grace J.R., Local heat transfer, solids concentration and erosion around membrane tubes in a cold model circulating fluidized bed, International Journal of Heat and Mass Transfer. 38 (13) (1995) 2403-2410.

Louge M.Y., Bricout V., Martin-Letellier S., On the dynamics of pressurized and atmospheric circulating fluidized bed risers, Chemical Engineering Science. 54 (12) (1999) 1811-1824.

Lu Y., Jin H., Guo L., Zhang X., Cao C., Guo X., Hydrogen production by biomass gasification in supercritical water with a fluidized bed reactor. International Journal of Hydrogen Energy. 33 (2008) 6066-6075.

Lv P., Xiong Z., Chang J., Wu C., Chen Y., Zhu J., An experimental study on biomass air–steam gasification in a fluidized bed. Bioresour Technol. 95 (2004) 95-101.

Mahalingam M., and Kolar A.K., Heat transfer model for the membrane wall of a high temperature circulating fluidized bed, in Circulating Fluidized Bed Technology Ill (Edited by P. Basu, M. Horio, and M. Hasatani), Pergamon Press, Oxford, 1991, pp. 239-246.

Mahanta P., (1992). Variation of heat transfer coefficient along the riser wall and a cross tube in a CFB, M. Thesis, Department of Mechanical Engineering, IIT Kharagpur.

Mansaray K., Ghaly A., Al-Taweel A., Hamdullahpur F., Ugursal V., Air gasification of rice husk in a dual distributor type fluidized bed gasifier. Biomass Bioenergy. 17 (1999) 315-332.

Mansaray K.G., and Ghaly A.E., Physical and thermochemical properties of rice husks. Energy Sources. 19(9) (1997) 989-1004.

Mansaray K.G., and Ghaly A.E., Determination of kinetic parameters of rice husks in oxygen using thermogravimetric analysis" Biomass and Bioenergy. 17 (1999) 19-31.

Marzocchella, A., and Salatino, P., Fluidization of solids with CO_2 at pressures from ambient to supercritical. American Institute of Chemical Engineers. 46 (5) (2000) 901-910.

McKendry P., Energy production form biomass (part 3): gasification technologies. Bioresource Technology. 83 (1) (2002) 55-63.

Meena K. L., (2004). Heat transfer characteristics on upper splash region and in cyclone separator of circulating fluidized bed unit, M. Tech. Thesis, Department of Mechanical Engineering, IIT Guwahati.

Miccio F, Piriou B, Ruoppolo G, Chirone R. Biomass gasification in a catalytic fluidized reactor with beds of different materials. Chemical Engineering Journal. 154 (2009) 369-374.

Mickley, H.S., Fairbanks, D.F., Mechanism of heat transfer to fluidized beds. American Institute of Chemical Engineers. 1 (1955) 374-384.

Mickley, H.S., Trilling, C.A., Heat transfer characteristics in fluidized beds. Journal of Industrial and Engineering Chemistry. 41 (1949) 1135.

Mishra P., Chakraverty A., Banerjee H.D., Studies on physical and thermal properties of Rise Husk related to its Industrial application. Journal of Material Science. 21 (1986) 2129-2132.

Moilanen A, Nasrullah M, Kurkela E. The effect of biomass feedstock type and process parameters on achieving the total carbon conversion in the large scale fluidized bed gasification of biomass. Environ Progress and Sustainable Energy. 28 (2009) 355–359.

Molerus O., Arguments on heat transfer in gas fluidized beds, Chemical Engineering Science. 48 (1993) 761-770.

Ministry of Power, Government of India (website: http://powermin.nic.in).

Munson T.R., and Spindler R.J., Transient thermal behaviour of decomposing materials – Part 1: General theory and application to convective heating, Avco Corporation RAD-TR-61-10, May 1961.

Murakami T., Xu G., Suda T., Matsuzawa Y., Tani H., Fujimori T., Some process fundamentals of biomass gasification in dual fluidized bed. Fuel. 86 (2007) 244–55.

Myung S.Y., Eom Y.J., Dong J.I., Park Y.K., Kang B.S., Jeon J.K., Characteristics of thermal decomposition of major components of biomass isolated from Wood. Journal of Korean Industrial and Engineering Chemistry. 15 (2004) 896.

Nag P.K., Power Plant Engineering, McGraw Hill Publication Company Pvt. Ltd., 2nd Edition, New Delhi, India, 2001.

Nag P.K., and Gupta A.V.S.S.K.S., A heat transfer model of pressurized circulating fluidized bed, in: J. Werther (Ed.), Circulating Fluidized Bed Technology. 6 (1999) 361-366.

Nag P.K., and Ali Moral M.N., Effect of probe size on heat transfer at the wall in circulating fluidized beds, International Journal of Energy Research. 14 (1990) 965-974.

Nag P.K., Nawsher M., Basu P., A mathematical model for the predicted of heat transfer from finned surfaces in a circulating fluidized bed, International Journal of Heat and Mass Transfer 38 (9) (1995) 1675–1681.

Nakamura, M., Hamada, Y., Toyama, S., Fouda, A.E., and Capes, C.E., An experimental investigation of minimum fluidization velocity at elevated temperatures and pressures, Canadian Journal of Chemical Engineering. 63(1) (1985) 8-13.

Namkung W., Kim S.W., Kim S.D., Hydrodynamics and flow regime in a fast fluidized bed, Chemical Engineering Journal. 72 (1999) 245-252.

Narvaez I., Orio A., Aznar M., Corella J., Biomass gasification with air in an atmospheric bubbling fluidized bed. Effect of six operational variables on the quality of the produced raw gas. Journal of Industrial Engineering and Chemical Research. 35 (1996) 2110-2120.

Nasser M.M., Kinetic studies on thermal degradation of nonwood plants. Wood Fiber Science. 17(2) (1985) 266-273.

Natarajan E., Nordin A., and Rao A.N., Overview of combustion and gasification of rice husk in fluidized bed reactors, Biomass and Bioenergy. 14(5/6) (1998) 533-546.

Nemtsov D.A., Zabaniotou A., Mathematical modelling and simulation approaches of agricultural residues air gasification in a bubbling fluidized bed reactor. Chemical Engineering Journal. 143 (2008) 10-31.

Nikoo M.B., and Mahinpey N., Simulation of biomass gasification in fluidized bed reactor using ASPEN PLUS. Biomass Bioenergy. 32 (2008) 1245–1254.

Niksa, S., and Lau, C.W., Impact of soot on the combustion characteristics of coal particles of various types, Combustion and Flame. 94 (1993) 293.

Noymer P.D., and Glicksman L.R., Cluster motion particle convection heat transfer at the wall of a circulating fluidized bed, International Journal of Heat Mass Transfer. 41(1) (1998) 147-158.

Oesch P., Leppamaki E., Stahlberg P., Sampling and characterization of highmolecular-weight polyaromatic tar compounds formed in the pressurized fluidized-bed gasification of biomass. Fuel. 75 (1996) 1406–1412.

Oka N. S., and Oka E.J.A. S., Fluidized bed combustion, Marcel Dekker Inc (CRC Press), New York, 2004.

Ozawa T., A new method of analyzing thermogravimetric data. Journal of Chemical society of Japan. 38(11) (1965) 1881-1886.

Pan Y.G., Roca X., Velo E., Puigjaner L., Removal of tar by secondary air in fluidized bed gasification of residual biomass and coal. Fuel. 78 (1999) 1703-1709.

Pan Y. G., E. Velo, X. Roca, J. J. Manyà, and L. Puigjaner, Fluidized-bed gasification of residual biomass/poor coal blends for fuel gas production. Fuel. 79 (2000) 1317-1326.

Panton R.L., Rittmann J.G., Analytical study of pyrolysis including effects of mass loss and competing reactions. (Paper presented at Fall meeting of the Western States Section of the Combustion Institute, La Jolla, California, October 1969).

Park D.K., Goo J.H., Kim S.D., Lee S.H., Lee J.G., Pyrolysis and Gasification Characteristics of Sawdust and Rice Husk, Proceedings of the Sixth Korea-China Workshop on Clean Energy Technology; 1 (2006) 321–331.

Pfeifer C., Puchner B., Hofbauer H., Comparison of dual fluidized bed steam gasification of biomass with and without selective transport of CO_2. Chemical Engineering Science. 64 (23) (2009) 5073-5083.

Pinto F., F. Carlos, R.N. Andre, C. Travares, M. Dias, I. Gulyrtlu, Cabrita I., Effect of experimental conditions on co-gasification of coal, biomass and plastics wastes with air/steam mixtures in fluidized bed system. Fuel. 82 (2003) 1967-1976.

Praghanmor, R.R., (2009). Study of heat transfer characteristics of cold circulating fluidized bed risers. M.Tech. Thesis, Department of Mechanical Engineering, IIT Guwahati, India.

Puchner B., Pfeifer C., Hofbauer H., Bed material and parameter variation for a pressurized biomass fluidized bed process, Proceedings of the 20th International Conference on Fluidized bed Combustion, Springer Dordrecht Heidelberg London (Tsinger University Press, Beijing), China, 2009, pp.700-705.

Qin Yu-Hong, Feng Jie, Li Wen-Ying, Formation of tar and its characterization during air–steam gasification of sawdust in a fluidized bed reactor, Fuel. 89 (2010) 1344–1347.

Qu Tingting, Guo Wanjun, Shen Laihong, Xiao Jun, Zhao Kun, Experimental study of biomass pyrolysis based on three major components: hemicellulose, cellulose and lignin. Industrial & Engineering Chemical Research. 50(18), 10424-33(2011).

Radmanesh R., Chaouki J., Guy C., Biomass gasification in a bubbling fluidized bed reactor: experiments and modeling. American Institute of Chemical Engineers Journal. 52 (12) (2006) 4258-4272.

Ramiah, M.V., Thermogravimetric and differential thermal analysis of cellulose, hemicelIuIose and lignin, Journal of Applied Polymer Science. 14 (1970) 1323-1337.

Rapagna S., Mazziotti di Celso G., Devolatilization of wood particles in a hot fluidized bed: product yields and conversion rates. Biomass Bioenergy. 32 (2008) 1123-1129.

Reddy B.V., and Basu P., Estimation of the effect of system pressure and CO2 concentration on radiation heat transfer in a pressurized circulating fluidized bed combustor, Institution Of Chemical Engineers. 80 (Part A) (2002) 178-182.

Reddy B.V., and Basu P., A model for heat transfer in a pressurized circulating fluidized furnace, International Journal of Heat and Mass Transfer. 44 (15) (2001) 2877-2887.

Reddy B.V., Nag P.K., Effect of lateral and extended fins on heat transfer in a circulating fluidized bed, International Journal of Heat and Mass Transfer 41 (1) (1998) 139–146.

Richtberg M., Richter R., Wirth K.E., Characterization of the flow patterns in a pressurized circulating fluidized bed. Powder Technology. 155 (2) (2005) 145-152.

Sadaka S.S., Ghaly A.E., Sabbah M.A., Two phase biomass air–steam gasification model for fluidized bed reactors: Part I—model development. Biomass Bioenergy. 22 (2002) 439-462.

Sadaka SS, Ghaly A.E., Sabbah M.A., Two phase biomass air-steam gasification model for fluidized bed reactors: Part II—model sensitivity. Biomass Bioenergy. 22 (2002) 463-477.

Sadaka S.S., Ghaly A.E., Sabbah M.A., Two-phase biomass air–steam gasification model for fluidized bed reactors: Part III—model validation. Biomass Bioenergy. 22 (2002) 479-487.

Sanz A., and Corella J., Modeling circulating fluidized bed biomass gasifiers. Results from a pseudo-rigorous 1-dimensional model for stationary state. Fuel Processing Technology. 87 (3) (2006) 247-258.

Saxena, S.C., and Vogel, G.J., The measurement of incipient fluidization velocities in a bed of coarse dolomite at temperature and pressure, Transactions of Institution of Chemical Engineers. 55(3) (1977) 184-189.

Schaub G., Reimert R., and Albrecht J., Investigation of emission rates from large scale CFB combustion plants, in 1989, In Proceedings of the l0th International Conference on Fluidized Bed Combustion (Edited by A. Manaker), ASME, New York, 1989, pp. 685-691.

Shamsuddin A.H., and Williams P.T., Devolatilisation studies of oil-palm solid wastes by thermogravimetric analysis. Journal of the Institute of Energy. 65(1) (1992) 31-34.

Shankarrao P.R., (2011). Parametric studies and effect of scale-up on heat transfer characteristics of circulating fluidized beds, PhD Thesis, Centre for Energy, IIT Guwahati.

Sharma K.A., Ravi M.R., Kohli S., Modeling product of composition in slow pyrolysis of wood. Journal of Solar Energy Society of India. 16 (2006) 1-11.

Shen L., Gao Y., Xiao J., Simulation of hydrogen production from biomass gasification in interconnected fluidized beds. Biomass Bioenergy. 32 (2008) 120–127.

Shen X., Zhou N., Xu Y., Experimental study on heat transfer in a pressurized circulating fluidized bed, in: P. Basu, M. Hasatani, M. Hario (Eds.), Circulating Fluidized Bed Technology, vol. III, Pergamon, New York, 1991, pp.451–456.

Sheth Pratik N., Amita U., Basu B.V., *AIChE Annual Meeting, Conference Proceedings*, (Salt Lake City, UT, United Sates, Nov.7-12; 2010), a142/1-a142/16.

Shi, D., Nicolai, R., Reh, L., Wall-to-bed heat transfer in circulating fluidized beds. Journal of Chemical Engineering Processing. 34 (7) (1998) 287-293.

Sidorenko I., and Rhodes M.J., Influence of pressure on fluidization properties, Powder Technology. 141 (1-2) (2004) 137-154.

Sidorenko I., and Rhodes M.J., Pressure effects on gas-solid fluidized bed behavior, International Journal of Chemical Reactor Engineering, 1 (2003) 1-33.

Simmons G.M., and Lee W.H., In Fundamentals of thermochemical biomass conversion, (Eds R P Overend, T A Milne, L K Mudge, Elsevier, London; 1985, pp.385-395.

Singh N.P., Overview of renewable energy in India. In: 25 years of renewable energy in India. New Delhi: Ministry of New and Renewable Energy, 2007, pp.1-16.

Singh V., and Sharma P., (2008). Studies on hydrodynamics and heat transfer characteristics of the circulating fluidized bed. B. Tech. Project Report, Department of Mechanical Engineering, IIT Guwahati, India.

Skoulou V., Koufodimos G., Samaras Z., Zabaniotou A., Low temperature gasification of olive kernels in a 5-kW fluidized bed reactor for H2-rich producer gas, International Journal of Hydrogen Energy. 33 (22) (2008) 6515-6524.

Sobreiro, L.E.L., and Monteiro, J.L.F., The effect of pressure on fluidized bed behavior, Powder Technol. 33 (1982) 95-100.

Sommariva S., Maffei T., Migliavacca G., Faravelli T., Ranzi E., A predictive multi-step kinetic model of coal devolatilization, Fuel 89 (2) (2009) 318-328.

Srivastava V.K., Sushil, Jalan R.K., Prediction of concentration in the pyrolysis of biomass material. Energy Conversion and Management. 37 (4) (1996) 473-483.

Subbarao, D., and Basu, P., A model of heat transfer in circulating fluidized beds. International Journal of Heat and Mass Transfer. 29 (3) (1986) 487-489.

Suneerat P., Nigel P., Denis D., Rafael K., Kinetic modelling of coal pyrolysis in an atmospheric wire-mesh reactor, the Joint International conference on Sustainable Eneregy and Environment (SEE), Hua Hin, Thailand, 1-3 December 2004, pp.549-594.

Tang J.T., and Engstrom F., Technical assessment on the Ahlstrom pyroflow circulating and conventional bubbling tluidized bed combustion systems, In Proceedings of the 9th International Conference on Fluidized Bed Combustion (Edited by J. P. Mustonen), ASME, New York, 1987, pp.38-54.

Teng H., Lin H., Ho J., Thermogravimetric analysis on global mass loss kinetics of rice hull pyrolysis. Industrial and Engineering Chemistry Research. 36 (1997) 3974-3977.

Tripathi A.K., Renewable energy development in India. In: Multiple choice questions on renewable energy. New Delhi: TERI Press; 2008. pp.1–12.

Tsukada M., Nakanishi D., Horio M., Effect of pressure on transport velocity in a circulating fluidized bed, in: 4th International Conference on CFB, Pennsylvania (pre print volume), 1994, pp.248-253.

Umeki K., Yamamoto K., Namioka T., Yoshikawa K. High temperature steam only gasification of woody biomass. Applied Energy. 87 (3) (2010) 791-798.

Varhegyi G., Szabo P., Antal M.J., Reaction kinetics of the thermal decomposition of cellulose and hemicellulose in biomass materials. In: Bridgwater AV, editor. Advances in Thermochemical Biomass Conversion. London: Blackie Academic and Professional, 1994, pp.760-770.

Varhegyi G., Antal M.J., Jakab E., Szabó P., Kinetic modeling of biomass pyrolysis. Journal of Analytical and Applied Pyrolysis. 42 (1997) 73–87.

Vélez J., Chejne F., Valdés C.F., Emergy E.J., and Londoño C.A., Co-gasification of Colombian coal and biomass in fluidized bed: An experimental study. Fuel. 88 (3) (2009) 424-430.

Vogt C., Schreiber, R., Werther, J., and Brunner, G., Fluidization at supercritical fluid conditions, in "Fluidization X", M. Kwauk, J. Li, and W. C. Yang, eds., United Engineering Foundation, New York, 2001, pp.117-124.

Wang L., Weller C., Jones D., Hanna M., Contemporary issues in thermal gasification of biomass and its application to electricity and fuel production, Biomass Bioenergy. 32 (7) (2008) 573–581.

Weerachanchai P., Horio M., Tangsathitkulchai C., Effects of gasifying conditions and bed materials on fluidized bed steam gasification of wood biomass. Bioresource Technology. 100 (3) (2009) 1419–1427.

Weinstein, W., Graff, R.A., Meller, M., Shao, M.J., The effect of the imposed pressure drop across a fast fluidized bed, Fluidization, Kunii, D., and Toei, R., (eds), (Engineering Foundation, United Engineering Trustees, Inc., New York), 1983, pp.299-306.

Wen C.Y., and Yu Y.H., A generalized method for predicting the minimum fluidization velocity, American Institute of Chemical Engineers Journal. 12(3) (1966a) 610-612.

Wen C.Y., and Miller F.N., Heat transfer in solid-gas transport lines. Journal of Industrial and Engineering Chemistry. 53 (1961) 51-53.

Werderman C.C., and Werther J., Solids flow pattern and heat transfer in an industrial-scale fluidized bed heat exchanger, Proc. 12th Int. Conf. Fluidized Bed Combustion, ASME, New York, 1993, pp.985-990.

Werther J., Potentials of biomass co-combustion in coal-fired boilers, Proceedings of the 20th International Conference on fluidized bed combustion, Springer Dordrecht Heidelberg London (Tsinger University Press, Beijing), China, 2009, pp.27-42.

Williams P.T., and Besler S., Thermogravimetric analysis of the components of biomass. In: Bridgwater AV, editor. Advances in Thermochemical Biomass Conversion. London: Blackie Academic and Professional, 1994. p.771-783.

Wiman J., and Almstedt A.E., Hydrodynamics, erosion and heat transfer in a pressurized fluidized bed: influence of pressure, fluidization velocity, particle size and tube bank geometry, Chemical Engineering Science. 52(16) (1997) 2677-2695.

Winaya N.S., and Basu P., Effect of pressure and carbon dioxide concentration on heat transfer at high temperature in a pressurized circulating fluidized bed (PCFB) combustor, International Journal of Heat and Mass Transfer. 44 (2001) 2965-2971.

Wirth K.E., Heat transfer in circulating fluidized beds, Chemical Engineering Science. 50 (1995) 2137-2151.

Wu C., Yin X., Ma L., Zhou Z., Chen H., Operational characteristics of a 1.2-MW biomass gasification and power generation plant. Biotechnology Advances. 27 (2009) 588-592.

Wu R., Lim C. J., Chauki J., and Grace J. R., Heat transfer from a circulating fluidized bed to membrane water wall cooling surfaces. American Institute of Chemical Engineers Journal. 33 (1987) 1888-1893.

Xiao X., Le D.D., Morishita K., Zhang S., Li L., Takarada T., Multi-stage biomass gasification in internally circulating fluidized-bed gasifier (ICFG): test operation of animal-waste-derived biomass and parametric investigation at low temperature. Fuel Processing Technology. 91 (8) (2010) 895-902.

Yassin L., Lettieri P., Simons S., Germana A., Techno-economic performance of energy-from waste fluidized bed combustion and gasification processes in the UK context. Chemical Engineering Journal. 146 (2009) 315-327.

Yates J.G., Effects of temperature and pressure on gas-solid fluidization, Chemical Engineering Science. 51(2) (1996) 167-205.

Yates J.G., Experimental observations of voidage in gas fluidized beds, in: J. Chaouki, F. Larachi, M.P. Duducovic (Eds.), Non-Invasive Monitoring of Multiphase Flows, Elsevier, Amsterdam, 1997, pp.141-160.

Yue G., Lu J., Zhang H., Yong H., Zhang J., and Liu Q., (2005). Design theory of circulating fluidized boilers, In the Proceedings of the 18th International Conference on Fluidized Bed Combustion, Jia, L., Ed., ASME, New York, paper: FBC 78134.

Zaror C.A., and Pyle D.L., The pyrolysis of biomass. A general review. Proceedings- Indian Academy of Science, Engineering Sciences. 5(4) (1982) 269-285.

Zhang Jun, Yuan Zhen-wei, Wei Xin-li, An automatic shake mechanism for the biomass pyrolysis feeding system, Powder Technology. 207 (1) (2011) 348–352.

Zhao Y., Sun S., Zhou H., Sun R., Tian H., Luan J., Qian Juan, Experimental study on sawdust air gasification in an entrained-flow reactor, Fuel Processing Technology, 91 (8) (2010) 910-914.

Zhou J., Chen Q., Zhao H., Cao X., Mei Q., Luo Z., Biomass-oxygen gasification in a high-temperature entrained-flow gasifier. Biotechnology Advances. 27 (2009) 606–611.

Zhou Z., Ma L., Yin X., Wu C., Huang L., Wang C., Study on biomass circulation and gasification performance in a clapboard-type internal circulating fluidized bed gasifier. Biotechnology Advances 27 (2009) 612–615.

APPENDICES

Appendix – I
Design of Orifice Plate

Applying Bernoulli's theorem to the upstream tapping (1) and to the orifice (2), of the Fig.I.1 we can write,

$$\frac{V_1^2}{2g} + H_1 = \frac{V_2^2}{2g} + H_2 \tag{I.1}$$

Assuming that the pipe is running full and for the moment that no expansion of the fluid takes place, then

$$A_1 V_1 = A_2 V_2 \tag{I.2}$$

$$\text{or, } V_1 = \frac{A_2}{A_1} V_2 = m_1 V_2$$

$$\text{where } m_1 = \frac{A_2}{A_1}$$

Now substituting the expression of V_1 to equation (I.1),

$$V_2^2 = \frac{2g\left(H_1 - H_2\right)}{1 - m_1^2} \tag{I.3}$$

where $(H_1 - H_2)$ is the difference of pressure heads between points (1) and (2) of Fig.I.1 and expressed in meter of air. Now if we substitute $(H_1 - H_2)$ in terms of (Δp) and express in cm of water, then we can write,

$$p_1 = \rho_a \times g \times H_1 \text{ and } p_2 = \rho_a \times g \times H_1 \tag{I.4}$$

$$\text{Hence, } p_1 - p_2 = \rho_a \times g \times \left(H_1 - H_2\right)$$

$$\therefore H_1 - H_2 = \frac{p_1 - p_2}{\rho_a \times g} = \frac{\Delta p}{\rho_a \times g} \text{ m of water column}$$

$$or, H_1 - H_2 = \frac{\Delta p \times 100}{\rho_a \times g} \text{ cm of water column}$$

$$or, H_1 - H_2 = \frac{10 \times \Delta p}{\rho_a}$$

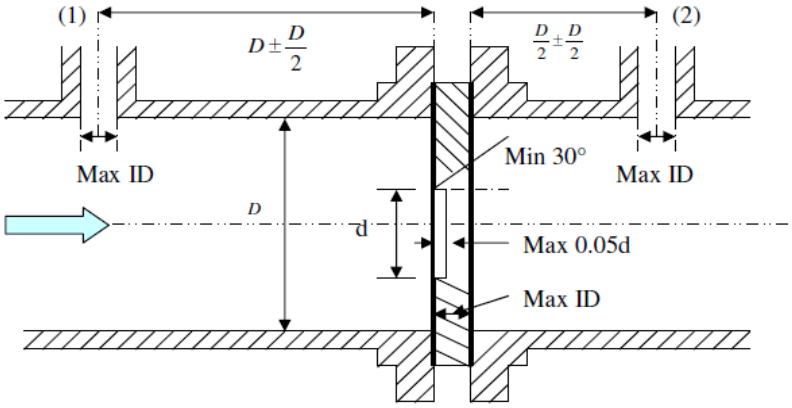

Fig.IV.1 Orifice meter with D and D/2 tappings

where Δp is the difference in height of manometric fluid (water) in cm of water.

Now substituting the expression of $(H_1 - H_2)$ in equation (I.3) we can write

$$V_2^2 = \frac{2g\left(\frac{10 \times \Delta p}{\rho_a}\right)}{1 - m_1^2} \quad \text{or} \quad V_2 = \left[\frac{2g\left(\frac{10 \times \Delta p}{\rho_a}\right)}{1 - m_1^2}\right]^{1/2} \text{ m/s} \tag{I.5}$$

Theoretical mass flow rate (m_t) of air can be expressed as

$$m_t = \rho_a \times A_2 \times V_2 \qquad \text{kg/s}$$

$$\text{Or, } m_t = \rho_a \times \left[\frac{\pi}{4} \times \left(\frac{d_o}{100}\right)^2\right] \times \left[\frac{2g \times \left(\frac{10 \times \Delta p}{\rho_a}\right)}{1 - m_1^2}\right]^{1/2} \times 3600 \quad \text{kg/h}$$

$$\text{Or, } m_t = 3.96 \times d_o^2 \times \frac{(\Delta p \times \rho_a)^{1/2}}{(1 - m_1^2)^{1/2}}$$

$$m_t = 3.96 \times d_o^2 \times E \times (\Delta p \times \rho_a)^{1/2} \quad \text{kg/h} \tag{I.6}$$

where

$$E = \frac{1}{\left(1 - m_1^2\right)^{1/2}} = 1.013$$

$d_o =$ diameter of orifice in cm $= 4.2$ cm

$\Delta p =$ difference in manometric fluid height in cm of water

$\rho_a =$ density of air

$$m_1 = \frac{d}{D} = \frac{4.2^2}{10.5^2} = 0.16$$

$$\text{Re} = \frac{\rho VD}{\mu} = \frac{VD}{\nu} = \frac{0.105 \times 2.5}{16.04 \times 10^{-6}} = 16365.33$$

For the above Reynolds number and at β = 0.4, Value of discharge coefficient, C is found to be 0.6095 from IS code 14615 (Part 1):1999, page no.71

Now, equation (I.6) implies,

$$m_t = 3.96 \times 4.2^2 \times 1.013 \times \left(\Delta p \times 1.166\right)^{1/2} = 76.41 \times \sqrt{\Delta p} \text{ kg/hr} \quad \text{(I.7)}$$

The actual mass flow rate (m_a) can now be expressed as

$$m_a = C \times z \times m_t \text{ kg/h} \quad \text{(I.8)}$$

$$\text{or, } m_a = C \times z \times \left[3.96 \times d_o^2 \times E \times \left(\Delta p \times \rho_a\right)\right] 1/2$$

$$\text{or, } m = C \times Z \times 76.41 \times \sqrt{\Delta p} \text{ kg/h}$$

where

$C =$ Coefficient of discharge = 0.6095

$z =$ Velocity of approach factor = 1

$$\text{or, } m_a = 46.57 \times \sqrt{\Delta p} \text{ kg/h}$$

$$\text{or, } m_a = 0.012936 \times \sqrt{\Delta p} \text{ kg/s}$$

In the present case,

$$A_b = \frac{\pi}{4} \times \left(0.054\right)^2 = 0.00229 \text{ m}^2$$

Superficial velocity,

$$U = \frac{m_a}{\rho \times A_b} = \frac{0.012936 \times \sqrt{\Delta p}}{1.166 \times \frac{\pi}{4} \times \left(0.054\right)^2} = 4.844 \times \sqrt{\Delta p} \text{ m/s} \quad \text{(I.9)}$$

Appendix – II
Design of Distributor Plate

The distributor was fabricated based on the design procedure described by Kunii and Levenspiel (1991), and Basu (2006). It is a straight hole orifice type of distributor. The design considerations are given below:

Diameter of particle, $d_p = 0.41\,\text{mm}$

Bed inventory, $I = 2$ kg

Operating velocity, $U = 2.5\,\text{m/s}$

Voidage at maximum fluidization, $\varepsilon_{mf} = 0.5$

Cross sectional area of the bed, $A_b = \frac{\pi}{4}(0.054)^2 = 2.2902\times10^{-3}$ m^2

Density of the solid particle (sand), $\rho_s = 2600\,\text{kg/m}^3$

Density of air, $\rho_a = 1.166\,\text{kg/m}^3$

Acceleration due to gravity, $g = 9.81$ m/s^2

Height of the bed at minimum fluidization:

$$H_{mf} = \frac{\Delta p}{(1-\varepsilon_{mf})\times\rho_s\times g} = \frac{I\times g/A_b}{(1-\varepsilon_{mf})\times\rho_s\times g} = \frac{I}{A_b\times(1-\varepsilon_{mf})\times\rho_s} \qquad \text{(II.1)}$$

= 0.671 m

(i) Bed pressure drop (Δp_b)

$$\Delta p_b = \rho_s\times g\times H_{mf}\times(1-\varepsilon_{mf})$$

$$\text{or, } \Delta p_b = 8566.93 \text{ N/m}^2 \qquad \text{(II.2)}$$

(ii) Orifice diameter, (d_{or})

$$d_{or} = 3d_p = 3\times0.41\times10^{-3} = 1.23\times10^{-3}\,\text{m} \qquad \text{(II.3)}$$

(iii) Minimum distributor pressure drop for uniform distribution (Δp_D)

$$\Delta p_D = \Delta p_b \times [0.01 + 0.2\{1 - \exp(-D/2\times H_{mf})\}] = 153.24 \text{ N/m}^2 \quad \text{(II.4)}$$

(iv) Rearrangement resistance (Δp_R)

$$\Delta p_R = \rho_g \times \left[\frac{U \times (A_b/A_i)^2}{2g}\right] = 1.166 \times \frac{2.5 \times \left(\frac{0.054^2}{0.105^2}\right)^2}{2\times 9.81} = 0.01039 \text{ N/m}^2 < \Delta p_D/100 \quad \text{(II.5)}$$

(v) Thickness of the distributor plate (t): t = 5 mm = 0.005 m

(vi) Orifice discharge coefficient (C_D)

$$C_D = 0.82 \times (t/d_{or})^{0.13} = 0.82 \times \left(\frac{5\times 10^{-3}}{2\times 10^{-3}}\right)^{0.13} = 0.923 \quad \text{(II.6)}$$

(vii) Gas velocity through the Orifice (U_{or})

$$U_{or} = C_D \times \left[2\times \Delta p_D/\rho_g\right]^{1/2} = 0.923 \times \left[\frac{2\times 153.24}{1.166}\right]^{1/2} = 14.96 \text{ m/s} \quad \text{(II.7)}$$

(viii) Number of orifice per square meter of distributor (N_{or})

$$N_{or} = (U_{OP}/U_{or}) \times (1/A_{or}) = (U_{OP}/U_{or}) \times (4/\pi d_{or}^2)$$
$$\text{or } N_{or} = \frac{2.5\times 4}{14.96\times \pi \times (0.002)^2} = 53193.49 \text{ m}^{-2} \quad \text{(II.8)}$$

(ix) Total number of holes on perforated distributor $= N_{or} \times A_b = 53193.49 \times 0.00229 = 121.82$

(x) Pitch of the orifices in the distributor $= 1/(N_{or})^{1/2} = 1/(53193.49)^{1/2} = 5.006\times 10^{-3}$ m = 5 mm

(xi) Open area in the distributor $= \pi/4 \times (2\times 10^{-3})^2 \times 121 = 3.80\times 10^{-4} \text{ m}^2$

(xi) Percentage opening $= \left(\frac{3.80\times 10^{-4}}{A_b}\right) \times 100 = 16.59\%$.

(i) Maximum gas flow rate, Q_m:

$$Q_m = U_m \times A_b = 2.5 \times \frac{\pi}{4} \times 0.05^2 = 0.00490 \text{ m}^3/\text{s}$$

$$\text{or, } Q_m = 17.67 \text{ m}^3/\text{hr} \tag{III.1}$$

Design gas flow rate: 35 m^3/hr

Calculation of cyclone barrel diameter, D_c: The gas handling capacity of a stairmand high efficiency cyclone is given by the following equation

$$Q_d = \frac{V_{in}}{8} \times D_c^2 \tag{III.2}$$

The maximum flow rate at the inlet of cyclone and the riser exit are equal.

$$\text{where } V_{in} = 3 \times U_m, \; D_c = 0.080 \text{ m}$$

Cyclone design ratios: Using Stairmand's (1951) design data for the high efficiency cyclone, the various dimensions ratios are written down from which the cyclone dimensions are arrived at:

$$B_C / D_C = \frac{1}{4}, \Rightarrow B_C = \frac{1}{4} \times D_C = \frac{1}{4} \times 0.08 = 0.02 \text{ m}$$

$$H_C / D_C = \frac{1}{2}, \Rightarrow H_C = \frac{1}{2} \times D_C = \frac{1}{2} \times 0.08 = 0.04 \text{ m} \tag{III.3}$$

$$D_E / D_C = \frac{1}{4}, \Rightarrow D_E = \frac{1}{4} \times D_C = 0.02 \text{ m}$$

$$Z_C / D_C = L_C / D_C = 2, \Rightarrow L_C = 2 \times D_C = 0.16 \text{ m}; \; Z_C = 2 \times D_C = 0.16 \text{ m}$$

$$S_C / D_C = \frac{1}{8}, \; \Rightarrow S_C = \frac{1}{8} \times D_C = \frac{1}{8} \times 0.08 = 0.01 \text{ m}$$

$$J_C = D_C / 4 = 0.02 \text{ m} = 0.0254 \text{ (arbitrary)}$$

$$D_{in} = 2 \times \frac{B_c + H_c}{B_c + H_c} = 0.267 \text{ m}$$

Calculation of actual inlet velocity:

$$U_{cy,i} = \frac{Q_m/3600}{H_C \times B_C} = \frac{17.67/3600}{0.04 \times 0.02} = 6.13 \text{ m/s} \quad \text{(III.4)}$$

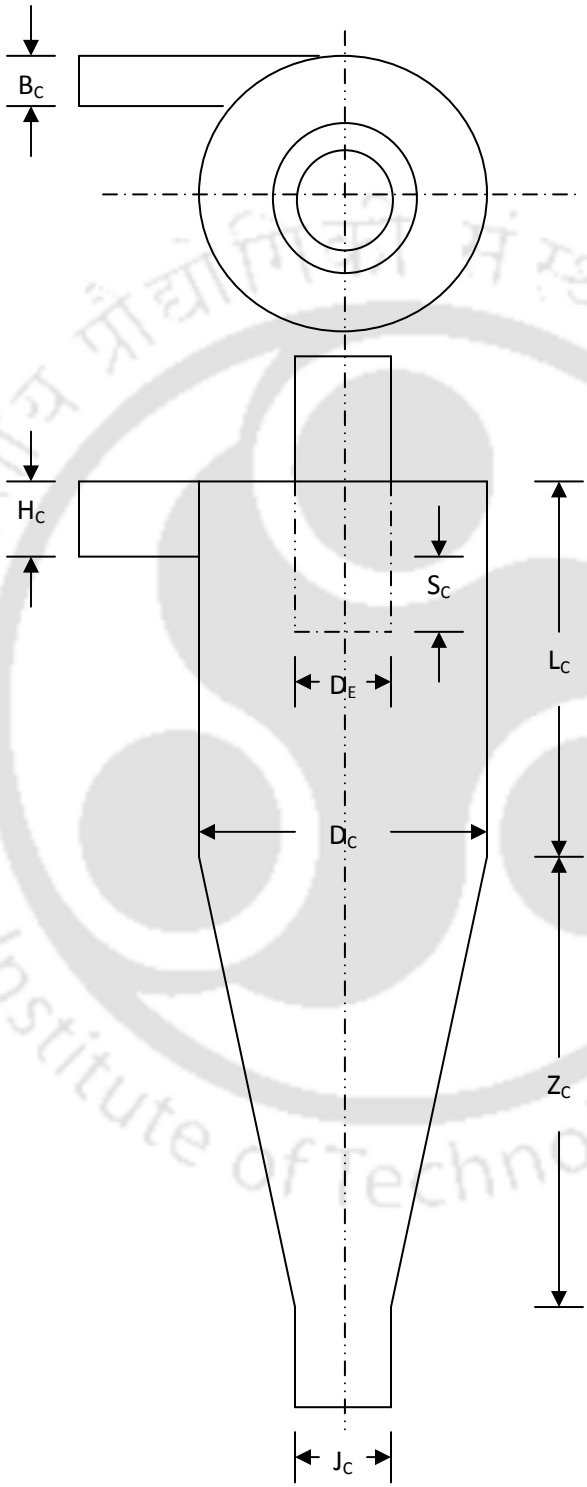

Fig.III.1 Schematics of cyclone separator

Appendix – IV
Mean Particle Size Analysis

To investigate the mean particle size the following procedure proposed by Kunii and Levenspiel, (1991) is followed with the following assumptions

(1) Volume of the particles remains constant

(2) Surface area of the particles remains constant

Let there be:

n_1 : Particles of diameter d_1

n_2 : Particles of diameter d_2

n_3 : Particles of diameter d_3

and so on.

By using assumption no.1:

$$N \times \frac{\pi \bar{d}_p^3}{6} = n_1 \times \frac{\pi d_1^3}{6} + n_2 \times \frac{\pi d_2^3}{6} + n_3 \times \frac{\pi d_3^3}{6} + \ldots \quad \text{(IV.1)}$$

where N is the number of replaced, uniformly sized particles of diameters $\bar{d}_p$.

$$N \times \bar{d}_p^3 = n_1 \times d_1^3 + n_2 \times d_2^3 + n_3 \times d_3^3 + \ldots \quad \text{(IV.2)}$$

By using assumption no.2:

$$N \times \pi \bar{d}_p^2 = n_1 \times \pi d_1^2 + n_2 \times \pi d_2^2 + n_3 \times \pi d_3^2 + \ldots$$

$$\text{or, } N \times \bar{d}_p^2 = n_1 \times d_1^2 + n_2 \times d_2^2 + n_3 \times d_3^2 + \ldots \quad \text{(IV.3)}$$

Let X_1 be the weight fraction of the solids of diameter d_1

$$\text{Therefore, } X_1 = \frac{\frac{n_1 \times \bar{d}_1^3}{6} \times \rho_s}{\frac{N \times \bar{d}_p^3}{6} \times \rho_s} = \frac{n_1 \times d_1^3}{N \times \bar{d}_p^3} \quad \text{(IV.4)}$$

where ρ_s represents the density of sand

$$\text{Similarly, } X_1 = \frac{\frac{n_2 \times \bar{d}_2^3}{6} \times \rho_s}{\frac{N \times \bar{d}_p^3}{6} \times \rho_s} = \frac{n_2 \times d_2^3}{N \times \bar{d}_p^3}$$

Hence, $n_1 \times d_1^2 = X_1 \times N \times \bar{d}_p^3 / d_1$ and $n_2 \times d_2^2 = X_2 \times N \times \bar{d}_p^3 / d_2$

$$N \times \bar{d}_p^2 = n_1 \times d_1^2 + n_2 \times d_2^2 + n_3 \times d_3^2 + \ldots$$
$$= X_1 \times N \times \bar{d}_p^3 / d_1 + X_2 \times N \times \bar{d}_p^3 / d_2 + X_3 \times N \times \bar{d}_p^3 / d_3$$

$$\text{or, } \frac{1}{\bar{d}_p} = \frac{X_1}{d_1} + \frac{X_2}{d_2} + \frac{X_3}{d_3} + \ldots$$

$$\text{or, } \frac{1}{\bar{d}_p} = \sum \frac{X_i}{d_i}$$

$$\text{or, } \bar{d}_p = \frac{1}{\sum \frac{X_i}{d_i}} \qquad \text{(IV.5)}$$

Table-IV.1 Particle size measurement

Mesh (BSS)	Mean particle size (d_i), µm	Weight in grams	Weight fraction $\left(X_i = \frac{W_i}{W}\right)$	X_i/d_i
18 - 22	858.33	288	0.3070362	3.577×10^{-4}
22 - 25	726.25	202	0.2153518	2.965×10^{-4}
25 - 30	610.18	82	0.0874200	1.433×10^{-4}
30 - 36	473.73	122	0.1300640	2.745×10^{-4}
36 - 44	370.07	72	0.0767591	2.074×10^{-4}
44 - 52	303.53	10	0.0106610	3.512×10^{-4}
52 - 60	254.08	36	0.0383795	1.510×10^{-4}
60 -72	214.69	62	0.0660981	3.078×10^{-4}
72 - Pan	195.80	64	0.0682303	3.484×10^{-4}

Hence, the mean particle size calculated based on the Eq. (IV.5) is found to be 410 µm.

Appendix – V
Calibration of Thermocouple

The calibration of thermocouple is done by keeping one junction of the two dissimilar metals (Copper-Constantan) at constant temperature (at 0 °C) and other junction is maintained at variable temperatures. In order to maintain variable temperature, a water circulating bath is used. A high precision multi-meter is connected in the circuit to see the emf generation. In every 5 °C, the increase of water temperature the emf (millivolt) generation is recorded. The calibration curve so obtained is presented in Fig.V.1. Chormel-alumel thermocouple calibration chart was used for high temperature measurement.

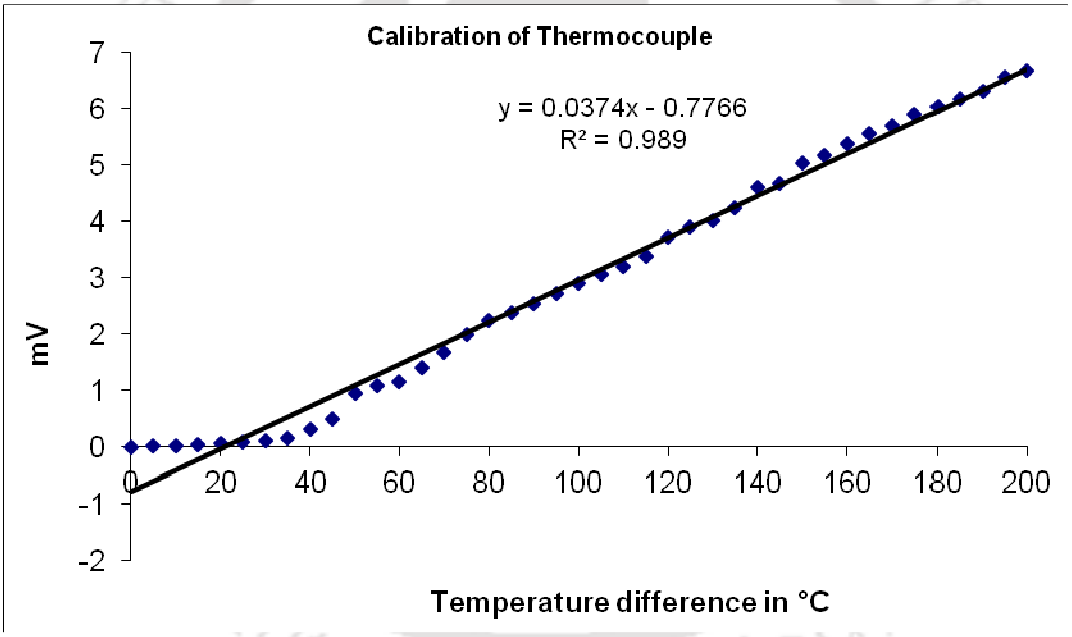

Fig.V.1 Calibration curve for copper-constantan thermocouple

Appendix – VI
Calibration of Blower for Biomass Feeding System

The flow rate of the blower used in the biomass feeding system is calibrated with voltages supply. The velocity of flow is measured by an anemometer at the blower exit. Fig.VI.1 presents the calibration curve of the blower.

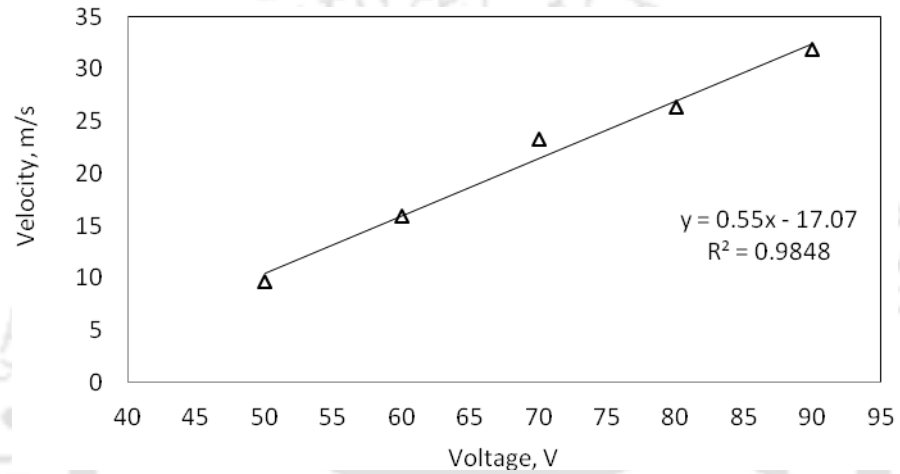

Fig.VI.1 Blower calibration curve

The flow using pipe without holes initiated at a supply voltage of 100 V while with holes the flow is initiated at 55 V. This implies that by using porous pipe power consumption may be reduced significantly. Further experiments with different particle sizes and different flow rates presented no difficulties, providing a consistent and constant feed supply.

Appendix – VII
Design Calculation of CFB Gasification

The design procedure of CFB biomass gasifier as outlined by Buragohain *et al.* (2009) has been followed. The various components of the gasifier such as riser, distributor plate and cyclone separator have been designed as per the procedure described by the hydrodynamics of fluidization. The main process parameters affecting the quality of gas are air or equivalence ratio and temperature of gasification. The step-by-step calculation of various parameters is presented in the following sections.

The dimensions and the materials for the construction of the CFB gasifier is decided based on the design hot CFB unit. Some of the operating variables are changed while operating the hot CFB unit in the gasification mode. The particles of biomass are rather light and are easily drifted out of the riser even with small velocities of gas. Therefore, in order to ensure an effective and a uniform distribution of the biomass particles in the riser, the biomass was mixed with sand particles of proper size and shape. Friction with the sand particles will help distribute the biomass uniformly in the riser. Sand particles will also help effective distribution of heat through the riser section due to their high heat capacity. Given below is a step-by-step calculation for the riser section of the gasifier along the distributor plate (Kunii and Levenspil, 1991).

- Particle size of sand: $d_{p1} = 278$ μm
- Sphericity of sand particles: $\phi_s = 0.86$
- Density of sand particles: $\rho_s = 2300$ kg/m^3

We take saw dust as the representative biomass. As far as hydrodynamics of the CFB gasifier is concerned, the relevant properties are particle size and density.

- Particle size of biomass: $d_{p1} = 407$ μm
- Density of biomass: $\rho_s = 210$ kg/m^3
- Sphericity of biomass particles: $\phi_s = 0.95$

Fluidizing gas is taken to be air at 800 K. As air is being heated in an internal passage, the rise in temperature is compensated by rise in pressure, and no significant reduction is seen in the density of air. As a conservative estimate, therefore, we take the density of air as 0.4412 kg/m^3, which is less than the corresponding value for ambient conditions (1.2 kg/m^3). The viscosity of air is taken at 800 K.

- Density of air at 800 K is : $\rho_{\text{air}} = 0.4412$ kg/m^3
- Viscosity of air at 800 K is: $\mu_{\text{air}} = 3.624\times10^{-5}$ kg/m-s
- Voidage at minimum fluidization: $\varepsilon_{mf} = 0.586$

Minimum fluidization velocity for sand;

$$u_{mf1} = \frac{d_{p1}^2(\rho_{s1} - \rho_{air})}{150\mu_{air}} \frac{\varepsilon_{mf}^3 \phi_s^2}{(1-\varepsilon_{mf})} = 6.0449\times10^{-3} \text{ m/s} \quad \text{(VII.1)}$$

Minimum fluidization velocity for biomass;

$$u_{mf2} = \frac{d_{p2}^2(\rho_{s1} - \rho_{air})}{150\mu_{air}} \frac{\varepsilon_{mf}^3 \phi_s^2}{(1-\varepsilon_{mf})} = 0.002801 \text{ m/s} \quad \text{(VII.2)}$$

Particle Reynolds No. of sand;

$$\text{Re}_{p,\text{ sand}} = 106.65 \quad \text{(VII.3)}$$

Particle Reynolds No. of biomass;

$$\text{Re}_{p,\text{ biomass}} = 6.606 \quad \text{(VII.4)}$$

To determine the actual air velocity required for having the pneumatic conveying regime, we determine non-dimensional terminal settling velocity (u_t^*) and the non-dimensional diameter of the particle (d_p^*) for sand particles. It needs to be mentioned that the sand particles (denoted by subscript 1 in the following formulae), being denser, are taken as the basis for choosing the gas velocity. The fluidization velocity for the biomass particles is smaller by one order of magnitude. Thus, the biomass particles will be assured to be in pneumatic conveying regime for these velocities.

Non-dimensional particle diameter;

$$d_{p1}^{*} = d_{p1}\left[\frac{\rho_{air}\left(\rho_{s1}-\rho_{air}\right)g}{\mu_{air}}\right]^{1/3} = 5.4068 \tag{VII.5}$$

Non-dimensional terminal settling velocity;

$$u_{t1}^{*} = \left[\frac{18}{d_{p1}^{*2}} + \frac{2.335-1.744\phi_s}{\sqrt{d_{p1}^{*}}}\right] = 0.97489 \tag{VII.6}$$

Actual terminal settling velocity;

$$u_{t1} = u_{t1}^{*}\left(\frac{\eta_{air}\left(\rho_{s1}-\rho_{air}\right)}{\rho_{air}^{2}}\right)^{1/3} = 1.572 \text{ m/s} \tag{VII.7}$$

Figure VII.1 shows the map of fluidization regimes developed by Grace (1986) and further modified by Kunii and Levenspiel (1997). For a given particles (particle properties) and operating velocity, the gas solid contact pattern can be determined using this diagram. Looking into it, we find that the non-dimensional range of superficial velocity, which gives pneumatic transport regime, is u_t^{*} = 4 to 12.

The actual fluidization velocity is then:

$$u_g = u_g^{*}\left[\frac{\left(\rho_{s1}-\rho_{air}\right)g}{\rho_{air}^{2}}\right]^{1/3} = 4.921 \text{ to } 14.764 \text{ m/s} \tag{VII.8}$$

Consideration the fact that the difference in the minimum fluidization velocity of sand and biomass particle is large, it is quite clear that the gas velocities for which these particles enter fast fluidization regime will also be different. Similar calculations of biomass particles show that fast fluidization is encountered for air velocities between 1.63 to 4.8 m/s. We, therefore, choose a velocity of 4.34 m/s for fluidizing medium which would give pneumatic conveyance regime for all biomass particles, while the sand particles will be in fast fluidization/pneumatic conveying regime.

The actual fluidization velocity in the present case will be:

$$u_g = u_g^* \left[\frac{(\rho_{s1} - \rho_{air})\, g}{\rho_{air}^2} \right]^{1/3} = 7 \text{ m/s} \qquad \text{(VII.9)}$$

From the calculation it is understood that u = 7 m/s is sufficient enough to circulate solids through the CFB loop.

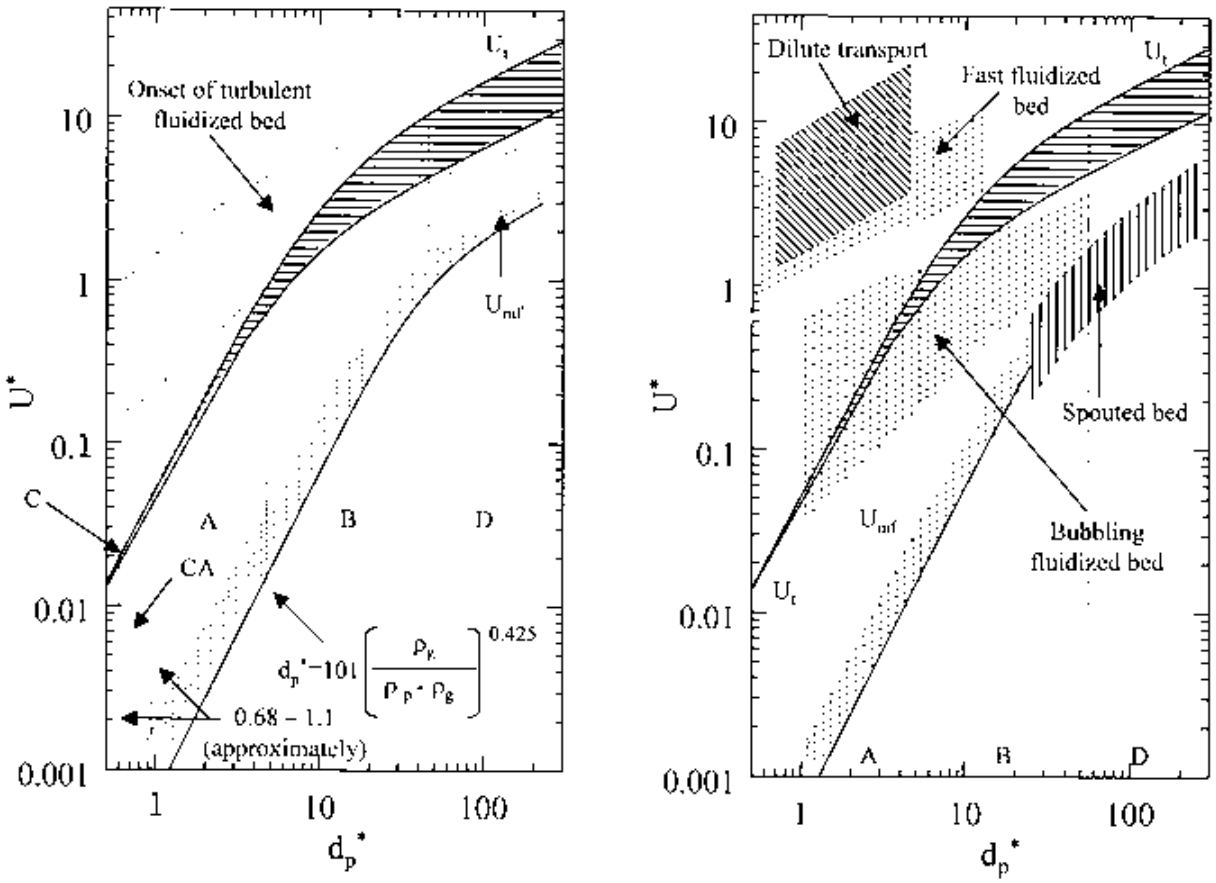

Fig.VII.1 Flow regime diagram (Kunii and Levenspiel, 1991)

Table VII.1 show the comparison of minimum fluidization velocity, minimum bubbling velocity, terminal velocity, transport velocity, fast transition velocity, transition velocity to pneumatic transport at two different bed temperatures of 27 °C and 827 °C for sand particle of size 307 µm and density 2300 kg/m^3.These stoichiometric information are the basic information necessary for the design of a CFB reactor.

Table VII.1 Comparison of stoichiometric information

Particulars	Values at 27 °C	Values at 827 °C
Archimedes Number	2235.71	102.31
Minimum fluidization velocity, U_{mf}	0.0841 m/s	0.0354 m/s
Minimum bubbling velocity, U_{mb}	0.0841 m/s	0.0354 m/s
Transition to turbulent Re No., Re_c	35.661	8.317
Transition to turbulent Re No., Re_k	55.626	12.973
Transition to turbulent velocity, U_c	1.842 m/s	3.849 m/s
Transition to turbulent velocity, U_k	2.874 m/s	6.004 m/s
Terminal velocity, U_t	2.296 m/s	2.637 m/s

Appendix – VIII
Heisler Chart

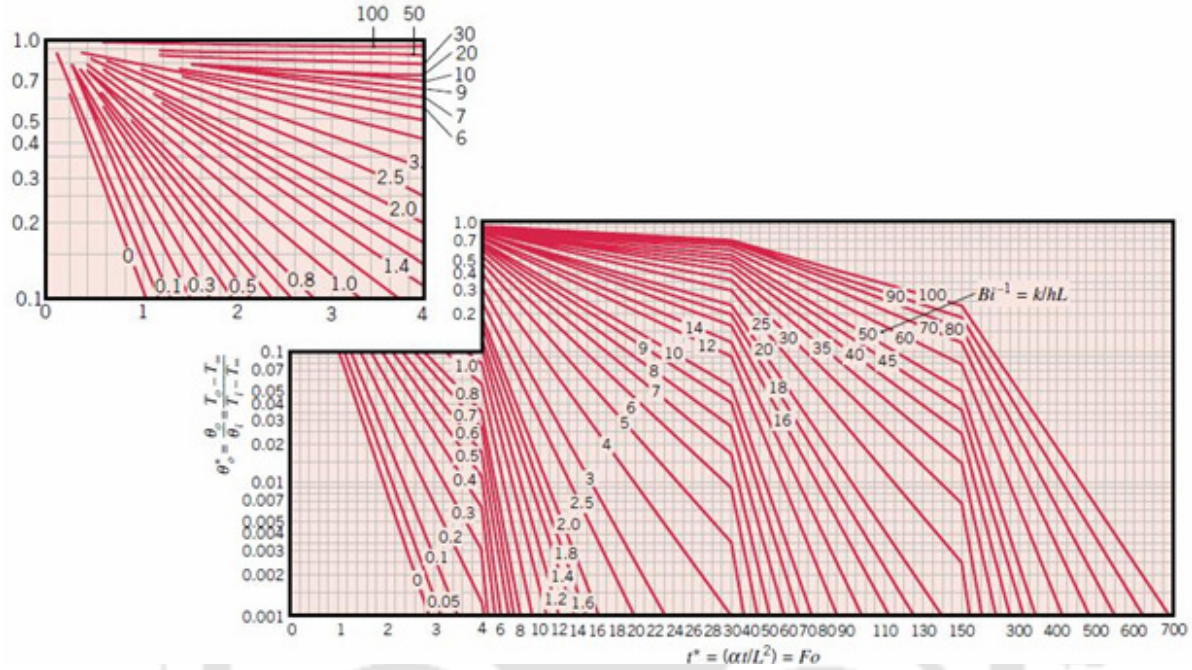

Fig.VIII.1 Midplane temperature as a function of time for a plane wall of thickness 2L

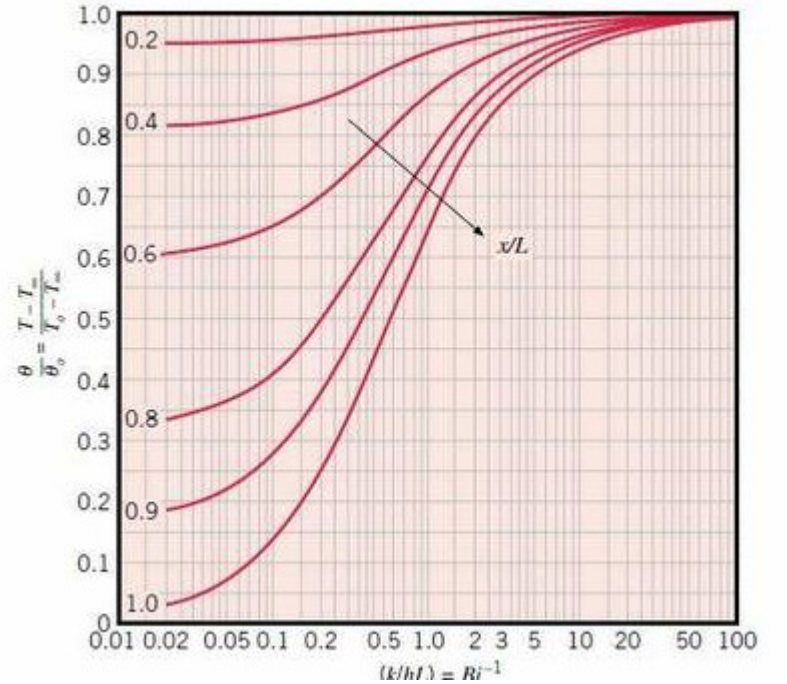

Fig.VIII.2 Temperature distribution in a plane wall of thickness 2L

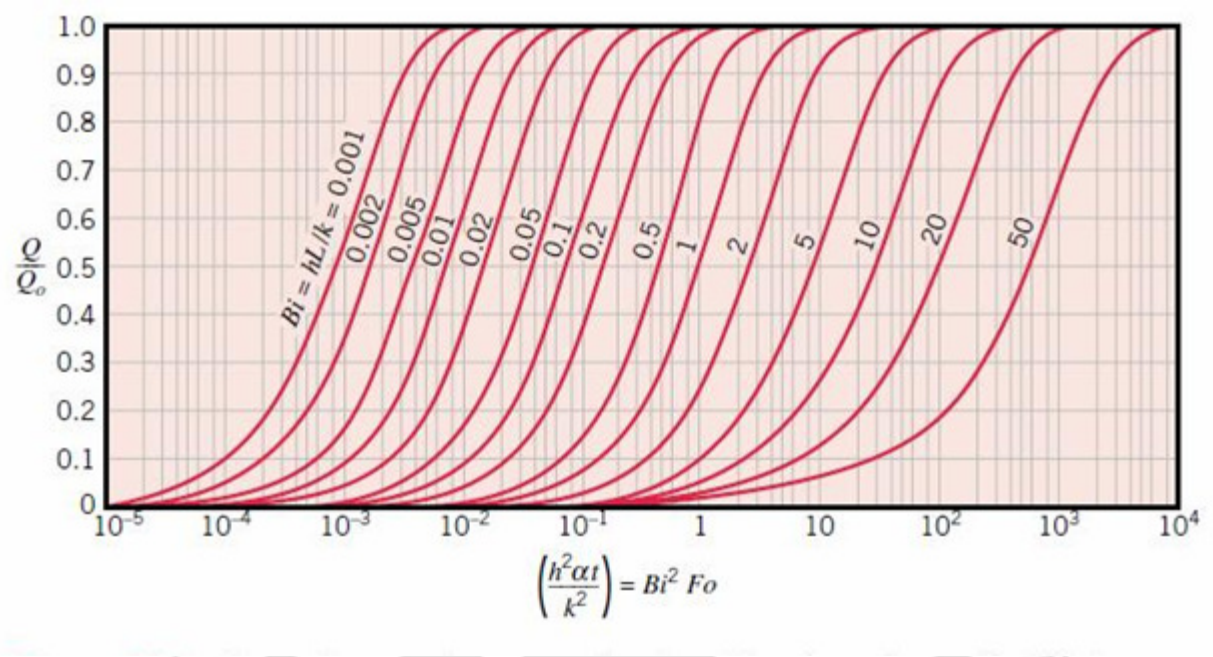

Fig.VIII.3 Internal energy change as function of time for a plane wall of thickness 2L

The following values of the rice husk properties were considered for the analysis of transit temperature by using Heisler Chart

Density: $\rho = 1030.93$ kg/m^3

Specific heat: $C_p = 1.69071$ kJ/kg °C

Thermal conductivity: $K = 0.0523$ W/m °C

Thermal diffusivity may be defined as,

$$\alpha = \frac{K}{\rho C_p} = 3.0\times10^{-8}\ \text{m}^2/\text{s} \qquad \text{(VIII.1)}$$

Let, the thickness ($2l$) of the material is 10 cm

$$\therefore l = 5\times10^{-3}\ \text{m} \qquad \text{(VIII.2)}$$

Biot number,

$$\frac{1}{Bi} = \frac{K}{hl} = 0.2615 \qquad \text{(VIII.3)}$$

From the transient temperature chart, at the above Fourier No and Biot No. the value of $\frac{\theta_c}{\theta_i}$ is found to be 0.9. As temperature of the plate is a function of centre line temperature in an infinite plate of thickness $2l$. Hence, the temperature at the various locations may be calculated by using the Heisler transient temperature chart.

Table VIII.1 Centre line temperature reading

Time and Fourier Number $t = 24$ s, $F_o = 0.0288$			Time and Fourier Number $t = 8$ min, $F_o = 0.576$			Time and Fourier Number $t = 16.67$ min, $F_o = 1.2$			Time and Fourier Number $t = 25$ min, $F_o = 1.8$		
$\frac{x}{l}$	Temperature		$\frac{x}{l}$	Temperature		$\frac{x}{l}$	Temperature		$\frac{x}{l}$	Temperature	
	°C	K		°C	K		°C	K		°C	K
0	459.90	**732.9**	0	288.85	**561.85**	0	239.09	**512.09**	0	201.77	**474.77**
0.2	445.05	**718.05**	0.2	286.13	**559.13**	0.2	237.61	**510.61**	0.2	201.225	**474.22**
0.4	414.36	**687.36**	0.4	274.15	**547.15**	0.4	231.11	**504.11**	0.4	198.83	**471.83**
0.6	389.25	**662.25**	0.6	258.37	**531.37**	0.6	222.54	**495.54**	0.6	195.67	**468.67**
0.8	339.03	**612.03**	0.8	243.13	**516.13**	0.8	214.27	**487.27**	0.8	192.62	**465.62**
0.9	302.76	**575.76**	0.9	227.89	**500.89**	0.9	205.99	**478.99**	0.9	189.57	**462.57**
1.0	280.44	**553.44**	1.0	216.46	**489.46**	1	199.79	**472.79**	1.0	187.29	**460.29**

Appendix – IX
Kinetic Parameters of Various Biomass Samples

Kinetic parameters for 5 (five) biomass samples (rice husk, sawdust, rice straw, water hyacinth and tea waste) were evaluated by using regression analysis. The result of the analysis with temperature ranges of both active pyrolysis zone (first reaction zone) and second reaction zone are presented in the following Table (Table IX.1).

Table IX.1 Values of reaction kinetics of biomass

Biomass	**RICE HUSK**							Heating Rate – 10 °C/min
First Reaction Zone					**Second Reaction Zone**			
Temperature Range in °C	Weight range in mg		Kinetic parameters	Regression	Temperature Range in °C	Weight range in mg	Kinetic parameters	Regression
180 – 350	W_o	9.157310	E (kJ/mol)	54.113	350 – 490	W_o 4.539802	E (kJ/mol)	50.265
	W_f	4.543011	A (min^{-1})	1.218×10^4		W_f 2.024864	A (min^{-1})	929.600
			n	0.485			n	0.619
Biomass	RICE HUSK							Heating Rate – 30 °C/min
First Reaction Zone					**Second Reaction Zone**			
Temperature Range in °C	Weight range in mg		Kinetic parameters	Regression	Temperature Range in °C	Weight range in mg	Kinetic parameters	Regression
191 – 368	W_o	7.917016	E (kJ/mol)	58.839	369 – 531	W_o 3.896528	E (kJ/mol)	46.937
	W_f	3.896528	A (min^{-1})	7.412×10^4		W_f 1.634948	A (min^{-1})	1.009×10^3
			n	0.518			n	0.656
Biomass	RICE HUSK							Heating Rate – 80 °C/min
First Reaction Zone					**Second Reaction Zone**			
Temperature Range in °C	Weight range in mg		Kinetic parameters	Regression	Temperature Range in °C	Weight range in mg	Kinetic parameters	Regression
181 - 380	W_o	4.506176	E (kJ/mol)	51.917	381 – 581	W_o 2.2482460	E (kJ/mol)	37.053
	W_f	2.260982	A (min^{-1})	3.057×10^4		W_f 0.9448632	A (min^{-1})	339.52
			n	0.360			n	0.676
Biomass	**RICE STRAW**							Heating Rate – 10 °C/min
First Reaction Zone					**Second Reaction Zone**			
Temperature Range in °C	Weight range in mg		Kinetic parameters	Regression	Temperature Range in °C	Weight range in mg	Kinetic parameters	Regression
185 – 380	W_o	5.829232	E (kJ/mol)	38.327	381 – 506	W_o 2.1111400	E (kJ/mol)	144.564
	W_f	2.113014	A (min^{-1})	395.42		W_f 0.6347989	A (min^{-1})	2.025×10^{10}
			n	0.658			n	1.280
Biomass	RICE STRAW							Heating Rate – 30 °C/min
First Reaction Zone					**Second Reaction Zone**			
Temperature Range in °C	Weight range in mg		Kinetic parameters	Regression	Temperature Range in °C	Weight range in mg	Kinetic parameters	Regression
180 – 370	W_o	6.412382	E (kJ/mol)	49.085	371 – 521	W_o 2.5497070	E (kJ/mol)	72.023
	W_f	2.558008	A (min^{-1})	1.405×10^4		W_f 0.4650733	A (min^{-1})	8.239×10^4
			n	0.712			n	0.758

Biomass	RICE STRAW							Heating Rate – 80 °C/min
First Reaction Zone					**Second Reaction Zone**			
Temperature Range in °C	Weight range in mg		Kinetic parameters	Regression	Temperature Range in °C	Weight range in mg	Kinetic parameters	Regression
183 – 401	W_o	6.488919	E (kJ/mol)	47.360	402 – 531	W_o 2.1397340	E (kJ/mol)	4.485
	W_f	2.151442	A (min^{-1})	2.228×10^4		W_f 0.0801541	A (min^{-1})	2.433
			n	0.884			n	0.52
Biomass	**TEA WASTE**							Heating Rate – 10 °C/min
First Reaction Zone					**Second Reaction Zone**			
Temperature Range in °C	Weight range in mg		Kinetic parameters	Regression	Temperature Range in °C	Weight range in mg	Kinetic parameters	Regression
188 – 335	W_o	5.448367	E (kJ/mol)	43.433	336 – 500	W_o 3.0444960	E (kJ/mol)	35.475
	W_f	3.046954	A (min^{-1})	1.497×10^3		W_f 0.3416212	A (min^{-1})	36.408
			n	0.364			n	0.387

Biomass	**TEA WASTE**							**Heating Rate – 30** °C/min
First Reaction Zone					**Second Reaction Zone**			
Temperature Range in °C	Weight range in mg		Kinetic parameters	Regression	Temperature Range in °C	Weight range in mg	Kinetic parameters	Regression
180 – 378	W_o	**3.386152**	E (kJ/mol)	43.239	379 – 515	W_o **1.7171840**	E (kJ/mol)	75.239
	W_f	**1.720396**	A (s^{-1})	2.910×10^3		W_f **0.1945011**	A (s^{-1})	8.883×10^4
			n	0.568			n	0.541
Biomass	TEA WASTE							**Heating Rate – 80** °C/min
Temperature Range in °C	Weight range in mg		Kinetic parameters	Regression	Temperature Range in °C	Weight range in mg	Kinetic parameters	Regression
200 – 380	W_o	**5.259683**	E (kJ/mol)	50.168	381 – 600	W_o **2.8412910**	E (kJ/mol)	89.389
	W_f	**2.851640**	A (min^{-1})	3.901×10^4		W_f **0.3913109**	A (min^{-1})	2.629×10^6
			n	0.701			n	1.066
Biomass	**TEA WASTE – combination of 1st and 2nd Reaction (single reaction)**							**Heating Rate – 80** °C/min
Temperature Range in °C			Weight range in mg		Kinetic parameters		Regression	
200 – 600			W_o	5.2596830	E (kJ/mol)		72.545	
			W_f	0.3913109	A (min^{-1})		1.158×10^6	
					n		1.417	
Biomass	**WATER HYACINTH**							**Heating Rate – 10** °C/min
First Reaction Zone					**Second Reaction Zone**			
Temperature Range in °C	Weight range in mg		Kinetic parameters	Regression	Temperature Range in °C	Weight range in mg	Kinetic parameters	Regression
208 – 350	W_o	**3.872861**	E (kJ/mol)	71.010	351 – 531	W_o **1.9147440**	E (kJ/mol)	89.586
	W_f	**1.915560**	A (s^{-1})	9.360×10^5		W_f **0.5955276**	A (s^{-1})	5.502×10^5
			n	0.776			n	0.418
Biomass	WATER HYACINTH							**Heating Rate – 30** °C/min
First Reaction Zone					**Second Reaction Zone**			
Temperature Range in °C	Weight range in mg		Kinetic parameters	Regression	Temperature Range in °C	Weight range in mg	Kinetic parameters	Regression
190 – 342	W_o	**5.603742**	E (kJ/mol)	79.647	343 – 470	W_o **2.8702420**	E (kJ/mol)	91.014
	W_f	**2.874396**	A (s^{-1})	1.403×10^7		W_f **0.7353219**	A (s^{-1})	2.040×10^6
			n	0.751			n	0.441

Biomass	WATER HYACINTH							**Heating Rate – 80** °C/min
First Reaction Zone					**Second Reaction Zone**			
Temperature Range in °C	Weight range in mg		Kinetic parameters	Regression	Temperature Range in °C	Weight range in mg	Kinetic parameters	Regression
190 – 342	W_o	**5.504908**	E (kJ/mol)	85.793	343 – 461	W_o **2.9193200**	E (kJ/mol)	83.079
	W_f	**2.928435**	A (min^{-1})	1.276×10^{8}		W_f **0.7377498**	A (min^{-1})	1.018×10^{6}
			n	0.832			n	0.7961
Biomass	**SAW DUST**							**Heating Rate – 10** °C/min
First Reaction Zone					**Second Reaction Zone**			
Temperature Range in °C	Weight range in mg		Kinetic parameters	Regression	Temperature Range in °C	Weight range in mg	Kinetic parameters	Regression
197 – 332	W_o	**3.944974**	E (kJ/mol)	111.827	333 - 471	W_o **1.48019000**	E (kJ/mol)	47.534
	W_f	**1.482550**	A (min^{-1})	3.948×10^{9}		W_f **0.00455028**	A (min^{-1})	712.200
			n	0.751			n	0.699
Biomass	SAW DUST							**Heating Rate – 30** °C/min
First Reaction Zone					**Second Reaction Zone**			
Temperature Range in °C	Weight range in mg		Kinetic parameters	Regression	Temperature Range in °C	Weight range in mg	Kinetic parameters	Regression
251 – 362	W_o	**5.426730**	E (kJ/mol)	100.467	363 – 606	W_o **2.0936900**	E (kJ/mol)	101.463
	W_f	**2.099430**	A (min^{-1})	8.050×10^{8}		W_f **0.2934735**	A (min^{-1})	2.655×10^{7}
			n	0.906			n	0.780
Biomass	SAW DUST							**Heating Rate – 80** °C/min
First Reaction Zone					**Second Reaction Zone**			
Temperature Range in °C	Weight range in mg		Kinetic parameters	Regression	Temperature Range in °C	Weight range in mg	Kinetic parameters	Regression
210 - 361	W_o	**5.438789**	E (kJ/mol)	112.025	362 - 491	W_o **2.4005930**	E (kJ/mol)	31.269
	W_f	**2.366596**	A (min^{-1})	1.540×10^{10}		W_f **0.3904172**	A (min^{-1})	159.530
			n	0.684			n	0.170

Appendix – X
Uncertainty Analysis

For overall uncertainty measurement consider the following quantities:

- Orifice : ± 0.5 mm
- Manometer : ± 0.2 mm
- Temperature : ± 0.5 °C
- Distributor plate : ± 0.6 % opening area
- Center to center pressure tapings: 1 mm (error)
- Pressure gauge error: ± 0.5
- Loss of inventory: ± 1 gm
- Error in calculating recirculation: ± 1 mm
- Visual Error : ± 0.5
- Bulk temperature calculation: ± 1°C
- Thermocouple temperature measurement error: ± 0.5 °C

1. Uncertainty in calculating wall-to-bed heat transfer coefficient (h in W/m^2-K)

Individual uncertainties are:

$$q = 1.9017 \pm 0.1 \text{ W}$$

$$D = 0.054 \pm 0.005 \text{ m}$$

$$L = 0.50 \pm 0.001 \text{ m}$$

$$T_s = 68 \pm 0.5 \ ^{o}\text{C}$$

$$T_b = 35 \pm 0.5 \ ^{o}\text{C}$$

Heat transfer coefficient is calculated by using the following expression,

$$h = \frac{q}{A_s \left(T_s - T_b\right)} = \frac{q}{\pi \times D \times L \times \left(T_s - T_b\right)} \qquad \text{X-A}$$

Differentiating the above equation with respect to q D, L, T_s, and T_b, we have,

$$\frac{\partial h}{\partial q} = \frac{1}{\pi \times D \times L \times (T_s - T_b)} \quad \text{X.1}$$

$$\frac{\partial h}{\partial D} = -\frac{q}{\pi \times D^2 \times L \times (T_s - T_b)} \quad \text{X.2}$$

$$\frac{\partial h}{\partial L} = -\frac{1}{\pi \times D \times L^2 \times (T_s - T_b)} \quad \text{X.3}$$

$$\frac{\partial h}{\partial T_s} = \frac{q}{\pi \times D \times L}\left[\frac{-1}{(T_s - T_b)^2}\right] = -\frac{q}{\pi \times D \times L \times (T_s - T_b)^2} \quad \text{X.4}$$

$$\frac{\partial h}{\partial T_b} = \frac{q}{\pi \times D \times L \times (T_s - T_b)^2} \quad \text{X.5}$$

The overall uncertainty in calculating heat transfer coefficient is expressed as,

$$U_h = \sqrt{\left(\frac{\partial h}{\partial q}\right)^2 \times (\Delta q)^2 + \left(\frac{\partial h}{\partial D}\right)^2 \times (\Delta D)^2 + \left(\frac{\partial h}{\partial L}\right)^2 \times (\Delta L)^2 + \left(\frac{\partial h}{\partial T_s}\right)^2 \times (\Delta T_s)^2 + \left(\frac{\partial h}{\partial T_b}\right)^2 \times (\Delta T_b)^2} \quad \text{X.6}$$

$$= 0.039085$$

% Uncertainty is ± 3.91 X.7

2. Uncertainty in calculating solid circulation rate (G_s in kg m^{-2}s^{-1})

Individual uncertainties are:

$$\rho_s = 2300 \pm 5 \text{ kg}$$

$$L_a = 0.135 \pm 0.002 \text{ m}$$

$$d_D = 0.0254 \pm 0.002 \text{ m}$$

$$d_B = 0.054 \pm 0.005 \text{ m}$$

$$t = 30 \pm 0.2 \text{ s}$$

Solid circulation rate is calculated by using the following expression,

$$G_s = \frac{\rho_s \times L_a \times A_D \times (1 - \varepsilon_{mf})}{A_B \times t} \quad \text{X-B}$$

or,

$$G_s = \frac{\rho_s \times L_a \times d_D^2 \times \left(1-\varepsilon_{mf}\right)}{d_B^2 \times t} \quad \text{X.8}$$

Differentiating the above equation with respect to ρ_s, L_a, d_D, d_B, and t, we have,

$$\frac{\partial G_s}{\partial \rho_s} = \frac{L_a \times d_D^2 \times \left(1-\varepsilon_{mf}\right)}{d_B^2 \times t} \quad \text{X.9}$$

$$\frac{\partial G_s}{\partial L_a} = \frac{\rho_s \times d_D^2 \times \left(1-\varepsilon_{mf}\right)}{d_B^2 \times t} \quad \text{X.10}$$

$$\frac{\partial G_s}{\partial d_D} = \frac{2 \times \rho_s \times L_a \times d_D \times \left(1-\varepsilon_{mf}\right)}{d_B^2 \times t} \quad \text{X.11}$$

$$\frac{\partial G_s}{\partial d_B} = -\frac{2 \times \rho_s \times L_a \times d_D^2 \times \left(1-\varepsilon_{mf}\right)}{d_B^3 \times t} \quad \text{X.12}$$

$$\frac{\partial G_s}{\partial t} = -\frac{\rho_s \times L_a \times d_D^2 \times \left(1-\varepsilon_{mf}\right)}{d_B^2 \times t^2} \quad \text{X.13}$$

The overall uncertainty in calculating solid circulation rate is expressed as,

$$U_{G_s} = \sqrt{\left(\frac{\partial G_s}{\partial \rho_s}\right)^2 \times (\Delta \rho_s)^2 + \left(\frac{\partial G_s}{\partial L_a}\right)^2 \times (\Delta L_a)^2 + \left(\frac{\partial G_s}{\partial d_D}\right)^2 \times (\Delta d_D)^2 + \left(\frac{\partial G_s}{\partial d_B}\right)^2 \times (\Delta d_B)^2 + \left(\frac{\partial G_s}{\partial t}\right)^2 \times (\Delta t)^2} \quad \text{X.14}$$

$$= 0.0532$$

% Uncertainty is ± 5.32 X.15

3. **Uncertainty in calculating bed-to-wall heat transfer coefficient (*h* in W/m^2-K)**

Individual uncertainties are:

$T_B, T_s = \pm 1\ ^{o}\text{C}$

$T_{in}, T_{out} = \pm\ 0.5\ ^{o}\text{C}$

$m_w = \pm\ 2$ ml/min

$D = \pm\ 1$ mm

$L = \pm\ 1$ mm

The heat transfer coefficient is calculated by using the following expression,

$$h = \frac{m_w C_{p_w} (T_{in} - T_{out})}{A_{ts} (T_B - T_S)} \qquad \text{X-C}$$

Differentiating the above equation with respect to ρ_s, L_a, d_D, d_B, and t, we have,

$$\frac{\partial h}{\partial m_w} = \frac{C_{p_w} (T_{in} - T_{out})}{A_{ts} (T_B - T_S)} \qquad \text{X.16}$$

$$\frac{\partial h}{\partial T_{in}} = \frac{m_w C_{p_w}}{A_{ts} (T_B - T_S)} \qquad \text{X.17}$$

$$\frac{\partial h}{\partial T_{out}} = -\frac{m_w C_{p_w}}{A_{ts} (T_B - T_S)} \qquad \text{X.18}$$

$$\frac{\partial h}{\partial T_B} = -\frac{m_w C_{p_w} (T_{in} - T_{out})}{A_{ts} (T_B - T_S)^2} \qquad \text{X.19}$$

$$\frac{\partial h}{\partial T_S} = \frac{m_w C_{p_w} (T_{in} - T_{out})}{A_{ts} (T_B - T_S)^2} \qquad \text{X.20}$$

$$\frac{\partial h}{\partial A_{ts}} = -\frac{m_w C_{p_w} (T_{in} - T_{out})}{A_{ts}^2 (T_B - T_S)} \qquad \text{X.21}$$

The overall uncertainty in calculating heat transfer coefficient is expressed as,

$$U_{G_s} = \sqrt{\left(\frac{\partial h}{\partial m_w}\right)^2 \times (\Delta m_w)^2 + \left(\frac{\partial h}{\partial T_{in}}\right)^2 \times (\Delta T_{in})^2 + \left(\frac{\partial h}{\partial T_{out}}\right)^2 \times (\Delta T_{out})^2 + \left(\frac{\partial h}{\partial T_B}\right)^2 \times (\Delta T_B)^2 + \left(\frac{\partial h}{\partial T_S}\right)^2 \times (\Delta T_S)^2 + \left(\frac{\partial h}{\partial A_{ts}}\right)^2 \times (\Delta A_{ts})^2} \qquad \text{X.22}$$

$$= 0.123$$

% Uncertainty is ± 12.3 X.23

4. Uncertainty in calculating bed voidage

The expression of bed voidage calculation is:

$$\varepsilon = 1 - \frac{10 \times \Delta h}{\rho_s \times L_m} \qquad \text{X-D}$$

$$\frac{\partial \varepsilon}{\partial (\Delta h)} = -\frac{10}{\rho_s \times L_m} \quad \text{X.24}$$

$$\frac{\partial \varepsilon}{\partial L_m} = \frac{10 \times \Delta h}{\rho_s \times L_m^2} \quad \text{X.25}$$

$$\frac{\partial \varepsilon}{\partial \rho_s} = \frac{10 \times \Delta h}{\rho_s^2 \times L_m} \quad \text{X.26}$$

Overall uncertainty may be calculated as;

$$U = \sqrt{\left(\frac{\partial \varepsilon}{\partial (\Delta h)}\right)^2 \times (\Delta h)^2 + \left(\frac{\partial \varepsilon}{\partial L_m}\right)^2 \times (\Delta L_m)^2 + \left(\frac{\partial \varepsilon}{\partial \rho_s}\right)^2 \times (\Delta \rho_s)^2} = \pm 0.005 - 0.659\% \quad \text{X.27}$$

Uncertainty associated with solid density is assumed to be ± 5 kg/m^3

By using the above mathematical expression the uncertainties at different inventories and at different operating pressures are calculated and presented in the following tables:

Table X.1 Variation of uncertainty at inventory of I = 400 g

Riser height from the distributor in mm	L_m in m	ΔL_m in m	Δh in cm			$\Delta(\Delta h)$ in m	Overall uncertainty in %		
			P = 1 bar	P = 3 bar	P = 5 bar		P = 1 bar	P = 3 bar	P = 5 bar
120	0.18	0.005	0.3	0.3	0.5	0.003	0.021	0.021	0.034
192.5	0.145	0.005	3.3	4.2	5.3	0.003	0.342	0.435	0.549
370	0.28	0.005	12	18	23.6	0.010	0.336	0.503	0.659
495	0.30	0.005	0.2	0.1	0.1	0.003	0.007	0.005	0.005
970	0.30	0.005	0.1	0.05	0.1	0.003	0.005	0.005	0.005
1570	0.30	0.005	1.1	1.4	1.9	0.003	0.027	0.034	0.046

Table X.2 Variation of uncertainty at inventory of I = 600 g

Riser height from the distributor in mm	L_m in m	ΔL_m in m	Δh in cm			$\Delta(\Delta h)$ in m	Overall uncertainty in %		
			P = 1 bar	P = 3 bar	P = 5 bar		P = 1 bar	P = 3 bar	P = 5 bar
120	0.18	0.005	0.3	0.2	0.5	0.003	0.021	0.015	0.034
192.5	0.145	0.005	4.7	4.6	4.0	0.003	0.487	0.477	0.415
370	0.28	0.005	21.8	23.6	20.4	0.010	0.609	0.659	0.570
495	0.30	0.005	0.2	0.2	0.2	0.003	0.007	0.007	0.007
970	0.30	0.005	0.1	0.1	0.1	0.003	0.005	0.005	0.005
1570	0.30	0.005	1.6	1.8	1.8	0.003	0.039	0.044	0.044

Table X.3 Variation of uncertainty at inventory of I = 800 g

Riser height from the distributor in mm	L_m in m	ΔL_m in m	Δh in cm			$\Delta(\Delta h)$ in m	Overall uncertainty in %		
			P = 1 bar	P = 3 bar	P = 5 bar		P = 1 bar	P = 3 bar	P = 5 bar
120	0.18	0.005	0.2	0.3	0.3	0.003	0.015	0.021	0.021
192.5	0.145	0.005	3.4	3.0	1.8	0.003	0.352	0.311	0.187
370	0.28	0.005	17.0	20.0	20.3	0.010	0.475	0.559	0.567
495	0.30	0.005	0.3	0.2	0.1	0.003	0.009	0.007	0.005
970	0.30	0.005	0.1	0.1	0.05	0.003	0.005	0.005	0.005
1570	0.30	0.005	1.3	1.4	1.5	0.003	0.032	0.034	0.037

Table X.4 Variation of uncertainty at inventory of I = 1000 g

Riser height from the distributor in mm	L_m in m	ΔL_m in m	Δh in cm			$\Delta(\Delta h)$ in m	Overall uncertainty in %		
			P = 1 bar	P = 3 bar	P = 5 bar		P = 1 bar	P = 3 bar	P = 5 bar
120	0.18	0.005	0.4	0.4	0.3	0.003	0.028	0.028	0.021
192.5	0.145	0.005	3.0	2.2	3.2	0.003	0.311	0.228	0.332
370	0.28	0.005	17.9	19.9	16.6	0.010	0.050	0.556	0.464
495	0.30	0.005	0.05	0.4	0.2	0.003	0.005	0.011	0.007
970	0.30	0.005	0.1	0.1	0.1	0.003	0.005	0.005	0.005
1570	0.30	0.005	1.5	1.8	1.8	0.003	0.037	0.044	0.044

Appendix – XI
Experimental Data at Varied Blending of Biomass

Bed voidage, suspension density, solid circulation rate, axial and radial heat transfer coefficient at four % blending of biomass in sand and two weight composition ratios are presented in this appendix. Effect of operating pressure and superficial velocity are also presented in the following tables.

Table XI.1 Voidage , ε at U_{sup} = 5 m/s, P = 1 bar

Vertical distance from the distributor plate, mm	2.5 % blend		7.5 % blend		15.0 % blend		20.0 % blend	
	10:400 (B:S) G_s: 0.816	**15:600 (B:S) G_s: 1.586**	**30:400 (B:S) G_s: 0.946**	**45:600 (B:S) G_s: 1.072**	**60:400 (B:S) G_s: 0.773**	**90:600 (B:S) G_s: 0.912**	**80:400 (B:S) G_s: 0.205**	**120: 600 (B:S) G_s: 0.0817**
120	0.990337	0.983090	0.990337	0.975847	0.978261	0.915460	0.973428	0.833331
192.5	0.904050	0.925039	0.910044	0.928036	0.904050	0.925039	0.916043	0.910044
370	0.978261	0.968943	0.965837	0.976708	0.968943	0.975155	0.973602	0.975155
495	0.999276	0.982607	0.976813	0.998550	0.989854	0.994204	0.996375	0.994204
970	0.999276	0.998550	0.997101	0.998550	0.995653	0.992755	0.995653	0.997101
1570	0.982607	0.978261	0.986957	0.981158	0.984060	0.981158	0.978988	0.979710

Table XI.2 Suspension density, ρ_{sus} (kg/m^3) at U_{sup} = 5 m/s, P = 1 bar

Vertical distance from the distributor plate, mm	2.5 % blend		7.5 % blend		15.0 % blend		20.0 % blend	
	10:400 (B:S)	**15:600 (B:S)**	**30:400 (B:S)**	**45:600 (B:S)**	**60:400 (B:S)**	**90:600 (B:S)**	**80:400 (B:S)**	**120: 600 (B:S)**
120	23.38	40.04	23.38	56.69	51.14	195.51	62.25	384.31
192.5	221.74	173.49	207.96	166.60	221.74	173.49	194.17	207.96
370	51.14	72.56	79.70	54.71	72.56	58.28	61.85	58.28
495	2.83	41.15	54.47	4.50	24.49	14.49	9.50	14.49
970	2.83	4.50	7.83	4.50	11.16	17.82	11.16	7.83
1570	41.15	51.14	31.15	44.48	37.81	44.48	49.47	47.81

Table XI.3 Axial heat transfer coefficient, h (W/m^2-K) at U_{sup} = 5 m/s and at P = 1 bar

Vertical distance from the distributor plate, m	2.5 % blend		7.5 % blend		15.0 % blend		20.0 % blend	
	10:400 (B:S)	**15:600 (B:S)**	**30:400 (B:S)**	**45:600 (B:S)**	**60:400 (B:S)**	**90:600 (B:S)**	**80:400 (B:S)**	**120: 600 (B:S)**
1.4	106.73	106.31	122.69	90.49	101.46	101.86	89.6	85.18
1.5	111.01	109.95	128.38	95.05	106.13	109.09	95.14	91.57
1.6	114.38	117.42	132.06	96.15	110.95	110.54	96.47	94.06
1.7	115.33	119.79	136.40	99.61	111.55	117.09	100.68	100.68
1.8	120.34	124.08	142.48	102.57	116.56	119.10	103.95	102.41

Table XI.4 Radial heat transfer coefficient, h (W/m^2-K) at U_{sup} = 5 m/s and at P = 1 bar

Radial distance (d/D)	2.5 % blend		7.5 % blend		15.0 % blend		20.0 % blend	
	10:400 (B:S)	**15:600 (B:S)**	**30:400 (B:S)**	**45:600 (B:S)**	**60:400 (B:S)**	**90:600 (B:S)**	**80:400 (B:S)**	**120: 600 (B:S)**
0.8	264.45	204.93	362.93	310.30	334.29	401.53	463.38	486.17
0.6	160.92	131.97	198.27	156.20	171.42	190.98	195.29	177.89
0.4	125.06	556.55	150.21	111.07	123.49	134.63	131.14	114.25
0.3	130.15	188.21	147.02	105.43	128.06	139.14	122.26	104.48
0.2	114.38	117.42	132.06	96.15	110.95	120.55	110.54	94.06

Table XI.5 Voidage , ε at U_{sup} = 5 m/s, P = 3 bar

Vertical distance from the distributor plate, mm	2.5 % blend		7.5 % blend		15.0 % blend		20.0 % blend	
	10:400 (B:S) G_s: 1.164	**15:600 (B:S) G_s: 1.276**	**30:400 (B:S) G_s: 1.623**	**45:600 (B:S) G_s: 0.753**	**60:400 (B:S) G_s: 1.094**	**90:600 (B:S) G_s: 1.762**	**80:400 (B:S) G_s: 0.926**	**120: 600 (B:S) G_s: 0.1388**
120	0.997584	0.985508	0.992755	0.987923	0.995170	0.983090	0.987923	0.932368
192.5	0.820090	0.889055	0.868066	0.910044	0.835084	0.886058	0.904050	0.874065
370	0.951865	0.956520	0.945653	0.962732	0.927018	0.956520	0.959626	0.956520
495	0.995653	0.986957	0.969565	0.997101	0.973911	0.998550	0.991303	0.998550
970	0.999276	0.997101	0.998550	0.998550	0.998550	0.999276	0.997828	0.998550
1570	0.973911	0.975364	0.976813	0.975364	0.972463	0.973911	0.972463	0.972463

Table XI.6 Suspension density, ρ_{sus} (kg/m^3) at U_{sup} = 5 m/s, P = 3 bar

Vertical distance from the distributor plate, mm	2.5 % blend		7.5 % blend		15.0 % blend		20.0 % blend	
	10:400 (B:S)	**15:600 (B:S)**	**30:400 (B:S)**	**45:600 (B:S)**	**60:400 (B:S)**	**90:600 (B:S)**	**80:400 (B:S)**	**120: 600 (B:S)**
120	6.72	34.48	17.82	28.93	12.27	40.04	28.93	156.64
192.5	414.75	256.21	304.46	207.96	380.28	263.10	221.74	290.67
370	111.82	101.12	126.10	86.84	168.94	101.12	93.98	101.12
495	11.16	31.15	71.13	7.83	61.14	4.50	21.16	4.50
970	2.83	7.83	4.50	4.50	4.50	2.83	6.16	4.50
1570	61.14	57.80	54.47	57.80	64.47	61.14	64.47	64.47

Table XI.7 Axial heat transfer coefficient, h (W/m^2-K) at U_{sup} = 5 m/s and at P = 3 bar

Vertical distance from the distributor plate, m	2.5 % blend		7.5 % blend		15.0 % blend		20.0 % blend	
	10:400 (B:S)	**15:600 (B:S)**	**30:400 (B:S)**	**45:600 (B:S)**	**60:400 (B:S)**	**90:600 (B:S)**	**80:400 (B:S)**	**120: 600 (B:S)**
1.4	112.70	120.55	131.39	93.76	103.85	115.78	99.18	94.53
1.5	116.82	125.28	137.48	98.20	108.18	120.83	103.64	100.48
1.6	117.15	127.20	137.48	98.43	109.03	121.90	104.16	101.71
1.7	121.61	129.99	142.68	102.82	111.97	124.46	107.39	106.95
1.8	124.53	133.33	147.75	104.37	114.76	127.12	109.09	110.66

Table XI.8 Radial heat transfer coefficient, h (W/m^2-K) at U_{sup} = 5 m/s and at P = 3 bar

Radial distance (d/D)	2.5 % blend		7.5 % blend		15.0 % blend		20.0 % blend	
	10:400 (B:S)	**15:600 (B:S)**	**30:400 (B:S)**	**45:600 (B:S)**	**60:400 (B:S)**	**90:600 (B:S)**	**80:400 (B:S)**	**120: 600 (B:S)**
0.8	313.58	386.58	340.32	322.35	327.43	378.82	313.11	398.45
0.6	180.99	194.56	215.12	161.05	169.60	194.38	161.17	175.04
0.4	133.33	144.97	160.92	112.58	124.38	137.66	117.42	122.04
0.3	123.42	141.99	142.68	107.06	117.68	131.97	113.25	109.49
0.2	117.15	127.20	137.48	98.43	109.03	121.90	104.16	101.71

Table XI.9 Voidage , ε at U_{sup} = 5 m/s, P = 5 bar

Vertical distance from the distributor plate, mm	2.5 % blend		7.5 % blend		15.0 % blend		20.0 % blend	
	10:400 (B:S) G_s: 0.952	**15:600 (B:S) G_s: 1.455**	**30:400 (B:S) G_s: 1.798**	**45:600 (B:S) G_s: 1.350**	**60:400 (B:S) G_s: 1.637**	**90:600 (B:S) G_s:1.327**	**80:400 (B:S) G_s:0.989**	**120: 600 (B:S) G_s:0.3033**
120	0.998793	0.990337	0.990337	0.987923	0.987923	0.983090	0.992755	0.939615
192.5	0.832083	0.907047	0.865069	0.901048	0.847077	0.871063	0.922037	0.871063
370	0.951865	0.964285	0.976708	0.956520	0.936336	0.951865	0.968943	0.961179
495	0.997828	0.984060	0.969565	0.995653	0.966668	0.998550	0.991303	0.998550
970	0.999276	0.997101	0.998550	0.997828	0.999276	0.998550	0.999276	0.998550
1570	0.973911	0.975364	0.975364	0.973911	0.975364	0.972463	0.971014	0.973911

Table XI.10 Suspension density, ρ_{sus} kg/m^3) at U_{sup} = 5 m/s, P = 5 bar

Vertical distance from the distributor plate, mm	2.5 % blend		7.5 % blend		15.0 % blend		20.0 % blend	
	10:400 (B:S)	**15:600 (B:S)**	**30:400 (B:S)**	**45:600 (B:S)**	**60:400 (B:S)**	**90:600 (B:S)**	**80:400 (B:S)**	**120: 600 (B:S)**
120	3.94	23.38	23.38	28.93	28.93	40.04	17.82	139.98
192.5	387.18	214.85	311.35	228.64	352.71	297.57	180.39	297.57
370	111.82	83.27	54.71	101.12	147.52	111.82	72.56	90.41
495	6.16	37.81	71.13	11.16	77.79	4.50	21.16	4.50
970	2.83	7.83	4.50	6.16	2.83	4.50	2.83	4.50
1570	61.14	57.80	57.80	61.14	57.80	64.47	67.80	61.14

Table XI.11 Axial heat transfer coefficient, h (W/m^2-K) at U_{sup} = 5 m/s and at P = 5 bar

Vertical distance from the distributor plate, m	2.5 % blend		7.5 % blend		15.0 % blend		20.0 % blend	
	10:400 (B:S)	**15:600 (B:S)**	**30:400 (B:S)**	**45:600 (B:S)**	**60:400 (B:S)**	**90:600 (B:S)**	**80:400 (B:S)**	**120: 600 (B:S)**
1.4	116.95	121.05	117.75	99.47	121.19	114.69	100.38	96.33
1.5	121.76	126.20	122.62	104.21	126.74	120.00	104.69	102.26
1.6	121.76	126.97	122.26	104.21	129.10	122.47	105.22	103.28
1.7	126.97	130.15	127.12	107.73	132.82	124.68	108.52	108.12
1.8	130.56	133.07	128.70	109.43	139.04	129.34	110.54	111.01

Table XI.12 Radial heat transfer coefficient, h (W/m^2-K) at U_{sup} = 5 m/s and at P = 5 bar

Radial distance (d/D)	2.5 % blend		7.5 % blend		15.0 % blend		20.0 % blend	
	10:400 (B:S)	**15:600 (B:S)**	**30:400 (B:S)**	**45:600 (B:S)**	**60:400 (B:S)**	**90:600 (B:S)**	**80:400 (B:S)**	**120: 600 (B:S)**
0.8	334.83	380.90	281.29	308.92	425.40	411.08	313.11	403.09
0.6	187.02	196.77	187.36	164.50	204.93	196.77	161.80	175.93
0.4	138.86	145.17	141.90	117.48	148.49	137.94	118.42	123.94
0.3	128.54	141.70	127.51	113.01	145.37	137.94	114.50	111.91
0.2	121.76	126.97	122.26	104.21	129.10	122.47	105.22	103.28

Table XI.13 Voidage , ε at U_{sup} = 7 m/s and at P = 1 bar

Vertical distance from the distributor plate, mm	2.5 % blend		7.5 % blend		15.0 % blend		20.0 % blend	
	10:400 (B:S) G_s: 1.296	**15:600 (B:S) G_s: 1.406**	**30:400 (B:S) G_s: 1.565**	**45:600 (B:S) G_s: 1.261**	**60:400 (B:S) G_s: 1.137**	**90:600 (B:S) G_s: 1.451**	**80:400 (B:S) G_s: 1.064**	**120: 600 (B:S) G_s: 0.1921**
120	0.997584	0.987923	0.990337	0.980675	0.987923	0.980675	0.980675	0.968600
192.5	0.889055	0.913045	0.922037	0.922037	0.904050	0.910044	0.913045	0.904050
370	0.976708	0.964285	0.967390	0.965837	0.964285	0.967390	0.972049	0.967390
495	0.998550	0.976813	0.973911	0.995653	0.978261	0.997101	0.994204	0.998550
970	0.999276	0.998550	0.998550	0.998550	0.998550	0.998550	0.998550	0.999276
1570	0.975364	0.976086	0.979710	0.976813	0.978261	0.976813	0.976813	0.975364

Table XI.14 Suspension density, ρ_{sus} (kg/m^3) at U_{sup} = 7 m/s and at P = 1 bar

Vertical distance from the distributor plate, mm	2.5 % blend		7.5 % blend		15.0 % blend		20.0 % blend	
	10:400 (B:S)	**15:600 (B:S)**	**30:400 (B:S)**	**45:600 (B:S)**	**60:400 (B:S)**	**90:600 (B:S)**	**80:400 (B:S)**	**120: 600 (B:S)**
120	6.72	28.93	23.38	45.59	28.93	45.59	45.59	73.35
192.5	256.21	201.06	180.39	180.39	221.74	207.96	201.06	221.74
370	54.71	83.27	76.13	79.70	83.27	76.13	65.42	76.13
495	4.50	54.47	61.14	11.16	51.14	7.83	14.49	4.50
970	2.83	4.50	4.50	4.50	4.50	4.50	4.50	2.83
1570	57.80	56.14	47.81	54.47	51.14	54.47	54.47	57.80

Table XI.15 Axial heat transfer coefficient, h (W/m^2-K) at U_{sup} = 7 m/s and at P = 1 bar

Vertical distance from the distributor plate, m	2.5 % blend		7.5 % blend		15.0 % blend		20.0 % blend	
	10:400 (B:S)	**15:600 (B:S)**	**30:400 (B:S)**	**45:600 (B:S)**	**60:400 (B:S)**	**90:600 (B:S)**	**80:400 (B:S)**	**120: 600 (B:S)**
1.4	109.55	96.02	109.43	91.61	104.27	117.55	97.05	92.97
1.5	113.75	100.43	113.32	95.40	108.07	122.40	101.31	97.78
1.6	114.69	101.66	115.84	96.73	110.36	124.23	104.63	99.42
1.7	118.29	105.27	117.15	99.04	112.15	126.89	105.16	103.90
1.8	121.76	104.48	121.26	100.97	117.22	131.30	111.07	106.29

Table XI.16 Radial heat transfer coefficient, h (W/m^2-K) at U_{sup} = 7 m/s and at P = 1 bar

Radial distance (d/D)	2.5 % blend		7.5 % blend		15.0 % blend		20.0 % blend	
	10:400 (B:S)	**15:600 (B:S)**	**30:400 (B:S)**	**45:600 (B:S)**	**60:400 (B:S)**	**90:600 (B:S)**	**80:400 (B:S)**	**120: 600 (B:S)**
0.8	288.32	529.57	270.66	287.92	323.86	436.12	301.30	416.85
0.6	175.18	189.24	162.56	151.42	167.28	200.38	156.79	174.01
0.4	128.94	120.90	129.18	110.95	123.13	139.23	115.72	116.10
0.3	121.05	109.43	128.38	104.79	125.74	139.23	121.83	109.66
0.2	114.69	101.66	115.84	96.73	110.36	124.23	104.63	99.42

Table XI.17 Voidage , ε at U_{sup} = 7 m/s, P = 3 bar

Vertical distance from the distributor plate, mm	2.5 % blend		7.5 % blend		15.0 % blend		20.0 % blend	
	10:400 (B:S) G_s: 1.275	**15:600 (B:S) G_s: 1.123**	**30:400 (B:S) G_s: 2.089**	**45:600 (B:S) G_s: 1.205**	**60:400 (B:S) G_s: 1.434**	**90:600 (B:S) G_s: 1.861**	**80:400 (B:S) G_s: 1.352**	**120: 600 (B:S) G_s: 0.2609**
120	0.997584	0.980675	0.990337	0.987923	0.990337	0.978261	0.987923	0.903380
192.5	0.823087	0.883056	0.901048	0.910044	0.871063	0.898051	0.904050	0.895054
370	0.986026	0.953418	0.954971	0.961179	0.944100	0.961179	0.959626	0.965837
495	0.996375	0.991303	0.973911	0.994926	0.975364	0.998550	0.991303	0.997101
970	0.999276	0.996375	0.997828	0.998550	0.999276	0.998550	0.999276	0.998550
1570	0.973189	0.975364	0.976813	0.975364	0.973911	0.973911	0.972463	0.973911

Table XI.18 Suspension density, ρ_{sus} (kg/m^3) at U_{sup} = 7 m/s, P = 3 bar

Vertical distance from the distributor plate, mm	2.5 % blend		7.5 % blend		15.0 % blend		20.0 % blend	
	10:400 (B:S)	**15:600 (B:S)**	**30:400 (B:S)**	**45:600 (B:S)**	**60:400 (B:S)**	**90:600 (B:S)**	**80:400 (B:S)**	**120: 600 (B:S)**
120	6.72	45.59	23.38	28.93	23.38	51.14	28.93	223.28
192.5	407.86	270.00	228.64	207.96	297.57	235.53	221.74	242.42
370	33.29	108.25	104.68	90.41	129.67	90.41	93.98	79.70
495	9.50	21.16	61.14	12.83	57.80	4.50	21.16	7.83
970	2.83	9.50	6.16	4.50	2.83	4.50	2.83	4.50
1570	62.80	57.80	54.47	57.80	61.14	61.14	64.47	61.14

Table XI.19 Axial heat transfer coefficient, h (W/m^2-K) at U_{sup} = 7 m/s and at P = 3 bar

Vertical distance from the distributor plate, m	2.5 % blend		7.5 % blend		15.0 % blend		20.0 % blend	
	10:400 (B:S)	**15:600 (B:S)**	**30:400 (B:S)**	**45:600 (B:S)**	**60:400 (B:S)**	**90:600 (B:S)**	**80:400 (B:S)**	**120: 600 (B:S)**
1.4	116.56	118.49	131.22	97.42	108.07	118.29	98.85	92.22
1.5	120.62	123.05	136.84	101.71	112.46	122.84	102.77	97.64
1.6	120.98	126.43	137.75	101.96	113.69	124.68	104.32	99.04
1.7	124.98	131.22	141.51	105.32	116.23	126.97	105.91	104.53
1.8	129.26	136.40	147.54	106.40	120.62	131.81	109.84	105.59

Table XI.20 Radial heat transfer coefficient, h (W/m^2-K) at U_{sup} = 7 m/s and at P = 3 bar

Radial distance (d/D)	2.5 % blend		7.5 % blend		15.0 % blend		20.0 % blend	
	10:400 (B:S)	**15:600 (B:S)**	**30:400 (B:S)**	**45:600 (B:S)**	**60:400 (B:S)**	**90:600 (B:S)**	**80:400 (B:S)**	**120: 600 (B:S)**
0.8	318.88	372.70	323.35	291.97	342.56	384.43	269.60	394.66
0.6	181.94	187.53	205.13	158.35	177.28	194.92	157.87	169.33
0.4	135.59	142.48	158.23	115.59	126.89	138.86	114.69	117.88
0.3	126.50	141.99	142.48	108.35	127.28	137.94	115.65	108.07
0.2	120.98	126.43	137.75	101.96	113.69	124.68	104.32	99.04

Table XI.21 Voidage , ε at U_{sup} = 7 m/s, P = 5 bar

Vertical distance from the distributor plate, mm	2.5 % blend		7.5 % blend		15.0 % blend		20.0 % blend	
	10:400 (B:S) G_s: 1.093	**15:600 (B:S) G_s: 1.455**	**30:400 (B:S) G_s: 2.012**	**45:600 (B:S) G_s: 1.260**	**60:400 (B:S) G_s: 1.389**	**90:600 (B:S) G_s: 1.650**	**80:400 (B:S) G_s: 1.332**	**120: 600 (B:S) G_s: 0.3533**
120	0.996375	0.987923	0.992755	0.987923	0.980675	0.978261	0.990337	0.949277
192.5	0.871063	0.913045	0.880059	0.904050	0.853072	0.907047	0.931033	0.895054
370	0.958073	0.967390	0.948759	0.959626	0.945653	0.968943	0.973602	0.968943
495	0.997101	0.986957	0.973911	0.995653	0.992755	0.998550	0.991303	0.999711
970	0.999276	0.997101	0.998550	0.998550	0.997101	0.997101	0.998550	0.999563
1570	0.973911	0.975364	0.975364	0.973911	0.971014	0.975364	0.973911	0.973911

Table XI.22 Suspension density, ρ_{sus} (kg/m^3) at U_{sup} = 7 m/s, P = 5 bar

Vertical distance from the distributor plate, mm	2.5 % blend		7.5 % blend		15.0 % blend		20.0 % blend	
	10:400 (B:S)	**15:600 (B:S)**	**30:400 (B:S)**	**45:600 (B:S)**	**60:400 (B:S)**	**90:600 (B:S)**	**80:400 (B:S)**	**120: 600 (B:S)**
120	9.50	28.93	17.82	28.93	45.59	51.14	23.38	117.77
192.5	297.57	201.06	276.89	221.74	338.93	214.85	159.71	242.42
370	97.55	76.13	118.96	93.98	126.10	72.56	61.85	72.56
495	7.83	31.15	61.14	11.16	17.82	4.50	21.16	1.83
970	2.83	7.83	4.50	4.50	7.83	7.83	4.50	2.17
1570	61.14	57.80	57.80	61.14	67.80	57.80	61.14	61.14

Table XI.23 Axial heat transfer coefficient, h (W/m^2-K) at U_{sup} = 7 m/s and at P = 5 bar

Vertical distance from the distributor plate, m	2.5 % blend		7.5 % blend		15.0 % blend		20.0 % blend	
	10:400 (B:S)	**15:600 (B:S)**	**30:400 (B:S)**	**45:600 (B:S)**	**60:400 (B:S)**	**90:600 (B:S)**	**80:400 (B:S)**	**120: 600 (B:S)**
1.4	121.83	107.90	123.35	100.04	110.36	118.83	100.04	94.10
1.5	126.66	112.27	128.30	104.32	114.95	123.79	104.32	99.04
1.6	127.05	113.81	128.70	104.85	119.24	126.81	104.85	100.24
1.7	131.47	116.04	132.39	108.12	121.33	128.38	107.56	104.79
1.8	135.77	119.03	135.42	109.55	126.50	135.06	110.42	107.23

Table XI.24 Radial heat transfer coefficient, h (W/m^2-K) at U_{sup} = 7 m/s and at P = 5 bar

dial distance (d/D)	2.5 % blend		7.5 % blend		15.0 % blend		20.0 % blend	
	10:400 (B:S)	**15:600 (B:S)**	**30:400 (B:S)**	**45:600 (B:S)**	**60:400 (B:S)**	**90:600 (B:S)**	**80:400 (B:S)**	**120: 600 (B:S)**
0.8	352.45	388.75	299.56	294.46	370.04	386.58	280.53	387.30
0.6	193.29	185.52	189.93	160.92	186.02	195.47	161.55	170.02
0.4	143.76	131.47	147.44	117.95	133.84	140.08	116.63	118.22
0.3	133.59	124.01	135.42	112.52	137.39	143.46	114.69	110.07
0.2	127.05	113.81	128.70	104.85	119.24	126.81	104.85	100.24

Note: B: S = Biomass to sand ratio; G_s = Solid circulation rate in kg m^{-2}s^{-1}

Appendix – XII
List of Equipment/Instrument Used

List of instrument used

- Data acquisition system: Agilent 34970A (Data acquisition switch unit with multiplexer)
- Twin Lobe Blower : Capacity-1275 M^3/HP, pressure - 2000 MMWC, speed - 1300 rpm, motor for blower - 3 phase induction motor, 20 HP, 1400 rpm, 28.5 amp (Model:710)
- Compressor: Capacity - 225 litres, Maximum working pressure - 12.30 kg/cm^2, run by a 3 hp motor (manufacture by Ingersoll Rand (IR), Model: S-01480)
- Weighing balance: measuring range: max-15 kg, min-0.04 kg, error - 2 gm (Model: SP/p1s-15-FLP, manufactured by M/s. Shyaam Switchgears Pvt. Ltd.)
- Gas analyzer (Make: Testo, Model: 350 XL)
- Auto transformer (Make: VARIVOLT (0-270 V), 6 amp and 15 amp)
- Pressure guage (Make: Swagelok, Model: EN837-1)
- Pressure regulator (Make: Swagelok)
- Sieve machine for particle size measurement (manufactured by M/s. Scientific Engineering Corporation)
- Stop watch, Ball valve, Gate valve, Butter fly valve, Flow control valve, Bye pass valve, Air control valve
- Water tube manometer board – In-house fabrication
- Pressure tapings – In-house fabrication
- Installation of Orifice plate with U-tube water filled manometer - In-house fabrication
- Thermocouple sensor [Copper-Constantan (T-Type) and Chromel-Alumel (K-type)]
- Non contact type thermo meter (infrared)
- Thermocouple calibrator with constant temperature bath (Make: Julabo).

LIST OF PUBLICATIONS

JOURNALS

(1) **P. Kalita**, U. K. Saha, and P. Mahanta, Effect of biomass blending on hydrodynamics and heat transfer behavior in a cold pressurized circulating fluidized bed unit, *International Journal of Heat and Mass Transfer*, 60 (2013) 531-541. (doi:http://dx.doi.org/10.1016/j.ijheatmasstransfer.2013.01.043)

(2) **P. Kalita,** M. Clifford, K. Kalita, P. Mahanta, and U. K. Saha, Characterization and Analysis of Thermal Response of Rice Husk for Gasification Applications, *Journal of Renewable and Sustainable Energy*, 5, 013119 (2013). (doi: http://dx.doi.org/10.1063/1.4792487)

(3) **P. Kalita**, U. K. Saha, and P. Mahanta, Parametric study on the hydrodynamics and heat transfer along the riser of a pressurized circulating fluidized bed unit, *Experimental Thermal and Fluid Science*, 44 (2013) 620–630. **(doi:** http://dx.doi.org/10.1016/j.expthermflusci.2012.09.001)

(4) **P. Kalita**, U. K. Saha, and P. Mahanta, An experimental investigation of hydrodynamics and heat transfer with biomass blending in a riser of a pressurized circulating fluidized bed unit, *International Energy Journal*, 13 (2) (2012) 63-74. **(**www.rericjournal.ait.ac.th)

(5) **P. Kalita**, N. Golla, K. P. Vivek, U. K. Saha, and P. Mahanta, Design and Charactrization of a novel loose biomass feeding system, *Journal of Scientific and Industrial Research* (JSIR), 72 (2013) 511-514**.**

(6) **P. Kalita,** U. K. Saha, and P. Mahanta, Some studies on wall-to-bed heat transfer in a pressurized circulating fluidized bed unit, 5th BSME International Conference on Thermal Engineering, *Procedia Engineering* 56 (2013) 163-172. (http://dx.doi.org/10.1016/j.proeng.2013.03.103).

(7) **P. Kalita,** P. Mahanta and U. K. Saha, Study of bed-to-wall heat transfer with twisted tape at the upper splash region of a pressurized circulating fluidized bed unit, *International Journal of Heat and Mass Transfer* (Under Review) 2013.

(8) **P. Kalita,** P. Mahanta and U. K. Saha, Hydrodynamic Characteristics of Loop-seal in a CFB Boiler - A Review, *Journal of Power and Energy* (Under Review) 2013.

CONFERENCES

(9) **P. Kalita,** U. K. Saha, and P. Mahanta, Evaluation of gasification potential of sawdust in a pressurized circulating fluidized bed unit, *International Conference on ENERGY*, on 8th November, 2012, at the Université catholique de Louvain (UCL), Belgium.

(10) **P. Kalita**, P. Mahanta and U. K. Saha, 2011, Effect of operating parameters on the performance of a pressurized circulating fluidized bed unit - a review, Summer School on *Efficient Fossil Energy Technologies*, July 4-10, 2011, IIT Guwahati.